SURFACTANT INTERCALATED KOPPIES AND BOANE BENTONITES FOR POLYMER NANOTECHNOLOGY

By

Pedro Horácio Massinga Júnior

Submitted in partial fulfilment of the requirements for the degree

Doctor Philosophiae

in the
Department of Chemistry
Faculty of Natural and Agricultural Sciences
University of Pretoria
Pretoria

December 2013

SYNOPSIS

This research aimed to develop technology and processes to further beneficiate two southern African bentonites for applications in polymer/clay nanotechnology. The bentonites were from the Koppies mine in South Africa, and the Boane mine in Mozambique. The work was divided into two parts: (i) preparation of organomodified nanoparticulate smectite clays, and (ii) preparation of their poly(ethylene-co-vinylacetate) nanocomposites.

Nanoparticulate organobentonites were prepared using purified bentonites. The conventional organomodification process uses a very low concentration of bentonites at 80 ^{o}C. In this study, a novel method was developed: concentrated slurries of naturally occurring Ca-bentonite partially activated with soda ash in the presence of a proprietary dispersant were contacted at ambient temperature with quaternary ammonium surfactants. A known amount of bentonite dispersion was placed in a planetary mixer before the mixture. Likewise, a known amount of surfactant, up to 50% excess, based on the estimated cation exchange capacity (CEC) of the bentonites, was added while mixing the dispersion. The surfactants added were either in solution or in powdered form. The intercalated bentonite was recovered by centrifugation and washed repeatedly with water until halide ions could not be detected using a 1M silver nitrate solution. The solids were dried at ambient temperature and humidity, and then crushed and milled into a fine powder using a mortar and pestle.

Several instrumental techniques were used to characterise and examine the properties of the bentonite samples before and after organic treatment.The X-ray diffraction (XRD) results were consistent with: (i) paraffin-type extended chain intercalation; and (ii) interdigitated monolayer intercalation of the C12 and C14 single-chain alkyl surfactants and bilayer intercalation of the single-chain C16 surfactant and the surfactants with double alkyl chains. Fourier transform infrared (FTIR) spectroscopy analysis of the organobentonite powders confirmed disordered chain conformations. XRD also detected significant amounts of cristobalite in the samples of Boane bentonite (from Mozambique). This impurity could not be removed cost-effectively. The onset decomposition temperature ofthe present organobentonites was around 200 ºC, which is within the typical range of polymer/organoclay processing temperatures. The thermal stability of the organobentonites was independent of both the number of alkyl chain substituents and their length, and also independent of the degree of clay intercalation.

Poly(ethylene-co-vinylacetate) nanocomposites were prepared with South African Koppies bentonite, organomodified with single-chain C12 (and polar 2-hydroxyethyl side chain) and double-chains C18 alkyl ammonium cationic surfactants. The later surfactant was intercalated both below and above the clay CEC. Nanocomposites were prepared by twin-screw melt compounding. Transmission electron microscopy (TEM) indicated the presence of mixed nano- and micron-sized clay morphologies. XRD studies revealed that the crystallinity of the particles improved and that the d-spacing values increased on incorporation of the modified bentonites in the polymer matrix. It is postulated that, rather than indicating polymer co-intercalation, this was caused by further intercalation of either excess surfactants or surfactant residues that were released by shear delamination of the clays during compounding. Improved mechanical properties were realised, especially when using the bentonite containing the longer double-chains surfactant intercalated at levels in excess of the CEC of the clay. The nanocomposites showed improved tensile modulus and elongation at break values at the expense of a reduction in impact strength, while tensile strength was about the same as for the neat polymer.

Keywords: Intercalation, exfoliation, organobentonite, poly(ethylene-co-vinylacetate), nanocomposites.

PUBLICATIONS GENERATED AS PART OF THIS RESEARCH

Massinga Jr, P., Focke, W., del Fabbro, O., Radusch, H., 2013. EVA nanocomposites based on South African Koppies clay, *Journal of Vinyl and Additive Technology*, accepted for publication.

Massinga Jr, P., Focke, W., 2012. Intercalating cationic surfactants in Koppies bentonite, *Molecular Crystals and Liquid Crystals*, 555:1, 85–93.

Merckel, R., Focke, W.; Sibanda, M.; Massinga Jr, P.; Crowther, N., 2012. Co-intercalation of insecticides with hexadecyltrimethylammonium chloride in Mozambican bentonite, *Molecular Crystals and Liquid Crystals*, 555:1, 76–84.

Massinga Jr, P., Focke, W., De Vaal, P., Atanasova, M., 2010. Alkyl ammonium intercalation of Mozambican bentonite, *Applied Clay Science* 49, 142–148.

AKNOWLEDGEMENTS

I am grateful to:

Prof. Walter W Focke, my advisor, for his suggestions. Walter, much of what is good in this thesis comes from you.

Mr Ollie del Fabbro and Mrs Suzette Seymore for their assistance during the course of this research.

Dan Molefe, Herminio Muiambo, Lumbi Moyo, Mthokozisi Sibanda, Nontete Nhlapo, Shepherd Tichapondwa and Washington Mikhe – my colleagues at the Institute of Applied Materials in the University of Pretoria. My folks, your tremendous support is gratefully acknowledged.

The National Research Foundation (NRF) for financial support via the Institutional Research Development Programme (IRDP) and the South Africa/Mozambique Collaboration Programme. G & W Base & Industrial Minerals for samples and technical support. The South African Council for Geoscience (Pretoria), the Laboratory for Microscopy and Microanalysis at the University of Pretoria, and the Center of Engineering Sciences at the Martin-Luther-Universität Halle-Wittenberg (German), all for technical support. The University Eduardo Mondlane, my employer, for giving me the opportunity to further my studies and for financial assistance.

Rose Massinga, my wife, for bringing out the best in me.

Jesus Christ – the Lord God Almighty. Dear Lord, your will always guides me to where your grace protects me. “Let all who take refuge in you be glad; let them ever sing for joy (Psalm 5:11).” Blessed be your glorious name.

DECLARATION

I, the undersigned, declare that the thesis that I hereby submit for the degree PhD at the University of Pretoria is my own work, and has not previously been submitted for a degree or examination at this or any other institution.

Pretoria, December 2013

Pedro Horácio Massinga Júnior

Table of contents

LIST OF FIGURES

LIST OF TABLES

LIST OF SYMBOLS AND ABBREVIATIONS

ASTM	American Society for Testing and Materials
BP	Boane powder
BS	Boane slurry
BSE	backscattered electron
CP-MS	cone-and-plate measuring system
CEC	cation exchange capacity (meq/100 g dry clay)
d_L or d_{001}	basal spacing of clay mineral particles (nm)
DMA	dynamic mechanical analysis
E' or G'	storage modulus (Pa)
E" or G"	loss modulus (Pa)
EVA	ethylene vinyl acetate
FESEM	field emission scanning electron microscopy
FTIR	Fourier transform infrared spectroscopy
KP	Koppies powder
KS	Koppies slurry
L/D	length per diameter
LVE	linear viscoelastic region
meq	milliequivalent
MFI	melt flow index (g/10 min at 190 ^{o}C/2.16 kg)
MMT	montmorillonite
pH	hydrogenionic potential
PLSN	polymer-layered silicate nanocomposite
rpm	revolutions per minute
SEM/BSE	scanning electron microscopy with backscattered electron
SEM/EDX	scanning electron microscopy fitted with an energy dispersive X-ray analyser
TEM	transmission electron microscopy
Tg	glass transition temperature
TGA	thermogravimetric analysis
T_{onset}	thermogravimetric decomposition onset temperature
T_{peak}	main decomposition step in thermogravimetric analysis
VA	vinyl acetate

XRD	X-ray diffraction
XRF	X-ray fluorescence

Greek Symbols

ε_{es}	interaction between EVA and silicate particles (J.mol^{-1})
ε_{ss}	interaction between silicateand silicate particles (J.mol^{-1})
η^*	complex viscosity (Pa.s)
λ	radiation wavelength (nm)
θ	angle between incident and scattered X-rays (^{o})
ω	angular frequency (rad.s^{-1})

CHAPTER 1 INTRODUCTION

1.1 Rationale

Widespread future application of clay minerals in automotive, electronic, food packaging and biotechnology polymer nanocomposites has been predicted (Konta, 1995; Wang et al., 2004; Rehab and Salahuddin, 2005). It is related to (i) the polymer property enhancement that can be obtained by addition of clay minerals at lower loadings of about 5 mass %, and (ii) the inherently low processing costs of clay minerals due to their natural abundance in nearly pure mineralogical form.

Smectite clays intercalated with alkylammonium cations are the organoclays most widely used to prepare polymer nanocomposites (Sinha Ray and Okamoto, 2003). When dispersed as high aspect ratio particles in the polymer matrix, organoclays enhance desirable properties (LeBaron et al., 1999; Alexandre and Dubois, 2000; Sinha Ray and Okamoto, 2003; Paul & Robeson, 2008; Pavlidou & Papaspyrides, 2008; Camargo et al., 2009). Such properties include strength and stiffness, dimensional stability, flame retardancy, gas barrier properties and UV stability, among others (LeBaron et al., 1999; Alexandre and Dubois, 2000; Fischer, 2003; Sinha Ray and Okamoto, 2003; Lee and Lee, 2004; Wang et al., 2004; Ahmadi et al., 2005; Patel et al., 2007).

The enhancement of polymeric properties requires exfoliation or at least significant delamination of clay platelets (Fornes et al., 2002). Exfoliated structures are those in which the clay platelets are delaminated and individually dispersed in the polymer matrix. When polymer chains and silicate layers alternate in a well-ordered multilayer arrangement with a well-defined and preserved interlayer distance, the structures are intercalated. In exfoliated nanocomposite structures, silicate platelets are interspaced extensively. Such extensive interlayer separations disrupt coherent layer stacking. The ordering of the resulting clay platelets is not sufficient to produce a scattering peak. Hence, a featureless XRD diffraction pattern is recorded.

Complete exfoliation of individual clay sheets is difficult to achieve in the absence of favourable interactions between the polar clay's surfaces and the matrix polymer (Alexandre

and Dubois, 2000).There is an intrinsic incompatibility between the hydrophilic clay surfaces and the hydrophobic polymer chains.

Matching the surface energies requires appropriate organic modification of the clays. This is usually accomplished by means of an intercalation process through ion exchange reactions. Inorganic cations in the clay interlayer space, e.g. Ca^{2+} or Na^{+}, can be directly exchanged with organic cations. The exchange can be partial or complete, and may even exceed the cation exchange capacity (CEC) of clays (Lagaly, 1986; Klapyta et al., 2001; Xu and Boyd, 1995).

Organic intercalation modifies the hydrophilic nature of clay surfaces to organophilic. Simultaneously, it expands the basal or d-spacing (d_{001}) of clays. Organic species frequently intercalated into clay minerals include quaternary alkylammonium salts, known as quats. Long-chain quats are preferred as they lead to larger interlayer spacing. This, in turn, facilitates further penetration of polymer chains into the clay interlayer space. In addition, large basal spacing maximises the configurational freedom of organosilicate chains dispersed in the polymer matrix. Thus, organosilicate chains gain entropy, balancing the entropy loss caused by polymer chain confinement in the nanocomposites.

The d_{001} of smectite minerals expands with increasing loading of cationic surfactants. A limiting d_{001} is realised at a certain critical surfactant loading, beyond which no further expansion occurs (Xi et al., 2005). This critical surfactant loading depends on the clay CEC. At the critical loading, the alkyl chain length of the surfactant determines maximum d_{001} (He et al., 2010). Increasing the chain length tends to increase the maximum d-spacing. Ultimately, it is the surfactant conformation, rather than its amount intercalated or its chain length that determines the maximum d-spacing (He et al., 2010). This does not detract from the roles that the amount of surfactant intercalated and its chain length play with regard to the d-spacing.

The effects of surfactant loading and its alkyl chain length on the d-spacing of organoclays, as well as the arrangement and state of the intercalated surfactants, have been the subject of numerous investigations (Xi et al., 2005). Quats with two long alkyl chains are preferred as they lead to a larger interlayer spacing (Zhang et al., 2003). This allows easy penetration of

polymer chains into the organoclay interlayer space during composite preparation. Consequently, further expansion, delamination and dispersion of organoclay particles in a polymer matrix are facilitated.

The most environmentally friendly method for the preparation of polymer nanocomposites is melt intercalation. The method is also versatile and compatible with current processing equipment. Melt intercalation consists of blending molten polymer matrices with clay minerals. Polymer chains may diffuse from the matrix into the silicate interlayer. Thermodynamic factors related to the surface energies of polymers and silicates are critical.

Conventionally, polymer chains should first intercalate into the silicate interlayers. Subsequently, the chains may push the silicate platelets further apart. Individual silicate particles may thus exfoliate into the polymer matrix. Delaminating silicate platelets and achieving exfoliation requires strong shear forces (Garcia-Lopez et al., 2003; Wang et al., 2004; Pavlidou & Papaspyrides, 2008). Exfoliation is a key requirement for improving polymer properties. It can lead to a very large surface area for the interaction of stiff silicate particles with polymer chains.

Alexandre and Dubois (2000) obtained partially intercalated and partially exfoliated nanocomposite morphologies with poly(ethylene-co-vinylacetate), EVA, even at low vinylacetate content (12 mass %). However, no nanocomposites were formed when organomontmorillonite (functionalised with dimethyl dioctadecyl ammonium) was melt compounded into high-density polyethylene.

EVA $\{–(CH_2CH_2)_n[CH_2CH(OCOCH_3)]_m– \}$ is a copolymer with polarity that can be tailored depending on its vinylacetate (VA) units. Higher content of VA [$–CH_2CH(OCOCH_3)–$] affords polarity for interaction with (OH groups of) pristine silicates (Gupta et al., 2005; Cui et al., 2007). However, good surface affinity between EVA and silicates alone is not enough to achieve exfoliation. Prior break-up and expansion of intrinsic silicate stacks is required. Break-up of the silicate stacks is, generally, achieved by mechanical shear forces during intercalation of surfactants into the silicate layers.

Silicate stacks are explained as follows: layered silicates comprise particles with thickness in the nanometric range; their aspect ratio is very large, exceeding 200; there is a propensity for the aggregation and packing of such particles due to the flat surface area. However, the intercalation of long-chain surfactants expands the silicate interlayers, facilitating the diffusion of polymer chains into them. This, in turn, promotes exfoliation of silicate platelets in polymer matrices. Ultimately, a large interfacial area for interaction between polymer chains and silicate particles is thus created.

Over the last decade, EVA copolymer melt intercalated with clay minerals has been extensively researched. Such studies have considered the influence of various parameters on the degree of dispersion of the clay in the polymer matrix and the ultimate physical properties. These parameters include the nature of the pristine clay (Zanetti et al., 2001; Riva et al., 2002; Costache et al., 2005; Peeterbroeck et al. 2005), the clay organomodifier (Alexandre and Dubois, 2000; Alexandre et al., 2001; Zanetti et al., 2001; Jeon et al., 2003; Zhang et al., 2003; Peeterbroeck et al., 2005), the vinyl acetate content of the polymer (Alexandre and Dubois, 2000; Alexandre et al., 2001; Zannetti et al., 2001; Cser & Bhattacharya, 2003; Jeon et al., 2003; Zang et al., 2003; Pasanovic-Zujo et al., 2004; Zhang and Sundararaj, 2004; Gupta et al., 2005; Cui et al., 2007; Marini et al., 2009), the processing techniques (Zhang and Sundararaj, 2004; Chaudary et al., 2005a; Chaudary et al., 2005b; La Mantia & Tzankova Dintcheva, 2006; Pistor et al., 2010), and the presence of external compatibilisers (Suh et al., 2004; Jeon et al., 2003).

To date, however, the preparation of fully exfoliated EVA-layered silicate nanocomposites remains elusive. Most authors have reported mixed morphologies comprising both intercalated tactoids and exfoliated sheets. Exfoliation was favoured using EVA grades with higher vinylacetate content (Zhang et al., 2003). Clays functionalised with alkyl substituent only are partially exfoliated, with the microstructure of the composites being dominated by an intercalated structure (Zhang et al., 2003, Peeterbroeck et al., 2005). Nanocomposites based on clay melt intercalated with methyl dihydroxyethyl hydrogenated tallow ammonium displayed the highest amount of exfoliation and clay stacking destruction, characterised by the absence of a characteristic X-ray diffraction (XRD) reflection (Peeterbroeck et al., 2005).

The present study considered whether a surfactant with only a single hydroxyethyl substituent would perform similarly to that containing dihydroxyethyl. Furthermore, most studies employed clays with surfactants intercalated at approximately the cationic exchange capacity. However, intercalation can proceed to higher levels and the effect of this on nanocomposite morphology and properties was also investigated in this study.

The suitability of organoclays for the preparation and performance of polymer nanocomposites is not limited to good surface affinity with polymer chains. Thermal stability of organoclays is also relevant: lower degradation onset temperatures limit the processing temperatures of the composites. The thermogravimetric decomposition onset temperature (T_{onset}) provides an indicator of the thermal stability of organoclays. A previous study recorded no effects of different lengths of quat surfactants on the thermal decomposition of organoclays (Xie et al., 2001). The present study investigated the effect of a number of substituents of quaternary alkylammonium surfactants on the thermal decomposition of organoclays. In addition, it examined the influence of the number and length of the long-chain alkyl substituents of the surfactant on the nature of the chains in the interlayer.

1.2 Objectives of current research

This study aimed at rendering bentonites from Boane (Mozambique) and Koppies (South Africa) suitable for the preparation of bentonite-based polymer nanocomposites. Further, Koppies organobentonites were incorporated into an EVA matrix. The specific objectives of this research were to:

- Examine the influence of the number and length of long-chain alkyl substituents of surfactants, as well as the surfactant loading, on the degree of clay intercalation and on the nature of the chains in the interlayer.
- Evaluate the effect of the number and length of substituents of quaternary alkylammonium surfactants and the degree of clay intercalation on the thermal decomposition of organobentonites.
- Determine the effects of the structure of the surfactant (single long chain with one polar 2-hydroxyethyl side group) and the degree of clay intercalation on the exfoliation behaviour and the ultimate physical properties of poly(ethylene-co-vinylacetate)-clay composites.

1.3 Dissertation outline

Chapter 1 is the introduction, in which the rationale for the research is explained, the aim of the work presented, and the dissertation structure outlined.

Chapter 2 reviews the literature: a background to clay minerals and its organic intercalation is provided; likewise, a background to polymers and its nanocomposites is provided. In addition, peer-reviewed works on melt intercalated nanocomposites of EVA with layered silicates published over the last decade are critically assessed.

Chapter 3 outlines the experimental design and presents the raw materials and the instruments that were available for laboratory work. The methods and procedures followed in the laboratory are also described in this chapter.

Chapter 4 analyses the experimental results and explains eventual modifications to the experimental design.

Chapter 5 presents the conclusions, and all the references used are listed in Chapter 6. Additional supporting information is given in the Appendix.

CHAPTER 2 LITERATURE REVIEW

2.1 Clay minerals and their intercalation chemistry

The use of inorganic materials as reinforcing fillers for polymeric materials is widespread. Filled polymers take advantage of hybrid properties synergistically derived from polymer materials (e.g. the easy processability) and from inorganic materials (e.g. high mechanical strength and high thermal resistance) (Rehab & Salahuddin, 2005).

Clay minerals have been extensively researched to reinforce polymer materials mechanically and thermally. There are about 30 different aluminosilicate-layered minerals comprising natural clays. Each of these phyllosilicates consists of lamellar elements. Its crystal structure consists of a stack of plate-shaped layers interspaced by an interlayer, also known as a gallery (Utracki, 2004). The smallest stack of layers could be about 10 nm thick (Pavlidou and Papaspyrides, 2008). The nanometric dimensions, coupled with the two-dimensional structure, make the clay minerals interesting reinforcing fillers for polymer materials. The large surface area of the flake morphology and its high aspect ratio aids the stiffness and contributes to high in-plane strength of the lamellar elements (Rehab & Salahuddin, 2005).

Of all layered clay minerals, those of the smectite group are most often used to prepare polymer nanocomposites. This is due to the group's relatively high swelling properties and high cation exchange capacity (CEC). The high swelling ability of the smectite minerals allows a huge expansion of its interlayers. This facilitates the separation of individual clay layers, allowing larger molecular structures to intercalate. In turn, the high CEC indicates the presence of a high number of exchangeable cations in the interlayer. This allows the smectite to exchange the hydrated interlayer cations with a high number and wide range of like-polarity chemical groups (Sinha Ray and Okamoto, 2003).

The clay minerals belonging to the smectite group include montmorillonite, vermiculite, beidellite, saponite, talc, nontrolite, sauconite and pyrophyllite. Their crystal structure consists of a layer comprising two tetrahedral sheets sandwiching one octahedral sheet. Each sheet, either tetrahedral or octahedral, is about 0.22 nm thick. In between the two layers lie Ca^{2+} and Na^{+} cations as well as water molecules. The minimum thickness of an individual smectite platelet (basal spacing) in its natural state is considered to be 0.96 nm. It includes,

besides the octahedral and tetrahedral sheets, a hydrated interlayer with a minimum thickness of 0.30 nm (corresponding to a water monolayer). The lateral dimensions of an individual smectite platelet are more than two orders of magnitude larger (Paul et al., 2005; Utracki, 2004; Vaccari, 1998). The aspect ratio is $p \leq 1000$, i.e. the largest dimension of the platelet is 1000 nm (Utracki, 2004; Powell & Beall, 2006).

The crystal layer unit-cell of smectite clay minerals is generally characterised by six octahedral sites and eight tetrahedral sites. The octahedral sheet may consist of central Al^{3+}, Mg^{2+} or Fe^{2+}cations coordinated by six oxygen atoms (Powell & Beall, 2006). Two of these oxygen atoms are bonded to hydrogen atoms, forming OH groups. Each tetrahedral sheet is formed from central Si^{4+}, Al^{3+} or Fe^{3+}cations coordinated by four oxygen atoms. One oxygen atom is shared between each octahedral and each tetrahedral site (Utracki, 2004).

Isomorphic substitutions within the tetrahedral and/or octahedral sheets of native smectite clays generate a negative charge in the clay layers. Within tetrahedral sheets, a certain number of Al^{3+} cations can replace the same number of Si^{4+} cations. In the octahedral sheet, Al^{3+}cations can be replaced by the same number of Mg^{2+}cations and, less frequently, by Fe^{2+}cations. The general chemical formula of smectite minerals, often reported on the basis of the half unit-cell content, is:

$$(M^{n+}_{x+y/n}\, nH_2O)(Al^{3+}_{2-y}\, M^{2+}_{y})O_2(OH)_2(Si^{4+}_{4-x}\, Al^{3+}_{x})O_8$$

In this formula, $M^{n+}_{x+y/n}\, nH_2O$ indicates hydrated cations of different valency counter balancing the negative charge on the surfaces to restore the electroneutrality of the clays. M^{2+}_{y} refers to the generic divalent cation of the clay structure. X indicates the layer charge resulting from substitutions in tetrahedral sites. The layer charge of octahedral sites is indicated by Y, while “n” indicates the number of water molecules hydrating the cations (Utracki, 2004).

Clay surface charge is not constant throughout the whole mineral crystal: it varies from layer to layer. However, its average value is considered over the entire crystal. It is this charge that

is known as the CEC of the clay, generally expressed in meq/100g (milliequivalents per hundred grams) of dry clay (Sinha Ray & Okamoto, 2003).

Alkali and/or alkaline earth cations are the most common ions within the gallery of cationic clays. The decreasing order of preferential adsorption of some common cations is: $H^+ > Al^{3+} > Ba^{2+} > Sr^{2+} > Ca^{2+} > Mg^{2+} > NH_4^+ > K^+ > Na^+ > Li^+$. This order parallels the increasing degree of hydration for these cations (Perez, 1974, Voyutsky, 1978, Konta 1980). The sequence indicates that, although Ca^{2+} is preferentially adsorbed in the gallery of cationic clays than Na^+, the latter is more highly hydrated than Ca^{2+}.

There are three modes of hydration, and they have been recognised as pH dependent: (i) hydration at internal surfaces (interlayer hydration) of clay mineral particles; (ii) continuous hydration of internal and external clay surfaces, due to unlimited adsorption of water; and (iii) capillary condensation of free water in micropores (Utracki, 2004).

The interlayer hydration consists of three main elements: (i) hydration of adsorbed cations; (ii) interaction of hydrated cations with the internal surfaces of the clay mineral; and (iii) water activity in the clay-water system. The interaction of hydrated cations with the surfaces of the clay mineral involves the inner sphere of hydration and/or the outer sphere of hydration. When one side of the interlayer cation is directly bound to the clay mineral surface and the other side is bound to a number of water molecules, an inner sphere of hydration is formed. Further, when the interlayer cation is completely surrounded by water molecules and interacts, through these ligands, with the clay mineral surface, it is recognised as the outer sphere of hydration. Adsorption of water initiates by solvation of the interlayer cations and is followed by occupancy of the remaining interlayer space (Utracki, 2004).

Due to water penetrating the interlayer molecular spaces and to concomitant adsorption, some smectites expand considerably more than others. The amount of expansion depends largely on the type of exchangeable cation contained in the mineral interlayer. Some factors affecting interlayer hydration are: (i) the hydration energy of the interlayer cation; and (ii) the water polarisation power of the interlayer cation.

Hydration energy of the cation is the energy change when a cation is solvated in water. The structure of a hydrated cation consists of water molecules surrounding the central cation. The water molecules arrange themselves with oxygen lone pairs of electrons oriented towards the positive cation charge. There is a greater solvent ordering around small cations than around large ions. The smaller the cationic radius, the closer the water molecules will be packed. However, fewer water molecules can be closely packed around a small ion than around a large one. Cations of small size and of high charge produce a more intense electrostatic field at their surfaces. Consequently, their water polarisation power is strong, the degree of hydration is greater, and they become less mobile. Therefore, the presence of sodium as the predominant exchangeable cation instead of calcium can result in the clay swelling to several times its original volume (Kornmann et al., 1998).

Swelling of smectites is strongly related to isomorphic substitutions since the basal oxygen atoms acquire an excess negative charge. Their electron-donating capacity increases whether the layer charge derives from substitution in the octahedral or tetrahedral sheets. This results in a strong tendency to form hydrogen bonds with water molecules, especially those coordinated to interlayer cations. Such water molecules are Lewis acids, which have a tendency to receive electrons. The preference for H-bonding is, however, higher for oxygen atoms substituted in tetrahedral sheets than in octahedral ones. This is because the basal surface oxygen atoms of a smectite are those of tetrahedral sheets. It is the swelling and the CEC properties that confer very rich intercalation chemistry on smectites (Rehab & Salahudin, 2005).

2.2 Organic intercalation of clay minerals

Individual layers of clay minerals are potentially the most suitable for the preparation of polymer layered silicate nanocomposites (PLSNs). A high aspect ratio of clay particles is an important factor in polymer property enhancement. Exfoliation of montmorillonite (MMT) layers in a polymer matrix leads to a very large interfacial surface area for interaction with the polymer chains. However, complete delamination of individual clay mineral layers into a polymer matrix is doubtful (Pavlidou and Papaspyrides, 2008).

Dispersion of neat clay particles is difficult owing to an intrinsic incompatibility between the hydrophobic polymer matrix and the hydrophilic clay mineral surfaces. Better matching of the surface polarities can be achieved by appropriate organic modification of the clays. This

is usually accomplished via ion exchange reactions (de Paiva et al., 2008). The inorganic cations in the clay interlayer space, e.g. Ca^{2+} or Na^{+}, can be directly exchanged with organic cations by means of an intercalation process. The substitution with organic cations can be partial or complete, and in some cases it may even exceed the CEC (Utracki, 2004; Zhu et al., 2008).

The adsorption of organic molecules by clay is influenced by the hydration state of the clay and the polarising power of the interlamellar cations. When interlayer water is present, the cohesion forces of the clay are greatly reduced and, consequently, penetration of the sorbate molecule is facilitated.

Intercalation of organic cations is an important first step in the preparation of PLSNs. The replacement of small inorganic cations from interlayers aims to (LeBaron et al., 1999; Alexandre & Dubois, 2000; Sinha Ray and Okamoto, 2003; Goldstein & Beer, 2004; Lee and Lee, 2004; Powell and Beall, 2006):

- impart an organophilic character to the clay surface; this provides an effective mechanism for attracting polymers of like polarity into the clay interlayer
- increase the interlayer distance; this provides accessibility for large molecules like polymers.

The interlayer distance of organomodified clays, and consequently, the size and type of polymeric molecule that can be further intercalated, depends decisively on the selection of the cationic surfactant. Utracki (2004) stated that a preferred intercalating agent should possess:

(i) good kinetics for diffusion into the interlayer
(ii) high bonding strength with clay platelets
(iii) strong interaction with the polymer matrix.

Quaternary ammonium salts (quats) are the most extensively used intercalants in commercially available organoclays. They behave like a compatibiliser, providing good stress transfer between the clay and the polymer. Quats are preferred for the following reasons (Utracki, 2004):

(i) Oxygen atoms on the clay surface are suited for hydrogen bonding with organic surfactants comprising nitrogen atoms. This satisfies the first and second criteria for the selection of a cationic surfactant.

(ii) They have potential for bonding with electron-deficient aluminium atoms on the clay surface. This bonding may occur via the Lewis acid/base mechanism. This non-ionic interaction provides good kinetics for the diffusion of quats into the interlayer.

(iii) They behave like a compatibiliser, providing good stress transfer between the clay and the polymer.

LeBaron et al. (1999) recommend selecting long-chain surfactants for increasing the interlayer distance to the extent that a monomer or pre-polymer can be intercalated or eventually exfoliated. Zhang et al. (2003) found that surfactants with two long alkyl chains are ideal for yielding organosilicates with wider basal spacing. Further, it was found that the hydrophilic/hydrophobic balance of an organoclay depends on the length and packing density of the alkyl chains (Utracki, 2004).

The effect of alkyl chain length and surfactant loading on the d-spacing of organoclays, as well as the arrangement and state of the intercalated surfactants, have been the subject of numerous investigations (Xi et al., 2005). It is well known that the d-spacing increases with increasing surfactant loading. The loading may exceed the CEC of the clay mineral. The maximum d-spacing is realised at a certain critical surfactant loading, beyond which no further expansion occurs (Xi et al., 2005). This critical surfactant loading depends on the CEC of the clay. At the critical loading, the surfactant's alkyl chain length influences the maximum d-spacing (He et al., 2010). Increasing the chain length tends to increase the maximum d-spacing. Ultimately, it is the surfactant conformation, rather than the amount intercalated or its chain length that essentially determines the d-spacing that can be achieved (He et al., 2010). This does not detract from the roles that the amount of surfactant intercalated and its chain length play with regard to the d-spacing.

Preparation and performance of clay-polymer composites does not depend only on larger interlayer spacing of organoclays. It is also affected by the thermal stability of organoclays: lower degradation onset temperatures limit the processing temperatures of the

nanocomposites. An indicator for the thermal stability of an organoclay is its thermogravimetric decomposition onset temperature, T_{onset}. A previous study concluded that different lengths of quat surfactants have no effect or very little effect on the thermal decomposition of organoclays (Xie et al., 2001). It would be interesting to determine whether surfactants with different numbers of alkylammonium chains affect the thermal stability of organoclays.

2.2 Generalities about polymers

Polymers are natural or synthetic compounds of high molecular mass (macromolecules). They contain at least one repeating structural unit in their chains, inter-linked by covalent bonds. Such a repeat unit is equivalent to that of the starting material from which the polymer is made, and is known as a *monomer*. In each covalent bond, inter-linked atoms share the electronic pair equally. The total number of repeat units determines the length of the polymer chains. In addition, the monomers determine the degree of polymerisation and define the molecular size/mass of the polymer.

A polymer that contains identical monomers is a *homopolymer.* However, if different kinds of monomer comprise the polymer, it is classified as a *copolymer*. Polymer chains may be linear or branched. The structure of a polymer with a linear chain is quite simple and flexible. It consists of monomers connected to no more than two other monomers. A polymer structure consisting of a chain with at least one side chain, with a monomer connected to more than two other monomers to form three-dimensional networks, is classified as *branched polymer*.

Polymer molecules that are chemically and geometrically regular in structure are typically crystalline. Chain branching and co-polymerisation cause occasional structural irregularities of polymers. Both limit the extent of crystallisation, though do not prevent its occurrence. Co-polymers with significant amounts of both monomers, or with quite different monomer constituents, are typically non-crystalline polymers. Other irregularities of structures caused by the size and the bulkiness of the substituent groups yield non-crystalline polymers. A polymer may have a structure that is intermediate in kind between crystalline and amorphous.

Polymers can also be classified as thermoplastic, thermoset or elastomeric. *Thermoplastic polymers* comprise linear chains with weak van der Waals intermolecular bonds. These can be easily broken when the polymer is heated and individual chains move freely. They

constitute the most common category of plastics, since they are recyclable. *Thermoset polymers* consist of cross-linked chains whose bonds do not break easily on heating. The cross-links break at high temperatures, when the covalent bonds between monomers tend to break simultaneously, degrading the polymer. Cross-links prevent individual chain flow and lessen interchain interactions. Thus, cross-linking enhances the mechanical strength of polymers. However, it also makes it difficult to recycle the polymer. *Elastomeric polymers* (elastomers) are an intermediate category between thermoplastics and thermosets. They are not hard as thermosets, but are likewise difficult to melt; they also degrade. Elastomers consist of a few cross-linked chains as compared with thermoset polymers.

The structure of a polymer decisively affects its physical properties and applications. The application of a polymer depends on its properties: mechanical, electrical, thermal and optical, among others. Generally, polymers possess low electrical and thermal conductivity, and low mechanical and thermal resistance. They can bear external pressure without fracture, and even return to their initial shape when the external pressure is removed.

Polymer matrices consist of polymer chains in an environment of similar chains. At low temperatures, polymer molecules do not have enough energy to move with respect to one another. They are ‘frozen’ in a hard and brittle solid state known as the *glass state*. In this state, polymers are crystalline, vibrate with low energy, and have properties like hardness, stiffness and brittleness. When heated, polymer molecules vibrate with enhanced energy; a transition occurs from the glass state to the *elastomeric state*. The temperature at which the polymer softens and the transition occurs is known as the *glass transition temperature*, Tg. Polymer interchain interactions may decrease when Tg is reached, and individual chains gain freedom to move and assume many different conformations. The movement of polymer segments results from their increased thermal energy. In the elastomeric state, polymer chains may adopt an ordered arrangement and their free volume increases. The thermal expansion and the elasticity of the polymer may also increase. When the polymer is heated above its Tg, it may melt. Thermoset polymers do not melt on heating, while thermoplastics melt on heating and re-solidify on cooling. The chain orientations and molecular weight affect the softening and melting properties of thermoplastics.

There are polymers that are usable below their softening temperature. Others exhibit better performance above the Tg. The properties of a polymer at a required temperature determine its choice for a particular application. Owing to the ability of thermoplastics to melt on heating and re-solidify on cooling, they are preferred for the preparation of polymer/clay composites via melt compounding.

2.3 Overview of some characterisation techniques for polymer-clay composites and their precursors

2.3.1 X-ray diffraction (XRD)

XRD is a powerful tool used for assessing the orderly arrangements of atoms and molecules. It is the single most commonly used technique for probing composite structure due to its ease of use and its availability.

X-rays are usually produced by bombarding a target metal inside a vacuum tube with a beam of high-voltage electrons. The wavelengths of the X-rays produced depend on the applied voltage and the target metal. The detection of diffracted X-rays is made possible by a radiation counter and electronic equipment feeding data to a computer. This detection method allows precise measurement of the intensity of the diffracted beam. However, the action of diffracted X-rays on photographic films may also be used for their detection. This method, in turn, allows qualitative examination of the diffraction pattern and accurate measurement of angles and distances.

X-rays of a given wavelength are diffracted for the same specific orientations of the sample. Randomly oriented, minute powdered particles will have all orientations of the particles investigated simultaneously and included within the sample; it is not possible to investigate orientations about one crystal axis at a time, as with a single crystal. Though analysis of randomly oriented, minute powdered particles is more convenient, it gives less information than investigation of a single crystal.

XRD is an analytical method based on the interaction of electromagnetic radiation with structures comparable in size to the wavelength of its radiation. Such interaction gives interference effects that are sharpened when the structures are arranged in a lattice with an orderly array of points. In this case, the radiation is diffracted or scattered only under specific

experimental conditions. It is the knowledge of these conditions that gives information regarding the geometry of scattering structures.

The wavelength of X-rays is comparable to the interatomic distances in crystals. Low-angle X-ray scattering can detect larger periodicities of lamellar crystallites. A wide-angle XRD pattern describes the spatial arrangement of atoms. The periodicity of a structure is characterised by the existence of ordered three-dimensional repeat units. The characterisation of the structure of polymer-clay composites using XRD is partially based on the changes observed in the thickness and intensity of the basal reflection peaks (Pavlidou & Papaspyrides, 2008). The sharp features in XRD patterns are associated with regions of three-dimensional order or crystallinity. By contrast, diffuse XRD features are characteristic of three-dimensional disorder of an amorphous material. The occurrence of both sharp and diffuse features is evidence that ordered and disordered regions coexist.

XRD analysis of polymer-clay composites and their precursors consists essentially in monitoring the position, shape and intensity of basal reflections from the silicate layers. Subsequently, the interlayer spaces between diffractional silicate planes can be determined using Bragg's law (Equation 1).

$$n\lambda = 2d \sin\theta \quad (1)$$

where:
n is an integer
λ is the wavelength of incident wave
d is the interplanar distance between adjacent atomic lattices
θ is the angle between the incident ray and scattering planes

When characterising polymer-clay composites using XRD, organoclay basal peaks are often used as a reference. If such basal reflections do not change, the polymer is immiscible. If the basal peak position shifts towards a lower angle, coupled with peak broadening and an intensity decrease, the nanocomposite is intercalated (Pavlidou & Papaspyrides, 2008; Preschilla et al., 2008). However, a basal peak shift to lower angles coupled with an intensity

decrease to eventual disappearance are indicative of exfoliated nanocomposites (Preschilla et al., 2008).

It is doubtful whether complete exfoliation of clays can be achieved. The majority, if not all of polymer nanocomposites so far reported in the literature presented intercalated or mixed intercalated/exfoliated structures. This is due to the anisotropy and the large lateral dimensions of the silicate layers. They can reach a length of 1000 nm when delaminated and hence it is practically impossible to separate them completely in the polymer matrix (Pavlidou & Papaspyrides, 2008).

2.3.2 Transmission electron microscopy (TEM)

Composite structures determined solely on the basis of XRD patterns are not completely certain. TEM better analyses the size, morphology and degree of clay distribution on the composites. This technique provides qualitative visual evaluation of the internal composite structure. Heavier elements, such as Al, Si and O, compose the silicate layers. The surrounding polymer matrix and the silicate interlayers comprise C, H and N. The latter elements are relatively lighter, and are visualised as bright or white zones upon composite formation. Conversely, the cross-sections of silicate layers appear as dark lines (Pavlidou & Papaspyrides, 2008; Pereira de Abreu et al., 2007).

Sample preparation for TEM analysis is time-consuming since very thin sections of about 10^{-6} cm are required. Further, TEM requires a large set of images and a tedious analysis for quantification. The aim is to produce estimations representative of the whole material. The properties at the surface of samples may be different from those in the bulk (Pavlidou & Papaspyrides, 2008; Preschilla et al., 2008). In addition, the orientation at which the sample is prepared corresponds to one axis at a time. The endeavour to obtain representative TEM samples involves preparing them in all possible orientations, by rotating the sample about one of its axes.

2.3.3 Rheological analysis

Rheology is also powerful for complementing XRD. This technique can assess the degree of dispersion, and the morphology and size of clays in the polymer matrix (Dal Castel et al., 2009). The extent of clay exfoliation can be estimated from the shear thinning behaviour of

polymer composites (Szép et al., 2006). High zero-shear viscosities suggest a strong interaction between exfoliated nanoclay platelets and polymer chains. The internal nanocomposite network remains unaffected by the imposed low shear rate. When the shear rate is increased, the network breaks down and the platelets orientate in the direction of flow. Owing to this platelet alignment, the viscosity decreases to the level of the neat polymer (Gupta et al., 2005; Szép et al., 2006).

To analyse the rheological properties of polymer composites, oscillatory tests are most commonly used. Such tests provide information on the following functions: η^*, G' and G". These parameters are respectively referred to as the complex viscosity, the storage modulus and the loss modulus. The storage modulus, G', is a measure of the energy storage of the material. It indicates how well structured a material is and corresponds to its elastic contribution. The loss modulus, G", is a measure of energy dissipation. It corresponds to the viscous contribution of the material (Shenoy, 1999).

Oscillatory experiments are performed in the linear viscoelastic (LVE) region. In this region, the structure of the viscoelastic material remains unbroken throughout the measurements. The LVE range is frequently determined by a shear strain amplitude sweep test. It consists of exposing the sample to increasing strain amplitude at constant frequency and temperature. This test is carried out as the first oscillatory test with every unknown sample (Mezger, 2006). The mid-point of the LVE range is the value of the strain amplitude that is subsequently used in the frequency sweep test. This test is carried out to further characterise the viscoelastic structure. A typical frequency sweep test consists of exposing a sample to a stepwise increase in frequency at a constant strain amplitude and temperature. Cone-and-plate geometry is preferred to ensure uniform shear rates across the sample.

2.3.4 Dynamic mechanical analysis (DMA)

DMA measures the mechanical response of a material to a cyclic deformation as a function of temperature. Usually, tension and three-point bending are the types of cyclic deformation applied. DMA results are expressed by three main parameters: (i) the storage modulus, *E'*or *G';* (ii) the loss modulus, *E"* or *G"*; and (iii) the damping factor, tan δ or *E"/E' orG"/G'*.

The storage modulus corresponds to the elastic response of a certain material to the deformation. Typically, upon dispersion of a layered silicate in a polymer, DMA assesses whether G' increases. For exfoliated composite structures, G' increases, probably owing to the creation of a three-dimensional network of interconnected long silicate layers. These strengthen the polymer material through mechanical percolation. The increase in G' is, generally, larger above the Tg – the glass transition temperature. It is above this temperature that polymers soften, and the reinforcement effect of the clay particles becomes more prominent. Such reinforcement is derived from the restricted movement of the polymer chains.

The loss modulus, G", corresponds to the plastic response of the material to deformation. Enhancement of the loss modulus is discussed far less directly in the literature than G'. Finally, the damping factor, tan δ, measures the ratio of the loss modulus to the storage modulus. Tan δ is useful for determining the occurrence of molecular mobility transitions such as the glass transition temperature. Depending on the polymer matrix, values of tan δ are affected in different ways upon nanocomposite formation (Pavlidou & Papaspyrides, 2008).

2.3.5 Thermogravimetric analysis (TGA)

The thermal stability of a polymer and its nanocomposites can be investigated using TGA. A stepwise increase in temperature is used to monitor the mass loss of the polymer (Beyer, 2002; Szép et al., 2006). An atmosphere of air or oxygen is preferred for TGA of a polymer and its nanocomposites. Such an atmosphere allows oxidative decomposition reactions of the polymer to take place. TGA uses a precision balance that is very sensitive to the mass loss of the sample. However, the derivative of the thermogravimetric curve is more characteristic and informative (Szép et al., 2006). It indicates the temperatures at which each event occurs.

2.3.6 Fourier Transform Infrared (FTIR) spectroscopy

Infrared (IR) spectroscopy is a method of chemical analysis whereby the sample is illuminated with incident radiation in order to excite molecular vibrations. The frequency of the incident radiation, usually in cm^{-1} wavenumbers, is varied continuously. When the molecule absorbs a particular discrete amount of energy, it causes a vibration. The vibrational energy corresponds to the absorption of energy by a molecule as the component atoms vibrate about the mean centre of their chemical bonds. Only the vibrations producing a change in the

molecule's dipole moment are detected in the infrared spectrum. A change in the dipole moment during the vibration for the molecule or the functional group under study is the fundamental requirement for absorption of IR radiation.

The IR spectrum is formed when absorption of electromagnetic radiation occurs at frequencies that correlate to the vibrations of specific sets of chemical bonds. The transmittance of the radiation through the sample is plotted, in the spectrum, against the incident frequency.

Based on the spectral region, there are three forms of vibrational spectroscopy: far-IR (500-150 cm^{-1}), mid-IR (4000-400 cm^{-1}), and near-IR (13300-3300 cm^{-1}). The common vibrational energies of organic and non-metallic inorganic species are in the mid-IR.

Mid-IR spectroscopy is the most commonly used, and for this samples are prepared by grinding the analyte in an alkali halide. The mixture is pressed into a pellet or ground in mineral oil to form a mull (a very thick suspension), which is spread between two alkali halide plates. Water gives a prominent and obstructive mid-IR background. Therefore, mid-IR samples must be free of moisture.

2.3.7 Mechanical analysis (tensile and impact testing)

Mechanical reinforcement of polymers by layered silicates is due to the rigidity of these fillers. Layered silicates have high strength moduli and inherent resistance to strain. In intercalated or exfoliated structures, the polymer adjacent to the filler is restrained mechanically owing to its confinement, and the filler bears a significant portion of the load applied to the nanocomposite. Fillers with a larger surface area therefore provide a much greater reinforcing effect as they strengthen a much larger region of the polymer matrix. Conversely, aggregation of clay layers causes a reduction in mechanical properties. The stacking of platelets is detrimental to composite stiffness since it reduces the filler aspect ratio and surface area (Pavlidou & Papaspyrides, 2008).

Tensile properties

Typically, a tensile test consists of a sample (specimen) clamped at both ends. The grip sites are large to prevent premature failure due to stress concentration. The centre of the specimen is thin to encourage the sample to fail at this portion and not at the grip sites. The specimen is

pulled apart, with one end moving relative to the other at a constant rate of elongation. Multiple specimen samples are tested to allow statistical evaluation of the results.

Very informative mechanical data are gathered, recording a stress-strain curve in tension. The initial linear region (slope) of the stress-strain curve measures the stiffness of the material; this is the Young's modulus or modulus of elasticity. The strain at which the specimen breaks is termed the 'elongation at break' (Chacko et al., 2009). The initial region where the stress begins to level off corresponds to the stress at yield.

Generally, the Young's modulus and the amplitude or tensile strength of nanocomposites are significantly higher than those of virgin polymers. The increase in modulus and yield stress is attributable to the clay reinforcement effect. Conversely, elongation at break typically decreases relative to virgin polymers due to the clay reinforcement effect.

Notched impact strength

Notched impact strength is measured, commonly, by hitting the specimen with a pendulum with a massive striking edge (Charpy test). The energy required to break the specimen is calculated from the travel of the pendulum after it has broken the specimen.

2.4 Melt intercalation and performance of polymer-clay composites

Polymers filled with particles reduce production costs and, further, enhance desirable properties, e.g. stiffness and toughness, barrier properties, and resistance to fire and ignition, among others. However, the addition of microparticulate fillers does impart drawbacks to the resulting composites (e.g. brittleness and opacity). Thus a new class of composites – polymer nanocomposites – has emerged (Alexandre & Dubois, 2000).

Polymer nanocomposites are particle-filled polymers for which at least one dimension of the dispersed particles is in the nanometre range. Nanocomposites characterised by only one dimension in the nanometre range consist of filler present in the form of sheets of one to a few nanometres thick and hundreds to thousands of nanometres long. Such composites can be gathered under the name of polymer-layered silicate nanocomposites (PLSNs).

A uniform dispersion of fillers in the nanometre range is a key requirement for improving the mechanical and barrier properties of polymer nanocomposites. To date, the preparation of fully exfoliated PLSNs remains elusive. The use of varied processing equipment and conditions has yielded disparate nanocomposite structures and properties. So has the use of polymers with diverse features, silicates and organic modifiers of different types, modifiers with several chain lengths and polarity, and intercalation into silicates in dissimilar amounts. It is, therefore, necessary to understand the influence of materials, instruments and processing conditions on the properties of created composites.

Alexandre and Dubois (2000) found that no nanocomposites were formed when melt compounding organomontmorillonite (functionalised with dimethyl dioctadecyl ammonium) into high-density polyethylene. However, partially intercalated and partially exfoliated morphologies were obtained with EVA copolymers even at low vinyl acetate content (12 mass %). For this reason poly(ethylene-co-vinylacetate), EVA, was chosen as the polymer matrix in this study.

The literature review within the scope of this study focused on composites whose structures have been determined by TEM. Structures probed solely by XRD are not completely certain. When no XRD peak is observed, it could be deduced as exfoliation. However, the presence of a small quantity of ordered stacks may also yield a featureless XRD diffractogram. Moreover, the presence of a high number of non-uniformly dispersed clay stacks likewise yields a featureless pattern or interlayer variations. In turn, any presence of homogeneous distribution of the clay nanoplatelets could be interpreted as intercalation. Further, the presence of a few silicate stacks could be deemed to be conventional microcomposites. Certainly, the presence of recalcitrant XRD reflections confirms the occurrence of intercalated or unmodified silicate regions. However, exfoliated regions may perhaps co-exist and even predominate. TEM is critical since it gives direct evidence of composite structures. However, it may also fall short when a few samples not representative of the whole material are viewed. The research work reviewed in this project is likely to have been subject to this dilemma.

Table A.1 and Table A.2 in the Appendix summarise, respectively, diverse EVA grades and organosilicates melt blended to prepare EVA composites. Table A.3 summarises the melt processing equipment used in the works reviewed, together with processing parameters.

2.4.1 Effect of processing equipment and conditions on the dispersion of EVA composites

A co-rotating twin-screw extruder is considered the most effective mixing device for the dispersion of silicate platelets. This is because the screws rotate in the same direction, intermesh and pass resin over and under one screw to another. The material is thus subjected to an identical amount of shear and is unlikely to become stagnant. Chaudary et al. (2005a), Chaudary et al. (2005b) and Pistor et al. (2010) reported similar EVA nanocomposite structures. Partial intercalation and exfoliation were the predominant characteristics reported in all these articles. Further, it was stated that all samples contained small tactoid fractions (Chaudary et al., 2005a; Chaudary et al., 2005b; Pistor et al., 2010). However, the processing equipment and conditions employed by these authors were different (Table A.4).

La Mantia & Tzankova Dintcheva (2006) prepared equivalent samples using two different extruders. They reported similar EVA nanocomposite structures comprising intercalated silicate domains, as detected by XRD. The d_{001} was slightly increased for samples compounded in a twin-screw extruder (La Mantia & Tzankova Dintcheva, 2006). Likewise, in the works done by Chaudary et al. (2005a), Chaudary et al. (2005b) and Pistor et al. (2010), the overall nanocomposite structures seemed independent of the processing equipment used. In addition, all the nanocomposite structures appeared to be insensitive to different processing temperatures and shear forces.

2.4.2 Effect of silicate type on the dispersion of EVA composites

The effect of silicate type on the dispersion of EVA composites was investigated (Zanetti et al., 2001; Riva et al., 2002; Costache et al., 2005; Peeterbroeck et al., 2005). EVA matrices were melt blended with hectorite, fluorohectorite, magadiite and montmorillonite (MMT), all organically modified. The dispersion of hectorite-type clays was found to be better than that of MMT clays. This may be attributed to the large interfacial area available for the interaction of polymer chains with hectorite-like minerals. The interactionof high surface area silicate with polymer chains yields excellent dispersion (Chaudhary et al., 2005a). Hectorite had an aspect ratio (a quotient of the length of the particle to its diameter) of approximately 5000, while MMT has a ratio of less than 1000. Magadiite did not yield nanocomposites, only microcomposites. However, a large aspect ratio may be disadvantageous since the sheets will

tend to agglomerate. In such cases, the formation of a well-dispersed phase in a polymer matrix is doubtful.

2.4.3 Effect of organic modification of silicates on the dispersion of EVA composites

Nanocomposite creation was found to depend on the type of silicate modification (Alexandre et al., 2001; Zanetti et al., 2001). Suitable silicate modification should render it compatible with the polymer matrix. Silicates modified with ammonium cations bearing carboxylic acid moiety yielded conventional microcomposites. They were independent of the vinyl acetate (VA) content of EVA matrices. In contrast, organosilicates with non-functionalised alkyl ammonium chains (one and two) displayed affinity towards EVA chains. They yielded nanocomposites whatever the VA content (12, 19, 27 mass %) of the matrix. Exfoliated silicate sheets were observed together with stacks of intercalated and unmodified silicates. The nanocomposite structures were considered intercalated/exfoliated (Alexandre and Dubois, 2000; Alexandre et al., 2001; Zanetti et al., 2001). Higher amounts of stacks were observed in EVA12 nanocomposites (Alexandre et al., 2001). These authors speculated that such a small extent of exfoliation was due to low polarity of the EVA12 matrix. Organosilicates with one long alkyl chain likewise yielded nanocomposites with relatively high numbers of stacks (Alexandre et al., 2001). Table A.5 presents the effect of organic modification of silicates on the dispersion of EVA composites.

The effect of different types of silicate modification on the characteristics and properties of EVA nanocomposites was further investigated. Riva et al. (2002) used MMT modified with $(CH_2CH_2OH)_2N^+CH_3$(tallow) and EVA19. The polarity of MMT was increased, further improving its affinity towards polar EVA matrices. Exfoliated structure was reported for a nanocomposite based on EVA19. In addition, stacks of unmodified silicates were observed (Riva et al., 2002).

Zhang et al. (2003) increased the number of long alkyl chains used to modify MMT up to three. They anticipated that such an increase would decrease the polarity of organo-MMT. Nevertheless, they found it necessary for yielding larger organo-MMT basal spacings. They aimed at a proper balance between the two as it would ease migration and penetration of EVA chains into the silicate layers. The morphological features of EVA-MMT nanocomposites were examined. They were found to depend on the basal spacing of the organically modified MMT and the polarity of the EVA. Increasing both promoted better

dispersions. The chains of EVA diffused more easily into the MMT layers. Two long alkyl chains were found to be sufficient to yield organosilicates with wider basal spacing (Zhang et al., 2003). These authors recorded further marginal expansion of d_{001} for organoclay with triple chains.

2.4.4 Effect of VA content on the dispersion of EVA composites

The effect of changing the matrix VA content on the dispersion of EVA composites was assessed by several authors (Alexandre et al., 2001; Zannetti et al., 2001; Cser & Bhattacharya, 2003; Jeon et al., 2003; Zhang et al., 2003; Pasanovic-Zujo et al., 2004; Zhang & Sundararaj, 2004; Chaudhary et al., 2005a; Chaudhary et al., 2005b; Costache et al., 2005; Prasad et al., 2006; Cui et al., 2007; Marini et al., 2009). Increasing the VA content, i.e. EVA polarity, lowers the thermodynamic energy barrier for polymer interaction with silicates. Therefore, polymer chains diffuse more easily in between the silicate layers (Zhang et al., 2003). Increased matrix amorphousness (with increasing VA units) further facilitates stabilisation of the polymer chains within the silicate galleries (Chaudhary et al., 2005a; Chaudhary et al., 2005b). The latter authors claimed that higher amorphous content prevents re-crystallisation of polymer chains during annealing, allowing the chains to remain diffused within the silicate layers (Chaudhary et al., 2005a; Chaudhary et al., 2005b).

Whatever the VA content, organosilicates with OH groups along the alkyl N substituents appeared well dispersed. This may be due to strong intermolecular interactions between the OH groups of the organic modifier and the ester functions of the EVA matrix (Peeterbroeck et al., 2005). Increasing the VA content improved the degree of organosilicate dispersion. This was independent of the type of silicate modification. When the number of long chains was the same, organosilicates with higher chain lengths dispersed better. This may be related to the interlayer spacing of the organosilicate. Densely packing modifier into the silicate did not aid dispersion. Chaudhary et al. (2005a) claimed that it reduces the number of EVA chains penetrating the interlayer spaces. Table A.6 presents the effect of VA content on the dispersion of EVA composites.

Zhang and Sundararaj (2004) investigated the extent of dispersion of some organosilicates comprising double chains in EVA matrices with five VA contents (6, 9, 12, 18 and 28 mass %). The organosilicate employed is coded OC_{25} in Table A.2. It was found that all EVA matrices further expanded the organoclay interlayer. Increasing the VA content from 6 to 12

mass % expanded the silicate interlayer considerably. Above such a VA content, no further interlayer expansion was recorded. An intercalation-limiting effect of the polarity after a certain critical VA content has been established (Zhang and Sundararaj, 2004). This critical VA content was found to approximate 15 mass % (Jeon et al., 2003). The degree of intercalation of EVA into organoclay with double chains increased only at VA contents up to about 15 mass %. Above such a critical VA content, expansion of the basal spacing ceased. The interlayer expansion was attributed to increased diffusion of EVA (Zhang et al., 2003). The diffusion of polymer depends strongly on how well it flows. The latter is determined by the melt flow index, MFI.

2.4.5 Effect of MFI on the dispersion of EVA composites

The propensity of EVA with higher VA content to diffuse into the silicate interlayers has been established (Zhang et al., 2003). Zhang and Sundararaj (2004) examined the influence of MFI on the structure of nanocomposites. They used five EVA28 matrices with different MFIs (3, 6, 25, 43 and 150 g/10min). The influence of MFI on the effect of EVA polarity on limiting intercalation into double-tailed organoclay has been investigated. Lowering the MFI from 150 to 25 did not cause any detectable change in the basal spacing. However, decreasing the MFI further to 6 expanded the silicate interlayer. Below this MFI, the silicate interlayer collapsed. It was therefore concluded that effective polymer diffusion requires a conjugation between its mobility and its shear force (Zhang and Sundararaj, 2004). The latter should: (i) create shear tensions during nanocomposite processing; (ii) aid the breaking up of organo-silicate agglomerations; (iii) disperse silicate platelets or a few tactoids throughout the matrix; and (iv) keep the silicate platelets or tactoids apart. However, polymer mobility should be enough to promote its diffusion and penetration into the silicate layers before layer re-stacking. Although the existence of an intercalation-limiting effect of EVA into double-tailed organoclay was confirmed, it seemed to be dependent on the MFI of the matrix rather than that of its VA content. This speculation is contrary to that of Jeon et al. (2003). These authors recorded increasing interlayer distances with increasing VA content from 3 to 15 mass %. No further expansion was recorded for organo-MMT intercalated by EVA22 with different MFIs (2 and 3 g/10 min). In turn, Zhang and Sundararaj (2004) recorded increasing interlayer spacing when the MFI of EVA28 was lowered from 25 to 6. Thus, it is speculated that EVA resins possessing good mobility and sufficient shear force will have MFIs in the range 3–25. Marini et al. (2009) agreed that matrix viscosity is the driving force for polymer chain mobility within clay lamellae. In addition, matrix viscosity was thought to be

responsible for imposed shear tension causing lamellae slippage and clay dispersion. It was confirmed that adequate affinity between the polymer matrix and the organosilicate was indispensable.

The effects of diverse material features, varied processing equipment and different conditions on the structures of created composites have been reviewed. Next, the influence of such composite structures on the mechanical, rheological, thermal and fire properties of organoclays will be reviewed.

2.4.6 Influence of composite structure on the mechanical properties

The mechanical properties of created composites have been evaluated through tensile testing (Table A.7). Typically, silicate particles have a higher modulus than polymer matrices. Combining them increases the initial resistance of the composite to an applied stress.With increasing concentration of nanofiller, there is an increase in Young's modulus (stiffness) of the nanocomposites. Alexandre et al. (2001), using 5 mass % MMT, prepared nanocomposites with double the Young's modulus of pure EVA27. In turn, EVA19 and EVA12 increased the Young's modulus by 50%. The variation in the modulus of nanocomposites was explained by the difference in the structures of the nanocomposites. The dispersion of individual clay platelets responsible for the large increase in modulus was higher in EVA27 nanocomposite (Alexandre et al., 2001).

Apart from polymer polarity, silicate modification with surfactants having non-functionalised chains compatible with polymer matrices is also critical. The ductility of EVA27 nanocomposite decreased only slightly compared with that of pure polymer. This was in spite of a large increase in the nanocomposite's stiffness. For microcomposites, neither EVA polarity nor filler concentration was efficient in increasing substantially the Young's modulus.

Zhang and Sundararaj (2004) recorded ever-increasing Young's moduli of EVA nanocomposites with increasing concentration of nanofiller. In parallel, they proposed the existence of a 'platelet saturation effect'. Such an effect reduces the extent of platelet dispersion in the polymer matrix. The saturation effect has been explained as follows: lLayered silicates have a large aspect ratio, exceeding 200. Interaction between them is quite strong because of the large packing area. Exfoliation and dispersion of the silicate layers

depend mainly on two factors: EVA-silicate interaction (ε_{es}) and silicate-silicate interaction (ε_{ss}).When $\varepsilon_{es} > \varepsilon_{ss}$, exfoliation of the silicate layers is possible. Conversely, when $\varepsilon_{es} < \varepsilon_{ss}$, exfoliation is impossible. An increase in clay content then leads to a larger ε_{ss}; this is due to a shorter distance between the silicate aggregates (Zhang and Sundararaj, 2004).

The effect of interplay between EVA polarity (amorphicity) and silicate concentration (mass %) on the Young's modulus has been evaluated. It has been accepted that platelet 'randomisation' characterises exfoliated nanocomposite structures. Typically, such effective dispersion of the nanosilicate suppresses the matrix's ability to absorb energy when the EVA matrix has a lower VA content (Chaudhary et al., 2005a). Nanosilicates increase spatial hindrance for polymeric chain movement. They impart rigidity to the polymer matrix, creating a 'rigid' amorphous phase. Platelet–polymer and platelet-platelet interactions tend to create a flexible silicate network structure in the matrix. Owing to polymer entanglement, this network increases the initial resistance of polymeric chains moving under stress. The initial deformation energy is then absorbed by the silicate network. Simultaneously, the flexible network increases the nanocomposite's modulus. With increasing VA content, the silicate network increases its flexibility. Consequently, the resistance of the polymeric chains to movement is lowered. A 'mobile' amorphous phase therefore develops, and the network's ability to absorb deformation energy decreases. This occurs in spite of platelet–polymer and platelet-platelet interactions in the flexible silicate network. Stress is then partially transferred to the polymer chains, allowing them to absorb higher deformation energy. Hence, the modulus appears to be dominated by the extent of matrix crystallinity/amorphousness rather than by the silicate network.

Rigidity may also be imparted without the formation of a silicate network structure. There needs to be good interaction between the silicate platelets (or clusters of tactoids) and the matrix in which they are dispersed and appropriately oriented. However, tensile strength is likely to be reduced (Zhang and Sundararaj, 2004). Favourable interactions at the polymer/silicate interface are critical for efficient stress transfer, but tensile strength does not increase when polymer–clay interactions are sufficiently developed. The tensile strength of the nanocomposite reduces with increasing flexibility of the silicate network structure. Increasing matrix polarity tends to maximise the extent of diffusion of EVA chains into the silicate layers. A higher specific surface area then becomes available for polymer-silicate

interactions (Chaudhary et al., 2005a). However, effective polymer diffusion leading to exfoliation requires a balance between the network's mobility and its shear force (Zhang and Sundararaj, 2004).

2.4.7 Influence of composite structure on its steady shear rheological properties

The degree of dispersion of silicates in a polymer matrix affects the rheological behaviour of nanocomposites. Measurement of complex viscosity by an oscillatory test is useful to estimate the degree of exfoliation of composites. The viscosity of highly dispersed nanocomposites, with exfoliated structure, increases extensively when the shear rate changes. In turn, the viscosity of poor dispersions increases moderately with shear rate. At a low shear rate, exfoliated nanocomposites have a propensity to display solid-like behaviour. This has been attributed to the formation of a network structure by the dispersed silicate layers (Gupta et al., 2005). Polymer chains are trapped within the network and because there are unable to flow, viscosity increases. High zero-shear viscosities indicate that the network of dispersed layers remains unaffected by the imposed flow. Interactions between silicate layers and polymer chains are more pronounced in exfoliated systems than in fully intercalated ones. At the same silicate concentration, the elasticity (Young's) modulus is higher for exfoliated structures than for intercalated ones (Riva et al., 2002). Hence, solid-like behavior occurs at higher silicate loading in later systems. This leads to slower relaxation of the polymer chains (Gupta et al., 2005). The influence of composite structure on its steady shear rheological properties is presented in Table A.8.

High shear rates breakdown the silicate network and orient the platelets in the direction of flow. Therefore, nanocomposites exhibit shear thinning behaviour. The slope of the curves, the so-called 'shear thinning exponent' is used to estimate the extent of nanocomposite exfoliation. It has been accepted that higher absolute values of the exponent indicate a higher rate of exfoliation (Gupta et al., 2005; Szép et al., 2006). Marini et al. (2009) suggested that a significant increase in viscosity in the low shear region indicates strong matrix-organosilicate interactions. Both well-dispersed intercalated and/or exfoliated silicates can lead to a large increase in zero-shear viscosity (Marini et al., 2009).

La Mantia & Tzankova Dintcheva (2006) stated that matrix-organosilicate interactions increase in intensity with silicate interlayer spacing. When basal spacing increases, the surface area available for contact with polymeric chains also increases. Moreover, due to the

larger interplatelet distances, the volume concentration of the silicate increases (La Mantia & Tzankova Dintcheva, 2006). High interactions between the organosilicate and the polymer chains are critical for nanocomposite creation. However, they are not sufficient to guarantee effective clay dispersion and exfoliation (Zang and Sundararaj, 2004; Marini et al., 2009). Effective polymer diffusion requires balancing the mobility of the chain with its shear force (Zhang and Sundararaj, 2004).

Strong matrix-organosilicate interactions are indicated by a significant increase in zero-shear viscosity rather than simply by a high zero-shear viscosity. Marini et al. (2009) recorded huge rheological differences between various EVA nanocomposites, depending on the viscosity of the matrices. High-viscosity EVA12 (MFI = 0.3 g/10 min) and EVA19 (MFI = 2.1 g/10 min) consisted of fairly well-dispersed compact tactoids and had higher zero-shear viscosity than the respective EVA matrices. However, such viscosities were of the same order of magnitude or only differed by one order of magnitude. Further, pure matrices also displayed pseudoplastic behaviour. Absolute values of the shear thinning exponent calculated for EVA12 nanocomposite and its matrix were high. Similarly, nanocomposites produced with low viscosity, EVA18 (MFI = 150 g/10 min) and EVA28 (MFI = 25 g/10 min), exhibited higher zero-shear viscosity than the respective EVA matrices. However, such viscosities differed by more than one order of magnitude. Pure matrices also exhibited Newtonian behaviour. It was then concluded that organosilicate dispersion was dependent on the polarity and viscosity of the EVA matrix (Marini et al., 2009). Therefore, on its own, a high shear thinning exponent does not guarantee a higher rate of exfoliation. Likewise, a high zero-shear viscosity, on its own, does not guarantee strong matrix-organosilicate interactions.

2.4.8 Influence of composite structure on its thermal properties

EVA decomposes in two consecutive steps, regardless of whether there is an oxidative or an inert atmosphere. In air or oxygen, the first step occurs between 300 and 400°C and is attributed to the release of acetic acid. The acid splits off, forming an unsaturated or cross-linked backbone. The second step involves thermal dissociation and combustion of the resulting double bonds or cross-links (Beyer, 2002; Szép et al., 2006). Organoclays are well known for delaying polymer degradation. In fact, EVA nanocomposites exhibit a large increase in thermal stability under an oxidative environment. The maximum of the second degradation peak shifts to higher temperatures. The neat EVA is completely burnt without any residue. Therefore, increased stability of the nanocomposite is attributed to the

residue/char, which is yielded only under oxidative conditions (Beyer, 2002). Acetyl elimination in nanocomposites starts at a lower temperature compared with the virgin EVA. However, the rate of mass loss decreases significantly. This is considered to be due to the formation of a char barrier layer. Thus, both decomposition steps of the nanocomposites are affected by the clay platelets (Szép et al., 2006). Table A.9 presents the influence of the structure of composites on their thermal properties.

CHAPTER 3 EXPERIMENTAL

3.1 Materials

3.1.1 Clay samples

The bentonites used in this investigation were from the Boane deposit in Mozambique and from the Koppies mine in South Africa. G & W Base and Industrial Minerals supplied samples of the crude bentonites in milled powder form and in purified form as sodium-activated dispersions. The cation exchange capacities (CEC) of the purified bentonites were determined by the supplier using the methylene blue method (Hang and Brindley, 1970). The respective values were 70 and 85 meq/100 g dry clay for Boane bentonite and Koppies bentonite.

Bentonite dispersions were prepared as follows: 40 mass % crude Koppies or Boane clay was suspended in distilled water in a mixing tank. Soda ash, 4-5 mass %, was added to activate the bentonite in order to increase the swelling ability. The slurry was then passed through an industrial-sized centrifuge that removed most of the silica particles impurity. After this, 1-1.5 mass % proprietary dispersant was added and the slurry was thoroughly homogenised. The individual characteristics of the slurries were as follows.

Koppies slurry (KS)

The slurry of South African Koppies clay had a light brown colour. The colour was attributed to the presence of relatively high iron content. The chemical composition of the Koppies bentonite powder and related samples, as determined by XRF, is presented in Table 1 in Chapter 4. The solids content of KS was determined as 18.9% by the mass remaining in a thermogravimetric analysis at 150 °C (Figure 1). The pH of KS was 9.9.

Boane slurry (BS)

The Mozambican bentonite slurry (BS) exhibited an off-white colour. The iron and titanium content of the crude clay from Mozambique was considerably lower than that of the South African Koppies powdered sample (Table 1 in Chapter 4). The solids content of BS was determined as 19.2% by the mass remaining in a thermogravimetric analysis at 150 °C (Figure 2). The pH of BS was 7.4.

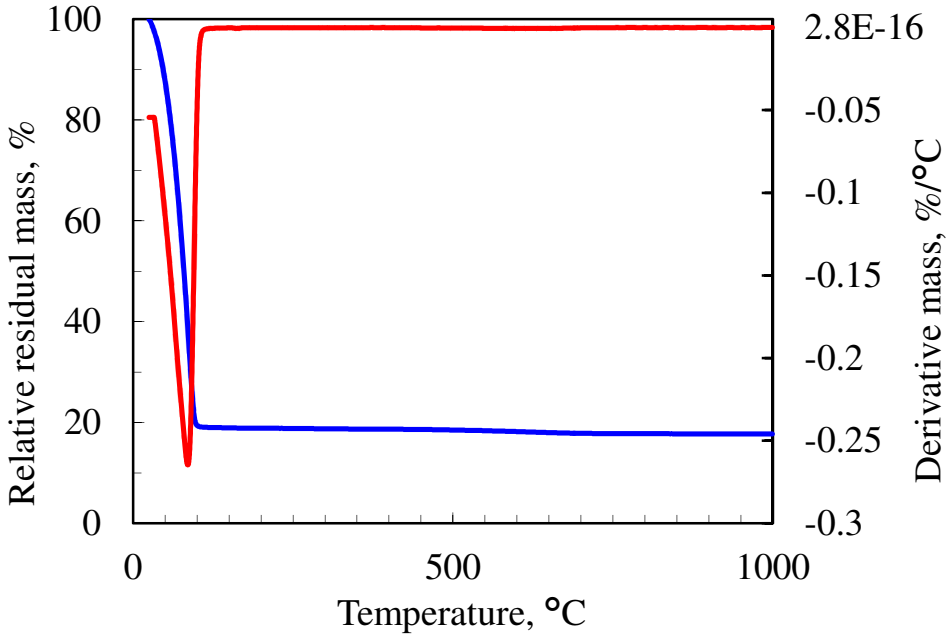

Figure 1. TG and DTG curves of South African Koppies slurry (KS)

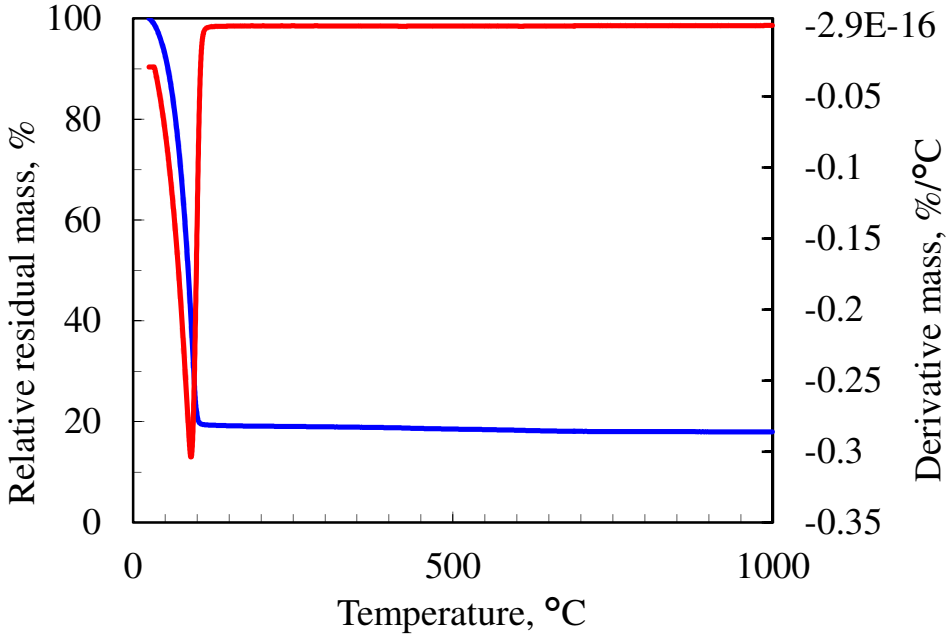

Figure 2. TG and DTG curves of Boane slurry (BS) from Mozambique

3.1.2 Intercalating agents

Quaternary ammonium surfactants (quats) with single and double alkyl chains were utilised as supplied. The following commercial quats were used.

Noramium M2SH-1 (DC18)

Noramium M2SH-1 is a double-chain surfactant manufactured by CECA (Arkema Group) and supplied by Akhulu Marchon. Chemically, it is N,N' di-hydrogenated tallow dimethyl ammonium chloride. The chain distribution is as follows: 64% C18 (saturated), 35% C16 (saturated) and 1% C18 (double bond). The composition is given in mass percent. The average molar mass of DC18 is approximately 529 g/mol. The surfactant was supplied as a 76% by mass solution in a water-isopropanol mixture.

Varisoft 432 CG (DC16)

Varisoft 432 CG is a product of Degussa (Goldschmidt GmbH). It is a double-chain quaternary ammonium ion with the chain lengths varying from 12 to 18 carbons. It contains mostly N,N'-dihexadecyl dimethyl ammonium chloride. The molar mass of the surfactant was estimated at 529.5 g/mol. DC16 surfactant is supplied as a 68% by mass solution in a water-isopropanol mixture.

Noramium M21080 (DC10)

Noramium M21080 is a product of CECA (Arkema Group), supplied by Akhulu Marchon. It contains the pure double-chain surfactant N,N' didecyl dimethyl ammonium chloride. The molar mass is 354 g/mol. DC10 is supplied as an 81% by mass solution of the surfactant in a water-isopropanol mixture.

CTAB (SC16)

Cetyl trimethyl ammonium bromide is a single-chain quat supplied by FEF Chemicals. Chemically, it consists of pure hexadecyl trimethyl ammonium bromide. The molar mass is 364 g/mol. SC16 is a white crystalline powder that melts at 230 ^{o}C. The solubility in water at 25 °C is 15 g/L.

Cetrimide BP (SC14)

Cetrimide BP (Purum grade, from FeF Chemicals A/S, Copenhagen) is essentially tetradecyl trimethyl ammonium bromide. SC14 is a white powder at ambient temperature. The molar mass is ca. 336 g/mol. It decomposes when heated to 245-250 ^{o}C. It is soluble in water and lower alcohols such as propanol.

Empigen HBC40 (SC12)

Empigen HBC40 is a trade name of lauryl dimethyl hydroxyethyl ammonium chloride (dodecyl[2-(2-hydroxyethoxy)ethyl]dimethyl ammonium chloride), from Huntsman Surface Sciences UK), supplied in its 40% aqueous solution. The molar mass of SC12 is at 293.5 g/mol.

3.1.3 Polymer matrix

EVA resin grade EV101 with 18 mass % vinyl acetate was supplied by APC (MFI 1.8 g/10 min at 190 °C/2.16 kg; density 0.941 g/cm^3). The polymer was milled into a fine powder using a Pallmann 300 Series pulveriser.

3.2 Methods

3.2.1 Organic intercalation of bentonite slurries

The CEC of the South African Koppies bentonite, 85 meq/100 g of dry clay, and that of Boane bentonite, from Mozambique, 70 meq/100 g of dry clay, were used to calculate the amount of each intercalating agent for the intercalation experiments (Appendix A.1).

The organoclays synthesised for this study were coded SCXX or DCXX. SC and DC indicate single and double chains respectively. XX represents the number of carbon atoms in each alkyl chain. A prefix of either K or B was introduced in each name, standing for Koppies and Boane respectively.

In the calculations of the amount of each intercalating agent required to synthesise the organoclays (Appendix A.1), it was assumed that surfactant DC16 (Varisoft 432 CG) comprised pure N,N'-dihexadecyl dimethylammonium chloride. For DC18 (Noramium®M2SH-1), with a mixture of chain lengths, the average molar mass was calculated. Some intercalation experiments were performed using a 50% excess of the

surfactants based on the estimated bentonite CEC. For the preparation of M-SC14, an excess of 80% surfactant was used.

Intercalation procedure

A typical intercalation experiment was performed as follows: the soda ash-activated bentonite dispersion (KS or BS) was placed in a planetary mixer. The surfactant solution or powder was added while mixing. Mixing was continued intermittently for about 5 h. The mixture was vigorously stirred for 3 min. During the initial 20 s, a dramatic decrease in the viscosity of Koppies slurry was noticed. After this period, the viscosity of the slurry increased again. It was speculated that the decrease in the slurry viscosity under the influence of high shear was due to the breakdown of the network of clay platelets and its subsequent alignment in the direction of flow.

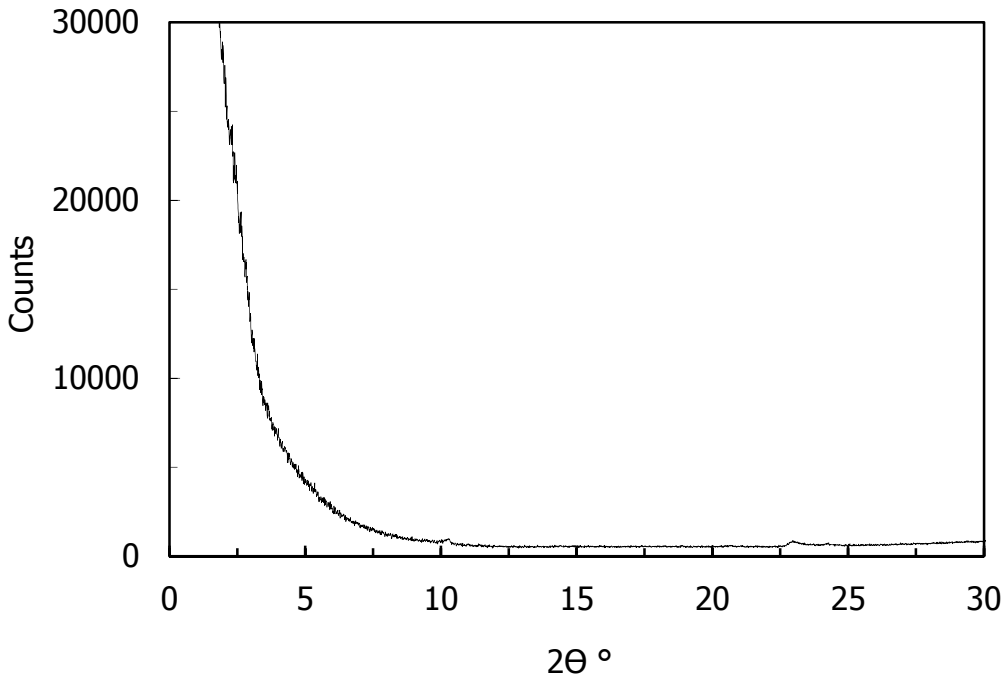

Figure 3. XRD pattern of South African Koppies slurry (KS)

To explain how the clay platelet network yielded an exfoliated (Figure 3) gel-like structure, van Olphen (1964) proposed that the flat face surface and the edge surface of plate-like clay crystallites expose two crystallographically different surfaces. The face surface has an interior net negative charge due to isomorphic substitutions. The charge is compensated by positive counter-ions adsorbed on the surface. On the other hand, disruption of the crystallites at the

edges exposes a broken bond surface (van Olphen, 1964). According to this author, indications are that the edges are negative under alkaline conditions, such as at the pH 9.9 of KS. The van der Waals attraction between edges or between edges and faces, or both, yields an exfoliated clay platelet network in water, with a gel-like structure.

Under the influence of high shear the network of clay platelets breaks down. Consequently, the viscosity of the slurry decreases due to the alignment of the platelets in the direction of flow. Utracki (2004) stated that as soon as the exchange reaction between the interlayer cations occurs and organic intercalant starts to enter the clay interlayer, platelet interactions cause the slurry viscosity to increase again.

After 3 min of stirring the surfactant into the bentonite slurry at high shear, the mixture was allowed to stand for 30 min. It was then stirred again, but for only 1 min, and allowed to stand again for 30 min. This procedure was repeated nine times to allow time for complete cation exchange. Next, the paste mixture was suspended in four parts of distilled water and allowed to stand overnight. Settling of the organophilic product was observed the following morning. The hydrophilic supernatant was decanted, and the organophilic product was re-dispersed in four parts of distilled water to remove halide salts and the excess of intercalant. The suspension was then centrifuged at 4000 rpm for 30 min. The presence of halides (chloride and/or bromide) was monitored by repeated product washing with distilled water, centrifugation and testing of the decanted supernatant with 1M $AgNO_3$. The aim of this successive washing procedure was to eliminate alkaline halide (the secondary product of the cationic exchange) and the excess of surfactant used. When no more precipitation of supernatant by solution $AgNO_3$ was observed, the halide-free product was filtered in a Buchner funnel under vacuum suction. Grade 2V Whatman folded filter paper was stretched and used to recover the product. The product was air-dried for a minimum of 2 days. It was further crushed and ground with a pestle and mortar, and thereafter its structural properties were analysed.

3.2.2 Compounding and injection moulding

Powdered organoclay plus EVA masterbatches were prepared as follows: EVA powder was mixed with organoclay powder in the mass ratio 4:1 and then compounded on a 28 mm co-rotating intermeshing twin-screw laboratory extruder (L/D = 16). The screw design comprised intermeshing kneader elements with a forward transport action. The barrel

temperature profile ranged from 170 to 180 °C and the screw speed was set at 168 rpm. The extruded masterbatch strand was dried, granulated and then pulverised. This powder was let down in virgin resin to set the required final clay content (targeted loading levels up to 6.5 mass % inorganic basis). EVA-organoclay composites were compounded twice at the same conditions in order to delaminate them and ensure a good dispersion of clay platelets. After compounding, the extruded strands were granulated and dried. Test bars, conforming to ASTM D638, were injection moulded on an Engel 3040 injection-moulding machine. Barrel temperatures varied from 170 to 180 °C for all samples. The injection and holding pressures were 180 and 80 bar respectively. The injection speed was 6 mm/s, the stroke was 22 mm and the clamping force was 350 kN.

3.2.2 Characterisation

Samples were characterised before and after organic treatment, as well as after compounding. Various instrument techniques were used to analyse the structural properties and to characterise the eventual sample transformations.

X-ray fluorescence (XRF)

The elemental composition was determined by X-ray fluorescence (XRF) spectroscopy. XRF spectrometer (ARL 9400 XP + XRF) wavelength dispersive was used. Ethyl cellulose was used to bind the powdered samples and produce pellets. The intercalated materials were ashed before analysis in order to reduce their bulk. The samples were ground to < 75 µm in a tungsten carbide mill and roasted at 1000 °C. Then 1 g sample was added to 9 g of $Li_2B_4O_7$ and fused into a glassed bead. Major element analysis was executed on the fused bead using an ARL9400XP+ spectrometer.

Thermogravimetric analysis/differential thermal analysis (TGA/DTA)

Thermal analysis was performed using the dynamic method on a Mettler Toledo A851 TGA/SDTA instrument. About 17 mg of powder was placed in open 70 µL alumina pans. Temperature was scanned from 25 to 1000 °C at a rate of 10 °C/min with air flowing at a rate of 50 mL/min.

Fourier transform infrared (FTIR) spectroscopy

FTIR spectra were recorded on a Perkin Elmer RX I FT-IR spectrometer. Approximately 2 mg of dry sample was combined with 100 mg of spectroscopic-grade KBr and ground into a fine powder. The mixture was pressed into a 13 mm ϕ die pellet. The reported spectra represent averages of 32 scans at a resolution of 2 cm^{-1}. The averaged data were background-corrected using a pure KBr pellet.

X-ray diffraction (XRD)

Mineral identification and composition assessment of pristine bentonite was performed by the South African Council for Geoscience. The XRD instrument used was a Bruker D8 Advance diffractometer using Cu Kα radiation (λ = 0.15406 nm). The system featured a Johansson crystal primary monochromator and LynxEye detector with 3.7° active area. XRD patterns were recorded for random powder preparations. The mineral identification was based on a Bruker Diffrac^{Plus} – EVA evaluation program. The phase concentrations were determined by Rietveld quantitative analysis with Diffrac^{Plus} – TOPAS software to an accuracy of ± 1%.

The basal spacings of all samples were determined in-house. XRD analysis of random powder samples of the organobentonites was performed on a PANalytical X-pert Pro machine. The instrument featured variable divergence and receiving slits and an X'celerator detector using Fe-filtered Co Kα radiation (λ=0.17901 nm). X'Pert High Score Plus software was used for data reduction.

Electron microscopy (SEM and TEM)

The surface morphology of the organoclays was examined by low-resolution scanning electron microscopy (SEM) using a JEOL 840 instrument. The powder samples were coated five times with gold using a SEM Polaron E5200. A SEM fitted with an energy dispersive X-ray analyser (SEM/EDS) was used to examine the morphological and mineralogical association of montmorillonite and cristobalite in Mozambican bentonite. A Leica Stereoscan 440 instrument linked to an Oxford INCA EDS with Oxford SDD detector was used. Polished stubs of the samples were prepared and coated with carbon for conductivity using an EMITECH K950X sputter coater. In addition, an Oberkochen Zeiss Ultra Plus microscope was used for field emission scanning electron microscopy (FESEM).

For transmission electron microscopy (TEM), EVA and its clay composite samples were cryo-sectioned with a diamond knife at a temperature below -110 °C on a Lecia-Riechert Ultracut R instrument with an EMFCS cryo attachment. The nominal sectioning thickness was 90 ± 10 nm. Each sample was mounted on a 300 mesh copper/palladium grid and viewed on a JEOL 2100F TEM using an acceleration voltage of 200 kV.

Rheometry

The rheological properties of neat EVA and its composites were determined in oscillatory mode at 170 ºC. An Advanced Rheometer AR 2000 (TA Instruments) was used, using a cone-and-plate measuring system. The diameter of the plate was 25 mm, the gap was set at 54 µm and the strain amplitude was set at 1%.

Tensile and impact testing

A Lloyds Instruments LRX machine was used for tensile testing (ASTM D638-M) of EVA and its clay composites at a cross-head speed of 50 mm/min. The tensile impact tests were done on a Zwick Impact Tester.

Dynamic mechanical analysis (DMA)

The viscoelastic behaviour was studied on an Eplexor 500 N Qualimeter dynamic mechanical analyser (DMA) from Gabo. The storage modulus (E'), loss modulus (E") and tan δ were determined as a function of temperature at a frequency of 1 Hz in tensile mode. The static load was 2.5 MPa with 2% maximum strain or 1.75 MPa with a maximum strain of 0.6%. The samples were heated from -60 °C to 60 °C at a scan rate of 1 °C/min.

CHAPTER 4 RESULTS AND DISCUSSION

4.1 Characteristics of natural and modified bentonites

4.1.1 Chemical and mineralogical composition

Table 1: Inorganic chemical composition (dry basis expressed as mass %) of bentonite samples before and after organic treatment

	SiO_2	Al_2O_3	Fe_2O_3	MgO	Na_2O	CaO	K_2O	P_2O_5	TiO_2	MnO
KP	64.66	20.03	5.73	4.29	0.37	2.90	1.34	0.17	0.37	0.15
KSC14	63.14	21.99	7.28	4.36	0.07	0.97	0.90	0.86	0.36	0.07
KSC16	64.27	21.67	6.14	4.31	0.08	1.48	0.89	0.76	0.35	0.06
KDC16	64.99	21.42	6.13	4.33	0.14	0.82	0.86	0.92	0.33	0.06
KDC18	65.32	21.40	5.98	4.25	0.08	0.87	0.89	0.83	0.33	0.06
BP	80.16	13.16	2.70	2.66	0.85	0.14	0.08	0.00	0.22	0.03
BSC14	82.77	12.66	2.49	1.75	0.03	0.00	0.05	0.01	0.22	0.01
BSC16	82.44	12.81	2.60	1.78	0.04	0.00	0.06	0.02	0.23	0.01
BDC10	82.42	12.73	2.52	1.76	0.20	0.00	0.12	0.01	0.22	0.01
BDC16	84.27	10.96	2.76	1.45	0.02	0.11	0.07	0.02	0.33	0.02
BDC18	80.87	13.13	2.79	1.88	0.97	0.12	0.03	0.00	0.19	0.01

Table 1 presents the chemical composition of the Koppies and Boane bentonite powders, as well as the ash from their organically treated samples, as determined by X-ray fluorescence (XRF). Boane bentonite has higher silica content than Koppies bentonite. This is attributed to the cristobalite present as a major impurity in Boane bentonite. The XRF results correlate with those of CEC provided by the supplier of the bentonites: Koppies (85 meq/100 g of dry clay) and Boane (70 meq/100 g of dry clay).

Cristobalite is a silica polymorph that in geological times appears as an intermediate in the process of transformation of amorphous silica (glass) to quartz (Velde, 1985). A high cristobalite content degrades the quality of bentonite and limits its utilisation. Rietveld quantitative analysis of the XRD data indicated that the crude Boane bentonite contained 60.3 mass % montmorillonite, 35.7

mass % cristobalite and 4.0 mass % quartz. Rietveld quantitative analysis of the XRD data of the crude Koppies bentonite indicated the following composition, in mass %: 38.9 montmorillonite, 26.7 quartz, 11.1 plagioclase, kaolinite and K-feldspar 10.4 each, 1.5 mica and about 1 calcite.

The montmorillonite phase was identified by the d_{001} around 1.50 nm, coupled with d_{060} = 0.15 nm and the Greene-Kelly test. The test consisted of Li-saturation, glycolation and heating to 300 ºC. After this treatment, the basal spacing collapsed to 0.96 nm, indicating montmorillonite (Greene-Kelly, 1955). Upon ethylene glycol saturation for 24 h, the d_{001} expanded to 1.72 nm and collapsed to 1.03 nm after heating for 1 h at 550 ºC (Brown and Brindley, 1980). Reflections characteristic of α-cristobalite were the following: d_{101} = 0.40 nm, d_{102} = 0.28 nm, d_{200} = 0.25 nm, d_{301} = 0.16 nm and d_{302} = 0.15 nm (Guven and Grim, 1972).

The chemical composition data (Table 1) showed a substantial reduction in the Na and Ca content following organic modification. This provided evidence for the successful intercalation of the organic cations, i.e. organic cations replaced the Na^+ and Ca^{2+} in the pristine bentonites by ion exchange.

4.1.2 Morphological appearance of the samples

The low-resolution SEM micrographs revealed flake-shaped particles (Figure A.1 in the Appendix). The aggregates of the crude bentonites appeared significantly larger than those of the organically modified samples. Figure 4 shows SEM/EDX images of pristine bentonite from Boane and of the organically modified sample, both embedded in an epoxy resin.

The SEM backscattered electron (BSE) images (Figure 4) highlighted some distinct differences between the crude Boane bentonite and its organic derivates. Typically, montmorillonite (smectite) and cristobalite (Si-oxide) appear as irregularly shaped aggregates, with a more or less distinguishable structure. The clay-cristobalite aggregations in the organically modified materials show interesting structures that have been affected to various extents by the modification. Lumps of finely mixed clay enclose tightly compacted aggregates of submicron-sized Si-oxide particles. These aggregates have a semi-rounded shape and appear in various sizes and clay-cristobalite proportions.

A B

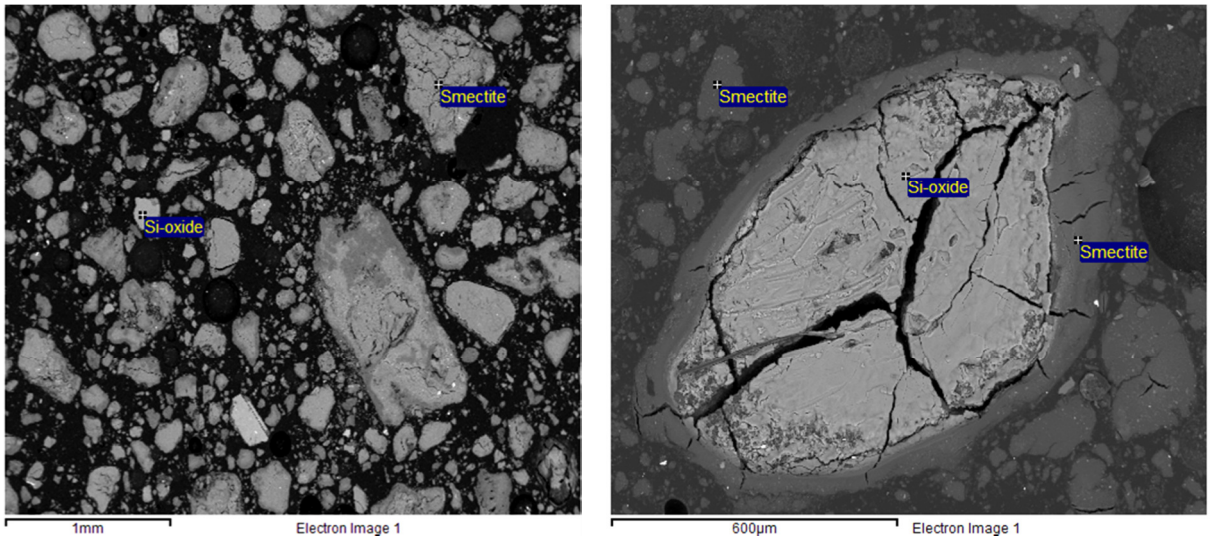

Figure 4. SEM/EDX backscattered electron images of crude clay BP [A] and organically modified clay based on BDC16 [B]

Incipient rigid cracks run through and around the aggregates and extend into the matrix. The cracking appears to be more pronounced within the cristobalite part of the aggregation, suggesting that it comprises a large agglomerate of much finer particles rather than a single large particle. This conjecture was confirmed by the FESEM images shown in Figure 5.

A B

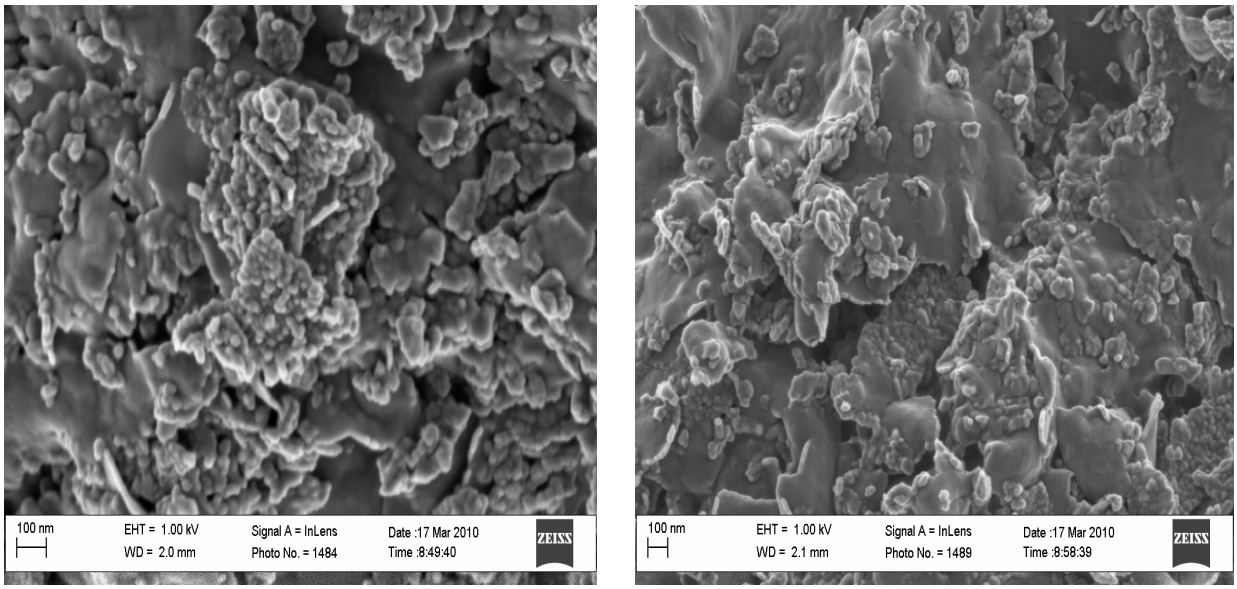

Figure 5. FESEM micrographs of untreated crude clay BP [A] and organically modified clay BSC14 [B]

Figure 5 shows the presence of rounded nano-sized particles on the surfaces of the clay mineral particles and also in aggregated form. Most of these particles were much smaller than 100 nm in size. The large aggregate shown in Figure 4 was attributed to the surface energy mismatch between the uncoated silica nanoparticles and the surfactant-coated bentonite flakes.

4.1.3 State of the intercalated alkylammonium ions

Organic cations introduced up to the CEC level by ion exchange (Lagaly, 1986) are electrostatically 'attached' to the clay mineral surfaces. The excess surfactant molecules are intercalated in their neutral salt form, i.e. together with their (hydrated) counter-ions (Klapyta et al., 2001; Lagaly, 1986). The incorporation of excess surfactant is driven by van der Waals interactions. Dense close-packing of the surfactants in the interlayer space improves the van der Waals interactions between long alkyl chains (Pan et al., 1997; Tahani et al., 1999; Yui et al., 2002; Janek and Lagaly, 2003; Kwolek et al., 2003; Calderon et al., 2008). Denser packing also requires better charge shielding of the same-charge surfactant head groups. Close-packing of long-chain surfactants can be facilitated by single-layer interdigitated intercalation, i.e. where the organic molecules are placed in such a way that the polar heads face opposite directions in order to minimise electrostatic repulsion between these head groups.

The state of the intercalated alkylammonium ions is derived by considering the basal spacing of the clay layers and the size and the shape of the guest molecule. The derived model compares the observed basal spacing and that calculated on the basis of the size and assumed shape of the guest alkylammonium. The model is accepted when good agreement between observed and calculated basal spacing is reached.

The physical arrangements of the alkyl chains of intercalated quaternary ammonium species (quats) have been the subject of intense debate (Lagaly, 1976; Lagaly, 1986; Vaia et al., 1994). At high surfactant loadings, two limiting cases are envisioned. One presumes that the chains are present as tilted, extended-chain paraffin-like arrangements. The alternative presumes disordered chain conformations containing numerous gauche conformers (Lagaly, 1976). These two different arrangements, although indistinguishable by XRD, nevertheless constitute very different molecular environments and interlayer structures (Vaia et al., 1994).

The d-spacing values observed for the present organobentonites are consistent with both options (Table 2).

Table 2. XRD basal spacings and FTIR CH_2 frequencies of bentonite samples

Sample	XRD *d*-spacing (Nm)	Chain tilt angle[1] °	FTIR $\nu_{as}(CH_2)$ (cm^{-1})	FTIR $\delta(CH_2)$ (cm^{-1})
BP	1.50	-	-	-
BSC12	1.82	25	-	-
BSC14	2.00	27	2920	1470
BSC16	3.81	32	2918	1470
BDC10	2.57	21	2924	1468
BDC16	3.89	33	2920	1469
BDC18	3.92	29	2918	1469
KP	1.52	-	-	-
KSC12	1.92	29	-	-
KSC14	1.84	22	2924	1476
KDC10	2.66	23	2925	1469
KDC16	3.82	32	2923	1468
KDC18	3.88	29	2918	1469

[1]Estimated from Equation (2) or Equation (3)

When the alkyl groups of intercalated surfactants adopt paraffin-like extended-chain conformations, they tilt at an angle α with respect to the plane of the clay mineral layers to yield a space-filled packing (Lagaly and Weiss, 1970a; Lagaly and Weiss, 1970b; Lagaly, 1986; He et al., 2006). The expected basal spacings for interdigitated monolayer intercalation and bilayer intercalation are given by the following approximate expressions (Lagaly and Weiss, 1970b; Kopka et al., 1998):

Monolayer: $$d_L = 1.18 + 0.127\, n_C \sin\alpha \quad (2)$$

Bilayer: $$d_L = 1.66 + 0.254\, n_C \sin\alpha \quad (3)$$

where:

d_L is the basal spacing

n_C is the number of carbon atoms in the alkyl chain

α is the tilt angle.

The values indicated for the constants in these equations are only approximate. They take into account the following contributions (Lagaly and Weiss, 1970a; Lagaly and Weiss, 1970b): the thickness of the bentonite layer (0.66 nm); the van der Waals radius of surface oxygen atoms (0.14 nm); the van der Waals radius of a methyl group (0.20 nm); the distance between a terminal methyl group and an oxygen atom (0.12 nm); the projected length of the C–N bond (0.12 nm); a correction accounting for the fact that methyl groups can actually penetrate the six-member oxygen rings of the silicate sheets (maximum depth 0.13 nm); and, finally, the gap between the terminal methyl groups for the case of bilayer intercalation (0.20 nm). These values yield separation distances of $xCH_3\cdots O \approx 0.12$ nm and $xN–CH_3\cdots O \approx 0.40$ nm.

The increased van der Waals energy between longer alkyl chains forces them into paraffin-type arrangements. Typically, alkylammonium chains are considered long at above eight carbon atoms. The strong interaction between long chains can shift the polar head groups out of their positions, for optimal hydrogen bond formation. Therefore, and in order that the volume accessible to the adsorptive surface will increase strongly, alkylammonium ions move from flat to perpendicular orientations (Utracki, 2004).

The powder XRD patterns for Boane crude and its organically modified derivatives are presented in Figure 6, while those for Koppies crude and its derivatives are shown in Figure 7. The measured basal spacings are presented in Table 2. The values obtained for single-chain surfactant-intercalated bentonites are consistent with a monolayer configuration. In turn, the basal spacings of the double-chain surfactant-intercalated bentonites are consistent with a bilayer configuration. The angle α at which the respective alkyl chains tilted with respect to the plane of the clay mineral layers is also presented in Table 2. The tilt angles were estimated from the measured basal spacing values using Equation (2) or Equation (3). The present angles are equivalent to about half the reported value of ca. 59 ° for typical paraffin-type conformations. This suggests that the chains adopted disordered conformations with numerous gauche conformers (Lagaly, 1986).

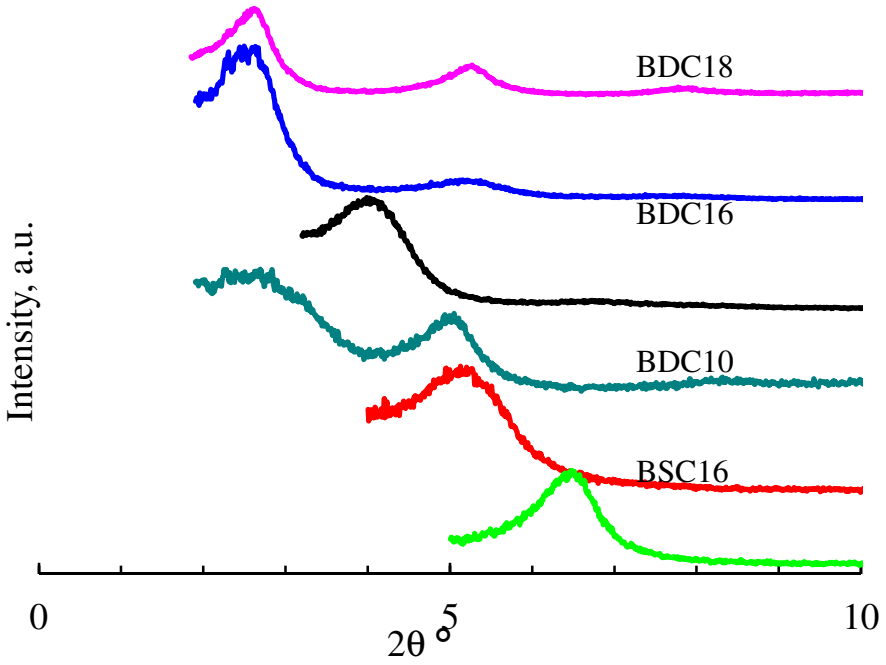

Figure 6. Powder XRD patterns for Boane crude and its organically modified derivatives

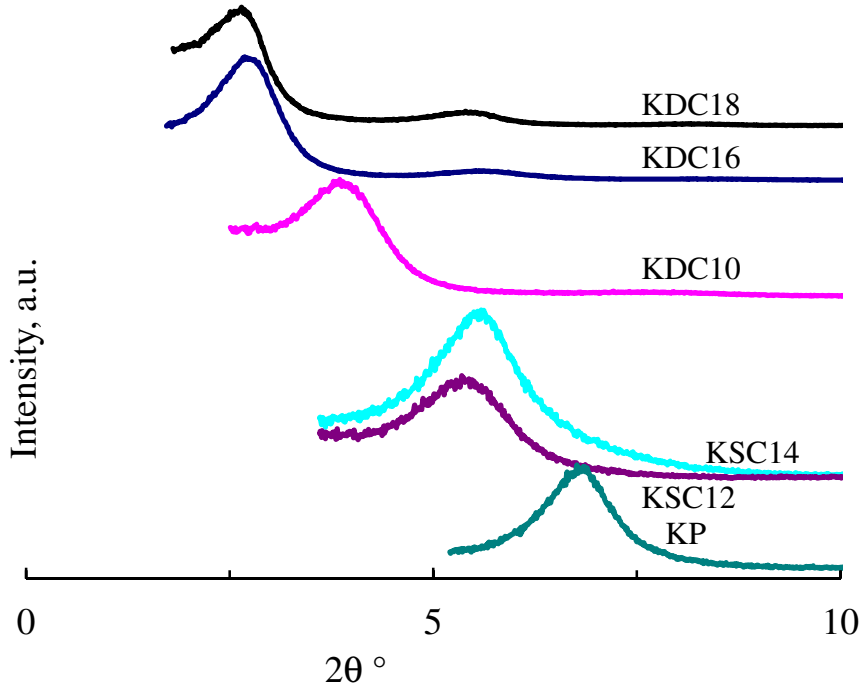

Figure 7. Powder XRD patterns for Koppies crude and its organically modified derivatives

The FTIR spectra for Koppies bentonite and its organoderivatives are shown in Figure 8 and those for the Boane counterparts are presented in Figure 9. Significant changes in the spectral profile of the organically modified samples can be observed. A more complex spectrum is observed for the organically treated samples than for the untreated samples. The spectra of the treated samples feature two strong bands in the wavenumber range 3000-2800 cm^{-1} (sharp bands at approximately 2920 and 2850 cm^{-1}), one additional band at 1470 cm^{-1} and another at 720 cm^{-1}. Altogether, these absorptions are indicative of the presence of a hydrocarbon with a long linear aliphatic chain. The strong band at about 2920 cm^{-1} may be assigned to $\nu_{as}(CH_2)$ stretching and that at 2850 cm^{-1} may be attributed to $\nu_s(CH_2)$ stretching. In turn, the band at 1470 cm^{-1} may be attributed to $\nu_{as}(CH_2)$ bending and that at 720 cm^{-1} may be assigned to $\nu_s(CH_2)$ bending. The presence of a weak band at approximately 1360 cm^{-1}, which is assigned to $\nu_s(CH_3)$ bending, corroborates the spectral data for the long linear aliphatic chain.

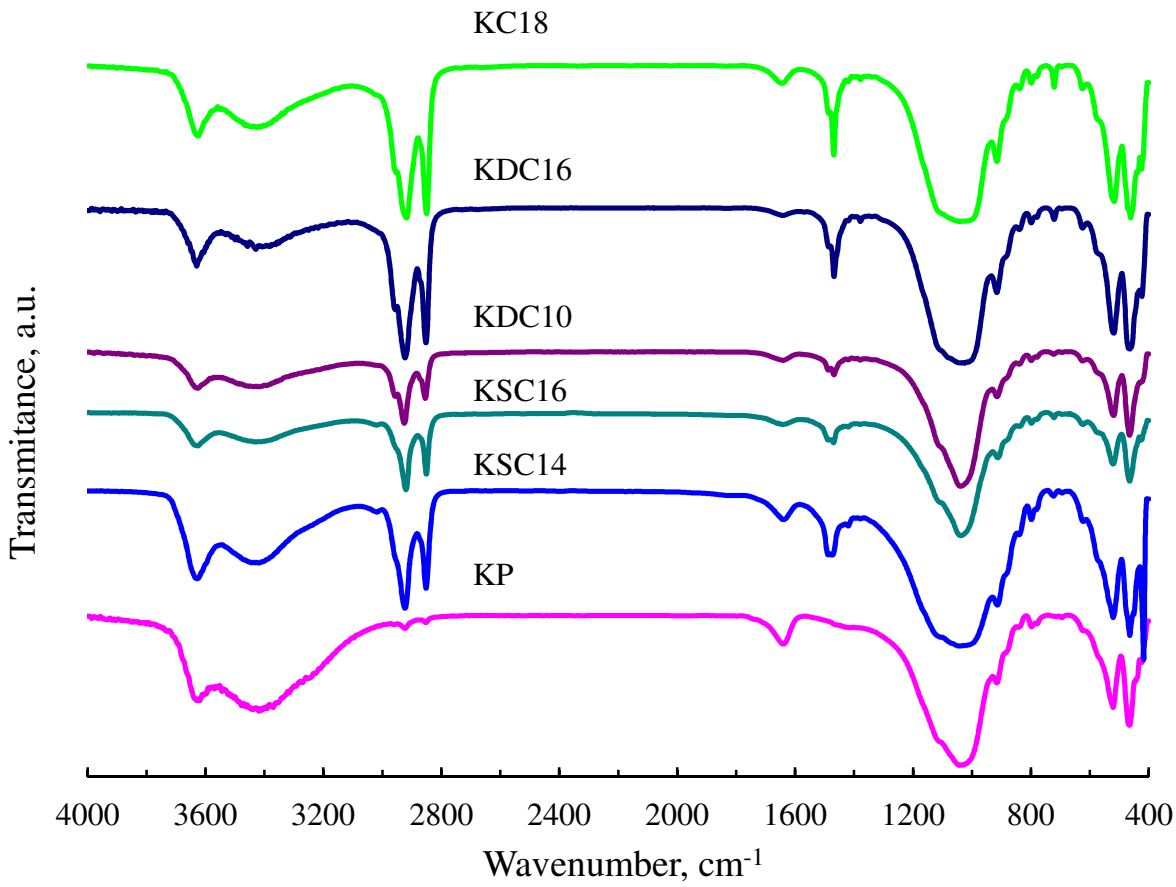

Figure 8. FTIR spectra for Koppies bentonite and its organoderivatives

The assignment of bands to CH_2 and CH_3 was based on a comparison of the relative intensities with increasing aliphatic chain length. The intensity of CH_2 absorption increases

with increasing chain length. Conversely, the intensity of the CH_3 band decreases with increasing chain length. The reverse is also true, i.e. the intensity of the CH_3 band increases with decreasing chain length, whereas the intensity of the CH_2 band decreases.

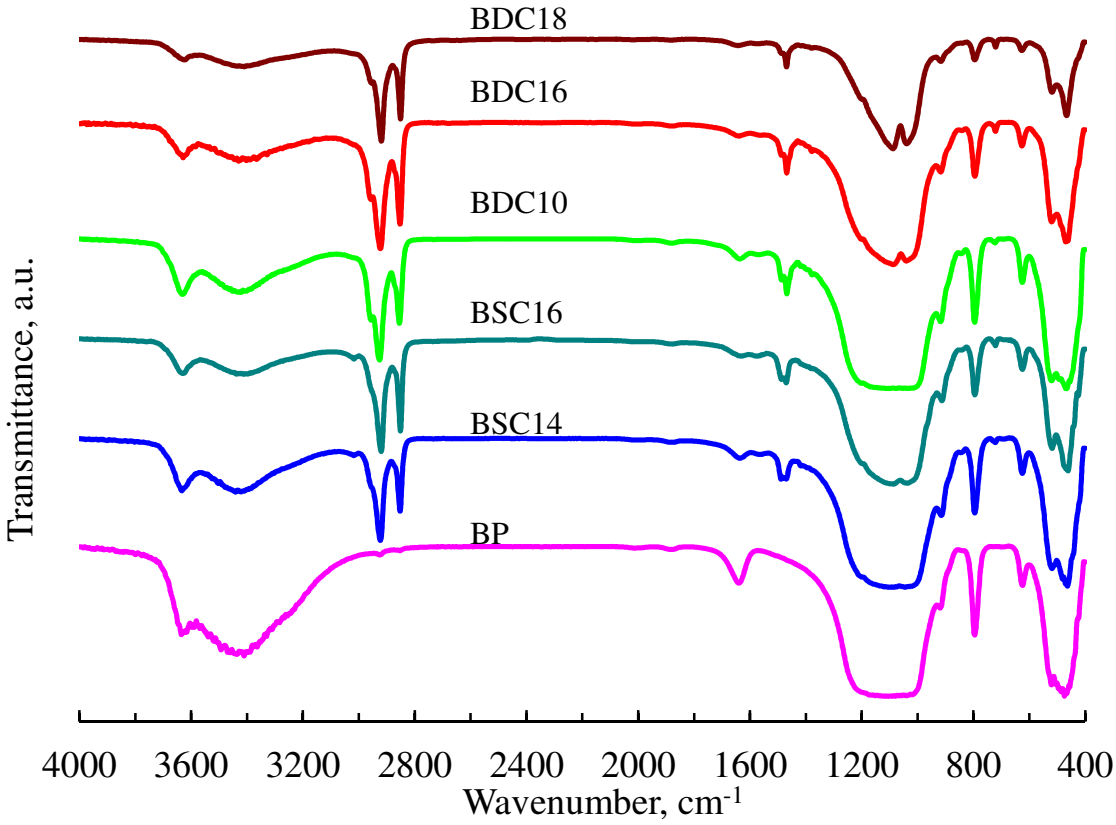

Figure 9. FTIR spectra for Boane bentonite and its organo-derivatives

Vaia et al. (1994) proposed the use of the $\nu_{as}(CH_2)$ band to probe the nature of the interlayer structure. Both the wavenumber and the width of this band are very sensitive to the gauche/trans conformer ratio and the packing density of the chain methylenes. The wavenumber varies from 2917.8 cm^{-1} for the methylene chains in the all-trans ordered state in a crystalline surfactant to 2928.9 cm^{-1} when the chains are in a liquid-like environment (Vaia et al., 1994; Hongping et al., 2004).

The frequencies of $\nu_{as}(CH_2)$ found for the present organobentonites are presented in Table 2. For all surfactants, regardless of the number of chains, the observed values shifted towards values more consistent with the all-trans ordered state with an increase in the alkyl chain lengths. It is speculated, however, that the intercalated alkyl chains did not adopt a rigid solid-like

configuration. Instead it is likely that they were mobile while simultaneously maintaining some degree of orientational order reminiscent of a liquid–crystalline state. Such trans-gauche disorder promotes dense packing of the chains and leads to improved surface mating between the terminal methyl groups and the silicate layers (Lagaly, 1976).

The FTIR CH_2 bending mode [$\delta(CH_2)$] reportedly provides useful additional information (He et al., 2004). A sharp and intense band located around 1472 cm^{-1} indicates strong interchain interactions. Conversely, band broadening coupled with decreased intensity at a position around 1466 cm^{-1} reflects reduced interactions between methylene groups on neighbouring chains (He et al., 2004). The $\delta(CH_2)$ wavenumbers found for the present organobentonites are presented in Table 2. Except for KSC12 and KSC14, the other $\delta(CH_2)$ wavenumbers were similar and were located in the middle of the range 1466-1472 cm^{-1}. As indicated above, the KSC12 and KSC14 organoclay samples feature interdigitated monolayer surfactant intercalation. The extent of interdigitation is such that interactions between different chain methylenes are intense. It is proposed, based on the XRD results, that BSC12 and BSC14 similarly feature interdigitated monolayer surfactant intercalation. However, the chains of the intercalated surfactants have weaker interactions. The other organobentonites comprise bilayer intercalated surfactants with weaker interactions between different chain methylenes.

Figure 8 and Figure 9 compare the FTIR spectra of organically treated clay with the spectra of untreated clay. A combination of narrow and broad absorption bands was observed for all samples between 3700-3200 cm^{-1}. The spectra are not affected, in terms of position (wavenumber), by the presence of organic cations and are characteristic for OH groups. Additional moderate and intense bands were observed from 1750-1360 cm^{-1}, as well as at about 1030 cm^{-1}; in the range 800-650 cm^{-1}they were used to investigate the nature of the OH group. The vibration at about 3618 cm^{-1} was assigned to the smectite structural OH-stretching band. This is a narrow band typical ofthe non-bonded hydroxy group. For clay minerals, OH absorption near 3620 cm^{-1} used to be assigned to inner hydroxyl groups – those located at the surface of octahedral sheets, opposite the tetrahedra. Madejová (2003) stated that smectites with high quantities of Al in the octahedra display absorption at 3620 cm^{-1} in the IR spectra. The broad OH band at approximately 3400 cm^{-1} was due to the presence of adsorbed water and resulted from the H–O–H vibrations of bound water. The intensity of this band decreases as water molecules are displaced by organic species with a larger size.

A typical broad Si–O stretching band is present in the spectra of all samples analysed at approximately 1030 cm^{-1} (Figure 8 and Figure 9). The bands at approximately 793 $cm^{-1}$are attributed to the presence of significant quantities of quartz in the samples. Bands at about 910 cm^{-1} may be assigned to Al_2OH (Madejová, 2003) or AlFeOH (Frost & Kloprogge, 2000). Two non-assigned bands were observed in the range 650-450 cm^{-1} for both untreated and treated clays.

The band structures between 3150 and 3000 cm^{-1} that were expected for KDC18 and BDC18, which would have been indicative of unsaturated aliphatic chains, were not observed. Neither were the C–H out-of-plane bending absorptions observed. Coates (2000) considers these bands to be the most informative regarding the location and spatial geometry of double bonds. The very low concentration of aliphatic C18 double-bonded chains in these samples may explain the absence of the C=C–H absorptions. The possibility that there might be an overlap obscuring the *cis* C–H out-of-plane bending was ruled out. This is because the $\nu_s(CH_2)$ bend at 720 cm^{-1} is not intense enough to obscure the *cis* C–H out-of-plane bending.

4.1.4 Thermal stability of organobentonites

Thermogravimetric analysis (TGA) provides information on the amount of intercalated surfactant (Xie et al., 2001; Xi et al., 2004; Xi et al., 2005; Li & Jiang, 2009). Figure 10 and Figure 11 report the TG mass losses recorded for samples based on Koppies and Boane bentonites respectively. As expected, mass loss increased with increasing number of alkyl chain substituents of surfactants. In addition, the mass loss increases mirrored the increase in the chain length, confirming its dependence on the amount of organic intercalated.

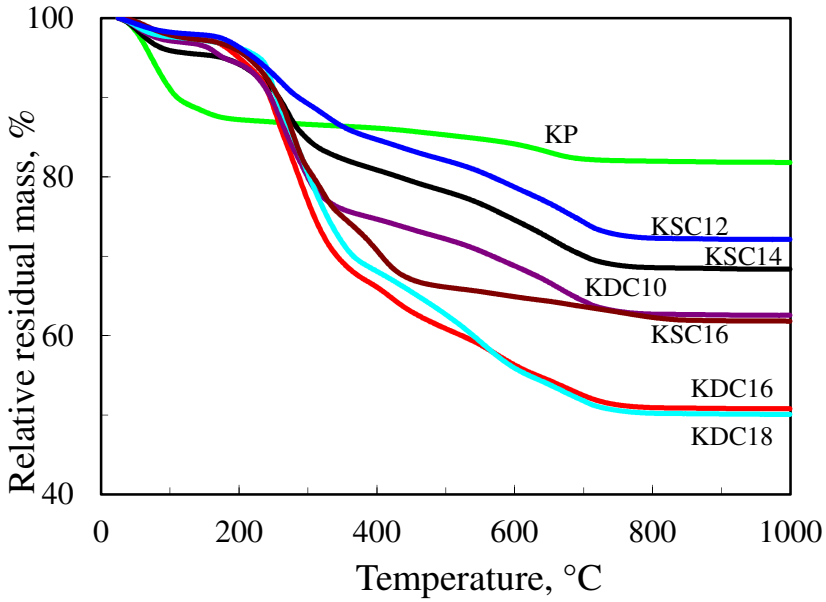

Figure 10. TG mass losses recorded for Koppies bentonite and its organoderivatives

The thermogravimetric decomposition onset temperature, T_{onset}, provides an indicator for the thermal stability of organoclays. T_{onset} is defined as the intercept of the tangent of the initial plateau and that of its main slope on the TG curves (Li & Jiang, 2009). The onset decomposition temperature of the present organobentonites is about 200 ºC (Figure 10 and Figure 11), irrespective of the alkyl chain length (Xie et al., 2001) and number of alkyl chains.

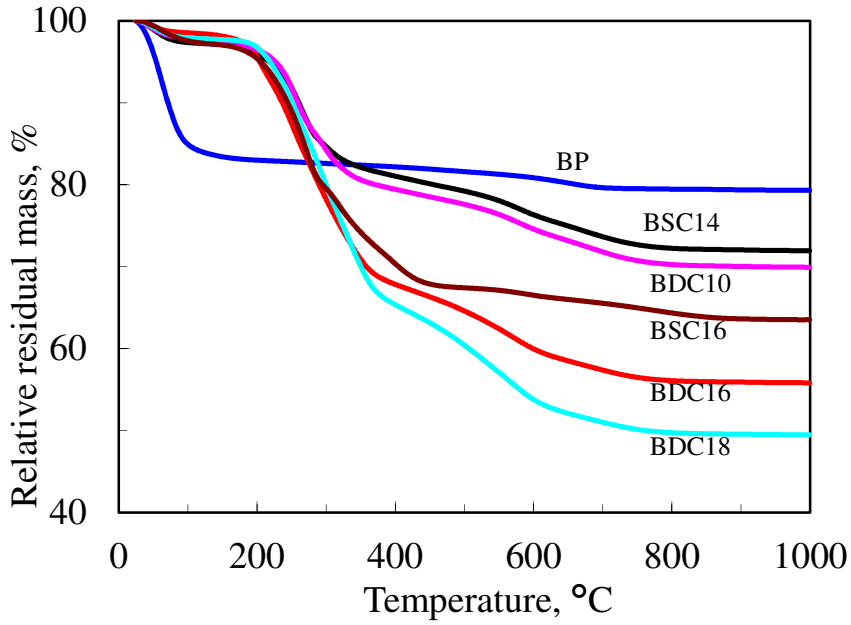

Figure 11. TG mass losses recorded for Boane bentonite and its organoderivatives

Figure 12 and Figure 13 present, respectively, the derivative TG curves for the Koppies and Boane bentonites and their respective organobentonites. These curves show several peaks, indicating that the degradation proceeds in several consecutive steps. These mass loss steps are related to the structure of the inserted molecule (Xi et al., 2004; Xi et al., 2005). For all the surfactants, most of the mass loss occurred in the same temperature range, i.e. 200-400 ºC, regardless of the length or number of alkyl chain substituents.

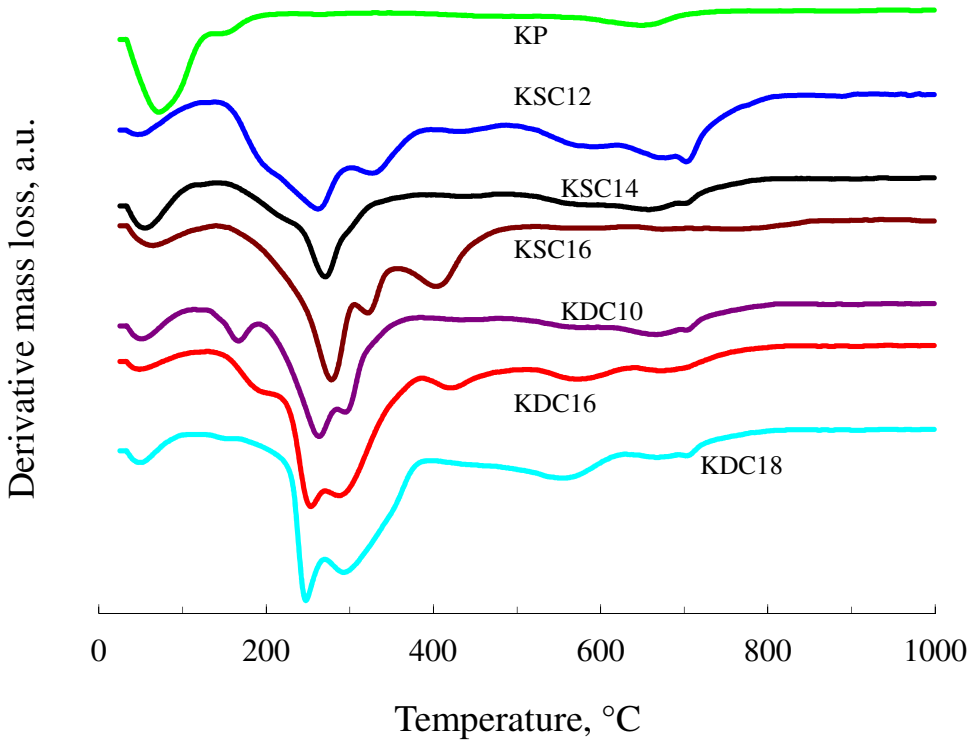

Figure 12. Derivative TG curves for Koppies bentonite and its organobentonites

The main decomposition step is tagged as T_{peak}, the peak temperature corresponding to the maximum mass loss rate. For single-chain intercalated surfactants, only hints of weak peaks were observed below T_{peak}. With the double-chain surfactants a more pronounced peak was observed below T_{peak}. The intensity of T_{peak} increased with chain length for single-chain surfactants. Conversely, T_{peak} decreased with increasing chain length for double-chain surfactants. Similar results for surfactants with two alkyl chains were previously reported (Li & Jiang, 2009). The decrease in T_{peak} was attributed to the development of ordered solid-like chain conformations (Li & Jiang, 2009). However, the T_{peak} trends observed for the present organobentonites are in contradiction to the trends indicated by the downward shift in FTIR

$\nu_{as}(CH_2)$. This suggests that the degradation mechanism of the surfactants might not be as sensitive to the molecular arrangements of the surfactants in the interlayer as has been surmised.

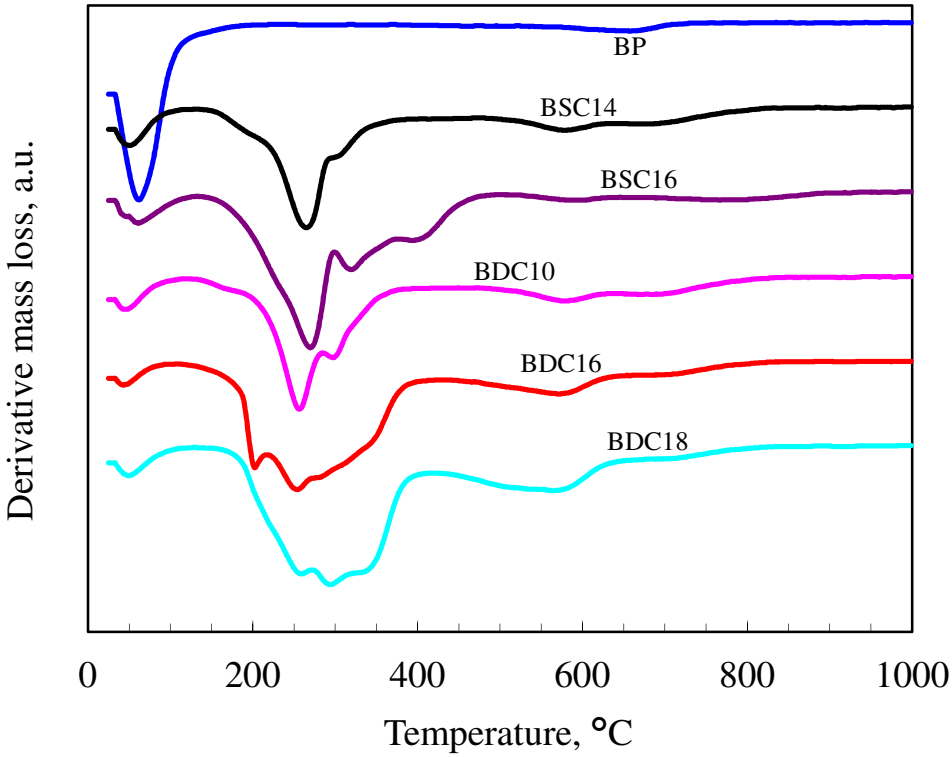

Figure 13. Derivative TG curves for Boane bentonite and its organobentonites

In the DTG curve of the crude bentonites (Figure 12 and Figure 13), only two major thermal events were observed. The DTG curves of the organobentonites showed additional thermal events. The endothermic peak displayed below 100 °C in the DTA curves (Figure 14 and Figure 15) was attributed to the loss of interlayer water. The mass loss associated with this dehydration event amounted to 16.6 mass % for crude bentonites and less than 4 mass % for organobentonites. The higher water content of the crude bentonites was expected as the Ca^{2+} and Na^{+} ions have a greater tendency for hydration than the oleophilic surfactant.

The DTA curves for the crude bentonites are almost featureless in the region between 150 and 600 ºC (Figure 14 and Figure 15). In contrast, the curves obtained for the organobentonites showed significant exothermic events in this temperature range. These were attributed to the oxidative decomposition of intercalated organic species in the air atmosphere (Hedley et al., 2007; Tiwari et

al., 2008). BSC14 and BDC10 featured broad exothermic peaks centred at ca. 330 and 350 ºC respectively.

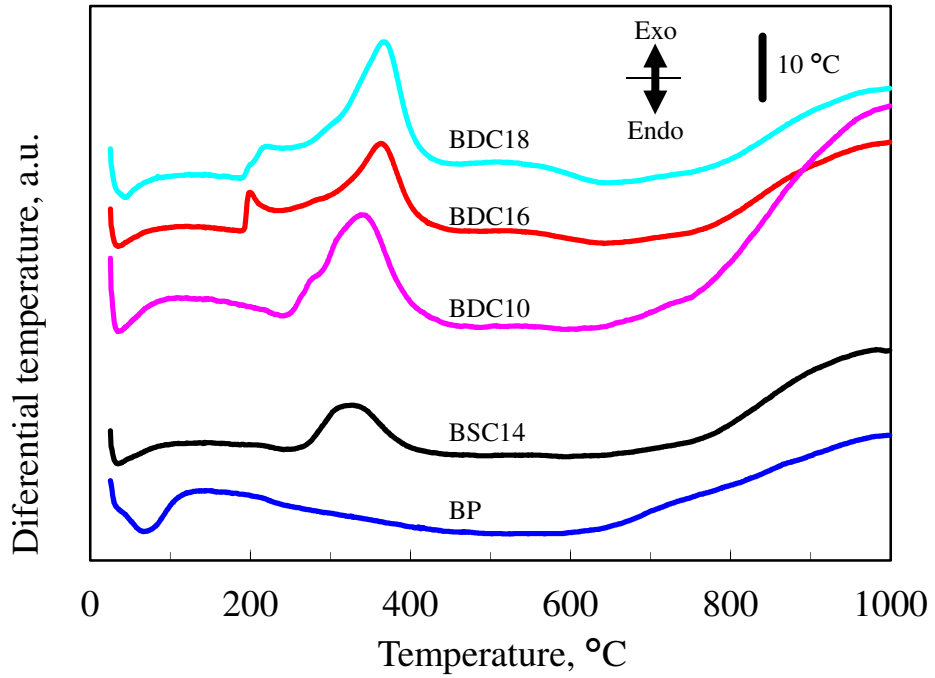

Figure 14. DTA curves for Boane bentonite and its organobentonites

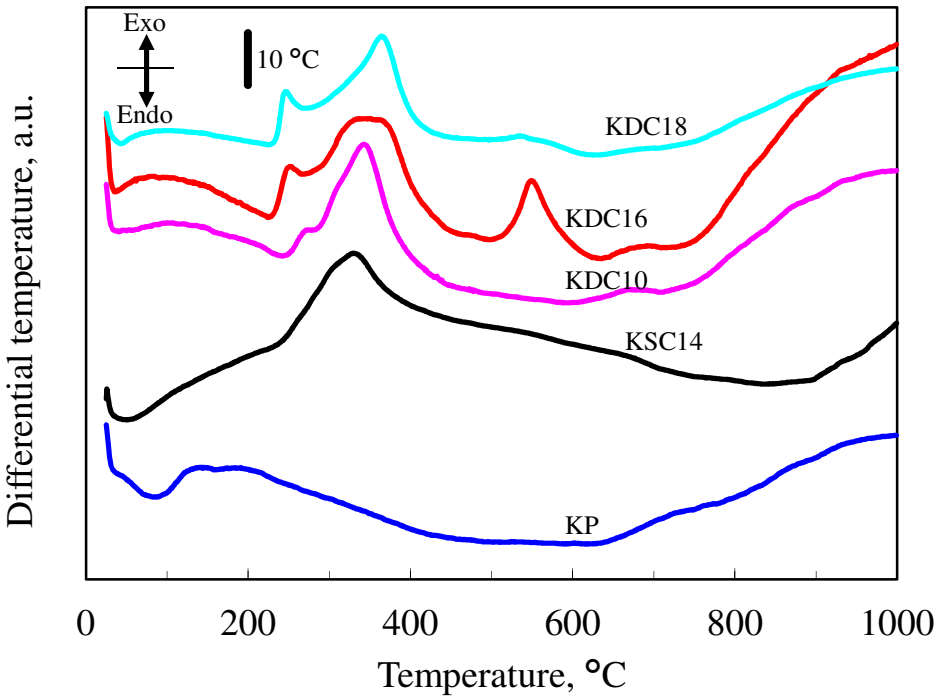

Figure 15. DTA curves for Koppies bentonite and its organobentonites

It is evident from Figure 14 that BDC16 and BDC18 organobentonites started to degrade earlier than all the other organobentonites. A well-defined exotherm onset was observed just below 200 ºC and was followed by a second broader peak centred at ca. 370 ºC (Figure 14). Nevertheless, current results seem to support the claim of Xie et al. (2001) that the decomposition onset temperatures of alkyl ammonium organoclays are independent of the alkyl chain length.

4.2 Characteristics of EVA–organobentonite composites

4.2.1 Morphological characteristics

The properties of clay-based nanocomposites are ultimately determined by their morphology. Homogeneous dispersion of large numbers of stiff high-aspect-ratio platelets in the polymer matrix is usually the desired outcome. This implies the need for extensive delamination and/or exfoliation of the clay particles during the preparation step. Factors that control the exfoliation of clay particles include the properties of the matrix and the organoclays, and the processing route used. Surfactant structural issues significantly affect the properties of organoclays and ultimately the nanocomposite morphology (Fornes et al., 2002). This study held the montmorillonite clay base, the polymer matrix and the melt processing technique constant and focused on the effect of the surfactant structure and its loading on the organoclay. Fornes et al. (2002) studied Nylon 6 composites and observed that decreasing the number of long alkyl chains from two to one, and using an equivalent amount of surfactant with the montmorillonite (as opposed to adding an excess) led to greater extents of silicate platelet exfoliation, increased moduli, higher yield strengths and lower values for the elongation at break. The current study found that the opposite holds for EVA-based micro-nanocomposites prepared by melt compounding. The present results are in better agreement with the findings of Shah et al. (2005) for nanocomposites from poly(ethylene-co-methacrylic acid) copolymers. In these systems four distinct surfactant structural effects lead to improved levels of delamination/exfoliation and higher stiffness for these nanocomposites. These effects are:(1) a higher number of alkyl chains on the amine rather than just one;(2) longer alkyl chains instead of shorter ones;(3) the use of 2-hydroxyethyl groups as opposed to methyl groups on the ammonium ion; and (4) an excess amount of the amine surfactant on the clay instead of an equivalent amount (Shah et al., 2005).

Figure 16 presents the XRD pattern of the soda ash-activated Koppies slurry (KS), neat Koppies powder (KP) bentonite and the organic derivatives. The diffractogram of KS is

featureless, indicating that the bentonite particles were present in an exfoliated form. The basal reflection observed at 2θ = 6.76º for KP bentonite corresponds to d_{001} = 1.52 nm (Table 2). This falls within the 1.2-1.6 nm range typical for smectite minerals under ambient temperature and humidity conditions (Utracki, 2004).

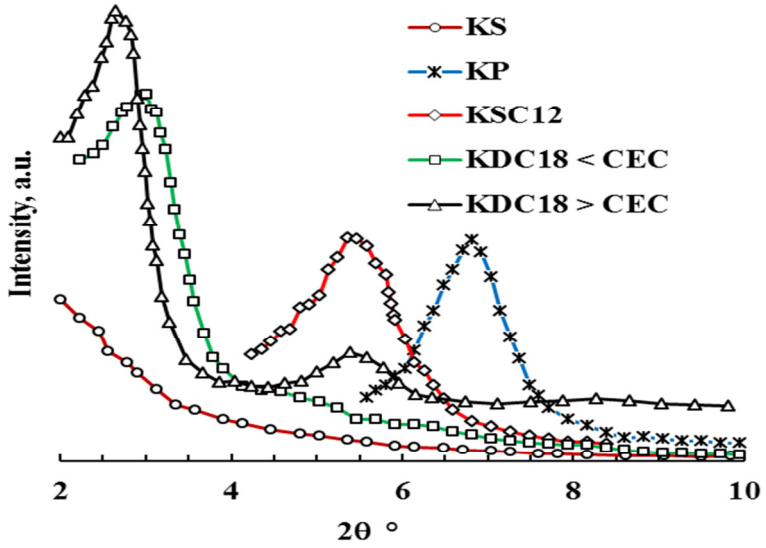

Figure 16. XRD pattern of the soda ash-activated Koppies slurry (KS), neat Koppies powder (KP) bentonite and the organic derivatives

The chain length, surfactant loading and configurations that the surfactant molecules assume in the interlayer determine the basal spacing of organoclays (Lagaly, 1986). The surfactant cations are electrostatically 'attached' to the clay surfaces with the alkyl chains preferring to pack tightly together in order to maximise van der Waals interactions. Excess surfactant intercalates in the neutral salt form, together with (hydrated) counter-ions (Lagaly, 1986; Klapyta et al., 2001).

The diffractograms for the organoclays showed reflections at lower 2θ values, confirming the intercalation of the surfactants. The observed XRD d-spacing for the single-chain surfactant organoclay sample KSC12 was 1.92 nm (Table 2). As previously reported by our laboratory (Massinga et al., 2010; Massinga &Focke, 2012), this value is consistent with interdigitated monolayer surfactant intercalation of the C12 single-chain surfactant. Organobentonites prepared in the presence of the C18 double-chain surfactant below and above the CEC of KP resulted in a nearly identical XRD diffractogram and content of intercalated surfactant

(Figure 16). The XRD-estimated d-spacings were 3.56 nm for the organoclay sample prepared with a stoichiometric amount (KDC18 < CEC) and 3.77 nm for the organoclay sample with an excess of the C18 double-chain surfactant (KDC18 > CEC). These values are consistent with bilayer surfactant intercalation. The additional reflection at 5.45°, in the diffractogram for the KDC18 > CEC sample, corresponds to a second-order basal reflection. This reflection was not observed for the KDC18 < CEC sample, suggesting that more ordered intercalation occurred in the former case.

The XRD diffractograms for EVA composites based on the C12 single-chain surfactant (Figure 17) did not show well-defined reflections, in contrast to those for the EVA-clay composites based on the C18 double-tail surfactant (Figure 18 and Figure 19).

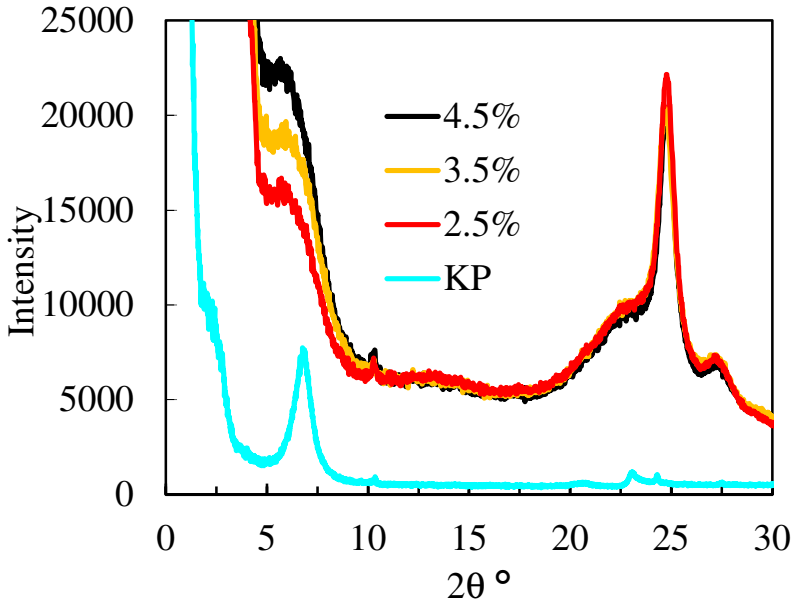

Figure 17. XRD diffractograms for EVA-organoclay composites based on Koppies bentonite with C12 single chain

The diffractogram for all the EVA composites with organoclays based on the C18 double-chain surfactant (Figure 18 and Figure 19) were virtually identical, irrespective of the clay loading. They all showed four clear reflections associated with an integral series of basal plane reflections. This indicates a homogeneous distribution of the alkylammonium cations in the MMT interlayers (Klapyta et al., 2001). Compared with the organoclays, the reflections

are sharper and their positions shifted to lower 2θ values. This implies an increase in perfection and an expansion of the clay gallery height to effect a d-spacing as high as 3.9 nm.

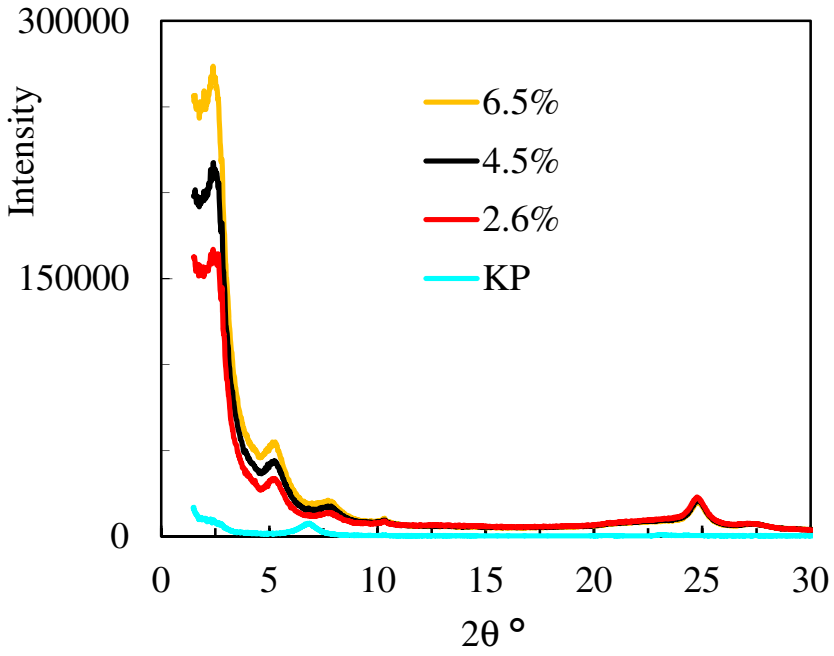

Figure 18. XRD diffractograms for EVA-organoclay composites based on Koppies bentonite with C18 double chain at CEC

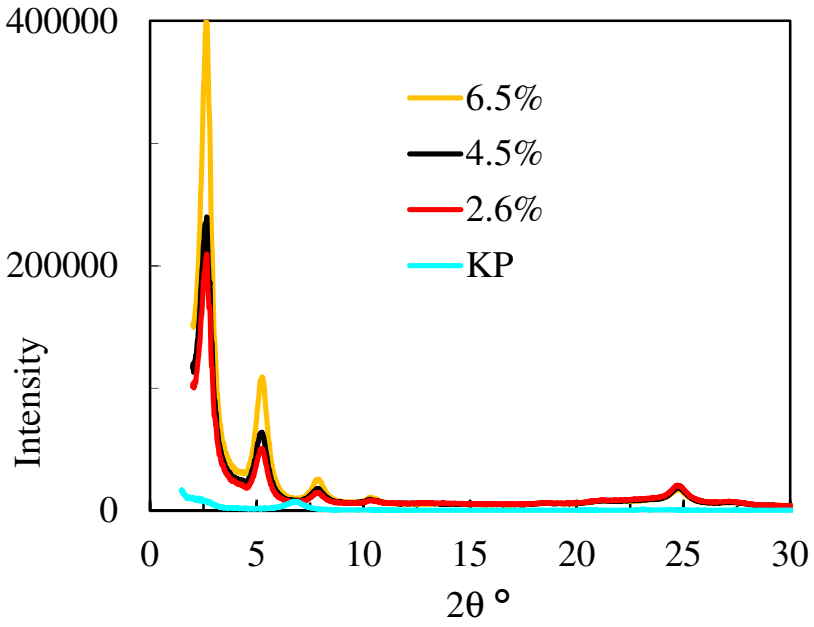

Figure 19. XRD diffractograms for EVA-organoclay composites based on Koppies bentonite with C18 double chain above CEC

The following tentative rationalisation for the results presented in this thesis is proposed. The XRD results indicated interdigitated monolayer intercalation of the single-tail surfactant in the clay, while the double-tail surfactant intercalated in a double-layer fashion (Massinga et al., 2010; Massinga & Focke, 2012). The basal spacing values of the neat organoclays were readily determined as the XRD diffractograms showed clear basal reflections. Incorporating the clays into the EVA by melt compounding changed these diffractograms dramatically. The XRD diffractograms of the KSC12-based nanocomposites became almost featureless, suggesting extensive disruption of the regular clay platelet stacking. Only hints of poorly resolved reflections remained. Such a drastic change is consistent with extensive clay delamination which reduces the remaining platelets to stacks comprising a few clay sheets. TEM provided some evidence for this possibility (Figure 20). An alternative possibility is a significant increase in the degree of disorder in the stacking of the platelets within the tactoids. Random co-intercalation of EVA polymer chains can result in such a severe disruption in the regularity of sheet stacking. The presence of a single hydroxyethyl substituent on the C12 surfactant appears sufficient to encourage co-intercalation of the EVA chains as it is capable of hydrogen bonding with the ester functional groups.

In contrast, the XRD diffractograms for the nanocomposites made using the double-tail surfactant showed sharpened reflections and, in some instances, the emergence of additional reflections attributable to multiple basal reflections. This is consistent with an increase in the structural order of the tactoids due to improved packing of the surfactants intercalated in the clay galleries. It is significant that the diffractograms, and thus the basal spacings, were virtually identical, irrespective of the amount of surfactant employed in the synthesis of the organoclays. Alexandre and Dubois (2000) previously noted an increase in the basal spacing of double-tail intercalated MMT when it was incorporated into EVA. They also found that the surfactant intercalated into the neat clay when both were individually dispersed in molten EVA (Alexandre et al., 2001). An increase in basal spacing has also been observed in other polymer matrices (Pavlidou & Papaspyrides, 2008) and it is generally taken as evidence that polymer intercalation into the clay galleries has occurred (Beyer, 2002). However, the sharpening of the reflection peaks observed in this study is not consistent with polymer intercalation into the clay galleries. Since the polymer chains vary in length and in composition, one would expect significant variations in the d-spacing values and thus a broadening of the XRD reflections if they were co-intercalated. This is in fact observed with

the clay intercalated with surfactant containing the hydroxyethyl substituent. The common shift to lower Bragg angles implies that, more likely, the EVA chains did not enter the clay galleries. Instead, it seems more probable that 'surplus' surfactant molecules released by the delamination and dispersion of the clay sheets during compounding were taken up in the remaining tactoids, resulting in improved ordering through tighter packing of the alkyl chains in the galleries. Nevertheless, it should be kept in mind that the XRD traces capture only the thicker tactoids and certainly not the well-dispersed single (exfoliated) clay sheets.

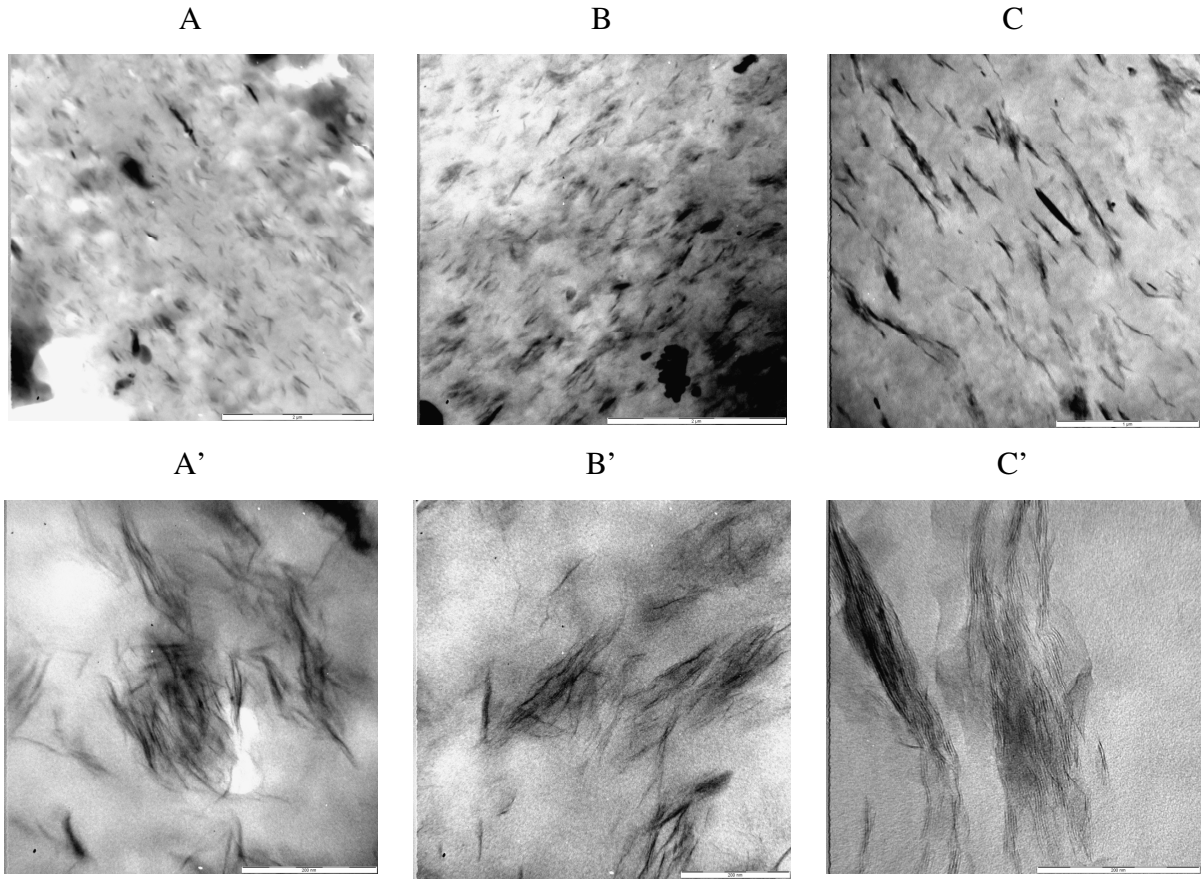

Figure 20. Representative TEM pictures for the EVA-organoclay composites at the micron scale (1 µm): [A] C12 single chain; [B] C18 double chain at CEC; [C] C18 double chain above CEC, and at the nanoscale (200 nm): [A'] C12 single chain; [B'] C18 double chain at CEC; [C'] C18 double chain above CEC

Figure 20 shows representative TEM micrographs of the EVA-organoclay composites at the micron scale (Figure 20A, B, C) and at the nanoscale (Figure 20A', B', C'). Small clay particles are visible at the micron scale but extensive delamination is evident in the

micrographs with nanoscale resolution. This implies that the EVA-organoclay compounds prepared in the present study were a combination of micro- and nanocomposites. The flake-like clay particles seen in the composites based on the single-tail organobentonite KSC12 were significantly smaller and thinner than those observed in the two composites comprising the double-tail surfactant. It seems reasonable to conclude that a surfactant with a single hydroxyethyl substituent facilitates clay sheet dispersions particularly well, similarly to those containing two hydroxyethyl substituents, when all other characteristics are similar.

4.2.2 Rheological and mechanical characteristics

The main consequence of delamination and exfoliation of clay particles is the enhancement of the viscosity of the liquid melt and the modulus in the solid state. Two main mechanisms operate to increase the modulus of composites comprising well-dispersed clay platelets (Pavlidou & Papaspyrides, 2008). The clay platelet particles are significantly stiffer than the polymer matrix. Thus, the first effect derives from their load-carrying ability. In addition, the apparent increase in matrix stiffness arises from the tendency of the clay surfaces to constrain the motion of adjacent polymer chains. Strong polymer chain-clay surface interactions strengthen this confinement effect. Both mechanisms benefit from an increase in the degree of clay exfoliation as the interfacial area also increases.

The rheological behaviour of molten polymer nanocomposites complements XRD and TEM information on the degree of exfoliation of clay platelets in a polymer matrix (Gupta et al., 2005). Figures 21-23 show the effect of clay content and shear rate on the melt viscosity of EVA-clay composites. The high viscosity at low shear rates points to strong interactions between the delaminated clay platelets and the polymer chains or, alternatively, the formation of network structures by clay particle interactions. Pronounced shear thinning indicates extensive clay exfoliation in certain systems (Wagener & Reisinger, 2003; Gupta et al., 2005; Szép et al., 2006). The nanocomposites' internal structure is retained at low shear rates but at high shear rates the clay network structures break down and the platelets tend to orient in the direction of flow. The resulting platelet alignment decreases the apparent viscosity so that it approaches that of the neat polymer melt (Wagener & Reisinger, 2003; Szép et al., 2006).

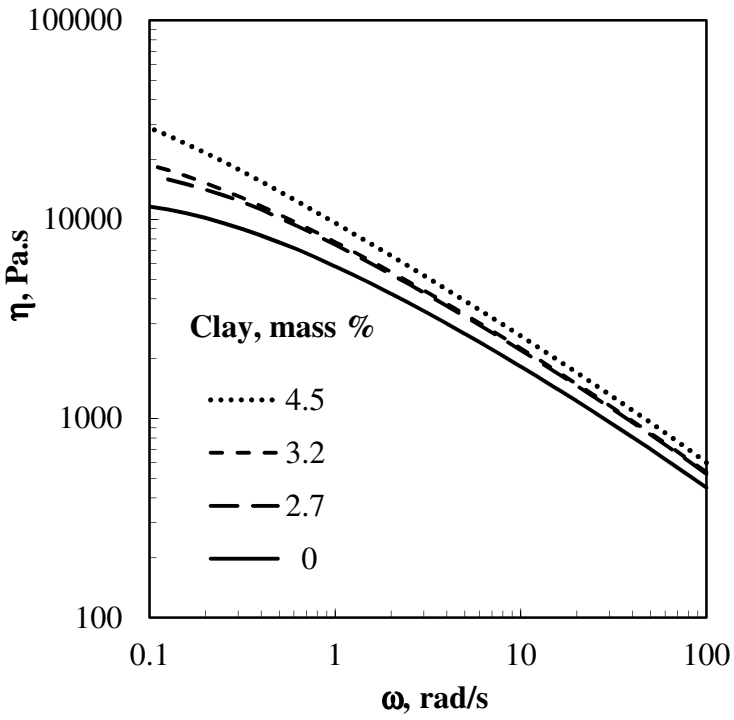

Figure 21. Rheology curves obtained at 170 °C for EVA-clay composites containing the clay prepared with C12 single chain

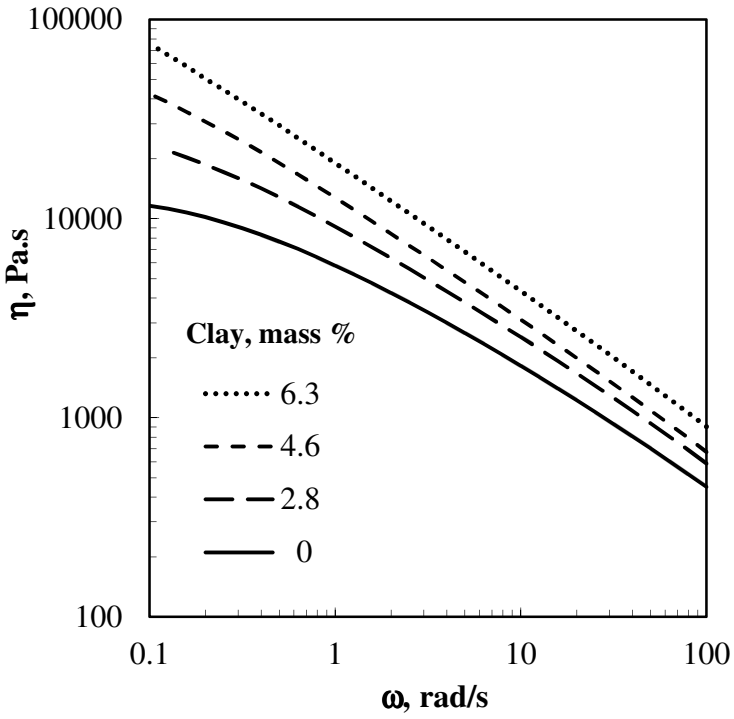

Figure 22. Rheology curves obtained at 170 °C for EVA-clay composites containing the clay prepared with C18 double chain at CEC

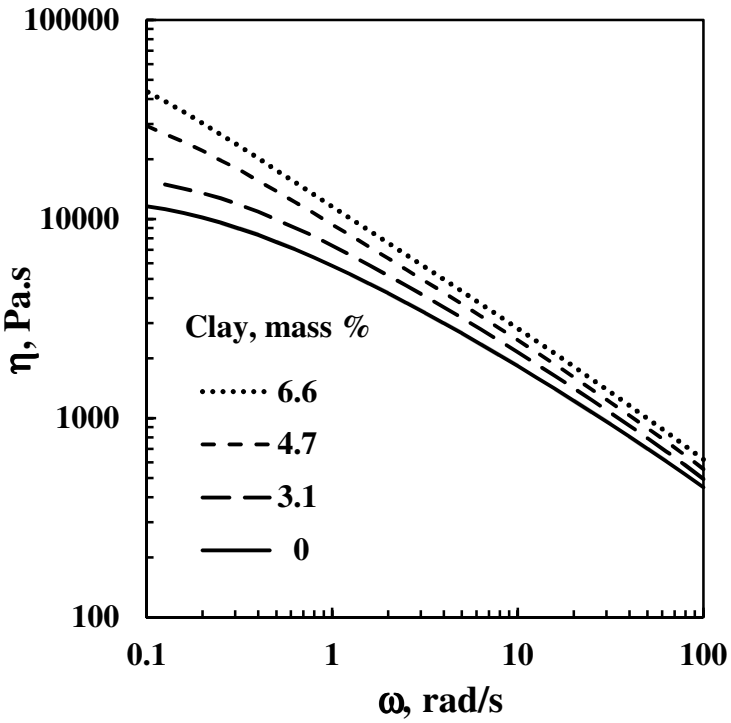

Figure 23. Rheology curves obtained at 170 °C for EVA-clay composites containing the clay prepared with C18 double chain above CEC

Figure 24 compares the relative viscosities scaled with respect to that of the neat EVA at a clay content of ca. 4.5 mass %. Interestingly, the highest melt viscosity is shown by the KDC18 < CEC sample. The melt viscosities of the other two clay composites were similar but significantly lower.

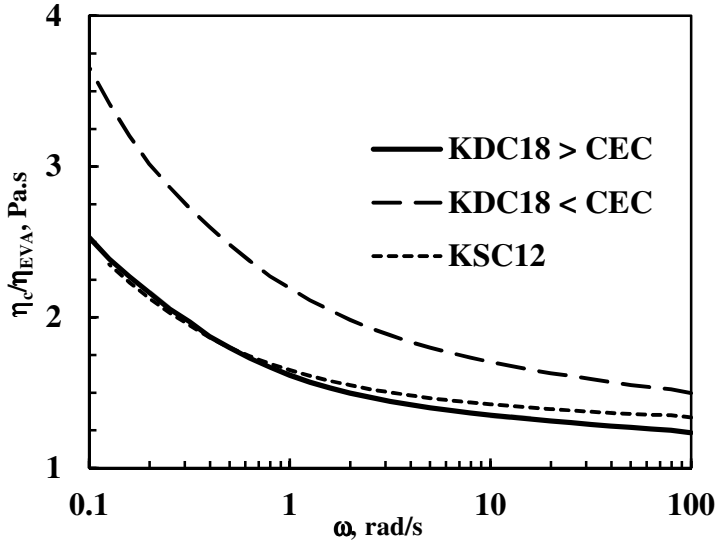

Figure 24. Relative viscosities of composites scaled with respect to that of the neat EVA at a clay content of ca. 4.5 mass %

Table 3 compare moduli for the composites at comparable clay contents. It is clear that the composites based on the double-tail modified clays performed better at modulus enhancement than the single-tail surfactant-modified clay, especially when intercalation beyond a CEC excess was achieved, despite the fact that the single-tail surfactant is more likely to interact with the EVA chains as discussed above. Thus it may be easier to exfoliate bilayer-intercalated clay than interdigitated monolayer intercalated clay. The increase in the melt viscosities mirrored the modulus enhancement for the composites based on the two clays prepared with an equivalent amount of surfactant. Surprisingly, this was not the case for the composite based on an excess of the DC18 surfactant. It provided the best performance in modulus improvement but featured a lower viscosity than the KDC18 < CEC sample. The lowering of the viscosity of the KDC18 > CEC composites was unexpected. However, this can be explained by assuming that some of the excess surfactant must have de-intercalated and that these surfactant molecules imparted an external lubrication effect.

Table 3. Clay content from TGA and mechanical properties of EVA-clay composites

EVA composite	Clay (mass %)	Tensile strength, (MPa)		Strain at break (%)		Young's modulus(MPa)		Tensile impact(MJ/m$^{2)}$	
Neat EVA	0.0	9.1	0.3	287	18	24.3	2.2	0.57	0.01
C12 single chain	2.7	9.0	0.2	250	14	34.1	2.4	0.41	0.06
(KSC12)	3.2	9.2	0.2	236	10	37.7	3.7	0.41	0.02
	4.5	9.3	0.2	245	12	33.1	2.6	0.39	0.02
C18 double chain	2.8	9.3	0.2	271	11	39.2	3.0	0.39	0.03
	3.9	9.4	0.3	274	19	37.3	2.9	0.40	0.02
(KDC18 < CEC)	4.6	9.3	0.2	274	7	42.3	2.5	0.45	0.03
	6.3	9.5	0.2	284	8	49.3	4.3	0.37	0.02
C18 double chain	3.1	12.4	0.3	445	19	38.1	1.5	0.40	0.03
(excess surfactant)	4.7	16.2	0.2	721	22	48.9	2.3	0.35	0.01
(KDC18 > CEC)	6.6	15.1	0.3	663	11	73.1	4.6	0.36	0.03

Note: The second number in each column indicates standard deviation in measured value.

Table 3 reports tensile and tensile impact properties for the EVA nanocomposites. The tensile impact strength decreased with clay loading for all samples. Adding clay reduced it by values between 21 and 38%, depending on the clay used. For the KSC12 and KDC18 < CEC composites, tensile strength increases marginally and elongation at break decreases slightly

with increase in clay content. In contrast, the KDC18 > CEC composites showed significant improvements in both tensile strength and ultimate elongation. Optimum results were obtained for the compound with intermediate clay content (4.7 mass % clay). In this case, the tensile strength and ultimate elongation were 78 and 151% higher than the corresponding values for the neat polymer. The tensile modulus data obtained from tensile strength tests, also summarised in Table 3, indicate that the composites differed markedly with respect to the increase in the Young's modulus. The composite based on the clay containing the double-tail surfactant intercalated in excess of the CEC showed the best performance. The modulus was three times higher than that of the neat EVA at a loading of 6.6 mass %. At a similar clay content, the composite prepared using the organoclay loaded with the same surfactant, but at a lower level, provided only a doubling of the modulus. Table 3 also shows that the increase in modulus with increasing clay content was less for the composites based on the single long alkyl chain surfactant. The nanocomposites displayed a large increase in the elongation at break. This could be due to the plasticising effect of the galleries, their contribution to the formation of dangling chains and conformational effects at the clay-matrix interface (Camargo et al., 2009).

4.2.3 Thermal and thermomechanical characteristics

Table 3 also reports the TGA-determined dry (inorganic) clay contents of the EVA-organoclay composites. Figures 25-27 show TGA results for EVA-organoclay composites based on Koppies bentonite intercalated with C12 single chain and C18 double chain below and above CEC.

Up to a temperature of about 400 °C, all samples showed a similar mass loss profile. Thereafter the observed mass loss was less for the samples with higher clay loadings. At high temperatures, the mass loss reached a plateau value corresponding to the calcined clay residue. This allowed the estimation of the actual clay content of the EVA composites from the residual mass observed at 1 000 °C.

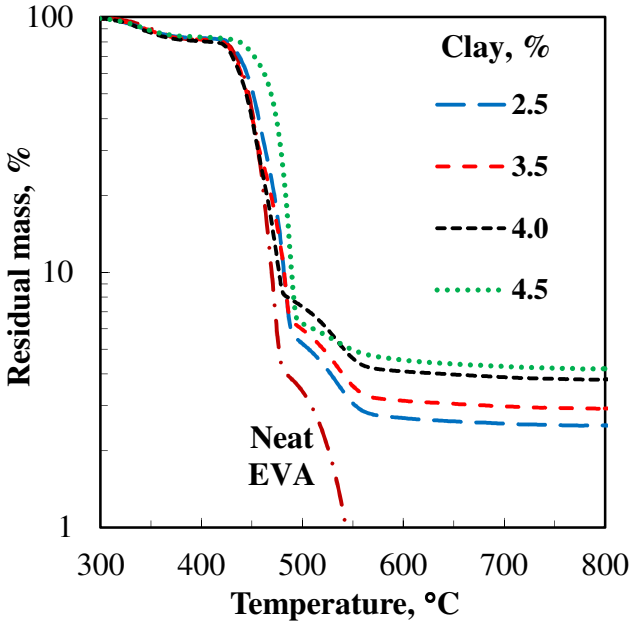

Figure 25. TGA curves for EVA-organoclay composites based on Koppies bentonite with C12 single chain

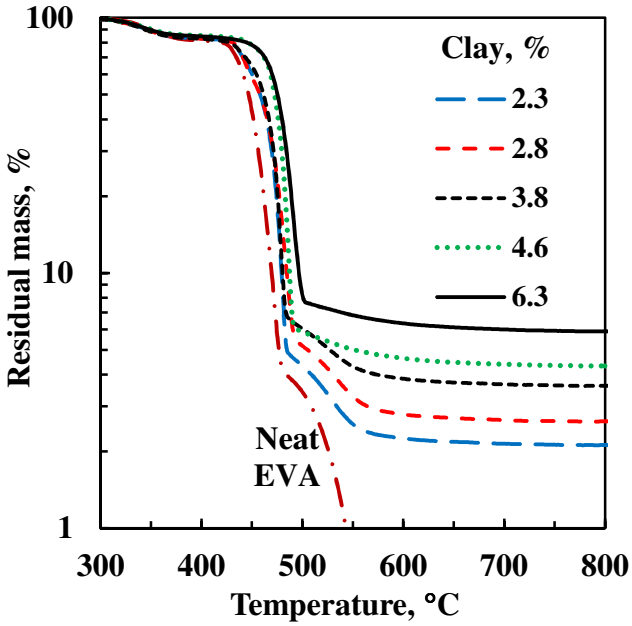

Figure 26. TGA curves for EVA-organoclay composites based on Koppies bentonite with C18 double chain at CEC

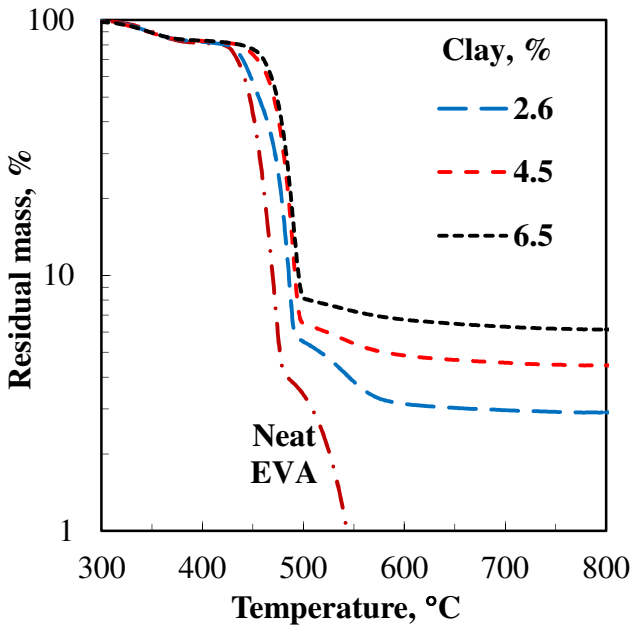

Figure 27. TGA curves for EVA-organoclay composites based on Koppies bentonite with C18 double chain above CEC

Figure 28 shows tan δ as a function of temperature and clay concentration for the composite based on the clay containing double-tail surfactant intercalated in excess of the clay CEC. The shape of the tan δ curve remains approximately the same, but the peak height decreases with increase in clay content. The tan δ curves for the composites made with the other two organoclays showed similar behaviour (Figure 29 and Figure 30). The peak in this curve can be associated with the glass transition temperature which was about -7 °C for the neat EVA as well as for all the composites. This suggests that the presence of the clay did not significantly affect the mobility of the polymer chains of the matrix.

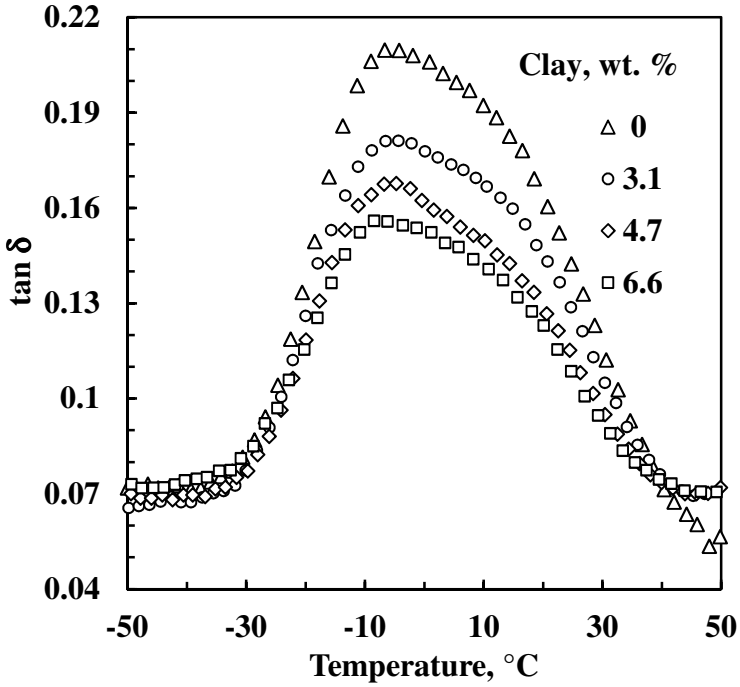

Figure 28. Effect of clay loading on tan δ for EVA-organoclay composites based on the clay containing C18 double chain above CEC

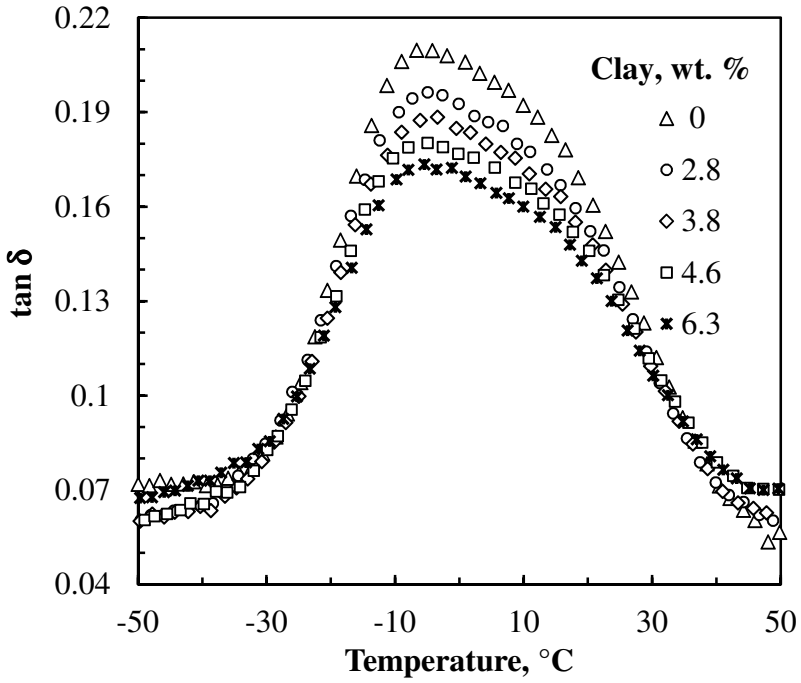

Figure 29. Effect of clay loading on tan δ for EVA-organoclay composites based on the clay containing C18 double chain at CEC

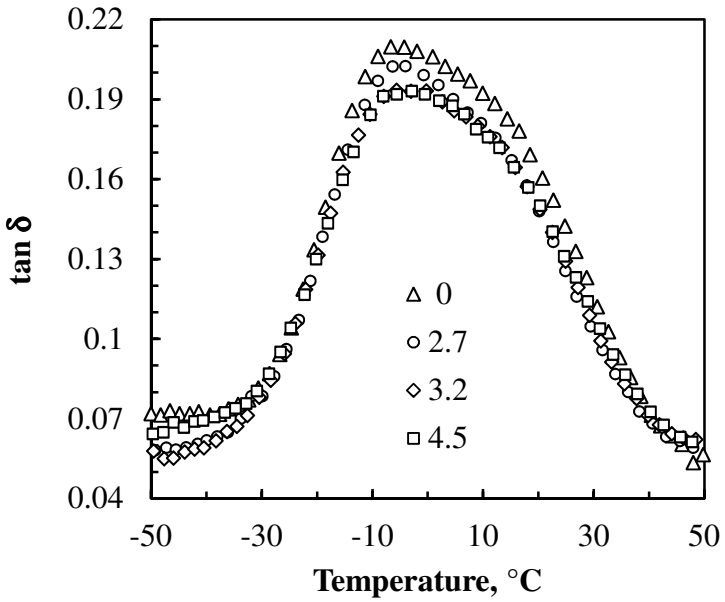

Figure 30. Effect of clay loading on tan δ for EVA-organoclay composites based on the clay containing C12 single chain

Figures 31-33 show the DMA-determined storage modulus as a function of temperature and clay concentration for the EVA-organoclay composites.The graphs show that the stiffness enhancement is limited at low temperatures where the polymer is in a glassy state and more pronounced in the temperature range corresponding to the rubbery plateau, i.e. above the glass transition temperature.

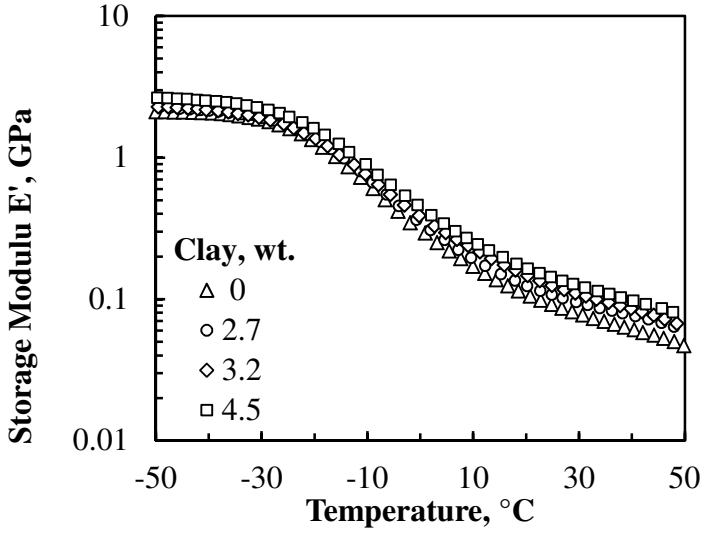

Figure 31. DMA-determined storage modulus for EVA-organoclay composites based on C12 single chain

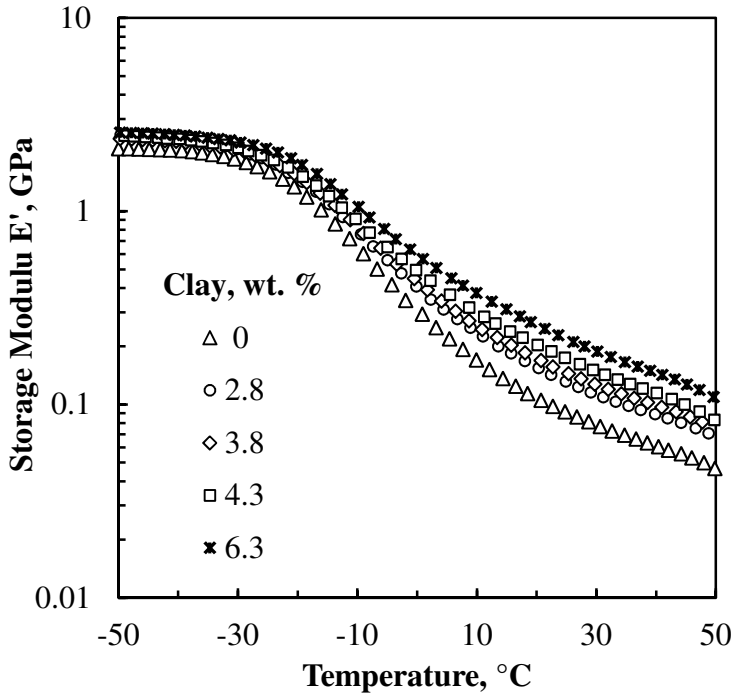

Figure 32. DMA-determined storage modulus for EVA-organoclay composites based on C18 double chain at CEC

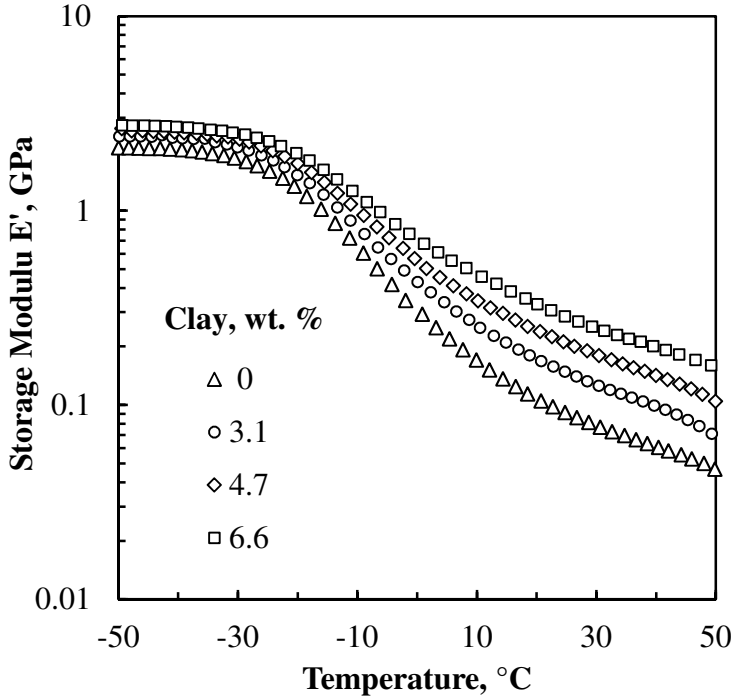

Figure 33. DMA-determined storage modulus for EVA-organoclay composites based on C18 double chain above CEC

Figure 34 compares the modulus enhancement E'_c/E'_p found for the composites containing approximately 4.5 mass % clay. Figures 31-34 confirm that the modulus enhancement trends observed with tensile testing (Table 3) hold over the full temperature range. They show that the enhancement achieved in the glassy region is small and similar for the different organoclay composites but that it becomes differentiated at elevated temperatures.

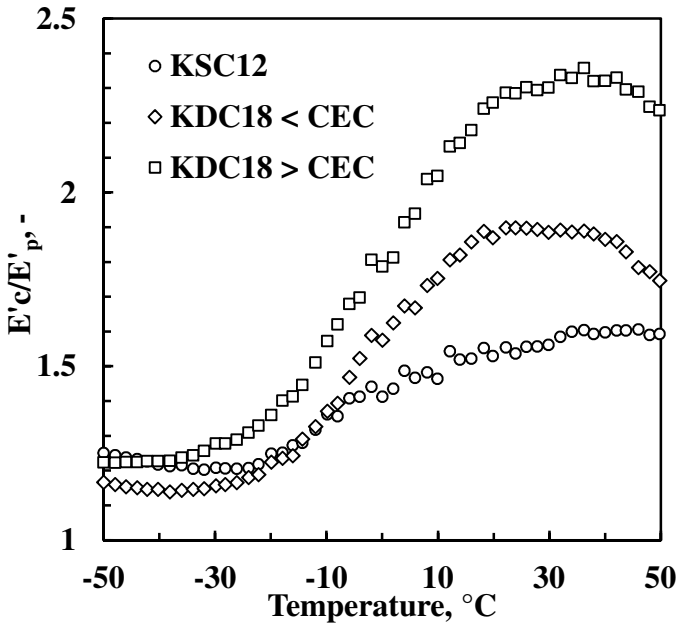

Figure 34. Modulus enhancement for the composites containing approximately 4.5 mass % clay

CHAPTER 5 CONCLUSIONS

Organobentonites were prepared using purified bentonites from the Boane deposit in Mozambique and from the Koppies mine in South Africa. Boane bentonite contained significant amounts of cristobalite that could not be removed cost-effectively. Quaternary ammonium surfactants (quats) were intercalated using soda ash-activated Koppies and Boane bentonite dispersions.

X-ray diffractometry (XRD), Fourier transform infrared (FTIR) spectroscopy and thermogravimetric analysis (TGA) were combined to describe the interlayer structures and their molecular environments. It was concluded that the organobentonite samples comprising single-chain C12 and C14 surfactant consist of monolayers of interdigitated surfactant configurations. The extent of interchain penetration caused strong hydrophobic interactions between the different chain methylenes. The single-chain C16 and double-chain C10, C16 and C18 alkyl surfactants intercalated as bilayers but XRD also hints at the presence of a minor phase comprising interdigitated surfactant configurations. However, FTIR analysis indicated disordered chain conformations. It is speculated that the intercalated alkyl chains did not adopt a rigid solid-like configuration. Instead it is likely that they were mobile while simultaneously maintaining some degree of orientational order reminiscent of a liquid–crystalline state. The interactions between the different chain methylenes of the organobentonites comprising bilayer intercalated surfactants were weaker.

The onset decomposition temperature of the present organobentonites, around 200 ºC, is within the typical range of polymer/organoclay processing temperatures. The thermal stability of the present organobentonites was independent of both the number of alkyl chain substituents and their length, as well as independent of the degree of clay intercalation.

TEM and XRD revealed that the EVA nanocomposites prepared by twin-screw melt compounding had mixed exfoliated/intercalated microstructures. The presence of a single hydroxyethyl substituent in the C12 surfactant appears to be sufficient to encourage co-intercalation of the EVA chains as it is capable of hydrogen bonding with the ester functional groups. It seems reasonable to conclude that a surfactant with a single hydroxyethyl substituent facilitates clay sheet dispersions particularly well, similarly to those containing two hydroxyethyl substituents, when all other characteristics are similar.

The XRD diffractograms for the nanocomposites made using the C18 double-tail surfactant showed sharpened reflections and, in some instances, the emergence of additional reflections attributable to multiple basal reflections. This is consistent with an increase in the structural order of the tactoids due to improved packing of the surfactants intercalated in the clay galleries. However, the sharpening of the reflection peaks observed does not seem consistent with polymer intercalation into the clay galleries. Since the polymer chains vary in length and in composition, one would expect significant variations in d-spacing values and thus a broadening of the XRD reflections if they were co-intercalated. This is in fact observed with the clay intercalated with the surfactant containing the hydroxyethyl substituent. The common shift to lower Bragg angles implies that, more likely, the EVA chains did not enter the clay galleries. Instead, it seems more probable that 'surplus' surfactant molecules released by the delamination and dispersion of the clay sheets during compounding were taken up in the remaining tactoids, resulting in improved ordering through tighter packing of the alkyl chains in the galleries.

Improved mechanical properties were realised, especially when using the bentonite containing the longer double-tail surfactant intercalated at levels in excess of the cation exchange capacity (CEC) of the clay. The nanocomposites showed improved tensile modulus and elongation at break values at the expense of a reduction in impact strength, while tensile strength was about the same as for the neat polymer. It is postulated that it was easier to delaminate these bilayer-intercalated clays and that excess surfactant acted as an external lubricant, thereby reducing the apparent melt viscosity.

CHAPTER 6 REFERENCES

Ahmadi, S., Huang, Y., Li, W., 2005. Fabrication and physical properties of EPDM-organoclay nanocomposites, *Compos. Sci. Technol*. 65, 1069-1076.

Alexandre, M., Dubois, P., 2000. Polymer-layered silicate nanocomposites: preparation, properties and uses of a new class of materials, *Mater. Sci. Eng*. 28, 1-63.

Alexandre, M., Beyer, G., Henrist, C., Cloots, R., Rulmont, A., Jéróme, R., Dubois, P., 2001. "One-pot" preparation of polymer/clay nanocomposites starting from Na^+ montmorillonite. 1. Melt intercalation of ethylene-vinyl acetate copolymer, *Chem. Mater*. 13, 3830-3832.

Bellucci, F., Camino, G., Frache, A., Ristori, V., Sorrentino, L., Iannace, S.,Bian, X., Guardasole, M., Vaccaro, S., 2006. Effect of organoclay impurities on mechanical properties of EVA-layered silicate nanocomposites, e-Polymers 014, 1-10.

Beyer, G., 2002. Nanocomposites: a new class of flame retardants for polymers, *Plastics Additives & Compounding* 4(10), 22-28.

Brown, G., Brindley, G., 1980. Crystal structure of clay minerals and their X-ray identification, Mineralogical Society, London, Monograph 5, 305-360.

Camargo, P., Satyanarayana, K., Wypych, F., 2009. Nanocomposites: synthesis, structure, properties and new application opportunities, *Mat. Res*. 12(1), 1-39.

Calderon, J., Lennox, B., Kamal, M., 2008. Thermal stable phosphonium-montmorillonite organoclays, *Appl. Clay Sci*. 40, 90-98.

Chacko, A., Sadiku, E., Vorster, O., 2009. The rheological and mechanical properties of ethylene-vinyl acetate (EVA) copolymer and organoclay nanocomposites, *J. Reinf. Plast. Comp.* 29, 558-570.

Chaudhary, D., Prasad, R., Gupta, R., Bhattacharya, S., 2005a. Morphological influence on mechanical characterisation of ethylene-vinyl acetate copolymer-clay nanocomposites, *Polym. Eng. Sci.* 45 (7), 889-897.

Chaudhary, D., Prasad, R., Gupta, R., Bhattacharya, S., 2005b. Clay intercalation and influence on crystallinity of EVA-based clay nanocomposites, *Thermochim. Acta* 433 (1-2), 187-195.

Coates, J., 2000. Interpretation of infrared spectra, A practical approach. In: Meyers, R. (Ed.), *Encyclopedia of Analytical Chemistry*, Chichester, Wiley, 10815-10837.

Costache, M., Jiang, D., Wilkie, C., 2005. Thermal degradation of ethylene-vinyl acetate copolymer nanocomposites, *Polymer* 46, 6947-6958.

Cser, F., Bhattacharya, S., 2003. Study of the orientation and the degree of exfoliation of nanoparticles in poly(ethylene-vinyl acetate) nanocomposites, *J. Appl. Polym. Sci*. 90, 3026-3031.

Cui, L., Ma, X., Paul, D., 2007. Morphology and properties of nanocomposites formed from ethylene-vinyl acetate copolymers and organoclays, *Polymer* 48, 6325-6339.

Dal Castel, C., Bianchi, O., Oviedo, M., Liberman, S., Mauler, R., Oliveira, R., 2009. The influence of interfacial agents on the morphology and viscoelasticity of PP/MMT nanocomposites, *Mat. Sci. Eng. C* 29 (2009) 602-606.

De Paiva, L., Morales, A., Diaz, F., 2008. Organoclays: Properties, preparation and applications, *Appl. Clay Sci*. 42, 8-24.

Duquesne, S., Jama, C., Le Brasa, M., Delobelb, R., Recourtc, P., Gloaguen, J., 2003. Elaboration of EVA-nanoclay systems-characterization, thermal behaviour and fire performance, Composites Science and Technology 63, 1141-1148.

Filippi, S., Paci, M., Polacco, G., Dintcheva, N., Magagnini, P., 2011. The interlayer spacing collapse of Cloisite® 30B organoclay, Polymer Degradation and Stability 96(5), 823-832.

Fischer, H., 2003. Polymer nanocomposites: From fundamental research to specific applications, *Mater. Sci. Eng. C* 23, 763-772.

Fornes, T., Yoon, P., Hunter, D., Keskkula, H., Paul, D., 2002. Effect of organoclay structure on nylon 6 nanocomposite morphology and properties, *Polymer* 43, 5915-5933.

Frost, R., Kloprogge, J., 2000. Vibrational spectroscopy of ferruginous smectite and nontronite, *Spectrochim. Acta A* 56, 2177-2189.

Garcia-Lopez, D., Picazo, O., Merino, J., Pastor, J., 2003. Polypropylene-clay nanocomposites: Effect of compatibilizing agents on clay dispersion, *Europ. Polym. J.* 39, 945-950.

Goldstein, A., Beer, M., 2004. Exfoliable organo-montmorillonite nano-fillers for polymer/ceramic composites, *J. Europ. Ceram. Soc.* 24, 3187-3194.

Greene-Kelly, R., 1955. Dehydration of the montmorillonite minerals. *Mineral Mag*. 228.

Gupta, R., Pasanovic-Zujo, V., Bhattacharya, S., 2005. Shear and extensional rheology of EVA/layered silicate-nanocomposites, *J. Non-Newtonian Fluid Mech*. 128, 116-125.

Guven, N., Grim, R., 1972. X-ray diffraction and electron optical studies on smectite and α-cristobalite associations, *Clays Clay Miner.* 20, 89-92.

Hang, P., Brindley, G., 1970. Methylene blue absorption by clay minerals. Determination of surface areas and cation exchange capacities (clay-organic studies xviii), *Clays Clay Miner*. 18, 203-212.

He, H.; Frost, R., Zhu, J., 2004. Infrared study of $HDTMA^+$ intercalated montmorillonite, *Spectrochim. Acta A* 60, 2853.

He, H., Frost, R., Bostrom, T., Yuan, P., Duong, L., Yang, D., Xi, Y., Kloprogge, T., 2006. Changes in the morphology of organoclays with $HDTMA^+$ surfactant loading, *Appl. Clay Sci*. 31, 262-271.

He, H., Ma, Y., Zhu, J., Yuan, P., Qing, Y., 2010. Organoclays prepared from montmorillonites with different cation exchange capacity and surfactant configuration, *Appl. Clay Sci*. 48, 67.

Hedley, C., Yuan, G., Theng, B., 2007. Thermal analysis of montmorillonites modified with quaternary phosphonium and ammonium surfactants, *Appl. Clay Sci*. 35, 180-188.

Hongping, H., Ray, F., Jianxi, Z., 2004. Infrared study of $HDTMA^+$ intercalated montmorillonite. *Spectrochim. Acta* 60, 2853-2859.

Janek, M., Lagaly, G., 2003. Interaction of a cationic surfactant with bentonite: A colloid chemistry study, *Colloid Polym. Sci*. 281, 293-301.

Jeon, C., Ryu, S., Chang, Y., 2003. Preparation and characterization of ethylene vinyl acetate copolymer/montmorillonite nanocomposite, *Polym. Int*. 52, 153-157.

Joseph, S., Focke, W.W., 2011. Poly (ethylene-vinyl co-vinyl acetate)/clay nanocomposites: Mechanical, morphology and thermal behavior.*Polym. Comp.*, 32(2), 252-258.

Klapyta, Z., Fujita, T., Iyi, N., 2001. Adsorption of dodecyl- and octadecyl trimethyl ammonium ions on a smectite and synthetic micas, *Appl. Clay Sci*. 19, 5-10.

Konta, J., 1980. Properties of ceramic raw materials. In: Bilke, W. E., Paetsch, D. (Eds), *Ceramic Monographs – Handbook of Ceramics,* Monograph 1.1.4, Freiburg, Germany, Verlag Schimdt GmbH.

Konta, J., 1995. Clay and man: Clay raw materials in the service of man, *Appl. Clay Sci*. 10, 275-335.

Kopka, H., Beneke, K., Lagaly, G., 1998. Anionic surfactants between double metal hydroxide layers, *J. Colloid Interf. Sci*. 123, 427-436.

Kornmann, X., Berglund, L., Sterte, J., 1998. Nanocomposites based on montmorillonite and unsaturated polyester, *Polym. Eng. Sci*., 38, 1351-1358.

Kwolek, T., Hodorowicz, M., Stadnicka, K., Czapkiewicz, J., 2003. Adsorption isotherms of homologous alkyl dimethyl benzyl ammonium bromides on sodium montmorillonite, *J. Colloid Interf. Sci*. 264, 14-19.

Lagaly, G., Weiss, A., 1970a. Anordnung und Orientierung kationischer Tenside auf Silicatoberflächen. II. Paraffinähnliche Strukturen bei den *n*-Alkylammonium-Schichtsilicaten mit hoher Schichtladung (Glimmer). *Kolloid-Z. u. Z. Polymere*237, 364-368.

Lagaly, G., Weiss, A., 1970b. Anordnung und Orientierung kationischer Tenside auf Silicatoberflächen. III. Paraffinartige Strukturen bei den *n*-Alkylammonium-Schichtsilicaten mit mittlerer Schichtladung (Vermiculite). *Kolloid-Z. u. Z. Polymere* 238, 485-493.

Lagaly, G., 1976. Kink-block and gauche-block structures of bimolecular films. *Angew. Chem. Int. Ed. Engl*. 15, 575-586.

Lagaly, G., 1986. Interaction of alkylamines with different types of layered compounds, *Solid State Ionics* 22, 43-51.

La Mantia, F., Tzankova Dintcheva, N., 2006. EVA copolymer-based nanocomposites: Rheological behavior under shear and isothermal and non-isothermal elongational flow, *Polym. Test*. 25, 701-708.

LeBaron, P., Wang, Z., Pinnavaia, T., 1999. Polymer-layered silicate nanocomposites: An overview, *Appl. Clay Sci.* 15, 11-29.

Lee, J., Lee, H., 2004. Characterization of organobentonite used for polymer nanocomposites, *Mater. Chem. Phys*. 85, 410-415.

Lee, H., Park, B., Choi, H., Gupta, R., Bhattachary, S., 2007. Preparation and rheological characteristics of ethylene-vinyl acetate copolymer/organoclay nanocomposites, J. Macromolecular Sci., Part B: Physics 46 B (2), 261-273.

Li, Z., Jiang, W., 2009. A thermogravimetric investigation of alkylammonium intercalation into rectorite, *Thermochim. Acta* 483, 58.

Madejová, J., 2003. FTIR techniques in clay mineral studies, *Vib. Spectrosc*. 31, 1-10.

Marini, J., Branciforti, M., Lotti, C., 2009. Effect of matrix viscosity on the extent of exfoliation in EVA/organoclay nanocomposites, *Polym. Adv. Technol.* 21 (6), 408-417.

Martins, C., Larocca, N., Paul, D., Pessan, L., 2009. Nanocomposites formed from polypropylene/EVA blends, Polymer 50, 1743-1754.

Massinga Jr., P.,Focke, W., De Vaal, P., Atanasova, M., 2010. Alkyl ammonium intercalation of Mozambican bentonite, *Appl. Clay Sci*., 49, 142-148.

Massinga Jr., P.,Focke, W., 2012. Intercalating cationic surfactants in Koppies bentonite, *Mol. Cryst. Liq. Cryst.*, 555(1), 85-93.

Mezger, T. (2006). *Rheology Handbook: For Users of Rotational and Oscillatory Rheometers*, 2nd ed.,Hanover, Germany, Vicentz Network GmbH.

Montanari, G., Cavallini, A., Guastavino, F., Coletti, G., Schifani, R., Di Lorenzo Del Casale, M., Camino, G., Deorsola, F., 2004. Microscopic and nanoscopic EVA composite investigation: Electrical properties and effect of purification treatment, Annual Report - Conference on Electrical Insulation and Dielectric Phenomena, CEIDP, 318-321.

Pan, J., Yang, G., Han, B., Yan, H., 1997. Studies on interaction of dodecyltrimethylammonium bromide with Na- and Al-montmorillonite, *J. Colloid Interf. Sci.*194, 276-280.

Pasanovic-Zujo, V., Gupta, R., Bhattacharya, S., 2004. Effect of vinyl acetate content and silicate loading on EVA nanocomposites under shear and extensional flow, *Rheolog. Acta*43(2), 99-108.

Patel, H., Somani, R., Bajaj, H., Jasra, R., 2007. Preparation and characterization of phosphonium montmorillonite with enhanced thermal stability, *Appl. Clay Sci*. 35, 194-200.

Paul, D., Zeng, Q., Yu, A., Lu, G., 2005. The interlayer swelling and molecular packing in organoclays, *J. Colloid Interf. Sci*. 292, 462-468.

Paul, D., Robeson, L., 2008. Polymer nanotechnology: Nanocomposites, M. *Polymer*, 49, 3187-3204.

Pavlidou, S., Papaspyrides, C., 2008. A review on polymer-layered silicate nanocomposites, *Prog. Polym. Sci*. 33, 1119-1198

Peeterbroeck, S., Alexandre, M., Jérôme, R., Dubois, P., 2005. Poly(ethylene-co-vinyl acetate)/clay nanocomposites: Effect of clay nature and organic modifiers on morphology, mechanical and thermal properties, *Polym. Degrad. Stab*. 90(2 Spec. Iss.), 288-294.

Pereira de Abreu, D., Losada, P., Angulo, I., Cruz, J., 2007. Development of new polyolefin films with nanoclays for application in food packaging, Europ. Polym. J. 43, 2229-2243.

Perez, E., 1974. Modificaciones de las Pastas Ceramicas por Medio de Electrolitos y Coloides Protectores, Madrid, Instituto Eduardo Torroja de la Construccion y del Cemento, 51.

Pistor, V., Lizot, A., Fiorio, R., Zattera, A., 2010. Influence of physical interaction between organoclay and poly(ethylene-co-vinyl acetate) matrix and effect of clay content on rheological melt state, *Polymer* 51, 5165-5171.

Powell, C., Beall, G., 2006. Physical properties of polymer/clay nanocomposites, *Curr. Opin. Solid State Mater. Sci.*10, 73-80.

Prasad, R., Gupta, R., Cser, F., Bhattachary, S., 2006. Experimental investigation of the linear viscoelastic response of EVA-based nanocomposites, *J. App. Polym. Sci*. 101, 2127-2135.

Preschilla, N., Sivalingam, G., Rasheed, A., Tyagi, S., Biswas, A., Bellare, J., 2008. Quantification of organoclay dispersion and lamellar morphology in poly(propylene)-clay nanocomposites with small angle X-ray scattering, *Polymer* 49, 4285-4297.

Rehab, A., Salahuddin, N., 2005. Nanocomposite materials based on polyurethane intercalated into montmorillonite clay, *Mater. Sci. Eng. A* 399, 368-376.

Riva, A., Zanetti, M., Braglia, M., Camino, G., Falqui, L., 2002. Thermal degradation and rheological behaviour of EVA/montmorillonite nanocomposites, *Polym. Degrad. Stab*. 77(2), 299-304.

Sinha Ray, S., Okamoto, M., 2003. Polymer/layered silicate nanocomposites: A review from preparation to processing, *Prog. Polym. Sci*. 28, 1539-1641.

Shah, R., Hunter, D., Paul, D., 2005. Nanocomposites from poly(ethylene-co-methacrylic acid) ionomers: effect of surfactant structure on morphology and properties, *Polymer* 46, 2646-2662.

Shenoy, A. (1999). *Rheology of Filled Polymer Systems*. London, UK, Kluwer Academic.

Suh, I., Ryu, S., Bae, J., Chang, Y., 2004. Effects of compatibilizer on the layered silicate/ethylene vinyl acetate nanocomposite, *J. Appl. Polym. Sci*., 94, 1057-1061.

Szép, A., Szabó, A., Tóth, N., Anna, P., Marosi, G., 2006. Role of montmorillonite in flame retardancy of ethylene vinyl acetate copolymer, *Polym. Degrad. Stab*. 91, 593-599.

Tahani, A., Karroua, M., Van Damme, H., Levitz, P., Bergaya, F., 1999. Adsorption of a cationic surfactant on Na-montmorillonite: Inspection of adsorption layer by X-ray and fluorescence spectroscopies, *J. Colloid Interf. Sci.*216, 242-249.

Tian, Y., Yu, H., Wu, S., Ji, G., 2004. Study on the structure and properties of EVA/MMT nanocomposites, J. Materials Sci. 39, 4301-4303.

Tiwari, R., Khilar, K., Natarajan, U., 2008. Synthesis and characterization of novel organo–montmorillonites, *Appl. Clay Sci*. 38, 203-208.

Utracki, L., 2004. *Clay-Containing Polymeric Nanocomposites*. Vol. 1, Shawbury, UK, Rapra Technology Limited.

Vaccari, A., 1998. Preparation and catalytic properties of cationic and anionic clays, *Catal. Today* 41, 53-71.

Vaia, R., Teukolsky, R., Giannelis, E., 1994. Interlayer structure and molecular environment of alkylammonium layered silicates, *Chem. Mater*. 6, 1017-1022.

van Olphen, H., 1964. Internal mutual flocculation in clay suspensions, J. colloid sci. 19, 313-322

Velde, B., 1985. *Clay Minerals – A Physico-Chemical Explanation of their Occurrence,* Amsterdam, Elsevier.

Voyutsky, S., 1978. *Colloid Chemistry*, Moscow, Mir Publishers, 560.

Wagener, R., Reisinger, T., 2003. A rheological method to compare the degree of exfoliation of nanocomposites. *Polymer* 44, 7513-7518.

Wang, S., Hu, Y., Zong, R., Tang, Y., 2004. Preparation and characterization of flame retardant ABS/montmorillonite nanocomposites, *Appl. Clay Sci*. 25, 49-55.

Xi, Y., Ding, Z., He, H., Frost, R., 2004. Structure of organoclays – An X-ray diffraction and thermogravimetric analysis study, *J. Colloid Interf. Sci*., 277, 116.

Xi, Y., Martens, W., He, H., Frost, R., 2005. Thermogravimetric analysis of organoclays intercalated with the surfactant octadecyl trimethyl ammonium bromide, *J. Therm. Anal. Calorim.*, 81, 91.

Xie, W., Gao, Z., Liu, K., Pan, W., Vaia, R., Hunter, D., Singh, A., 2001. Thermal characterization of organically modified montmorillonite, *Thermochim. Acta* 367-368, 339-350.

Xu, S., Boyd, S., 1995. Cationic surfactant adsorption by swelling and nonswelling layer silicates, *Langmuir*, 11, 2508-2514.

Yui, T., Yoshida, H., Tachibana, H., Tryk, D., Inoue, H., 2002. Intercalation of polyfluorinated surfactants into clay minerals and the characterization of the hybrid compounds, *Langmuir* 18, 891-896.

Zanetti, M., Camino, G., Thomann, R., Mülhaupt, R., 2001. Synthesis and thermal behaviour of layered silicate-EVA nanocomposites, *Polymer* 42(10), 4501-4507.

Zhang, W., Chen, D., Zhao, Q., Fang, Y., 2003. Effects of different kinds of clay and different vinyl acetate content on the morphology and properties of EVA/clay nanocomposites, *Polymer* 44 (26), 7953-7961.

Zhang, F., Sundararaj, U., 2004. Nanocomposites of ethylene-vinyl acetate copolymer (EVA) and organoclay prepared by twin-screw melt extrusion, *Polym. Comp.* 25(5), 535-542.

Zhu, R., Zhu, L., Zhu, J., Xu, L., 2008. Structure of cetyltrimethylammonium intercalated hydrobiotite, *Appl. Clay Sci*. 42, 224-231.

APPENDICES

Appendix A.1

The cation exchange capacity (CEC) of KP, from South Africa, is 0.85 meq/g of dry clay. The CEC of Mozambican BP clay is 0.70 meq/g of dry clay. These CECs were used to calculate the amount of each intercalating agent for intercalation experiments. The mass of organic cation (OC) equivalent to these clay CECs was calculated as follows:

$$\text{m OC (g)} = \text{Clay CEC (meq)} * \frac{1\,\text{eq}}{1000\,\text{eq}} * \frac{1\,\text{mol OC}}{1\,\text{eq OC}} * \frac{\text{M (g/mol) OC}}{1\,\text{mol OC}}$$

Where: m = mass; M = molar mass

Example

This example corresponds to the calculation for preparing KSC14 (Koppies slurry and quaternary ammonium salt SC14 (M = 336 g/mol). The CEC is 0.85 meq/g of dry clay.

$$m_{SC14} = 0.85\,\text{meq} * \frac{1\,\text{eq}}{1000\,\text{eq}} * \frac{1\,\text{mol C14TAB}}{1\,\text{eq C14TAB}} * \frac{336\,\text{g/mol C14TAB}}{1\,\text{mol C14TAB}} = 0.29\,\text{g}$$

The calculated mass of SC14 is equivalent to the CEC of 1 g of dry clay. However, for the synthesis of KSC14 an amount of clay slurry comprising 94.7 g of dry clay instead of 1 g was used. Therefore, the mass of SC14 required for 94.7 g of dry clay was:

$$m_{SC14} = 94.7 * 0.29 \text{ g SC14} = 27.45 \text{ g}$$

A mass of SC14 1.5 times the equivalent of the clay CEC was used instead of 27.45 g SC14.

$$M_{SC14\ (excess\ 50\%)} = 1.5 * 27.45 \text{ g C14TAB} = 41.2 \text{ g}$$

Since the intercalation experiments did not use dry clay, but clay slurry, it was necessary to calculate the amount of KS comprising 94.7 g of dry clay. In Figure 1, the solid content of

South African clay slurry KS was determined as 18.9 mass %. Therefore, the amount of clay slurry containing 94.7 g of dry clay was calculated as follows:

$$m_{KS} = \frac{94.7\text{g}}{0.189} = 501\,\text{g}$$

This mass of clay slurry was intercalated with 41 g of SC14, which is about 1.5 times the mass of organic cation equivalent to the clay's CEC.

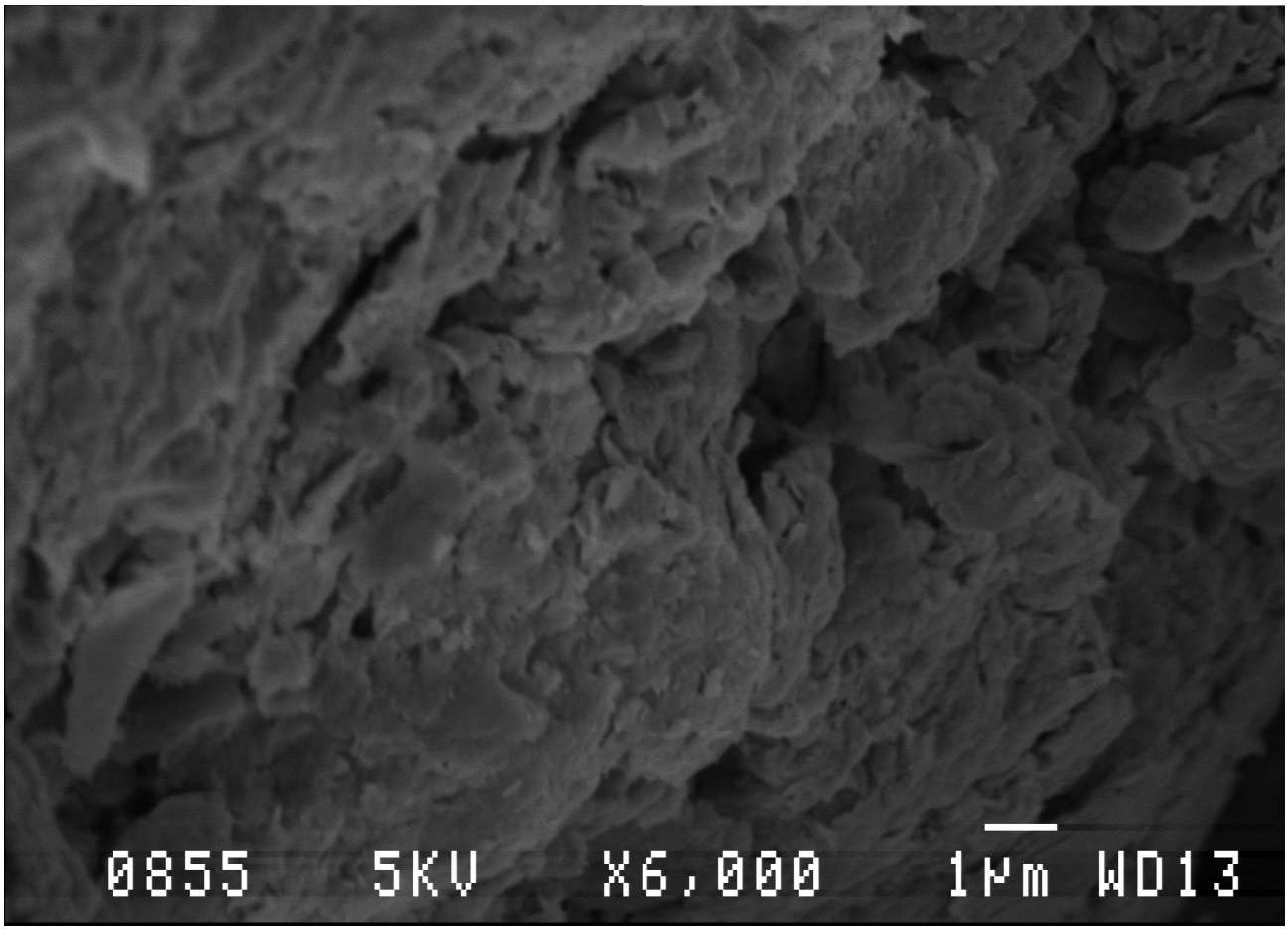

Figure A.1. Representative low-resolution SEM micrograph of organobentonite KSC14 revealed flake-shape particles

Table A.1. Summary of EVA melt intercalated with layered silicates in reviewed works

VA content (%)	MFI[a] (g/10 min)	Melting temperature (^oC)	Density g/cm^3	Reference
3	0.6	103[b]	(0.926[b])	Jeon et al., 2003
6	1.8	n.i.	n.i.	Zhang & Sundararaj, 2004
8	1	94[b]	0.930[b]	Jeon et al., 2003
9	n.i.	n.i.	n.i.	Cser & Bhattacharya, 2003; Pasanovic-Zujo et al., 2004; Chaudhary et al., 2005a; Chaudhary et al., 2005b; Costache et al., 2005
	1.1	n.i.	n.i.	Zang & Sundararaj, 2004
9.3	2	100	0.930	Cui et al., 2007
12	0.5	96	0.936	Alexandre et al., 2001a; Zanetti et al., 2001
	1.1	90[b]	0.932[b]	Jeon et al., 2003
12	0.8	n.i.	n.i.	Zang & Sundararaj, 2004
	0.3	95	0.929	Marini et al., 2009
14	0.3	93	0.935	La Mantia & Tzankova Dintcheva, 2006
14	0.3	93	0.935	Filippi et al., 2011
15	1.6	95[b]	0.938[b]	Jeon et al., 2003
18	n.i.	n.i.	n.i.	Pasanovic-Zujo et al., 2004; Chaudhary et al., 2005a; Chaudhary et al., 2005b
	1.6	n.i.	n.i.	Zhang & Sundararaj, 2004

VA content (%)	MFI[a] (g/10 min)	Melting temperature (^oC)	Density g/cm^3	Reference
18	2.5	88	0.941	Prasad et al., 2006; Cui et al., 2007
	2	86	0.940	Martins et al., 2009
	150	73	0.937	Marini et al., 2009
19	0.65	84	0.942	Alexandre et al., 2001a; Zanetti et al., 2001; Riva et al., 2002; Duquesne et al., 2003
	2	n.i.	n.i.	Costache et al., 2005
19	0.65	84	0.942	Bellucci et al., 2006
	2.1	86	0.940	Marini et al., 2009;
19	8	n.i.	n.i.	Marini et al., 2009
22	2	81[b]	0.945[b]	Jeon et al., 2003
22	3	87[b]	0.944[b]	Jeon et al., 2003
26	4	73[b]	0.950[b]	Jeon et al., 2003
27	3	71	0.951	Alexandre et al., 2001a; Alexandre et al., 2001b Peeterbroeck et al., 2005
28	n.i.	n.i.	n.i.	Beyer, 2001; Cser & Bhattacharya, 2003; Zhang et al., 2003; Pasanovic-Zujo et al., 2004; Tian et al., 2004; Chaudhary et al., 2005a; Chaudhary et al., 2005b; Costache et al., 2005; Szép et al., 2006

VA content (%)	MFI[a] (g/10 min)	Melting temperature (^oC)	Density g/cm^3	Reference
	3	71[b]	0.950[b]	Jeon et al., 2003
	3, 6, 25, 43, 150	n.i.	n.i.	Zhang & Sundararaj, 2004
	25	70	0.950	Gupta et al., 2005; Prasad et al., 2006
28	3	73	0.951	Cui et al., 2007
	150	68	0.950	Joseph & Focke, 2011
	2-3	100	0.920	Chacko et al., 2009
	24	73	0.947	Pistor et al., 2010
	25	70	0.921	Marini et al., 2009
	400	60	0.951	Joseph & Focke, 2011
40	n.i.	n.i.	n.i.	Zhang et al., 2003
	3	58	0.967	Cui et al., 2007; Lee et al., 2007
50	n.i.	n.i.	n.i.	Zhang et al., 2003
80	n.i.	n.i.	n.i.	Zhang et al., 2003

[a)] =measured at 190^o C under 2.16 kg load; [b)] = as indicated by the supplier; n.i. = not indicated

Table A.2. Summary of layered silicates and organic modifiers used in reviewed works

Code	Silicate mineral	CEC (meq/100 g)	Organic modifier	d_{001}, nm	Reference
OC_1	MMT	80–95	$(CH_3)_2N^+(HTallow)_2$	3.19 2.57	Alexandre et al., 2001a; Peeterbroeck et al., 2005;
OC_2	MMT	80–95	$(CH_3)_2[CH_3CH(CH_3CH_2)(CH_2)_4N^+(HTallow)$	2.07	Alexandre et al., 2001a; Peeterbroeck et al., 2005;
OC_3	MMT	80–95	$H_3N^+(CH_2)_{11}COOH$	1.63	Alexandre et al., 2001a
OC_4	MMT	80–95	$(CH_3)_3N^+(CH_2)_{21}COOH$	2.0	Alexandre et al., 2001a
OC_5	MMT	92	$(CH_3)_2N^+[(CH_2)_{17}CH_3]_2$	n.i.	Alexandre et al., 2001b
OC_6	MMT	n.i.	$(CH_3)_2N^+[(CH_2)_{17}CH_3]_2$	n.i.	Beyer, 2001
OC_7	FH	70–80	$H_2N(CH_2)_{11}COOH$	n.i.	Zanetti et al., 2001; Riva et al., 2002;
OC_8	FH	n.i.	$H_3N^+(CH_2)_{17}CH_3$	n.i.	Zanetti et al., 2001; Riva et al., 2002;
OC_9	MMT	n.i.	$H_3N^+(CH_2)_{17}CH_3$	n.i.	Zanetti et al., 2001
OC_{10}	MMT	n.i.	$(CH_2CH_2OH)_2N^+CH_3(Tallow)$	1.80	Riva et al., 2002; Costache et al., 2005; Cui et al., 2007

Code	Silicate mineral	CEC (meq/100 g)	Organic modifier	d_{001}, nm	Reference
OC_{11}	MMT	n.i.	$(CH_2CH_2OH)_2N^+CH_3(Tallow)$	1.88–1.84	Duquesne et al., 2003 Chaudhary et al., 2005a; Chaudhary et al., 2005b; Peeterbroeck et al., 2005; Prasad et al., 2006; Lee et al., 2007 Martins et al., 2009; Marini et al., 2009; Pistor et al., 2010;
OC_{11}	MMT	n.i.	$(CH_2CH_2OH)_2N^+CH_3(Tallow)$	1.88–1.84	Filippi et al., 2011
OC_{12}	MMT	n.i.	$(CH_3)_2N^+(HTallow)_2$	3.6	Riva et al., 2002
OC_{13}	MMT	85	$(CH_3)_3N^+(CH_2)_{15}CH_3$	1.96	Cser & Bhattacharya, 2003;
OC_{14}	MMT	n.i.	$(CH_2CH_2OH)_2N^+CH_3(CH_2)_{17}CH_3$	0.872	Jeon et al., 2003
OC_{15}	MMT	n.i.	$(CH_3)_2N^+[(CH_2)_{17}CH_3]_2$	2.239	Jeon et al., 2003
OC_{16}	MMT	n.i.	$(CH_3)_2(C_6H_5CH_2)N^+(CH_2)_{17}CH_3$	1.002	Jeon et al., 2003
OC_{17}	MMT	n.i.	$(CH_3)_2[CH_3CH(CH_3CH_2)(CH_2)_4N^+(CH_2)_{17}CH_3$	1.103	Jeon et al., 2003
OC_{18}	MMT	n.i.	$(CH_3)_3N^+(CH_2)_{17}CH_3$	1.983	Zhang et al., 2003
OC_{19}	MMT	n.i.	$(CH_3)_2N^+[(CH_2)_{17}CH_3]_2$	3.617	Zhang et al., 2003

Code	Silicate mineral	CEC (meq/100 g)	Organic modifier	d_{001}, nm	Reference
OC_{20}	MMT	n.i.	$CH_3N^+[CH_2)_{15}CH_3]_3$	3.723	Zhang et al., 2003
OC_{21}	MMT	n.i.	$(CH_3)_2N^+(HTallow)_2$	3.52	Chaudhary et al., 2005a;
OC_{21}	MMT	n.i.	$(CH_3)_2N^+(HTallow)_2$	3.52	Chaudhary et al., 2005b
OC_{22}	FH	70-80	$(CH_3)_2N^+(HTallow)_2$	4.55	Montanari et al., 2004; Bellucci et al., 2006
OC_{23}	MMT	85	$(CH_3)_2(CH_3CH_2)N^+(CH_2)_{15}CH_3$	2.00	Pasanovic-Zujo et al., 2004
OC_{24}	MMT	100	$H_3N^+(CH_2)_{17}CH_3$	2.01	Tian et al., 2004
OC_{25}	MMT	n.i.	$(CH_3)_2N^+(HTallow)_2$	2.4–2.7	Zhang and Sundararaj, 2004; Cui et al., 2007; Martins et al., 2009
OC_{26}	MMT	85	$(CH_3)_2(CH_3CH_2)N^+(CH_2)_{15}CH_3$	2.1	Gupta et al., 2005
OC_{27}	H	n.i.	$(CH_2CH_2OH)_2N^+CH_3(Tallow)$	2.1	Costache et al., 2005
OC_{28}	MG	n.i.	$(CH_2CH_2OH)_2N^+CH_3(Tallow)$	3.5	Costache et al., 2005
OC_{29}	FH	n.i.	$(CH_3)_2N^+(HTallow)_2$	3.11	Peeterbroeck et al., 2005
OC_{30}	MMT	n.i.	$(CH_3)_2N^+(Tallow)_2$	3.1–3.2	Montanari et al., 2004 Peeterbroeck et al., 2005; Bellucci et al., 2006; La Mantia & Tzankova Dintcheva, 2006

Code	Silicate mineral	CEC (meq/100 g)	Organic modifier	d_{001}, nm	Reference
OC_{31}	MMT	n.i.	$(CH_3)_2N^+(HTallow)_2$	2.24	Peeterbroeck et al., 2005
OC_{32}	MMT	n.i.	n.i.	1.82	Szép et al., 2006
OC_{33}	MMT	n.i.	$(CH_3)_3N^+(HTallow)$	1.8	Cui et al., 2007
OC_{34}	MMT	n.i.	$(CH_3)_2(C_6H_5CH_2)N^+(HTallow)$	1.865	Chacko et al., 2009

OC = organoclay; MMT = montmorillonite; FH = fluorohectorite; H = hectorite; MG = magadiite; n.i. = not indicated

Table A.3. Summary of equipment and parameters used to process the composites in reviewed works

Compounder/extruder	Temperature (°C)	Residence time (min)	Screw speed (rpm)	Reference
Two-roll mill (Agila)	160 EVA12) 130 (EVA19 & EVA27)	7	n.i	Alexandre et al., 2001a
Two-roll mill (Agila)	130	7	n.i.	Alexandre et al., 2001b
BUSS kneader	160	n.i.	n.i.	Beyer, 2001
Twin-screw minicompounder (DACA).	120	5 & 10	n.i.	Zanetti et al., 2001
Brabender	120	5	n.i.	Zanetti et al., 2001
Internal mixer (Brabender AEW330)	120±5	10	60	Riva et al., 2002
Twin-screw (Banbury)	80	40	70	Cser & Bhattacharya, 2003
Internal-mixer (Brabender Plasticorder PL2000)	160	n.i.	40/5/80	Duquesne et al., 2003
Mixer (Haake)	100	20	80	Jeon et al., 2003

Compounder/extruder	Temperature (°C)	Residence time (min)	Screw speed (rpm)	Reference
Rubber Mill	120	13	32 (3 min) & 64 (10 min)	Zhang et al., 2003
Leistriz ZSE27	140	n.i.	n.i.	Montanari et al., 2004
Twin-screw (Brabender)	80 (EVA28) & 90 (EVA18)	40	70	Pasanovic-Zujo et al., 2004
Twin-roll mill	120–125	10	n.i.	Tian et al., 2004
Twin-screw (Coperion, ZSK-25)	160	n.i.	200	Zhang & Sundararaj, 2004
Intermeshing counter-rotating twin-screw (Brabender)	110 (EVA9); 100 (EVA18 & EVA28)	25	70	Chaudhary et al., 2005a; Chaudhary et al., 2005b
Twin-screw (Brabender)	80	30	70	Gupta et al., 2005
Internal-mixer (Brabender Plasticorder)	120	20	60	Costache et al., 2005
Two-roll mill (AGILA)	140	12	15 m/s	Peeterbroeck et al., 2005
Internal mixer (Brabender)	125-130	3	60	Bellucci et al., 2006

Compounder/extruder	Temperature (°C)	Residence time (min)	Screw speed (rpm)	Reference
Single-screw (Brabender)	160	n.i.	60	La Mantia & Tzankova Dintcheva, 2006
Intermeshing counter-rotating twin-screw (Brabender)	160	n.i.	60	La Mantia & Tzankova Dintcheva, 2006
Twin-screw (Brabender)	100	n.i.	70	Prasad et al., 2006
Internal-mixer (Brabender Plasti Corder PL2000)	180	10	180	Szép et al., 2006
Intermeshing co-rotating twin-screw (Haake)	170	n.i.	280	Cui et al., 2007
Intermeshing counter-rotating twin-screw	110	25	70	Lee et al., 2007
Co-rotating twin-screw (Haake)	90–100	n.i.	280	Chacko et al., 2009
Twin-screw (B&P Process Equipment Systems)	195	n.i.	140	Martins et al., 2009

Compounder/extruder	**Temperature (°C)**	**Residence time (min)**	**Screw speed (rpm)**	**Reference**
Internal mixer (Haake Rheomix 600p)	150 150	5 (masterbatch) 5 nanocomposites)	120 120	Marini et al., 2009 Marini et al., 2009
Interpenetrating twin-screw co-rotating (MH-COR-20-32-LAB)	160	n.i.	400	Pistor et al., 2010
Static mixer (Brabender Plasticorder)	120	12.5	60	Fillippi et al., 2011
Two-roll mill	180	40	42	Joseph & Focke, 2011

Table A.4. Effect of processing equipment and conditions on dispersion of EVA composites

Nanocomposite	**Extruder/Compounder**	**Temperature (^oC)**	**Screw speed (rpm)**	**Reference**
EVA28 With OC_{11}	Counter-rotating intermeshing twin-screw	100	70	Chaudary et al., 2005a; Chaudary et al., 2005b
EVA28 with OC_{11}	Co-rotating interpenetrating twin-screw	160	400	Pistor et al., 2010
EVA14 with OC_{30}	Single screw	120–160	60	La Mantia & Tzankova Dintcheva, 2006
EVA14 with OC_{30}	Counter-rotating intermeshing twin-screw	120–160	60	La Mantia & Tzankova Dintcheva, 2006

Table A.5. Effect of organic modification of silicates on dispersion of EVA composites

Composite	Composite d_{001} (nm)	d_{002} (nm)	d_{003} (nm)	TEM results	O-clay load (mass %)	O-clay d_{001} (nm)	Reference
EVA9/OC_5	-	1.46	-	Int/exf & tactoids	5	1.820	Cui et al., 2007
EVA9/OC_{10}	4.41	Exists	-	Int & big tactoids	5	3.520	Chaudhary et al., 2005a
EVA9/OC_6	3.33	Exists	-	Int/exf & small tactoids	5	2.570	Cui et al., 2007
EVA9/OC_{25}	-	1.62	-	Tactoids	5	1.840	Cui et al., 2007
EVA18/OC_5	-	-	-	Int/exf & small tactoids	5	1.860	Chaudhary et al., 2005a
EVA18/OC_6	3.81	Exists	Exists	Int/exf & small tactoids	5	2.570	Cui et al., 2007
EVA19/OC_5	-	1.5	-	Exf & small tactoids	10	1.800	Riva et al., 2002
EVA19/OC_5	-	1.35	-	Exf & few tactoids	10	1.800	Duquesne et al., 2003
EVA19/OC_{4a}	-	1.4	-	Int/exf & small tactoids	10	2.000	Zanetti et al., 2001a
EVA19/OC_6	3.8	2	1.3	Int/exf & tactoids	10	3.600	Riva et al., 2002
EVA27/OC_5	-	Yes		Exf	5	1.800	Peeterbroeck et al., 2005
EVA27/OC_{23}	3.68	yes		Int/exf & tactoids	5	2.070	Peeterbroeck et al., 2005

Composite	Composite d_{001} (nm)	d_{002} (nm)	d_{003} (nm)	TEM results	O-clay load (mass %)	O-clay d_{001} (nm)	Reference
EVA27/OC_6	3.87	yes		Int/exf & tactoids	5	2.240	Peeterbroeck et al., 2005
EVA27/OC_{13}	4.02	yes		Int/exf & tactoids	5	2.900	Peeterbroeck et al., 2005
EVA28/OC_{19}	-	-	-	Exf & small tactoids	5	2.100	Gupta et al., 2002
EVA28/OC_1	4.4	yes	No	Int/exf & small tactoids	5	2.010	Tian et al., 2004
EVA28/OC_{27}	3.75	yes	Yes	Int & small tactoids*	5	2.620	Joseph and Focke, 2011
EVA28/OC_{13}	Yes	yes	Yes	Int/exf & small tactoids			Beyer, 2001
EVA28/OC_6	3.053	yes	Yes			2.293	Jeon et al., 2003

Int/exf = mixed morphology intercalated/exfoliated; * = Visualized in FESEM

Table A.6. Effect of VA content on dispersion of EVA composites

Composite	Composite d_{001} (nm)	d_{002} (nm)	d_{003} (nm)	TEM results	O-clay load (wt %)	O-clay d_{001} (nm)	Reference
EVA6/OC_6	3.2	Yes			2.5	2.500	Zhang and Sundararaj, 2004
EVA9/OC_6	3.5	Yes			2.5	2.500	Zhang and Sundararaj, 2004
EVA18/OC_6	3.81	Yes	Yes	Int/exf & small tactoids	5	2.570	Cui et al., 2007
EVA28/OC_6	3.85	Yes	Yes	Int/exf & small tactoids	5	2.570	Cui et al., 2007
EVA40/OC_6	4.18	Yes	Yes	Int/exf & small tactoids	5	2.570	Cui et al., 2007

Table A.7. Influence of composite structure on its mechanical properties

Material	Silicate content (%)	Internal structure	Modulus (MPa)	Strength (MPa)	Strain (%)	Reference
EVA27	0	-	12.1±1.2	28.4±0.7	1 406±28	Alexandre et al., 2001a
EVA27-OC_1	5	Int/exf	24.0±0.5	26.2±1.2	1 264±75	Alexandre et al., 2001a
EVA27-OC_2	5	Int/exf	23.1±1.0	27.0±0.8	1 341±16	Alexandre et al., 2001a
EVA27-OC_3	5	Int/exf	12.0±0.3	26.8±1.5	1 409±13	Alexandre et al., 2001a
*EVA15	0	-	58.8	15.7	800	Jeon et al., 2003
*EVA15-OC_{15}	2.5	Int***	80.4	14.7	760	Jeon et al., 2003
*EVA15-OC_{15}	5	Int***	94.1	14.2	756	Jeon et al., 2003
*EVA15-OC_{15}	7.5	Int***	101	12.7	711	Jeon et al., 2003
*EVA15-OC_{15}	10	Int***	109.8	11.3	678	Jeon et al., 2003
EVA6	0	-	84.5	-	1 146	Zhang & Sundararaj, 2004
EVA6-OC_{25}	2.5	Int***	97.7	-	946	Zhang & Sundararaj, 2004
EVA6-OC_{25}	5	Int***	113	-	600	Zhang & Sundararaj, 2004
EVA6-OC_{25}	10	Int***	127.2	-	36	Zhang & Sundararaj, 2004
EVA6-OC_{25}	20	Int***	152.4	-	18	Zhang & Sundararaj, 2004
*EVA9	0	-	8.6	15.6	-	Chaudhary et al., 2005a; Chaudhary et al., 2005b

Material	Silicate content (%)	Internal structure	Modulus (MPa)	Strength (MPa)	Strain (%)	Reference
*EVA9-OC_{11}	2.5	Int tactoid	54.3	7.8	-	Chaudhary et al., 2005a; Chaudhary et al., 2005b
*EVA9-OC_{11}	5	Int tactoid	64.3	8.9	-	Chaudhary et al., 2005a; Chaudhary et al., 2005b
*EVA9-OC_{11}	7.5	Int tactoid	74.3	9.4	-	Chaudhary et al., 2005a; Chaudhary et al., 2005b
*EVA18	0	-	5.7	13.3	-	Chaudhary et al., 2005a; Chaudhary et al., 2005b
*EVA18-OC_{11}	2.5	Int/exf	30	12.2	-	Chaudhary et al., 2005a; Chaudhary et al., 2005b
*EVA18-OC_{11}	5	Int/exf	34.3	15	-	Chaudhary et al., 2005a; Chaudhary et al., 2005b
*EVA18-OC_{11}	7.5	Int/exf	45.7	6.7	-	Chaudhary et al., 2005a; Chaudhary et al., 2005b
*EVA28	0	-	2.9	8.3	-	Chaudhary et al., 2005a; Chaudhary et al., 2005b
*EVA28-OC_{11}	2.5	Exf with small tactoids	8.6	5.3	-	Chaudhary et al., 2005a; Chaudhary et al., 2005b

Material	Silicate content (%)	Internal structure	Modulus (MPa)	Strength (MPa)	Strain (%)	Reference
*EVA28-OC_{11}	5	Exf with small tactoids	12.6	6.7	-	Chaudhary et al., 2005a; Chaudhary et al., 2005b
*EVA28-OC_{11}	7.5	Exf with small tactoids	17.1	5.6	-	Chaudhary et al., 2005a; Chaudhary et al., 2005b
EVA27	0	-	12.2±1.2	28.4±0.7	1406±28	Peeterbroeck et al., 2005
EVA27-OC_{31}	3	Int/exf & small tactoids	24.9±0.9	25.8±1.3	1231±46	Peeterbroeck et al., 2005
EVA27-OC_{2}	3	Int/exf & small tactoids	22.0±1.0	26.2±1.2	1259±25	Peeterbroeck et al., 2005
EVA27-OC_{11}	3	Int/exf & small tactoids	22.8±1.1	30.7±0.9	1266±24	Peeterbroeck et al., 2005
EVA27-OC_{1}	3	Int/exf & small tactoids	24.0±0.5	26.7±0.4	1291±45	Peeterbroeck et al., 2005
EVA27-OC_{29}	3	Int/exf & small tactoids	21.1±2.6	25.1±2.2	1270±51	Peeterbroeck et al., 2005
*EVA9.3	0	-	83.3	-	178.6	Cui et al., 2007
*EVA9.3-OC_{10}	1	Exf & small tactoids	91.7	-	174.2	Cui et al., 2007

Material	Silicate content (%)	Internal structure	Modulus (MPa)	Strength (MPa)	Strain (%)	Reference
*EVA9.3-OC_{10}	3	Exf & small tactoids	100	-	172.9	Cui et al., 2007
*EVA9.3-OC_{10}	5	Exf & small tactoids	125	-	160	Cui et al., 2007
*EVA9.3-OC_{10}	7	Exf & small tactoids	141.2	-	148.6	Cui et al., 2007
*EVA9.3-OC_{33}	1	Exf & small tactoids	79.2	-	174.2	Cui et al., 2007
*EVA9.3-OC_{33}	3	Exf & small tactoids	95.8	-	162.9	Cui et al., 2007
*EVA9.3-OC_{33}	5	Exf & small tactoids	104.2	-	157.1	Cui et al., 2007
*EVA9.3-OC_{33}	7	Exf & small tactoids	116.2	-	140	Cui et al., 2007
*EVA9.3-OC_{25}	1	Int/exf & small tactoids	112.5	-	170	Cui et al., 2007
*EVA9.3-OC_{25}	3	Int/exf & small tactoids	179.2	-	171.4	Cui et al., 2007

Material	Silicate content (%)	Internal structure	Modulus (MPa)	Strength (MPa)	Strain (%)	Reference
*EVA9.3-OC_{25}	5	Int/exf & small tactoids	250	-	151.4	Cui et al., 2007
*EVA9.3-OC_{25}	7	Int/exf & small tactoids	275	-	125.7	Cui et al., 2007
*EVA18	0	-	35.5	9.4	234.3	Cui et al., 2007
*EVA18-OC_{10}	1	Exf & small tactoids	45.2	-	242.9	Cui et al., 2007
*EVA18-OC_{10}	3	Exf & small tactoids	64.5	-	234.3	Cui et al., 2007
*EVA18-OC_{10}	5	Exf & small tactoids	90.3	-	234.3	Cui et al., 2007
*EVA18-OC_{10}	7	Exf & small tactoids	109.7	-	228.6	Cui et al., 2007
*EVA18-OC_{33}	1	Exf & small tactoids	38.7	-	251.4	Cui et al., 2007
*EVA18-OC_{33}	3	Exf & small tactoids	45.2	-	251.4	Cui et al., 2007

Material	Silicate content (%)	Internal structure	Modulus (MPa)	Strength (MPa)	Strain (%)	Reference
*EVA18-OC_{33}	5	Exf & small tactoids	58.1	-	257.1	Cui et al., 2007
*EVA18-OC_{33}	7	Exf & small tactoids	71.0	-	258.6	Cui et al., 2007
*EVA18-OC_{25}	1	Int/exf & small tactoids	51.6	10.1	257.1	Cui et al., 2007
*EVA18-OC_{25}	3	Int/exf & small tactoids	96.8	11.1	264.3	Cui et al., 2007
*EVA18-OC_{25}	5	Int/exf & small tactoids	161.3	11.9	248.6	Cui et al., 2007
*EVA18-OC_{25} *EVA18-OC_{25}	7 7	Int/exf & small tactoids	232.3 232.3	12.0 12.0	208.6 208.6	Cui et al., 2007 Cui et al., 2007
*EVA28	0	-	18	**	**	Cui et al., 2007
*EVA28-OC_{10}	1	Exf & small tactoids	21	**	**	Cui et al., 2007
*EVA28-OC_{10}	3	Exf & small tactoids	28.5	**	**	Cui et al., 2007

Material	Silicate content (%)	Internal structure	Modulus (MPa)	Strength (MPa)	Strain (%)	Reference
*EVA28-OC_{10}	5	Exf & small tactoids	36	**	**	Cui et al., 2007
*EVA28-OC_{10}	7	Exf & small tactoids	57	**	**	Cui et al., 2007
*EVA28-OC_{33}	1	Exf & small tactoids	19.5	**	**	Cui et al., 2007
*EVA28-OC_{33}	3	Exf & small tactoids	25.5	**	**	Cui et al., 2007
*EVA28-OC_{33}	5	Exf & small tactoids	36	**	**	Cui et al., 2007
*EVA28-OC_{33}	7	Exf & small tactoids	48	**	**	Cui et al., 2007
*EVA28-OC_{25} *EVA28-OC_{25}	1 1	Int/exf & small tactoids	24 24	** **	** **	Cui et al., 2007 Cui et al., 2007
*EVA28-OC_{25} *EVA28-OC_{25}	3 3	Int/exf & small tactoids	48 48	** **	** **	Cui et al., 2007 Cui et al., 2007
*EVA28-OC_{25}	5	Int/exf & small tactoids	72	**	**	Cui et al., 2007

Material	Silicate content (%)	Internal structure	Modulus (MPa)	Strength (MPa)	Strain (%)	Reference
*EVA28-OC_{25}	7	Int/exf & small tactoids	117	**	**	Cui et al., 2007
EVA28	0	-	7.1	4.05	454	Joseph & Focke, 2011
EVA28-OC_{25}	1	Int	7.8	4.10	483	Joseph & Focke, 2011
EVA28-OC_{25}	3	Int	10.9	4.13	473	Joseph & Focke, 2011
EVA28-OC_{25}	5	Int	15.8	4.46	475	Joseph & Focke, 2011
EVA28-OC_{25}	10	Int	20.1	3.80	391	Joseph & Focke, 2011
EVA28	0	-	3.96	1.62	374	Joseph & Focke, 2011
EVA28-OC_{25}	1	Int	4.2	1.68	427	Joseph & Focke, 2011
EVA28-OC_{25}	3	Int	5	1.7	508	Joseph & Focke, 2011
EVA28-OC_{25}	5	Int	5	1.7	509	Joseph & Focke, 2011
EVA19	0	-	43±1.1	25±0.5	820±22	Bellucci et al., 2006
EVA19-OC_{30}	5	Int	54±1.3	17±0.6	663±15	Bellucci et al., 2006
EVA19-OC_{22}	5	Exf	62±1.7	20±0.8	721±18	Bellucci et al., 2006

* = Estimated from graphs;** = Beyond instrument limit;***= Probed by XRD

Table A.8. Influence of composite structure on its steady shear rheological properties

Material	Silicate content (%)	Internal structure	η_0 (Pa.s)	T^a (^oC)	-n	G' (Pa)	Reference
EVA19	0	-		110		10^3	Riva et al., 2002
EVA19-OC_7	10	Tactoids		110		10^3	Riva et al., 2002
EVA19-OC_8	10	Int/exf		110		3.10^3	Riva et al., 2002
EVA19-OC_{10}	10	Int/exf		110		$1,5.10^4$	Riva et al., 2002
EVA19-OC_{12}	10	Int/exf		110		$1,9.10^3$	Riva et al., 2002
*EVA28	0	Int***					Pasanovic-Zujo et al., 2004
*EVA28-OC_{18}	3	Int***				10^9	Pasanovic-Zujo et al., 2004
*EVA28-OC_{18}	5	Int***					Pasanovic-Zujo et al., 2004
*EVA28-OC_{18}	10	Int***					Pasanovic-Zujo et al., 2004
*EVA28	0	-	4.10^3	130			Gupta et al., 2005
*EVA28-OC_{26}	2.5	Int***	$1,6.10^4$	130			Gupta et al., 2005
*EVA28-OC_{26}	5	Int***	4.10^4	130			Gupta et al., 2005
*EVA28-OC_{26}	7	Int***	9.10^4	130			Gupta et al., 2005
*EVA28-OC_{26}	10	Int***	$1,7.10^5$	130			Gupta et al., 2005
EVA14	0	-	$1,8.10^5$	160			La Mantia & Tzankova Dintcheva, 2006
EVA14-OC_{30}	5	Int tactoid	3.10^5	160	0.049		La Mantia & Tzankova Dintcheva, 2006
EVA14-OC_{30}	10	Int tactoid	$3,3.10^5$	160	0.058		La Mantia & Tzankova Dintcheva, 2006

Material	**Silicate content (%)**	**Internal structure**	**η_0 (Pa.s)**	**T^a (^oC)**	**-n**	**G' (Pa)**	**Reference**
EVA14	0	-	$1,6.10^5$	160			La Mantia & Tzankova Dintcheva, 2006
EVA14-OC_{30}	5	Int tactoid	$2,8.10^5$	160	0.042		La Mantia & Tzankova Dintcheva, 2006
EVA14-OC_{30}	10	-	$3,1.10^5$	160	0.054		La Mantia & Tzankova Dintcheva, 2006
*EVA28	0	-		130			Szép et al., 2006
*EVA28-OC_{32}	5	Int/exf	4.9	130	0.84		Szép et al., 2006
EVA40	0		$5,6.10^4$	130	0.62	3.10^3	Lee et al., 2007
EVA40-OC_{11}	2.5	-	$1,8.10^5$	130	0.49	$7,5.10^3$	Lee et al., 2007
EVA40-OC_{11}	5	Exf with small tactoids	4.10^5	130	0.34	$1,3.10^4$	Lee et al., 2007
EVA40-OC_{11}	7.5	Exf with small tactoids	$1,4.10^6$	130	0.25	$2,6.10^4$	Lee et al., 2007
EVA40-OC_{11}	10	Exf with small tactoids	$4,6.10^6$	130	0.22	$5,5.10^4$	Lee et al., 2007
EVA12	0	-	$5,5.10^5$	150	0.28		Marini et al., 2009
EVA12-OC_{31}	3	Int/exf & small tactoids	$6,6.10^5$	150	0.36		Marini et al., 2009
EVA19	3	Int/exf & small tactoids	4.10^4	150	0.02		Marini et al., 2009

Material	**Silicate content (%)**	**Internal structure**	**η_0 (Pa.s)**	**T^a (^oC)**	**-n**	**G' (Pa)**	**Reference**
EVA19-OC_{11}	3	Int/exf & small tactoids	10^5	150	0.08		Marini et al., 2009
EVA19	3	Int/exf & small tactoids	10^4	150	0.02		Marini et al., 2009
EVA19-OC_{29}	3	Int/exf & small tactoids	$4{,}2.10^4$	150	0.06		Marini et al., 2009
EVA28	0	-	$2{,}3.10^3$	150	0.02		Marini et al., 2009
EVA28-OC_{10}	1	Exf & small tactoids	$1{,}1.10^5$	150	0.46		Marini et al., 2009
EVA18	3	Exf & small tactoids	$2{,}4.10^2$	150	0.05		Marini et al., 2009
EVA18-OC_{10}	5	Exf & small tactoids	$3{,}8.10^4$	150	0.41		Marini et al., 2009
EVA19	0	-			0.22		Bellucci et al., 2006
EVA19-OC_{30}	5	Int			0.34		Bellucci et al., 2006
EVA19-OC_{22}	5	Exf			0.54		Bellucci et al., 2006
*EVA28	0	-	10^4	110		-	Prasad et al., 2006

Material	**Silicate content (%)**	**Internal structure**	**η_0 (Pa.s)**	**T^a (^oC)**	**-n**	**G' (Pa)**	**Reference**
*EVA28-OC_{11}	2.5	Exf & small tactoids	8.10^4	110	0.28	30	Prasad et al., 2006
*EVA28-OC_{11}	5	Int/exf & small tactoids	4.10^5	110	0.46	200	Prasad et al., 2006
*EVA28-OC_{11}	7.5	Int/exf & small tactoids	7.10^6	110	0.84	7.10^3	Prasad et al., 2006
*EVA18	0	-	$1,5.10^5$	110	0.25	-	Prasad et al., 2006
*EVA18-OC_{11}	2.5	Exf & small tactoids	$4,5.10^5$	110	0.33	100	Cui et al., 2007
*EVA18-OC_{11}	5	Exf & small tactoids	$1,2.10^6$	110	0.49	600	Prasad et al., 2006
*EVA18-OC_{11}	7.5	Exf & small tactoids	6.10^6	110	0.67	4.10^3	Prasad et al., 2006

η^o = Zero shear viscosity; T^a = Temperature; n = Shear thinning exponent; G'= storage modulus; *= Estimated from graphs

η^o and G' were taken at lower shear rates or frequencies

Table A.9. Influence of composite structure on its thermal properties

Material	Silicate content (%)	Internal structure	T_{max1} (°C)		T_{max2} (°C)		Reference
			Oxidative	Non-oxidative	Oxidative	Non-oxidative	
*EVA19	0	-	367	373	457	487	Beyer, 2001
*EVA28-OC_6	5		367	360	498	483	Beyer, 2001
EVA12	0				413		Zanetti et al., 2001
EVA12-OC_7	10				415		Zanetti et al., 2001
EVA12-OC_8	10				487		Zanetti et al., 2001
EVA12-OC_9	10				474		Zanetti et al., 2001
EVA19	0		335	348		468	Zanetti et al., 2001
EVA19-OC_7	10			348		468	Zanetti et al., 2001
EVA19-OC_8	10		288	283		479	Zanetti et al., 2001
EVA19-OC_9	10		335	296	475	468	Zanetti et al., 2001
*EVA19	0		332	350	423	464	Riva et al., 2002
*EVA19-OC_7	10		350	350	423	468	Riva et al., 2002
*EVA19-OC_8	10	Int/exf	293	284	477	470	Riva et al., 2002
*EVA19-OC_{10}	10	Int/exf	350	330	486	468	Riva et al., 2002
*EVA19-OC_{12}	10	Int/exf	350	350	486	457	Riva et al., 2002
EVA19	0		335		470		Duquesne et al., 2003
EVA19-OC_{11}	5		340		430		Duquesne et al., 2003

Material	Silicate	Internal	T_{max1} (°C)		T_{max2} (°C)		Reference
			Oxidative	Non-Oxidative	Oxidative	Non-Oxidative	
EVA19-OC_{11}	10		340		430, 470		Duquesne et al., 2003
*EVA27	0		352		448		Peeterbroeck et al., 2005
*EVA27-OC_1	3		352		490		Peeterbroeck et al., 2005
*EVA27-OC_{29}	3		352		504		Peeterbroeck et al., 2005
*EVA27-OC_{30}	3		352		476		Peeterbroeck et al., 2005
*EVA27	0		352		448		Peeterbroeck et al., 2005
*EVA27-OC_1	5		352		490		Peeterbroeck et al., 2005
*EVA27-OC_{29}	5		352		490		Peeterbroeck et al., 2005
*EVA27-OC_{30}	5		352		490		Peeterbroeck et al., 2005
*EVA28	0		341		458		Szép et al., 2006
*EVA28-OC_{32}	11		331		476		Szép et al., 2006

*Estimated from graphs

Table A.10. XRF analysis of major and trace elements in the bentonite samples

UNIVERSITEIT VAN PRETORIA
UNIVERSITY OF PRETORIA
YUNIBESITHI YA PRETORIA

XRF REPORT:

XRD & XRF Facility **Geology Department**

Direct Telephone: (012) 420-2137
Direct Telefax: (012) 420 2661 South Africa

CLIENT: Pedro

DATE: 12/03/08

ANALYSIS:

Should be considered semi-quantitative.

%	GSN Cert	GSN	KP	BP	KDC16	KDC10	KDC18>CEC	BSC14	BDC16	BDC10	BDC18>CEC	BDC18 >CEC
SiO_2	65.80	66.09	56.41	73.35	33.19	49.09	33.85	60.86	44.15	59.23	41.20	45.52
TiO_2	0.68	0.67	0.32	0.20	0.17	0.15	0.17	0.16	0.10	0.16	0.10	0.26
Al_2O_3	14.67	14.81	17.47	12.04	10.94	9.17	11.09	9.31	8.59	9.15	6.69	15.85
Fe_2O_3	3.75	3.73	5.00	2.47	3.13	1.11	3.10	1.83	1.40	1.81	1.42	5.25
MnO	0.06	0.05	0.13	0.03	0.03	0.00	0.03	0.01	0.00	0.00	0.01	0.05
MgO	2.30	2.19	3.74	2.43	2.21	1.39	2.20	1.29	1.54	1.26	0.96	3.14
CaO	2.50	2.46	2.53	0.13	0.42	0.00	0.45	0.00	0.32	0.00	0.06	0.70
Na_2O	3.77	3.76	0.32	0.78	0.07	0.57	0.04	0.02	0.80	0.14	0.49	0.05
K_2O	4.63	4.62	1.17	0.07	0.44	0.32	0.46	0.04	0.20	0.09	0.02	0.65
P_2O_5	0.28	0.28	0.15	0.00	0.47	0.01	0.43	0.01	0.01	0.01	0.00	0.62
Cr_2O_3	0.008	0.01	0.01	0.00	0.00	0.00	0.00	0.00	0.00	0.00	0.01	0.01
NiO	0.0043	0.01	0.00	0.01	0.00	0.00	0.00	0.00	0.00	0.00	0.02	0.01
V_2O_5	0.01	0.01	0.01	0.00	0.00	0.00	0.00	0.00	0.00	0.00	0.00	0.01
ZrO_2	0.03	0.02	0.02	0.05	0.01	0.04	0.01	0.05	0.04	0.05	0.12	0.04
LOI	1.32	1.29	10.72	7.65	47.75	37.58	48.51	25.89	43.05	27.04	49.47	28.69
TOTAL	99.82	100.0 0	97.99	99.22	98.85	99.44	100.36	99.47	100.21	98.96	100.56	100.85

ppm	GSNcert	GSN	KP	BP	KDC16	KDC10	KDC18>CEC	BSC14	BDC16	BDC10	BDC18>CEC	KSC14
As	1.6	3	3	3	3	4	3	228	6	7	3	5
Cu	20	27	10	9	11	13	8	121	37	95	66	11
Ga	22	20	20	23	11	14	11	22	11	16	10	17
Mo	1.2	1	1	1	1	1	1	1	1	1	1	1
Nb	21	20	25	92	5	10	5	64	66	61	37	15
Ni	34	38	13	9	8	11	8	23	15	15	10	9
Pb	53	52	34	21	5	11	8	3	11	18	13	15
Rb	185	182	52	3	18	23	17	58	2	2	2	31
Sr	570	578	150	36	30	34	27	3	3	3	3	66
Th	42	45	32	13	3	4	3	76	3	3	3	14
U	8	11	3	3	3	3	3	3	3	3	3	3
W*	450	543	6	10	6	6	6	8	8	8	6	6
Y	19	10	31	163	10	14	9	78	96	93	58	18
Zn	48	49	55	167	35	44	34	171	92	130	88	43
Zr	235	225	157	411	74	94	75	369	376	357	242	110
Cl*	450	692	697	5615	9560	4948	10916	114	13368	4329	19959	123
Co	65	69	6	2	7	167	8	2	2	3	2	14
Cr	55	57	7	7	7	7	7	7	7	7	7	24
F*	1050	2011	617	1328	611	837	668	1382	1451	1566	1431	100
S*	140	484	98	597	355	262	178	318	377	243	299	423
Sc	7	9	10	1	11	9	10	2	2	1	2	11
V	65	55	26	17	28	29	27	17	17	17	17	37
Cs	5	9	9	9	10	10	12	9	9	9	9	9
Ba	1400	1383	483	129	274	273	307	124	73	93	120	255

La	75	52	46	167	51	50	53	120	149	120	131	51
Ce	135	136	119	250	120	109	118	216	278	213	231	112

If you have any further queries, kindly contact the laboratory.

Analyst:

M.Loubser

SURFACTANT INTERCALATED KOPPIES AND BOANE BENTONITES FOR POLYMER NANOTECHNOLOGY

By

Pedro Horácio Massinga Júnior

Submitted in partial fulfilment of the requirements for the degree

Doctor Philosophiae

in the
Department of Chemistry
Faculty of Natural and Agricultural Sciences
University of Pretoria
Pretoria

December 2013

SYNOPSIS

This research aimed to develop technology and processes to further beneficiate two southern African bentonites for applications in polymer/clay nanotechnology. The bentonites were from the Koppies mine in South Africa, and the Boane mine in Mozambique. The work was divided into two parts: (i) preparation of organomodified nanoparticulate smectite clays, and (ii) preparation of their poly(ethylene-co-vinylacetate) nanocomposites.

Nanoparticulate organobentonites were prepared using purified bentonites. The conventional organomodification process uses a very low concentration of bentonites at 80 ^{o}C. In this study, a novel method was developed: concentrated slurries of naturally occurring Ca-bentonite partially activated with soda ash in the presence of a proprietary dispersant were contacted at ambient temperature with quaternary ammonium surfactants. A known amount of bentonite dispersion was placed in a planetary mixer before the mixture. Likewise, a known amount of surfactant, up to 50% excess, based on the estimated cation exchange capacity (CEC) of the bentonites, was added while mixing the dispersion. The surfactants added were either in solution or in powdered form. The intercalated bentonite was recovered by centrifugation and washed repeatedly with water until halide ions could not be detected using a 1M silver nitrate solution. The solids were dried at ambient temperature and humidity, and then crushed and milled into a fine powder using a mortar and pestle.

Several instrumental techniques were used to characterise and examine the properties of the bentonite samples before and after organic treatment.The X-ray diffraction (XRD) results were consistent with: (i) paraffin-type extended chain intercalation; and (ii) interdigitated monolayer intercalation of the C12 and C14 single-chain alkyl surfactants and bilayer intercalation of the single-chain C16 surfactant and the surfactants with double alkyl chains. Fourier transform infrared (FTIR) spectroscopy analysis of the organobentonite powders confirmed disordered chain conformations. XRD also detected significant amounts of cristobalite in the samples of Boane bentonite (from Mozambique). This impurity could not be removed cost-effectively. The onset decomposition temperature ofthe present organobentonites was around 200 ºC, which is within the typical range of polymer/organoclay processing temperatures. The thermal stability of the organobentonites was independent of both the number of alkyl chain substituents and their length, and also independent of the degree of clay intercalation.

Poly(ethylene-co-vinylacetate) nanocomposites were prepared with South African Koppies bentonite, organomodified with single-chain C12 (and polar 2-hydroxyethyl side chain) and double-chains C18 alkyl ammonium cationic surfactants. The later surfactant was intercalated both below and above the clay CEC. Nanocomposites were prepared by twin-screw melt compounding. Transmission electron microscopy (TEM) indicated the presence of mixed nano- and micron-sized clay morphologies. XRD studies revealed that the crystallinity of the particles improved and that the d-spacing values increased on incorporation of the modified bentonites in the polymer matrix. It is postulated that, rather than indicating polymer co-intercalation, this was caused by further intercalation of either excess surfactants or surfactant residues that were released by shear delamination of the clays during compounding. Improved mechanical properties were realised, especially when using the bentonite containing the longer double-chains surfactant intercalated at levels in excess of the CEC of the clay. The nanocomposites showed improved tensile modulus and elongation at break values at the expense of a reduction in impact strength, while tensile strength was about the same as for the neat polymer.

Keywords: Intercalation, exfoliation, organobentonite, poly(ethylene-co-vinylacetate), nanocomposites.

PUBLICATIONS GENERATED AS PART OF THIS RESEARCH

Massinga Jr, P., Focke, W., del Fabbro, O., Radusch, H., 2013. EVA nanocomposites based on South African Koppies clay, *Journal of Vinyl and Additive Technology*, accepted for publication.

Massinga Jr, P., Focke, W., 2012. Intercalating cationic surfactants in Koppies bentonite, *Molecular Crystals and Liquid Crystals*, 555:1, 85–93.

Merckel, R., Focke, W.; Sibanda, M.; Massinga Jr, P.; Crowther, N., 2012. Co-intercalation of insecticides with hexadecyltrimethylammonium chloride in Mozambican bentonite, *Molecular Crystals and Liquid Crystals*, 555:1, 76–84.

Massinga Jr, P., Focke, W., De Vaal, P., Atanasova, M., 2010. Alkyl ammonium intercalation of Mozambican bentonite, *Applied Clay Science* 49, 142–148.

AKNOWLEDGEMENTS

I am grateful to:

Prof. Walter W Focke, my advisor, for his suggestions. Walter, much of what is good in this thesis comes from you.

Mr Ollie del Fabbro and Mrs Suzette Seymore for their assistance during the course of this research.

Dan Molefe, Herminio Muiambo, Lumbi Moyo, Mthokozisi Sibanda, Nontete Nhlapo, Shepherd Tichapondwa and Washington Mikhe – my colleagues at the Institute of Applied Materials in the University of Pretoria. My folks, your tremendous support is gratefully acknowledged.

The National Research Foundation (NRF) for financial support via the Institutional Research Development Programme (IRDP) and the South Africa/Mozambique Collaboration Programme. G & W Base & Industrial Minerals for samples and technical support. The South African Council for Geoscience (Pretoria), the Laboratory for Microscopy and Microanalysis at the University of Pretoria, and the Center of Engineering Sciences at the Martin-Luther-Universität Halle-Wittenberg (German), all for technical support. The University Eduardo Mondlane, my employer, for giving me the opportunity to further my studies and for financial assistance.

Rose Massinga, my wife, for bringing out the best in me.

Jesus Christ – the Lord God Almighty. Dear Lord, your will always guides me to where your grace protects me. “Let all who take refuge in you be glad; let them ever sing for joy (Psalm 5:11).” Blessed be your glorious name.

DECLARATION

I, the undersigned, declare that the thesis that I hereby submit for the degree PhD at the University of Pretoria is my own work, and has not previously been submitted for a degree or examination at this or any other institution.

Pretoria, December 2013

Pedro Horácio Massinga Júnior

Table of contents

LIST OF FIGURES

LIST OF TABLES

LIST OF SYMBOLS AND ABBREVIATIONS

ASTM	American Society for Testing and Materials
BP	Boane powder
BS	Boane slurry
BSE	backscattered electron
CP-MS	cone-and-plate measuring system
CEC	cation exchange capacity (meq/100 g dry clay)
d_L or d_{001}	basal spacing of clay mineral particles (nm)
DMA	dynamic mechanical analysis
E' or G'	storage modulus (Pa)
E" or G"	loss modulus (Pa)
EVA	ethylene vinyl acetate
FESEM	field emission scanning electron microscopy
FTIR	Fourier transform infrared spectroscopy
KP	Koppies powder
KS	Koppies slurry
L/D	length per diameter
LVE	linear viscoelastic region
meq	milliequivalent
MFI	melt flow index (g/10 min at 190 ^{o}C/2.16 kg)
MMT	montmorillonite
pH	hydrogenionic potential
PLSN	polymer-layered silicate nanocomposite
rpm	revolutions per minute
SEM/BSE	scanning electron microscopy with backscattered electron
SEM/EDX	scanning electron microscopy fitted with an energy dispersive X-ray analyser
TEM	transmission electron microscopy
Tg	glass transition temperature
TGA	thermogravimetric analysis
T_{onset}	thermogravimetric decomposition onset temperature
T_{peak}	main decomposition step in thermogravimetric analysis
VA	vinyl acetate

XRD	X-ray diffraction
XRF	X-ray fluorescence

Greek Symbols

ε_{es}	interaction between EVA and silicate particles (J.mol^{-1})
ε_{ss}	interaction between silicateand silicate particles (J.mol^{-1})
η^*	complex viscosity (Pa.s)
λ	radiation wavelength (nm)
θ	angle between incident and scattered X-rays (^{o})
ω	angular frequency (rad.s^{-1})

CHAPTER 1 INTRODUCTION

1.1 Rationale

Widespread future application of clay minerals in automotive, electronic, food packaging and biotechnology polymer nanocomposites has been predicted (Konta, 1995; Wang et al., 2004; Rehab and Salahuddin, 2005). It is related to (i) the polymer property enhancement that can be obtained by addition of clay minerals at lower loadings of about 5 mass %, and (ii) the inherently low processing costs of clay minerals due to their natural abundance in nearly pure mineralogical form.

Smectite clays intercalated with alkylammonium cations are the organoclays most widely used to prepare polymer nanocomposites (Sinha Ray and Okamoto, 2003). When dispersed as high aspect ratio particles in the polymer matrix, organoclays enhance desirable properties (LeBaron et al., 1999; Alexandre and Dubois, 2000; Sinha Ray and Okamoto, 2003; Paul & Robeson, 2008; Pavlidou & Papaspyrides, 2008; Camargo et al., 2009). Such properties include strength and stiffness, dimensional stability, flame retardancy, gas barrier properties and UV stability, among others (LeBaron et al., 1999; Alexandre and Dubois, 2000; Fischer, 2003; Sinha Ray and Okamoto, 2003; Lee and Lee, 2004; Wang et al., 2004; Ahmadi et al., 2005; Patel et al., 2007).

The enhancement of polymeric properties requires exfoliation or at least significant delamination of clay platelets (Fornes et al., 2002). Exfoliated structures are those in which the clay platelets are delaminated and individually dispersed in the polymer matrix. When polymer chains and silicate layers alternate in a well-ordered multilayer arrangement with a well-defined and preserved interlayer distance, the structures are intercalated. In exfoliated nanocomposite structures, silicate platelets are interspaced extensively. Such extensive interlayer separations disrupt coherent layer stacking. The ordering of the resulting clay platelets is not sufficient to produce a scattering peak. Hence, a featureless XRD diffraction pattern is recorded.

Complete exfoliation of individual clay sheets is difficult to achieve in the absence of favourable interactions between the polar clay's surfaces and the matrix polymer (Alexandre

and Dubois, 2000).There is an intrinsic incompatibility between the hydrophilic clay surfaces and the hydrophobic polymer chains.

Matching the surface energies requires appropriate organic modification of the clays. This is usually accomplished by means of an intercalation process through ion exchange reactions. Inorganic cations in the clay interlayer space, e.g. Ca^{2+} or Na^{+}, can be directly exchanged with organic cations. The exchange can be partial or complete, and may even exceed the cation exchange capacity (CEC) of clays (Lagaly, 1986; Klapyta et al., 2001; Xu and Boyd, 1995).

Organic intercalation modifies the hydrophilic nature of clay surfaces to organophilic. Simultaneously, it expands the basal or d-spacing (d_{001}) of clays. Organic species frequently intercalated into clay minerals include quaternary alkylammonium salts, known as quats. Long-chain quats are preferred as they lead to larger interlayer spacing. This, in turn, facilitates further penetration of polymer chains into the clay interlayer space. In addition, large basal spacing maximises the configurational freedom of organosilicate chains dispersed in the polymer matrix. Thus, organosilicate chains gain entropy, balancing the entropy loss caused by polymer chain confinement in the nanocomposites.

The d_{001} of smectite minerals expands with increasing loading of cationic surfactants. A limiting d_{001} is realised at a certain critical surfactant loading, beyond which no further expansion occurs (Xi et al., 2005). This critical surfactant loading depends on the clay CEC. At the critical loading, the alkyl chain length of the surfactant determines maximum d_{001} (He et al., 2010). Increasing the chain length tends to increase the maximum d-spacing. Ultimately, it is the surfactant conformation, rather than its amount intercalated or its chain length that determines the maximum d-spacing (He et al., 2010). This does not detract from the roles that the amount of surfactant intercalated and its chain length play with regard to the d-spacing.

The effects of surfactant loading and its alkyl chain length on the d-spacing of organoclays, as well as the arrangement and state of the intercalated surfactants, have been the subject of numerous investigations (Xi et al., 2005). Quats with two long alkyl chains are preferred as they lead to a larger interlayer spacing (Zhang et al., 2003). This allows easy penetration of

polymer chains into the organoclay interlayer space during composite preparation. Consequently, further expansion, delamination and dispersion of organoclay particles in a polymer matrix are facilitated.

The most environmentally friendly method for the preparation of polymer nanocomposites is melt intercalation. The method is also versatile and compatible with current processing equipment. Melt intercalation consists of blending molten polymer matrices with clay minerals. Polymer chains may diffuse from the matrix into the silicate interlayer. Thermodynamic factors related to the surface energies of polymers and silicates are critical.

Conventionally, polymer chains should first intercalate into the silicate interlayers. Subsequently, the chains may push the silicate platelets further apart. Individual silicate particles may thus exfoliate into the polymer matrix. Delaminating silicate platelets and achieving exfoliation requires strong shear forces (Garcia-Lopez et al., 2003; Wang et al., 2004; Pavlidou & Papaspyrides, 2008). Exfoliation is a key requirement for improving polymer properties. It can lead to a very large surface area for the interaction of stiff silicate particles with polymer chains.

Alexandre and Dubois (2000) obtained partially intercalated and partially exfoliated nanocomposite morphologies with poly(ethylene-co-vinylacetate), EVA, even at low vinylacetate content (12 mass %). However, no nanocomposites were formed when organomontmorillonite (functionalised with dimethyl dioctadecyl ammonium) was melt compounded into high-density polyethylene.

EVA $\{–(CH_2CH_2)_n[CH_2CH(OCOCH_3)]_m– \}$ is a copolymer with polarity that can be tailored depending on its vinylacetate (VA) units. Higher content of VA [$–CH_2CH(OCOCH_3)–$] affords polarity for interaction with (OH groups of) pristine silicates (Gupta et al., 2005; Cui et al., 2007). However, good surface affinity between EVA and silicates alone is not enough to achieve exfoliation. Prior break-up and expansion of intrinsic silicate stacks is required. Break-up of the silicate stacks is, generally, achieved by mechanical shear forces during intercalation of surfactants into the silicate layers.

Silicate stacks are explained as follows: layered silicates comprise particles with thickness in the nanometric range; their aspect ratio is very large, exceeding 200; there is a propensity for the aggregation and packing of such particles due to the flat surface area. However, the intercalation of long-chain surfactants expands the silicate interlayers, facilitating the diffusion of polymer chains into them. This, in turn, promotes exfoliation of silicate platelets in polymer matrices. Ultimately, a large interfacial area for interaction between polymer chains and silicate particles is thus created.

Over the last decade, EVA copolymer melt intercalated with clay minerals has been extensively researched. Such studies have considered the influence of various parameters on the degree of dispersion of the clay in the polymer matrix and the ultimate physical properties. These parameters include the nature of the pristine clay (Zanetti et al., 2001; Riva et al., 2002; Costache et al., 2005; Peeterbroeck et al. 2005), the clay organomodifier (Alexandre and Dubois, 2000; Alexandre et al., 2001; Zanetti et al., 2001; Jeon et al., 2003; Zhang et al., 2003; Peeterbroeck et al., 2005), the vinyl acetate content of the polymer (Alexandre and Dubois, 2000; Alexandre et al., 2001; Zannetti et al., 2001; Cser & Bhattacharya, 2003; Jeon et al., 2003; Zang et al., 2003; Pasanovic-Zujo et al., 2004; Zhang and Sundararaj, 2004; Gupta et al., 2005; Cui et al., 2007; Marini et al., 2009), the processing techniques (Zhang and Sundararaj, 2004; Chaudary et al., 2005a; Chaudary et al., 2005b; La Mantia & Tzankova Dintcheva, 2006; Pistor et al., 2010), and the presence of external compatibilisers (Suh et al., 2004; Jeon et al., 2003).

To date, however, the preparation of fully exfoliated EVA-layered silicate nanocomposites remains elusive. Most authors have reported mixed morphologies comprising both intercalated tactoids and exfoliated sheets. Exfoliation was favoured using EVA grades with higher vinylacetate content (Zhang et al., 2003). Clays functionalised with alkyl substituent only are partially exfoliated, with the microstructure of the composites being dominated by an intercalated structure (Zhang et al., 2003, Peeterbroeck et al., 2005). Nanocomposites based on clay melt intercalated with methyl dihydroxyethyl hydrogenated tallow ammonium displayed the highest amount of exfoliation and clay stacking destruction, characterised by the absence of a characteristic X-ray diffraction (XRD) reflection (Peeterbroeck et al., 2005).

The present study considered whether a surfactant with only a single hydroxyethyl substituent would perform similarly to that containing dihydroxyethyl. Furthermore, most studies employed clays with surfactants intercalated at approximately the cationic exchange capacity. However, intercalation can proceed to higher levels and the effect of this on nanocomposite morphology and properties was also investigated in this study.

The suitability of organoclays for the preparation and performance of polymer nanocomposites is not limited to good surface affinity with polymer chains. Thermal stability of organoclays is also relevant: lower degradation onset temperatures limit the processing temperatures of the composites. The thermogravimetric decomposition onset temperature (T_{onset}) provides an indicator of the thermal stability of organoclays. A previous study recorded no effects of different lengths of quat surfactants on the thermal decomposition of organoclays (Xie et al., 2001). The present study investigated the effect of a number of substituents of quaternary alkylammonium surfactants on the thermal decomposition of organoclays. In addition, it examined the influence of the number and length of the long-chain alkyl substituents of the surfactant on the nature of the chains in the interlayer.

1.2 Objectives of current research

This study aimed at rendering bentonites from Boane (Mozambique) and Koppies (South Africa) suitable for the preparation of bentonite-based polymer nanocomposites. Further, Koppies organobentonites were incorporated into an EVA matrix. The specific objectives of this research were to:

- Examine the influence of the number and length of long-chain alkyl substituents of surfactants, as well as the surfactant loading, on the degree of clay intercalation and on the nature of the chains in the interlayer.
- Evaluate the effect of the number and length of substituents of quaternary alkylammonium surfactants and the degree of clay intercalation on the thermal decomposition of organobentonites.
- Determine the effects of the structure of the surfactant (single long chain with one polar 2-hydroxyethyl side group) and the degree of clay intercalation on the exfoliation behaviour and the ultimate physical properties of poly(ethylene-co-vinylacetate)-clay composites.

1.3 Dissertation outline

Chapter 1 is the introduction, in which the rationale for the research is explained, the aim of the work presented, and the dissertation structure outlined.

Chapter 2 reviews the literature: a background to clay minerals and its organic intercalation is provided; likewise, a background to polymers and its nanocomposites is provided. In addition, peer-reviewed works on melt intercalated nanocomposites of EVA with layered silicates published over the last decade are critically assessed.

Chapter 3 outlines the experimental design and presents the raw materials and the instruments that were available for laboratory work. The methods and procedures followed in the laboratory are also described in this chapter.

Chapter 4 analyses the experimental results and explains eventual modifications to the experimental design.

Chapter 5 presents the conclusions, and all the references used are listed in Chapter 6. Additional supporting information is given in the Appendix.

CHAPTER 2 LITERATURE REVIEW

2.1 Clay minerals and their intercalation chemistry

The use of inorganic materials as reinforcing fillers for polymeric materials is widespread. Filled polymers take advantage of hybrid properties synergistically derived from polymer materials (e.g. the easy processability) and from inorganic materials (e.g. high mechanical strength and high thermal resistance) (Rehab & Salahuddin, 2005).

Clay minerals have been extensively researched to reinforce polymer materials mechanically and thermally. There are about 30 different aluminosilicate-layered minerals comprising natural clays. Each of these phyllosilicates consists of lamellar elements. Its crystal structure consists of a stack of plate-shaped layers interspaced by an interlayer, also known as a gallery (Utracki, 2004). The smallest stack of layers could be about 10 nm thick (Pavlidou and Papaspyrides, 2008). The nanometric dimensions, coupled with the two-dimensional structure, make the clay minerals interesting reinforcing fillers for polymer materials. The large surface area of the flake morphology and its high aspect ratio aids the stiffness and contributes to high in-plane strength of the lamellar elements (Rehab & Salahuddin, 2005).

Of all layered clay minerals, those of the smectite group are most often used to prepare polymer nanocomposites. This is due to the group's relatively high swelling properties and high cation exchange capacity (CEC). The high swelling ability of the smectite minerals allows a huge expansion of its interlayers. This facilitates the separation of individual clay layers, allowing larger molecular structures to intercalate. In turn, the high CEC indicates the presence of a high number of exchangeable cations in the interlayer. This allows the smectite to exchange the hydrated interlayer cations with a high number and wide range of like-polarity chemical groups (Sinha Ray and Okamoto, 2003).

The clay minerals belonging to the smectite group include montmorillonite, vermiculite, beidellite, saponite, talc, nontrolite, sauconite and pyrophyllite. Their crystal structure consists of a layer comprising two tetrahedral sheets sandwiching one octahedral sheet. Each sheet, either tetrahedral or octahedral, is about 0.22 nm thick. In between the two layers lie Ca^{2+} and Na^{+} cations as well as water molecules. The minimum thickness of an individual smectite platelet (basal spacing) in its natural state is considered to be 0.96 nm. It includes,

besides the octahedral and tetrahedral sheets, a hydrated interlayer with a minimum thickness of 0.30 nm (corresponding to a water monolayer). The lateral dimensions of an individual smectite platelet are more than two orders of magnitude larger (Paul et al., 2005; Utracki, 2004; Vaccari, 1998). The aspect ratio is $p \leq 1000$, i.e. the largest dimension of the platelet is 1000 nm (Utracki, 2004; Powell & Beall, 2006).

The crystal layer unit-cell of smectite clay minerals is generally characterised by six octahedral sites and eight tetrahedral sites. The octahedral sheet may consist of central Al^{3+}, Mg^{2+} or Fe^{2+}cations coordinated by six oxygen atoms (Powell & Beall, 2006). Two of these oxygen atoms are bonded to hydrogen atoms, forming OH groups. Each tetrahedral sheet is formed from central Si^{4+}, Al^{3+} or Fe^{3+}cations coordinated by four oxygen atoms. One oxygen atom is shared between each octahedral and each tetrahedral site (Utracki, 2004).

Isomorphic substitutions within the tetrahedral and/or octahedral sheets of native smectite clays generate a negative charge in the clay layers. Within tetrahedral sheets, a certain number of Al^{3+} cations can replace the same number of Si^{4+} cations. In the octahedral sheet, Al^{3+}cations can be replaced by the same number of Mg^{2+}cations and, less frequently, by Fe^{2+}cations. The general chemical formula of smectite minerals, often reported on the basis of the half unit-cell content, is:

$$(M^{n+}_{x+y/n}\, nH_2O)(Al^{3+}_{2-y}\, M^{2+}_{y})O_2(OH)_2(Si^{4+}_{4-x}\, Al^{3+}_{x})O_8$$

In this formula, $M^{n+}_{x+y/n}\, nH_2O$ indicates hydrated cations of different valency counter balancing the negative charge on the surfaces to restore the electroneutrality of the clays. M^{2+}_{y} refers to the generic divalent cation of the clay structure. X indicates the layer charge resulting from substitutions in tetrahedral sites. The layer charge of octahedral sites is indicated by Y, while “n” indicates the number of water molecules hydrating the cations (Utracki, 2004).

Clay surface charge is not constant throughout the whole mineral crystal: it varies from layer to layer. However, its average value is considered over the entire crystal. It is this charge that

is known as the CEC of the clay, generally expressed in meq/100g (milliequivalents per hundred grams) of dry clay (Sinha Ray & Okamoto, 2003).

Alkali and/or alkaline earth cations are the most common ions within the gallery of cationic clays. The decreasing order of preferential adsorption of some common cations is: $H^+ > Al^{3+} > Ba^{2+} > Sr^{2+} > Ca^{2+} > Mg^{2+} > NH_4^+ > K^+ > Na^+ > Li^+$. This order parallels the increasing degree of hydration for these cations (Perez, 1974, Voyutsky, 1978, Konta 1980). The sequence indicates that, although Ca^{2+} is preferentially adsorbed in the gallery of cationic clays than Na^+, the latter is more highly hydrated than Ca^{2+}.

There are three modes of hydration, and they have been recognised as pH dependent: (i) hydration at internal surfaces (interlayer hydration) of clay mineral particles; (ii) continuous hydration of internal and external clay surfaces, due to unlimited adsorption of water; and (iii) capillary condensation of free water in micropores (Utracki, 2004).

The interlayer hydration consists of three main elements: (i) hydration of adsorbed cations; (ii) interaction of hydrated cations with the internal surfaces of the clay mineral; and (iii) water activity in the clay-water system. The interaction of hydrated cations with the surfaces of the clay mineral involves the inner sphere of hydration and/or the outer sphere of hydration. When one side of the interlayer cation is directly bound to the clay mineral surface and the other side is bound to a number of water molecules, an inner sphere of hydration is formed. Further, when the interlayer cation is completely surrounded by water molecules and interacts, through these ligands, with the clay mineral surface, it is recognised as the outer sphere of hydration. Adsorption of water initiates by solvation of the interlayer cations and is followed by occupancy of the remaining interlayer space (Utracki, 2004).

Due to water penetrating the interlayer molecular spaces and to concomitant adsorption, some smectites expand considerably more than others. The amount of expansion depends largely on the type of exchangeable cation contained in the mineral interlayer. Some factors affecting interlayer hydration are: (i) the hydration energy of the interlayer cation; and (ii) the water polarisation power of the interlayer cation.

Hydration energy of the cation is the energy change when a cation is solvated in water. The structure of a hydrated cation consists of water molecules surrounding the central cation. The water molecules arrange themselves with oxygen lone pairs of electrons oriented towards the positive cation charge. There is a greater solvent ordering around small cations than around large ions. The smaller the cationic radius, the closer the water molecules will be packed. However, fewer water molecules can be closely packed around a small ion than around a large one. Cations of small size and of high charge produce a more intense electrostatic field at their surfaces. Consequently, their water polarisation power is strong, the degree of hydration is greater, and they become less mobile. Therefore, the presence of sodium as the predominant exchangeable cation instead of calcium can result in the clay swelling to several times its original volume (Kornmann et al., 1998).

Swelling of smectites is strongly related to isomorphic substitutions since the basal oxygen atoms acquire an excess negative charge. Their electron-donating capacity increases whether the layer charge derives from substitution in the octahedral or tetrahedral sheets. This results in a strong tendency to form hydrogen bonds with water molecules, especially those coordinated to interlayer cations. Such water molecules are Lewis acids, which have a tendency to receive electrons. The preference for H-bonding is, however, higher for oxygen atoms substituted in tetrahedral sheets than in octahedral ones. This is because the basal surface oxygen atoms of a smectite are those of tetrahedral sheets. It is the swelling and the CEC properties that confer very rich intercalation chemistry on smectites (Rehab & Salahudin, 2005).

2.2 Organic intercalation of clay minerals

Individual layers of clay minerals are potentially the most suitable for the preparation of polymer layered silicate nanocomposites (PLSNs). A high aspect ratio of clay particles is an important factor in polymer property enhancement. Exfoliation of montmorillonite (MMT) layers in a polymer matrix leads to a very large interfacial surface area for interaction with the polymer chains. However, complete delamination of individual clay mineral layers into a polymer matrix is doubtful (Pavlidou and Papaspyrides, 2008).

Dispersion of neat clay particles is difficult owing to an intrinsic incompatibility between the hydrophobic polymer matrix and the hydrophilic clay mineral surfaces. Better matching of the surface polarities can be achieved by appropriate organic modification of the clays. This

is usually accomplished via ion exchange reactions (de Paiva et al., 2008). The inorganic cations in the clay interlayer space, e.g. Ca^{2+} or Na^{+}, can be directly exchanged with organic cations by means of an intercalation process. The substitution with organic cations can be partial or complete, and in some cases it may even exceed the CEC (Utracki, 2004; Zhu et al., 2008).

The adsorption of organic molecules by clay is influenced by the hydration state of the clay and the polarising power of the interlamellar cations. When interlayer water is present, the cohesion forces of the clay are greatly reduced and, consequently, penetration of the sorbate molecule is facilitated.

Intercalation of organic cations is an important first step in the preparation of PLSNs. The replacement of small inorganic cations from interlayers aims to (LeBaron et al., 1999; Alexandre & Dubois, 2000; Sinha Ray and Okamoto, 2003; Goldstein & Beer, 2004; Lee and Lee, 2004; Powell and Beall, 2006):

- impart an organophilic character to the clay surface; this provides an effective mechanism for attracting polymers of like polarity into the clay interlayer
- increase the interlayer distance; this provides accessibility for large molecules like polymers.

The interlayer distance of organomodified clays, and consequently, the size and type of polymeric molecule that can be further intercalated, depends decisively on the selection of the cationic surfactant. Utracki (2004) stated that a preferred intercalating agent should possess:

(i) good kinetics for diffusion into the interlayer
(ii) high bonding strength with clay platelets
(iii) strong interaction with the polymer matrix.

Quaternary ammonium salts (quats) are the most extensively used intercalants in commercially available organoclays. They behave like a compatibiliser, providing good stress transfer between the clay and the polymer. Quats are preferred for the following reasons (Utracki, 2004):

(i) Oxygen atoms on the clay surface are suited for hydrogen bonding with organic surfactants comprising nitrogen atoms. This satisfies the first and second criteria for the selection of a cationic surfactant.

(ii) They have potential for bonding with electron-deficient aluminium atoms on the clay surface. This bonding may occur via the Lewis acid/base mechanism. This non-ionic interaction provides good kinetics for the diffusion of quats into the interlayer.

(iii) They behave like a compatibiliser, providing good stress transfer between the clay and the polymer.

LeBaron et al. (1999) recommend selecting long-chain surfactants for increasing the interlayer distance to the extent that a monomer or pre-polymer can be intercalated or eventually exfoliated. Zhang et al. (2003) found that surfactants with two long alkyl chains are ideal for yielding organosilicates with wider basal spacing. Further, it was found that the hydrophilic/hydrophobic balance of an organoclay depends on the length and packing density of the alkyl chains (Utracki, 2004).

The effect of alkyl chain length and surfactant loading on the d-spacing of organoclays, as well as the arrangement and state of the intercalated surfactants, have been the subject of numerous investigations (Xi et al., 2005). It is well known that the d-spacing increases with increasing surfactant loading. The loading may exceed the CEC of the clay mineral. The maximum d-spacing is realised at a certain critical surfactant loading, beyond which no further expansion occurs (Xi et al., 2005). This critical surfactant loading depends on the CEC of the clay. At the critical loading, the surfactant's alkyl chain length influences the maximum d-spacing (He et al., 2010). Increasing the chain length tends to increase the maximum d-spacing. Ultimately, it is the surfactant conformation, rather than the amount intercalated or its chain length that essentially determines the d-spacing that can be achieved (He et al., 2010). This does not detract from the roles that the amount of surfactant intercalated and its chain length play with regard to the d-spacing.

Preparation and performance of clay-polymer composites does not depend only on larger interlayer spacing of organoclays. It is also affected by the thermal stability of organoclays: lower degradation onset temperatures limit the processing temperatures of the

nanocomposites. An indicator for the thermal stability of an organoclay is its thermogravimetric decomposition onset temperature, T_{onset}. A previous study concluded that different lengths of quat surfactants have no effect or very little effect on the thermal decomposition of organoclays (Xie et al., 2001). It would be interesting to determine whether surfactants with different numbers of alkylammonium chains affect the thermal stability of organoclays.

2.2 Generalities about polymers

Polymers are natural or synthetic compounds of high molecular mass (macromolecules). They contain at least one repeating structural unit in their chains, inter-linked by covalent bonds. Such a repeat unit is equivalent to that of the starting material from which the polymer is made, and is known as a *monomer*. In each covalent bond, inter-linked atoms share the electronic pair equally. The total number of repeat units determines the length of the polymer chains. In addition, the monomers determine the degree of polymerisation and define the molecular size/mass of the polymer.

A polymer that contains identical monomers is a *homopolymer.* However, if different kinds of monomer comprise the polymer, it is classified as a *copolymer*. Polymer chains may be linear or branched. The structure of a polymer with a linear chain is quite simple and flexible. It consists of monomers connected to no more than two other monomers. A polymer structure consisting of a chain with at least one side chain, with a monomer connected to more than two other monomers to form three-dimensional networks, is classified as *branched polymer*.

Polymer molecules that are chemically and geometrically regular in structure are typically crystalline. Chain branching and co-polymerisation cause occasional structural irregularities of polymers. Both limit the extent of crystallisation, though do not prevent its occurrence. Co-polymers with significant amounts of both monomers, or with quite different monomer constituents, are typically non-crystalline polymers. Other irregularities of structures caused by the size and the bulkiness of the substituent groups yield non-crystalline polymers. A polymer may have a structure that is intermediate in kind between crystalline and amorphous.

Polymers can also be classified as thermoplastic, thermoset or elastomeric. *Thermoplastic polymers* comprise linear chains with weak van der Waals intermolecular bonds. These can be easily broken when the polymer is heated and individual chains move freely. They

constitute the most common category of plastics, since they are recyclable. *Thermoset polymers* consist of cross-linked chains whose bonds do not break easily on heating. The cross-links break at high temperatures, when the covalent bonds between monomers tend to break simultaneously, degrading the polymer. Cross-links prevent individual chain flow and lessen interchain interactions. Thus, cross-linking enhances the mechanical strength of polymers. However, it also makes it difficult to recycle the polymer. *Elastomeric polymers* (elastomers) are an intermediate category between thermoplastics and thermosets. They are not hard as thermosets, but are likewise difficult to melt; they also degrade. Elastomers consist of a few cross-linked chains as compared with thermoset polymers.

The structure of a polymer decisively affects its physical properties and applications. The application of a polymer depends on its properties: mechanical, electrical, thermal and optical, among others. Generally, polymers possess low electrical and thermal conductivity, and low mechanical and thermal resistance. They can bear external pressure without fracture, and even return to their initial shape when the external pressure is removed.

Polymer matrices consist of polymer chains in an environment of similar chains. At low temperatures, polymer molecules do not have enough energy to move with respect to one another. They are ‘frozen’ in a hard and brittle solid state known as the *glass state*. In this state, polymers are crystalline, vibrate with low energy, and have properties like hardness, stiffness and brittleness. When heated, polymer molecules vibrate with enhanced energy; a transition occurs from the glass state to the *elastomeric state*. The temperature at which the polymer softens and the transition occurs is known as the *glass transition temperature*, Tg. Polymer interchain interactions may decrease when Tg is reached, and individual chains gain freedom to move and assume many different conformations. The movement of polymer segments results from their increased thermal energy. In the elastomeric state, polymer chains may adopt an ordered arrangement and their free volume increases. The thermal expansion and the elasticity of the polymer may also increase. When the polymer is heated above its Tg, it may melt. Thermoset polymers do not melt on heating, while thermoplastics melt on heating and re-solidify on cooling. The chain orientations and molecular weight affect the softening and melting properties of thermoplastics.

There are polymers that are usable below their softening temperature. Others exhibit better performance above the Tg. The properties of a polymer at a required temperature determine its choice for a particular application. Owing to the ability of thermoplastics to melt on heating and re-solidify on cooling, they are preferred for the preparation of polymer/clay composites via melt compounding.

2.3 Overview of some characterisation techniques for polymer-clay composites and their precursors

2.3.1 X-ray diffraction (XRD)

XRD is a powerful tool used for assessing the orderly arrangements of atoms and molecules. It is the single most commonly used technique for probing composite structure due to its ease of use and its availability.

X-rays are usually produced by bombarding a target metal inside a vacuum tube with a beam of high-voltage electrons. The wavelengths of the X-rays produced depend on the applied voltage and the target metal. The detection of diffracted X-rays is made possible by a radiation counter and electronic equipment feeding data to a computer. This detection method allows precise measurement of the intensity of the diffracted beam. However, the action of diffracted X-rays on photographic films may also be used for their detection. This method, in turn, allows qualitative examination of the diffraction pattern and accurate measurement of angles and distances.

X-rays of a given wavelength are diffracted for the same specific orientations of the sample. Randomly oriented, minute powdered particles will have all orientations of the particles investigated simultaneously and included within the sample; it is not possible to investigate orientations about one crystal axis at a time, as with a single crystal. Though analysis of randomly oriented, minute powdered particles is more convenient, it gives less information than investigation of a single crystal.

XRD is an analytical method based on the interaction of electromagnetic radiation with structures comparable in size to the wavelength of its radiation. Such interaction gives interference effects that are sharpened when the structures are arranged in a lattice with an orderly array of points. In this case, the radiation is diffracted or scattered only under specific

experimental conditions. It is the knowledge of these conditions that gives information regarding the geometry of scattering structures.

The wavelength of X-rays is comparable to the interatomic distances in crystals. Low-angle X-ray scattering can detect larger periodicities of lamellar crystallites. A wide-angle XRD pattern describes the spatial arrangement of atoms. The periodicity of a structure is characterised by the existence of ordered three-dimensional repeat units. The characterisation of the structure of polymer-clay composites using XRD is partially based on the changes observed in the thickness and intensity of the basal reflection peaks (Pavlidou & Papaspyrides, 2008). The sharp features in XRD patterns are associated with regions of three-dimensional order or crystallinity. By contrast, diffuse XRD features are characteristic of three-dimensional disorder of an amorphous material. The occurrence of both sharp and diffuse features is evidence that ordered and disordered regions coexist.

XRD analysis of polymer-clay composites and their precursors consists essentially in monitoring the position, shape and intensity of basal reflections from the silicate layers. Subsequently, the interlayer spaces between diffractional silicate planes can be determined using Bragg's law (Equation 1).

$$n\lambda = 2d \sin\theta \quad (1)$$

where:
n is an integer
λ is the wavelength of incident wave
d is the interplanar distance between adjacent atomic lattices
θ is the angle between the incident ray and scattering planes

When characterising polymer-clay composites using XRD, organoclay basal peaks are often used as a reference. If such basal reflections do not change, the polymer is immiscible. If the basal peak position shifts towards a lower angle, coupled with peak broadening and an intensity decrease, the nanocomposite is intercalated (Pavlidou & Papaspyrides, 2008; Preschilla et al., 2008). However, a basal peak shift to lower angles coupled with an intensity

decrease to eventual disappearance are indicative of exfoliated nanocomposites (Preschilla et al., 2008).

It is doubtful whether complete exfoliation of clays can be achieved. The majority, if not all of polymer nanocomposites so far reported in the literature presented intercalated or mixed intercalated/exfoliated structures. This is due to the anisotropy and the large lateral dimensions of the silicate layers. They can reach a length of 1000 nm when delaminated and hence it is practically impossible to separate them completely in the polymer matrix (Pavlidou & Papaspyrides, 2008).

2.3.2 Transmission electron microscopy (TEM)

Composite structures determined solely on the basis of XRD patterns are not completely certain. TEM better analyses the size, morphology and degree of clay distribution on the composites. This technique provides qualitative visual evaluation of the internal composite structure. Heavier elements, such as Al, Si and O, compose the silicate layers. The surrounding polymer matrix and the silicate interlayers comprise C, H and N. The latter elements are relatively lighter, and are visualised as bright or white zones upon composite formation. Conversely, the cross-sections of silicate layers appear as dark lines (Pavlidou & Papaspyrides, 2008; Pereira de Abreu et al., 2007).

Sample preparation for TEM analysis is time-consuming since very thin sections of about 10^{-6} cm are required. Further, TEM requires a large set of images and a tedious analysis for quantification. The aim is to produce estimations representative of the whole material. The properties at the surface of samples may be different from those in the bulk (Pavlidou & Papaspyrides, 2008; Preschilla et al., 2008). In addition, the orientation at which the sample is prepared corresponds to one axis at a time. The endeavour to obtain representative TEM samples involves preparing them in all possible orientations, by rotating the sample about one of its axes.

2.3.3 Rheological analysis

Rheology is also powerful for complementing XRD. This technique can assess the degree of dispersion, and the morphology and size of clays in the polymer matrix (Dal Castel et al., 2009). The extent of clay exfoliation can be estimated from the shear thinning behaviour of

polymer composites (Szép et al., 2006). High zero-shear viscosities suggest a strong interaction between exfoliated nanoclay platelets and polymer chains. The internal nanocomposite network remains unaffected by the imposed low shear rate. When the shear rate is increased, the network breaks down and the platelets orientate in the direction of flow. Owing to this platelet alignment, the viscosity decreases to the level of the neat polymer (Gupta et al., 2005; Szép et al., 2006).

To analyse the rheological properties of polymer composites, oscillatory tests are most commonly used. Such tests provide information on the following functions: η^*, G' and G". These parameters are respectively referred to as the complex viscosity, the storage modulus and the loss modulus. The storage modulus, G', is a measure of the energy storage of the material. It indicates how well structured a material is and corresponds to its elastic contribution. The loss modulus, G", is a measure of energy dissipation. It corresponds to the viscous contribution of the material (Shenoy, 1999).

Oscillatory experiments are performed in the linear viscoelastic (LVE) region. In this region, the structure of the viscoelastic material remains unbroken throughout the measurements. The LVE range is frequently determined by a shear strain amplitude sweep test. It consists of exposing the sample to increasing strain amplitude at constant frequency and temperature. This test is carried out as the first oscillatory test with every unknown sample (Mezger, 2006). The mid-point of the LVE range is the value of the strain amplitude that is subsequently used in the frequency sweep test. This test is carried out to further characterise the viscoelastic structure. A typical frequency sweep test consists of exposing a sample to a stepwise increase in frequency at a constant strain amplitude and temperature. Cone-and-plate geometry is preferred to ensure uniform shear rates across the sample.

2.3.4 Dynamic mechanical analysis (DMA)

DMA measures the mechanical response of a material to a cyclic deformation as a function of temperature. Usually, tension and three-point bending are the types of cyclic deformation applied. DMA results are expressed by three main parameters: (i) the storage modulus, *E'*or *G';* (ii) the loss modulus, *E"* or *G"*; and (iii) the damping factor, tan δ or *E"/E' orG"/G'*.

The storage modulus corresponds to the elastic response of a certain material to the deformation. Typically, upon dispersion of a layered silicate in a polymer, DMA assesses whether G' increases. For exfoliated composite structures, G' increases, probably owing to the creation of a three-dimensional network of interconnected long silicate layers. These strengthen the polymer material through mechanical percolation. The increase in G' is, generally, larger above the Tg – the glass transition temperature. It is above this temperature that polymers soften, and the reinforcement effect of the clay particles becomes more prominent. Such reinforcement is derived from the restricted movement of the polymer chains.

The loss modulus, G", corresponds to the plastic response of the material to deformation. Enhancement of the loss modulus is discussed far less directly in the literature than G'. Finally, the damping factor, tan δ, measures the ratio of the loss modulus to the storage modulus. Tan δ is useful for determining the occurrence of molecular mobility transitions such as the glass transition temperature. Depending on the polymer matrix, values of tan δ are affected in different ways upon nanocomposite formation (Pavlidou & Papaspyrides, 2008).

2.3.5 Thermogravimetric analysis (TGA)

The thermal stability of a polymer and its nanocomposites can be investigated using TGA. A stepwise increase in temperature is used to monitor the mass loss of the polymer (Beyer, 2002; Szép et al., 2006). An atmosphere of air or oxygen is preferred for TGA of a polymer and its nanocomposites. Such an atmosphere allows oxidative decomposition reactions of the polymer to take place. TGA uses a precision balance that is very sensitive to the mass loss of the sample. However, the derivative of the thermogravimetric curve is more characteristic and informative (Szép et al., 2006). It indicates the temperatures at which each event occurs.

2.3.6 Fourier Transform Infrared (FTIR) spectroscopy

Infrared (IR) spectroscopy is a method of chemical analysis whereby the sample is illuminated with incident radiation in order to excite molecular vibrations. The frequency of the incident radiation, usually in cm^{-1} wavenumbers, is varied continuously. When the molecule absorbs a particular discrete amount of energy, it causes a vibration. The vibrational energy corresponds to the absorption of energy by a molecule as the component atoms vibrate about the mean centre of their chemical bonds. Only the vibrations producing a change in the

molecule's dipole moment are detected in the infrared spectrum. A change in the dipole moment during the vibration for the molecule or the functional group under study is the fundamental requirement for absorption of IR radiation.

The IR spectrum is formed when absorption of electromagnetic radiation occurs at frequencies that correlate to the vibrations of specific sets of chemical bonds. The transmittance of the radiation through the sample is plotted, in the spectrum, against the incident frequency.

Based on the spectral region, there are three forms of vibrational spectroscopy: far-IR (500-150 cm^{-1}), mid-IR (4000-400 cm^{-1}), and near-IR (13300-3300 cm^{-1}). The common vibrational energies of organic and non-metallic inorganic species are in the mid-IR.

Mid-IR spectroscopy is the most commonly used, and for this samples are prepared by grinding the analyte in an alkali halide. The mixture is pressed into a pellet or ground in mineral oil to form a mull (a very thick suspension), which is spread between two alkali halide plates. Water gives a prominent and obstructive mid-IR background. Therefore, mid-IR samples must be free of moisture.

2.3.7 Mechanical analysis (tensile and impact testing)

Mechanical reinforcement of polymers by layered silicates is due to the rigidity of these fillers. Layered silicates have high strength moduli and inherent resistance to strain. In intercalated or exfoliated structures, the polymer adjacent to the filler is restrained mechanically owing to its confinement, and the filler bears a significant portion of the load applied to the nanocomposite. Fillers with a larger surface area therefore provide a much greater reinforcing effect as they strengthen a much larger region of the polymer matrix. Conversely, aggregation of clay layers causes a reduction in mechanical properties. The stacking of platelets is detrimental to composite stiffness since it reduces the filler aspect ratio and surface area (Pavlidou & Papaspyrides, 2008).

Tensile properties

Typically, a tensile test consists of a sample (specimen) clamped at both ends. The grip sites are large to prevent premature failure due to stress concentration. The centre of the specimen is thin to encourage the sample to fail at this portion and not at the grip sites. The specimen is

pulled apart, with one end moving relative to the other at a constant rate of elongation. Multiple specimen samples are tested to allow statistical evaluation of the results.

Very informative mechanical data are gathered, recording a stress-strain curve in tension. The initial linear region (slope) of the stress-strain curve measures the stiffness of the material; this is the Young's modulus or modulus of elasticity. The strain at which the specimen breaks is termed the 'elongation at break' (Chacko et al., 2009). The initial region where the stress begins to level off corresponds to the stress at yield.

Generally, the Young's modulus and the amplitude or tensile strength of nanocomposites are significantly higher than those of virgin polymers. The increase in modulus and yield stress is attributable to the clay reinforcement effect. Conversely, elongation at break typically decreases relative to virgin polymers due to the clay reinforcement effect.

Notched impact strength

Notched impact strength is measured, commonly, by hitting the specimen with a pendulum with a massive striking edge (Charpy test). The energy required to break the specimen is calculated from the travel of the pendulum after it has broken the specimen.

2.4 Melt intercalation and performance of polymer-clay composites

Polymers filled with particles reduce production costs and, further, enhance desirable properties, e.g. stiffness and toughness, barrier properties, and resistance to fire and ignition, among others. However, the addition of microparticulate fillers does impart drawbacks to the resulting composites (e.g. brittleness and opacity). Thus a new class of composites – polymer nanocomposites – has emerged (Alexandre & Dubois, 2000).

Polymer nanocomposites are particle-filled polymers for which at least one dimension of the dispersed particles is in the nanometre range. Nanocomposites characterised by only one dimension in the nanometre range consist of filler present in the form of sheets of one to a few nanometres thick and hundreds to thousands of nanometres long. Such composites can be gathered under the name of polymer-layered silicate nanocomposites (PLSNs).

A uniform dispersion of fillers in the nanometre range is a key requirement for improving the mechanical and barrier properties of polymer nanocomposites. To date, the preparation of fully exfoliated PLSNs remains elusive. The use of varied processing equipment and conditions has yielded disparate nanocomposite structures and properties. So has the use of polymers with diverse features, silicates and organic modifiers of different types, modifiers with several chain lengths and polarity, and intercalation into silicates in dissimilar amounts. It is, therefore, necessary to understand the influence of materials, instruments and processing conditions on the properties of created composites.

Alexandre and Dubois (2000) found that no nanocomposites were formed when melt compounding organomontmorillonite (functionalised with dimethyl dioctadecyl ammonium) into high-density polyethylene. However, partially intercalated and partially exfoliated morphologies were obtained with EVA copolymers even at low vinyl acetate content (12 mass %). For this reason poly(ethylene-co-vinylacetate), EVA, was chosen as the polymer matrix in this study.

The literature review within the scope of this study focused on composites whose structures have been determined by TEM. Structures probed solely by XRD are not completely certain. When no XRD peak is observed, it could be deduced as exfoliation. However, the presence of a small quantity of ordered stacks may also yield a featureless XRD diffractogram. Moreover, the presence of a high number of non-uniformly dispersed clay stacks likewise yields a featureless pattern or interlayer variations. In turn, any presence of homogeneous distribution of the clay nanoplatelets could be interpreted as intercalation. Further, the presence of a few silicate stacks could be deemed to be conventional microcomposites. Certainly, the presence of recalcitrant XRD reflections confirms the occurrence of intercalated or unmodified silicate regions. However, exfoliated regions may perhaps co-exist and even predominate. TEM is critical since it gives direct evidence of composite structures. However, it may also fall short when a few samples not representative of the whole material are viewed. The research work reviewed in this project is likely to have been subject to this dilemma.

Table A.1 and Table A.2 in the Appendix summarise, respectively, diverse EVA grades and organosilicates melt blended to prepare EVA composites. Table A.3 summarises the melt processing equipment used in the works reviewed, together with processing parameters.

2.4.1 Effect of processing equipment and conditions on the dispersion of EVA composites

A co-rotating twin-screw extruder is considered the most effective mixing device for the dispersion of silicate platelets. This is because the screws rotate in the same direction, intermesh and pass resin over and under one screw to another. The material is thus subjected to an identical amount of shear and is unlikely to become stagnant. Chaudary et al. (2005a), Chaudary et al. (2005b) and Pistor et al. (2010) reported similar EVA nanocomposite structures. Partial intercalation and exfoliation were the predominant characteristics reported in all these articles. Further, it was stated that all samples contained small tactoid fractions (Chaudary et al., 2005a; Chaudary et al., 2005b; Pistor et al., 2010). However, the processing equipment and conditions employed by these authors were different (Table A.4).

La Mantia & Tzankova Dintcheva (2006) prepared equivalent samples using two different extruders. They reported similar EVA nanocomposite structures comprising intercalated silicate domains, as detected by XRD. The d_{001} was slightly increased for samples compounded in a twin-screw extruder (La Mantia & Tzankova Dintcheva, 2006). Likewise, in the works done by Chaudary et al. (2005a), Chaudary et al. (2005b) and Pistor et al. (2010), the overall nanocomposite structures seemed independent of the processing equipment used. In addition, all the nanocomposite structures appeared to be insensitive to different processing temperatures and shear forces.

2.4.2 Effect of silicate type on the dispersion of EVA composites

The effect of silicate type on the dispersion of EVA composites was investigated (Zanetti et al., 2001; Riva et al., 2002; Costache et al., 2005; Peeterbroeck et al., 2005). EVA matrices were melt blended with hectorite, fluorohectorite, magadiite and montmorillonite (MMT), all organically modified. The dispersion of hectorite-type clays was found to be better than that of MMT clays. This may be attributed to the large interfacial area available for the interaction of polymer chains with hectorite-like minerals. The interactionof high surface area silicate with polymer chains yields excellent dispersion (Chaudhary et al., 2005a). Hectorite had an aspect ratio (a quotient of the length of the particle to its diameter) of approximately 5000, while MMT has a ratio of less than 1000. Magadiite did not yield nanocomposites, only microcomposites. However, a large aspect ratio may be disadvantageous since the sheets will

tend to agglomerate. In such cases, the formation of a well-dispersed phase in a polymer matrix is doubtful.

2.4.3 Effect of organic modification of silicates on the dispersion of EVA composites

Nanocomposite creation was found to depend on the type of silicate modification (Alexandre et al., 2001; Zanetti et al., 2001). Suitable silicate modification should render it compatible with the polymer matrix. Silicates modified with ammonium cations bearing carboxylic acid moiety yielded conventional microcomposites. They were independent of the vinyl acetate (VA) content of EVA matrices. In contrast, organosilicates with non-functionalised alkyl ammonium chains (one and two) displayed affinity towards EVA chains. They yielded nanocomposites whatever the VA content (12, 19, 27 mass %) of the matrix. Exfoliated silicate sheets were observed together with stacks of intercalated and unmodified silicates. The nanocomposite structures were considered intercalated/exfoliated (Alexandre and Dubois, 2000; Alexandre et al., 2001; Zanetti et al., 2001). Higher amounts of stacks were observed in EVA12 nanocomposites (Alexandre et al., 2001). These authors speculated that such a small extent of exfoliation was due to low polarity of the EVA12 matrix. Organosilicates with one long alkyl chain likewise yielded nanocomposites with relatively high numbers of stacks (Alexandre et al., 2001). Table A.5 presents the effect of organic modification of silicates on the dispersion of EVA composites.

The effect of different types of silicate modification on the characteristics and properties of EVA nanocomposites was further investigated. Riva et al. (2002) used MMT modified with $(CH_2CH_2OH)_2N^+CH_3$(tallow) and EVA19. The polarity of MMT was increased, further improving its affinity towards polar EVA matrices. Exfoliated structure was reported for a nanocomposite based on EVA19. In addition, stacks of unmodified silicates were observed (Riva et al., 2002).

Zhang et al. (2003) increased the number of long alkyl chains used to modify MMT up to three. They anticipated that such an increase would decrease the polarity of organo-MMT. Nevertheless, they found it necessary for yielding larger organo-MMT basal spacings. They aimed at a proper balance between the two as it would ease migration and penetration of EVA chains into the silicate layers. The morphological features of EVA-MMT nanocomposites were examined. They were found to depend on the basal spacing of the organically modified MMT and the polarity of the EVA. Increasing both promoted better

dispersions. The chains of EVA diffused more easily into the MMT layers. Two long alkyl chains were found to be sufficient to yield organosilicates with wider basal spacing (Zhang et al., 2003). These authors recorded further marginal expansion of d_{001} for organoclay with triple chains.

2.4.4 Effect of VA content on the dispersion of EVA composites

The effect of changing the matrix VA content on the dispersion of EVA composites was assessed by several authors (Alexandre et al., 2001; Zannetti et al., 2001; Cser & Bhattacharya, 2003; Jeon et al., 2003; Zhang et al., 2003; Pasanovic-Zujo et al., 2004; Zhang & Sundararaj, 2004; Chaudhary et al., 2005a; Chaudhary et al., 2005b; Costache et al., 2005; Prasad et al., 2006; Cui et al., 2007; Marini et al., 2009). Increasing the VA content, i.e. EVA polarity, lowers the thermodynamic energy barrier for polymer interaction with silicates. Therefore, polymer chains diffuse more easily in between the silicate layers (Zhang et al., 2003). Increased matrix amorphousness (with increasing VA units) further facilitates stabilisation of the polymer chains within the silicate galleries (Chaudhary et al., 2005a; Chaudhary et al., 2005b). The latter authors claimed that higher amorphous content prevents re-crystallisation of polymer chains during annealing, allowing the chains to remain diffused within the silicate layers (Chaudhary et al., 2005a; Chaudhary et al., 2005b).

Whatever the VA content, organosilicates with OH groups along the alkyl N substituents appeared well dispersed. This may be due to strong intermolecular interactions between the OH groups of the organic modifier and the ester functions of the EVA matrix (Peeterbroeck et al., 2005). Increasing the VA content improved the degree of organosilicate dispersion. This was independent of the type of silicate modification. When the number of long chains was the same, organosilicates with higher chain lengths dispersed better. This may be related to the interlayer spacing of the organosilicate. Densely packing modifier into the silicate did not aid dispersion. Chaudhary et al. (2005a) claimed that it reduces the number of EVA chains penetrating the interlayer spaces. Table A.6 presents the effect of VA content on the dispersion of EVA composites.

Zhang and Sundararaj (2004) investigated the extent of dispersion of some organosilicates comprising double chains in EVA matrices with five VA contents (6, 9, 12, 18 and 28 mass %). The organosilicate employed is coded OC_{25} in Table A.2. It was found that all EVA matrices further expanded the organoclay interlayer. Increasing the VA content from 6 to 12

mass % expanded the silicate interlayer considerably. Above such a VA content, no further interlayer expansion was recorded. An intercalation-limiting effect of the polarity after a certain critical VA content has been established (Zhang and Sundararaj, 2004). This critical VA content was found to approximate 15 mass % (Jeon et al., 2003). The degree of intercalation of EVA into organoclay with double chains increased only at VA contents up to about 15 mass %. Above such a critical VA content, expansion of the basal spacing ceased. The interlayer expansion was attributed to increased diffusion of EVA (Zhang et al., 2003). The diffusion of polymer depends strongly on how well it flows. The latter is determined by the melt flow index, MFI.

2.4.5 Effect of MFI on the dispersion of EVA composites

The propensity of EVA with higher VA content to diffuse into the silicate interlayers has been established (Zhang et al., 2003). Zhang and Sundararaj (2004) examined the influence of MFI on the structure of nanocomposites. They used five EVA28 matrices with different MFIs (3, 6, 25, 43 and 150 g/10min). The influence of MFI on the effect of EVA polarity on limiting intercalation into double-tailed organoclay has been investigated. Lowering the MFI from 150 to 25 did not cause any detectable change in the basal spacing. However, decreasing the MFI further to 6 expanded the silicate interlayer. Below this MFI, the silicate interlayer collapsed. It was therefore concluded that effective polymer diffusion requires a conjugation between its mobility and its shear force (Zhang and Sundararaj, 2004). The latter should: (i) create shear tensions during nanocomposite processing; (ii) aid the breaking up of organo-silicate agglomerations; (iii) disperse silicate platelets or a few tactoids throughout the matrix; and (iv) keep the silicate platelets or tactoids apart. However, polymer mobility should be enough to promote its diffusion and penetration into the silicate layers before layer re-stacking. Although the existence of an intercalation-limiting effect of EVA into double-tailed organoclay was confirmed, it seemed to be dependent on the MFI of the matrix rather than that of its VA content. This speculation is contrary to that of Jeon et al. (2003). These authors recorded increasing interlayer distances with increasing VA content from 3 to 15 mass %. No further expansion was recorded for organo-MMT intercalated by EVA22 with different MFIs (2 and 3 g/10 min). In turn, Zhang and Sundararaj (2004) recorded increasing interlayer spacing when the MFI of EVA28 was lowered from 25 to 6. Thus, it is speculated that EVA resins possessing good mobility and sufficient shear force will have MFIs in the range 3–25. Marini et al. (2009) agreed that matrix viscosity is the driving force for polymer chain mobility within clay lamellae. In addition, matrix viscosity was thought to be

responsible for imposed shear tension causing lamellae slippage and clay dispersion. It was confirmed that adequate affinity between the polymer matrix and the organosilicate was indispensable.

The effects of diverse material features, varied processing equipment and different conditions on the structures of created composites have been reviewed. Next, the influence of such composite structures on the mechanical, rheological, thermal and fire properties of organoclays will be reviewed.

2.4.6 Influence of composite structure on the mechanical properties

The mechanical properties of created composites have been evaluated through tensile testing (Table A.7). Typically, silicate particles have a higher modulus than polymer matrices. Combining them increases the initial resistance of the composite to an applied stress.With increasing concentration of nanofiller, there is an increase in Young's modulus (stiffness) of the nanocomposites. Alexandre et al. (2001), using 5 mass % MMT, prepared nanocomposites with double the Young's modulus of pure EVA27. In turn, EVA19 and EVA12 increased the Young's modulus by 50%. The variation in the modulus of nanocomposites was explained by the difference in the structures of the nanocomposites. The dispersion of individual clay platelets responsible for the large increase in modulus was higher in EVA27 nanocomposite (Alexandre et al., 2001).

Apart from polymer polarity, silicate modification with surfactants having non-functionalised chains compatible with polymer matrices is also critical. The ductility of EVA27 nanocomposite decreased only slightly compared with that of pure polymer. This was in spite of a large increase in the nanocomposite's stiffness. For microcomposites, neither EVA polarity nor filler concentration was efficient in increasing substantially the Young's modulus.

Zhang and Sundararaj (2004) recorded ever-increasing Young's moduli of EVA nanocomposites with increasing concentration of nanofiller. In parallel, they proposed the existence of a 'platelet saturation effect'. Such an effect reduces the extent of platelet dispersion in the polymer matrix. The saturation effect has been explained as follows: lLayered silicates have a large aspect ratio, exceeding 200. Interaction between them is quite strong because of the large packing area. Exfoliation and dispersion of the silicate layers

depend mainly on two factors: EVA-silicate interaction (ε_{es}) and silicate-silicate interaction (ε_{ss}).When $\varepsilon_{es} > \varepsilon_{ss}$, exfoliation of the silicate layers is possible. Conversely, when $\varepsilon_{es} < \varepsilon_{ss}$, exfoliation is impossible. An increase in clay content then leads to a larger ε_{ss}; this is due to a shorter distance between the silicate aggregates (Zhang and Sundararaj, 2004).

The effect of interplay between EVA polarity (amorphicity) and silicate concentration (mass %) on the Young's modulus has been evaluated. It has been accepted that platelet 'randomisation' characterises exfoliated nanocomposite structures. Typically, such effective dispersion of the nanosilicate suppresses the matrix's ability to absorb energy when the EVA matrix has a lower VA content (Chaudhary et al., 2005a). Nanosilicates increase spatial hindrance for polymeric chain movement. They impart rigidity to the polymer matrix, creating a 'rigid' amorphous phase. Platelet–polymer and platelet-platelet interactions tend to create a flexible silicate network structure in the matrix. Owing to polymer entanglement, this network increases the initial resistance of polymeric chains moving under stress. The initial deformation energy is then absorbed by the silicate network. Simultaneously, the flexible network increases the nanocomposite's modulus. With increasing VA content, the silicate network increases its flexibility. Consequently, the resistance of the polymeric chains to movement is lowered. A 'mobile' amorphous phase therefore develops, and the network's ability to absorb deformation energy decreases. This occurs in spite of platelet–polymer and platelet-platelet interactions in the flexible silicate network. Stress is then partially transferred to the polymer chains, allowing them to absorb higher deformation energy. Hence, the modulus appears to be dominated by the extent of matrix crystallinity/amorphousness rather than by the silicate network.

Rigidity may also be imparted without the formation of a silicate network structure. There needs to be good interaction between the silicate platelets (or clusters of tactoids) and the matrix in which they are dispersed and appropriately oriented. However, tensile strength is likely to be reduced (Zhang and Sundararaj, 2004). Favourable interactions at the polymer/silicate interface are critical for efficient stress transfer, but tensile strength does not increase when polymer–clay interactions are sufficiently developed. The tensile strength of the nanocomposite reduces with increasing flexibility of the silicate network structure. Increasing matrix polarity tends to maximise the extent of diffusion of EVA chains into the silicate layers. A higher specific surface area then becomes available for polymer-silicate

interactions (Chaudhary et al., 2005a). However, effective polymer diffusion leading to exfoliation requires a balance between the network's mobility and its shear force (Zhang and Sundararaj, 2004).

2.4.7 Influence of composite structure on its steady shear rheological properties

The degree of dispersion of silicates in a polymer matrix affects the rheological behaviour of nanocomposites. Measurement of complex viscosity by an oscillatory test is useful to estimate the degree of exfoliation of composites. The viscosity of highly dispersed nanocomposites, with exfoliated structure, increases extensively when the shear rate changes. In turn, the viscosity of poor dispersions increases moderately with shear rate. At a low shear rate, exfoliated nanocomposites have a propensity to display solid-like behaviour. This has been attributed to the formation of a network structure by the dispersed silicate layers (Gupta et al., 2005). Polymer chains are trapped within the network and because there are unable to flow, viscosity increases. High zero-shear viscosities indicate that the network of dispersed layers remains unaffected by the imposed flow. Interactions between silicate layers and polymer chains are more pronounced in exfoliated systems than in fully intercalated ones. At the same silicate concentration, the elasticity (Young's) modulus is higher for exfoliated structures than for intercalated ones (Riva et al., 2002). Hence, solid-like behavior occurs at higher silicate loading in later systems. This leads to slower relaxation of the polymer chains (Gupta et al., 2005). The influence of composite structure on its steady shear rheological properties is presented in Table A.8.

High shear rates breakdown the silicate network and orient the platelets in the direction of flow. Therefore, nanocomposites exhibit shear thinning behaviour. The slope of the curves, the so-called 'shear thinning exponent' is used to estimate the extent of nanocomposite exfoliation. It has been accepted that higher absolute values of the exponent indicate a higher rate of exfoliation (Gupta et al., 2005; Szép et al., 2006). Marini et al. (2009) suggested that a significant increase in viscosity in the low shear region indicates strong matrix-organosilicate interactions. Both well-dispersed intercalated and/or exfoliated silicates can lead to a large increase in zero-shear viscosity (Marini et al., 2009).

La Mantia & Tzankova Dintcheva (2006) stated that matrix-organosilicate interactions increase in intensity with silicate interlayer spacing. When basal spacing increases, the surface area available for contact with polymeric chains also increases. Moreover, due to the

larger interplatelet distances, the volume concentration of the silicate increases (La Mantia & Tzankova Dintcheva, 2006). High interactions between the organosilicate and the polymer chains are critical for nanocomposite creation. However, they are not sufficient to guarantee effective clay dispersion and exfoliation (Zang and Sundararaj, 2004; Marini et al., 2009). Effective polymer diffusion requires balancing the mobility of the chain with its shear force (Zhang and Sundararaj, 2004).

Strong matrix-organosilicate interactions are indicated by a significant increase in zero-shear viscosity rather than simply by a high zero-shear viscosity. Marini et al. (2009) recorded huge rheological differences between various EVA nanocomposites, depending on the viscosity of the matrices. High-viscosity EVA12 (MFI = 0.3 g/10 min) and EVA19 (MFI = 2.1 g/10 min) consisted of fairly well-dispersed compact tactoids and had higher zero-shear viscosity than the respective EVA matrices. However, such viscosities were of the same order of magnitude or only differed by one order of magnitude. Further, pure matrices also displayed pseudoplastic behaviour. Absolute values of the shear thinning exponent calculated for EVA12 nanocomposite and its matrix were high. Similarly, nanocomposites produced with low viscosity, EVA18 (MFI = 150 g/10 min) and EVA28 (MFI = 25 g/10 min), exhibited higher zero-shear viscosity than the respective EVA matrices. However, such viscosities differed by more than one order of magnitude. Pure matrices also exhibited Newtonian behaviour. It was then concluded that organosilicate dispersion was dependent on the polarity and viscosity of the EVA matrix (Marini et al., 2009). Therefore, on its own, a high shear thinning exponent does not guarantee a higher rate of exfoliation. Likewise, a high zero-shear viscosity, on its own, does not guarantee strong matrix-organosilicate interactions.

2.4.8 Influence of composite structure on its thermal properties

EVA decomposes in two consecutive steps, regardless of whether there is an oxidative or an inert atmosphere. In air or oxygen, the first step occurs between 300 and 400°C and is attributed to the release of acetic acid. The acid splits off, forming an unsaturated or cross-linked backbone. The second step involves thermal dissociation and combustion of the resulting double bonds or cross-links (Beyer, 2002; Szép et al., 2006). Organoclays are well known for delaying polymer degradation. In fact, EVA nanocomposites exhibit a large increase in thermal stability under an oxidative environment. The maximum of the second degradation peak shifts to higher temperatures. The neat EVA is completely burnt without any residue. Therefore, increased stability of the nanocomposite is attributed to the

residue/char, which is yielded only under oxidative conditions (Beyer, 2002). Acetyl elimination in nanocomposites starts at a lower temperature compared with the virgin EVA. However, the rate of mass loss decreases significantly. This is considered to be due to the formation of a char barrier layer. Thus, both decomposition steps of the nanocomposites are affected by the clay platelets (Szép et al., 2006). Table A.9 presents the influence of the structure of composites on their thermal properties.

CHAPTER 3 EXPERIMENTAL

3.1 Materials

3.1.1 Clay samples

The bentonites used in this investigation were from the Boane deposit in Mozambique and from the Koppies mine in South Africa. G & W Base and Industrial Minerals supplied samples of the crude bentonites in milled powder form and in purified form as sodium-activated dispersions. The cation exchange capacities (CEC) of the purified bentonites were determined by the supplier using the methylene blue method (Hang and Brindley, 1970). The respective values were 70 and 85 meq/100 g dry clay for Boane bentonite and Koppies bentonite.

Bentonite dispersions were prepared as follows: 40 mass % crude Koppies or Boane clay was suspended in distilled water in a mixing tank. Soda ash, 4-5 mass %, was added to activate the bentonite in order to increase the swelling ability. The slurry was then passed through an industrial-sized centrifuge that removed most of the silica particles impurity. After this, 1-1.5 mass % proprietary dispersant was added and the slurry was thoroughly homogenised. The individual characteristics of the slurries were as follows.

Koppies slurry (KS)

The slurry of South African Koppies clay had a light brown colour. The colour was attributed to the presence of relatively high iron content. The chemical composition of the Koppies bentonite powder and related samples, as determined by XRF, is presented in Table 1 in Chapter 4. The solids content of KS was determined as 18.9% by the mass remaining in a thermogravimetric analysis at 150 °C (Figure 1). The pH of KS was 9.9.

Boane slurry (BS)

The Mozambican bentonite slurry (BS) exhibited an off-white colour. The iron and titanium content of the crude clay from Mozambique was considerably lower than that of the South African Koppies powdered sample (Table 1 in Chapter 4). The solids content of BS was determined as 19.2% by the mass remaining in a thermogravimetric analysis at 150 °C (Figure 2). The pH of BS was 7.4.

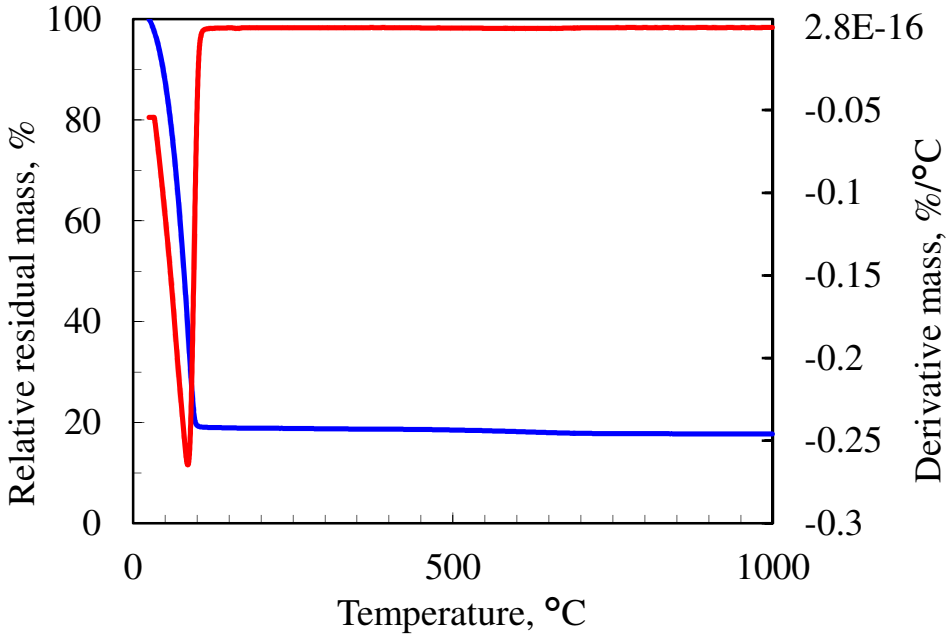

Figure 1. TG and DTG curves of South African Koppies slurry (KS)

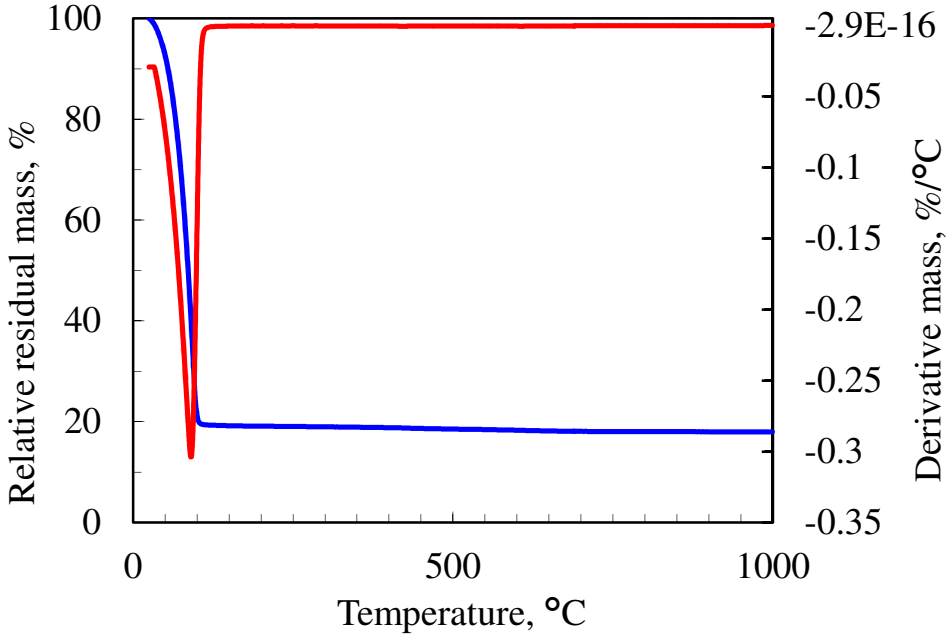

Figure 2. TG and DTG curves of Boane slurry (BS) from Mozambique

3.1.2 Intercalating agents

Quaternary ammonium surfactants (quats) with single and double alkyl chains were utilised as supplied. The following commercial quats were used.

Noramium M2SH-1 (DC18)

Noramium M2SH-1 is a double-chain surfactant manufactured by CECA (Arkema Group) and supplied by Akhulu Marchon. Chemically, it is N,N' di-hydrogenated tallow dimethyl ammonium chloride. The chain distribution is as follows: 64% C18 (saturated), 35% C16 (saturated) and 1% C18 (double bond). The composition is given in mass percent. The average molar mass of DC18 is approximately 529 g/mol. The surfactant was supplied as a 76% by mass solution in a water-isopropanol mixture.

Varisoft 432 CG (DC16)

Varisoft 432 CG is a product of Degussa (Goldschmidt GmbH). It is a double-chain quaternary ammonium ion with the chain lengths varying from 12 to 18 carbons. It contains mostly N,N'-dihexadecyl dimethyl ammonium chloride. The molar mass of the surfactant was estimated at 529.5 g/mol. DC16 surfactant is supplied as a 68% by mass solution in a water-isopropanol mixture.

Noramium M21080 (DC10)

Noramium M21080 is a product of CECA (Arkema Group), supplied by Akhulu Marchon. It contains the pure double-chain surfactant N,N' didecyl dimethyl ammonium chloride. The molar mass is 354 g/mol. DC10 is supplied as an 81% by mass solution of the surfactant in a water-isopropanol mixture.

CTAB (SC16)

Cetyl trimethyl ammonium bromide is a single-chain quat supplied by FEF Chemicals. Chemically, it consists of pure hexadecyl trimethyl ammonium bromide. The molar mass is 364 g/mol. SC16 is a white crystalline powder that melts at 230 ^{o}C. The solubility in water at 25 °C is 15 g/L.

Cetrimide BP (SC14)

Cetrimide BP (Purum grade, from FeF Chemicals A/S, Copenhagen) is essentially tetradecyl trimethyl ammonium bromide. SC14 is a white powder at ambient temperature. The molar mass is ca. 336 g/mol. It decomposes when heated to 245-250 ^{o}C. It is soluble in water and lower alcohols such as propanol.

Empigen HBC40 (SC12)

Empigen HBC40 is a trade name of lauryl dimethyl hydroxyethyl ammonium chloride (dodecyl[2-(2-hydroxyethoxy)ethyl]dimethyl ammonium chloride), from Huntsman Surface Sciences UK), supplied in its 40% aqueous solution. The molar mass of SC12 is at 293.5 g/mol.

3.1.3 Polymer matrix

EVA resin grade EV101 with 18 mass % vinyl acetate was supplied by APC (MFI 1.8 g/10 min at 190 °C/2.16 kg; density 0.941 g/cm^3). The polymer was milled into a fine powder using a Pallmann 300 Series pulveriser.

3.2 Methods

3.2.1 Organic intercalation of bentonite slurries

The CEC of the South African Koppies bentonite, 85 meq/100 g of dry clay, and that of Boane bentonite, from Mozambique, 70 meq/100 g of dry clay, were used to calculate the amount of each intercalating agent for the intercalation experiments (Appendix A.1).

The organoclays synthesised for this study were coded SCXX or DCXX. SC and DC indicate single and double chains respectively. XX represents the number of carbon atoms in each alkyl chain. A prefix of either K or B was introduced in each name, standing for Koppies and Boane respectively.

In the calculations of the amount of each intercalating agent required to synthesise the organoclays (Appendix A.1), it was assumed that surfactant DC16 (Varisoft 432 CG) comprised pure N,N'-dihexadecyl dimethylammonium chloride. For DC18 (Noramium®M2SH-1), with a mixture of chain lengths, the average molar mass was calculated. Some intercalation experiments were performed using a 50% excess of the

surfactants based on the estimated bentonite CEC. For the preparation of M-SC14, an excess of 80% surfactant was used.

Intercalation procedure

A typical intercalation experiment was performed as follows: the soda ash-activated bentonite dispersion (KS or BS) was placed in a planetary mixer. The surfactant solution or powder was added while mixing. Mixing was continued intermittently for about 5 h. The mixture was vigorously stirred for 3 min. During the initial 20 s, a dramatic decrease in the viscosity of Koppies slurry was noticed. After this period, the viscosity of the slurry increased again. It was speculated that the decrease in the slurry viscosity under the influence of high shear was due to the breakdown of the network of clay platelets and its subsequent alignment in the direction of flow.

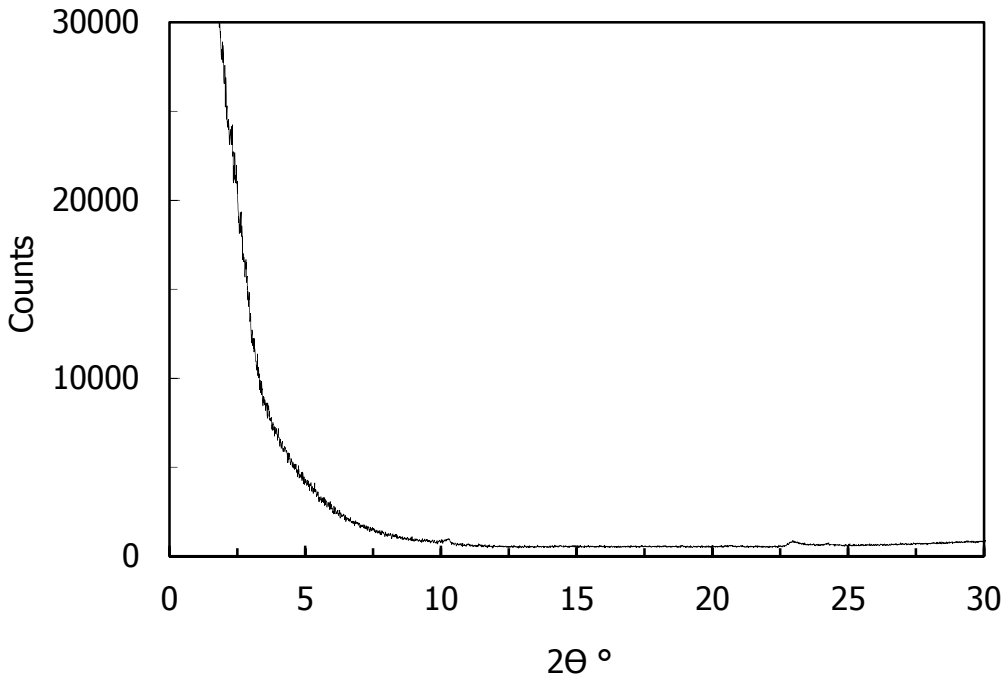

Figure 3. XRD pattern of South African Koppies slurry (KS)

To explain how the clay platelet network yielded an exfoliated (Figure 3) gel-like structure, van Olphen (1964) proposed that the flat face surface and the edge surface of plate-like clay crystallites expose two crystallographically different surfaces. The face surface has an interior net negative charge due to isomorphic substitutions. The charge is compensated by positive counter-ions adsorbed on the surface. On the other hand, disruption of the crystallites at the

edges exposes a broken bond surface (van Olphen, 1964). According to this author, indications are that the edges are negative under alkaline conditions, such as at the pH 9.9 of KS. The van der Waals attraction between edges or between edges and faces, or both, yields an exfoliated clay platelet network in water, with a gel-like structure.

Under the influence of high shear the network of clay platelets breaks down. Consequently, the viscosity of the slurry decreases due to the alignment of the platelets in the direction of flow. Utracki (2004) stated that as soon as the exchange reaction between the interlayer cations occurs and organic intercalant starts to enter the clay interlayer, platelet interactions cause the slurry viscosity to increase again.

After 3 min of stirring the surfactant into the bentonite slurry at high shear, the mixture was allowed to stand for 30 min. It was then stirred again, but for only 1 min, and allowed to stand again for 30 min. This procedure was repeated nine times to allow time for complete cation exchange. Next, the paste mixture was suspended in four parts of distilled water and allowed to stand overnight. Settling of the organophilic product was observed the following morning. The hydrophilic supernatant was decanted, and the organophilic product was re-dispersed in four parts of distilled water to remove halide salts and the excess of intercalant. The suspension was then centrifuged at 4000 rpm for 30 min. The presence of halides (chloride and/or bromide) was monitored by repeated product washing with distilled water, centrifugation and testing of the decanted supernatant with 1M $AgNO_3$. The aim of this successive washing procedure was to eliminate alkaline halide (the secondary product of the cationic exchange) and the excess of surfactant used. When no more precipitation of supernatant by solution $AgNO_3$ was observed, the halide-free product was filtered in a Buchner funnel under vacuum suction. Grade 2V Whatman folded filter paper was stretched and used to recover the product. The product was air-dried for a minimum of 2 days. It was further crushed and ground with a pestle and mortar, and thereafter its structural properties were analysed.

3.2.2 Compounding and injection moulding

Powdered organoclay plus EVA masterbatches were prepared as follows: EVA powder was mixed with organoclay powder in the mass ratio 4:1 and then compounded on a 28 mm co-rotating intermeshing twin-screw laboratory extruder (L/D = 16). The screw design comprised intermeshing kneader elements with a forward transport action. The barrel

temperature profile ranged from 170 to 180 °C and the screw speed was set at 168 rpm. The extruded masterbatch strand was dried, granulated and then pulverised. This powder was let down in virgin resin to set the required final clay content (targeted loading levels up to 6.5 mass % inorganic basis). EVA-organoclay composites were compounded twice at the same conditions in order to delaminate them and ensure a good dispersion of clay platelets. After compounding, the extruded strands were granulated and dried. Test bars, conforming to ASTM D638, were injection moulded on an Engel 3040 injection-moulding machine. Barrel temperatures varied from 170 to 180 °C for all samples. The injection and holding pressures were 180 and 80 bar respectively. The injection speed was 6 mm/s, the stroke was 22 mm and the clamping force was 350 kN.

3.2.2 Characterisation

Samples were characterised before and after organic treatment, as well as after compounding. Various instrument techniques were used to analyse the structural properties and to characterise the eventual sample transformations.

X-ray fluorescence (XRF)

The elemental composition was determined by X-ray fluorescence (XRF) spectroscopy. XRF spectrometer (ARL 9400 XP + XRF) wavelength dispersive was used. Ethyl cellulose was used to bind the powdered samples and produce pellets. The intercalated materials were ashed before analysis in order to reduce their bulk. The samples were ground to < 75 µm in a tungsten carbide mill and roasted at 1000 °C. Then 1 g sample was added to 9 g of $Li_2B_4O_7$ and fused into a glassed bead. Major element analysis was executed on the fused bead using an ARL9400XP+ spectrometer.

Thermogravimetric analysis/differential thermal analysis (TGA/DTA)

Thermal analysis was performed using the dynamic method on a Mettler Toledo A851 TGA/SDTA instrument. About 17 mg of powder was placed in open 70 µL alumina pans. Temperature was scanned from 25 to 1000 °C at a rate of 10 °C/min with air flowing at a rate of 50 mL/min.

Fourier transform infrared (FTIR) spectroscopy

FTIR spectra were recorded on a Perkin Elmer RX I FT-IR spectrometer. Approximately 2 mg of dry sample was combined with 100 mg of spectroscopic-grade KBr and ground into a fine powder. The mixture was pressed into a 13 mm ϕ die pellet. The reported spectra represent averages of 32 scans at a resolution of 2 cm^{-1}. The averaged data were background-corrected using a pure KBr pellet.

X-ray diffraction (XRD)

Mineral identification and composition assessment of pristine bentonite was performed by the South African Council for Geoscience. The XRD instrument used was a Bruker D8 Advance diffractometer using Cu Kα radiation (λ = 0.15406 nm). The system featured a Johansson crystal primary monochromator and LynxEye detector with 3.7° active area. XRD patterns were recorded for random powder preparations. The mineral identification was based on a Bruker Diffrac^{Plus} – EVA evaluation program. The phase concentrations were determined by Rietveld quantitative analysis with Diffrac^{Plus} – TOPAS software to an accuracy of ± 1%.

The basal spacings of all samples were determined in-house. XRD analysis of random powder samples of the organobentonites was performed on a PANalytical X-pert Pro machine. The instrument featured variable divergence and receiving slits and an X'celerator detector using Fe-filtered Co Kα radiation (λ=0.17901 nm). X'Pert High Score Plus software was used for data reduction.

Electron microscopy (SEM and TEM)

The surface morphology of the organoclays was examined by low-resolution scanning electron microscopy (SEM) using a JEOL 840 instrument. The powder samples were coated five times with gold using a SEM Polaron E5200. A SEM fitted with an energy dispersive X-ray analyser (SEM/EDS) was used to examine the morphological and mineralogical association of montmorillonite and cristobalite in Mozambican bentonite. A Leica Stereoscan 440 instrument linked to an Oxford INCA EDS with Oxford SDD detector was used. Polished stubs of the samples were prepared and coated with carbon for conductivity using an EMITECH K950X sputter coater. In addition, an Oberkochen Zeiss Ultra Plus microscope was used for field emission scanning electron microscopy (FESEM).

For transmission electron microscopy (TEM), EVA and its clay composite samples were cryo-sectioned with a diamond knife at a temperature below -110 °C on a Lecia-Riechert Ultracut R instrument with an EMFCS cryo attachment. The nominal sectioning thickness was 90 ± 10 nm. Each sample was mounted on a 300 mesh copper/palladium grid and viewed on a JEOL 2100F TEM using an acceleration voltage of 200 kV.

Rheometry

The rheological properties of neat EVA and its composites were determined in oscillatory mode at 170 ºC. An Advanced Rheometer AR 2000 (TA Instruments) was used, using a cone-and-plate measuring system. The diameter of the plate was 25 mm, the gap was set at 54 µm and the strain amplitude was set at 1%.

Tensile and impact testing

A Lloyds Instruments LRX machine was used for tensile testing (ASTM D638-M) of EVA and its clay composites at a cross-head speed of 50 mm/min. The tensile impact tests were done on a Zwick Impact Tester.

Dynamic mechanical analysis (DMA)

The viscoelastic behaviour was studied on an Eplexor 500 N Qualimeter dynamic mechanical analyser (DMA) from Gabo. The storage modulus (E'), loss modulus (E") and tan δ were determined as a function of temperature at a frequency of 1 Hz in tensile mode. The static load was 2.5 MPa with 2% maximum strain or 1.75 MPa with a maximum strain of 0.6%. The samples were heated from -60 °C to 60 °C at a scan rate of 1 °C/min.

CHAPTER 4 RESULTS AND DISCUSSION

4.1 Characteristics of natural and modified bentonites

4.1.1 Chemical and mineralogical composition

Table 1: Inorganic chemical composition (dry basis expressed as mass %) of bentonite samples before and after organic treatment

	SiO_2	Al_2O_3	Fe_2O_3	MgO	Na_2O	CaO	K_2O	P_2O_5	TiO_2	MnO
KP	64.66	20.03	5.73	4.29	0.37	2.90	1.34	0.17	0.37	0.15
KSC14	63.14	21.99	7.28	4.36	0.07	0.97	0.90	0.86	0.36	0.07
KSC16	64.27	21.67	6.14	4.31	0.08	1.48	0.89	0.76	0.35	0.06
KDC16	64.99	21.42	6.13	4.33	0.14	0.82	0.86	0.92	0.33	0.06
KDC18	65.32	21.40	5.98	4.25	0.08	0.87	0.89	0.83	0.33	0.06
BP	80.16	13.16	2.70	2.66	0.85	0.14	0.08	0.00	0.22	0.03
BSC14	82.77	12.66	2.49	1.75	0.03	0.00	0.05	0.01	0.22	0.01
BSC16	82.44	12.81	2.60	1.78	0.04	0.00	0.06	0.02	0.23	0.01
BDC10	82.42	12.73	2.52	1.76	0.20	0.00	0.12	0.01	0.22	0.01
BDC16	84.27	10.96	2.76	1.45	0.02	0.11	0.07	0.02	0.33	0.02
BDC18	80.87	13.13	2.79	1.88	0.97	0.12	0.03	0.00	0.19	0.01

Table 1 presents the chemical composition of the Koppies and Boane bentonite powders, as well as the ash from their organically treated samples, as determined by X-ray fluorescence (XRF). Boane bentonite has higher silica content than Koppies bentonite. This is attributed to the cristobalite present as a major impurity in Boane bentonite. The XRF results correlate with those of CEC provided by the supplier of the bentonites: Koppies (85 meq/100 g of dry clay) and Boane (70 meq/100 g of dry clay).

Cristobalite is a silica polymorph that in geological times appears as an intermediate in the process of transformation of amorphous silica (glass) to quartz (Velde, 1985). A high cristobalite content degrades the quality of bentonite and limits its utilisation. Rietveld quantitative analysis of the XRD data indicated that the crude Boane bentonite contained 60.3 mass % montmorillonite, 35.7

mass % cristobalite and 4.0 mass % quartz. Rietveld quantitative analysis of the XRD data of the crude Koppies bentonite indicated the following composition, in mass %: 38.9 montmorillonite, 26.7 quartz, 11.1 plagioclase, kaolinite and K-feldspar 10.4 each, 1.5 mica and about 1 calcite.

The montmorillonite phase was identified by the d_{001} around 1.50 nm, coupled with d_{060} = 0.15 nm and the Greene-Kelly test. The test consisted of Li-saturation, glycolation and heating to 300 ºC. After this treatment, the basal spacing collapsed to 0.96 nm, indicating montmorillonite (Greene-Kelly, 1955). Upon ethylene glycol saturation for 24 h, the d_{001} expanded to 1.72 nm and collapsed to 1.03 nm after heating for 1 h at 550 ºC (Brown and Brindley, 1980). Reflections characteristic of α-cristobalite were the following: d_{101} = 0.40 nm, d_{102} = 0.28 nm, d_{200} = 0.25 nm, d_{301} = 0.16 nm and d_{302} = 0.15 nm (Guven and Grim, 1972).

The chemical composition data (Table 1) showed a substantial reduction in the Na and Ca content following organic modification. This provided evidence for the successful intercalation of the organic cations, i.e. organic cations replaced the Na^+ and Ca^{2+} in the pristine bentonites by ion exchange.

4.1.2 Morphological appearance of the samples

The low-resolution SEM micrographs revealed flake-shaped particles (Figure A.1 in the Appendix). The aggregates of the crude bentonites appeared significantly larger than those of the organically modified samples. Figure 4 shows SEM/EDX images of pristine bentonite from Boane and of the organically modified sample, both embedded in an epoxy resin.

The SEM backscattered electron (BSE) images (Figure 4) highlighted some distinct differences between the crude Boane bentonite and its organic derivates. Typically, montmorillonite (smectite) and cristobalite (Si-oxide) appear as irregularly shaped aggregates, with a more or less distinguishable structure. The clay-cristobalite aggregations in the organically modified materials show interesting structures that have been affected to various extents by the modification. Lumps of finely mixed clay enclose tightly compacted aggregates of submicron-sized Si-oxide particles. These aggregates have a semi-rounded shape and appear in various sizes and clay-cristobalite proportions.

A B

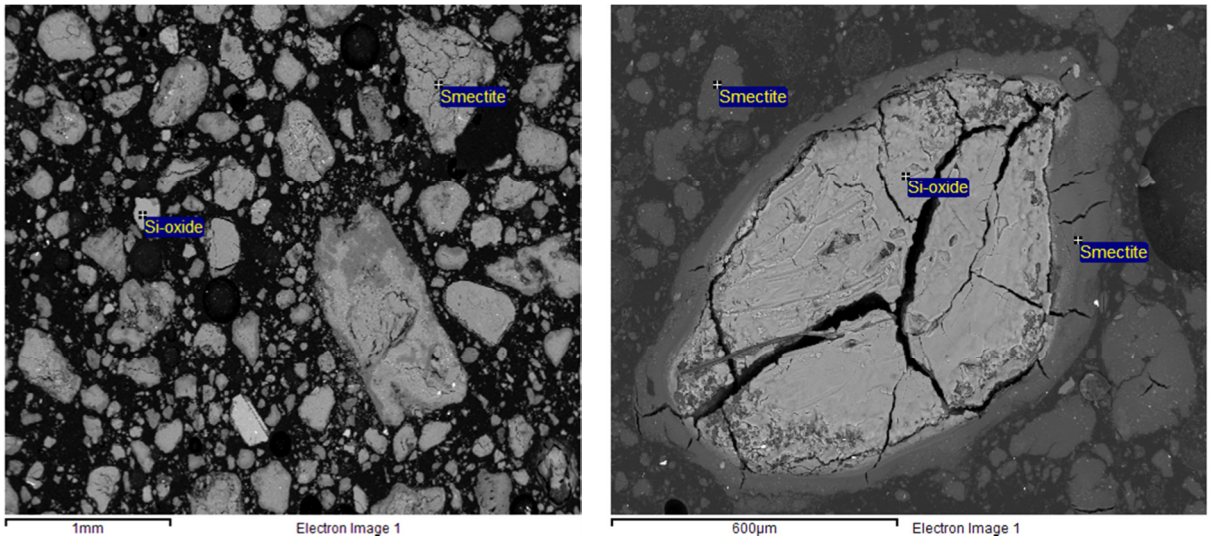

Figure 4. SEM/EDX backscattered electron images of crude clay BP [A] and organically modified clay based on BDC16 [B]

Incipient rigid cracks run through and around the aggregates and extend into the matrix. The cracking appears to be more pronounced within the cristobalite part of the aggregation, suggesting that it comprises a large agglomerate of much finer particles rather than a single large particle. This conjecture was confirmed by the FESEM images shown in Figure 5.

A B

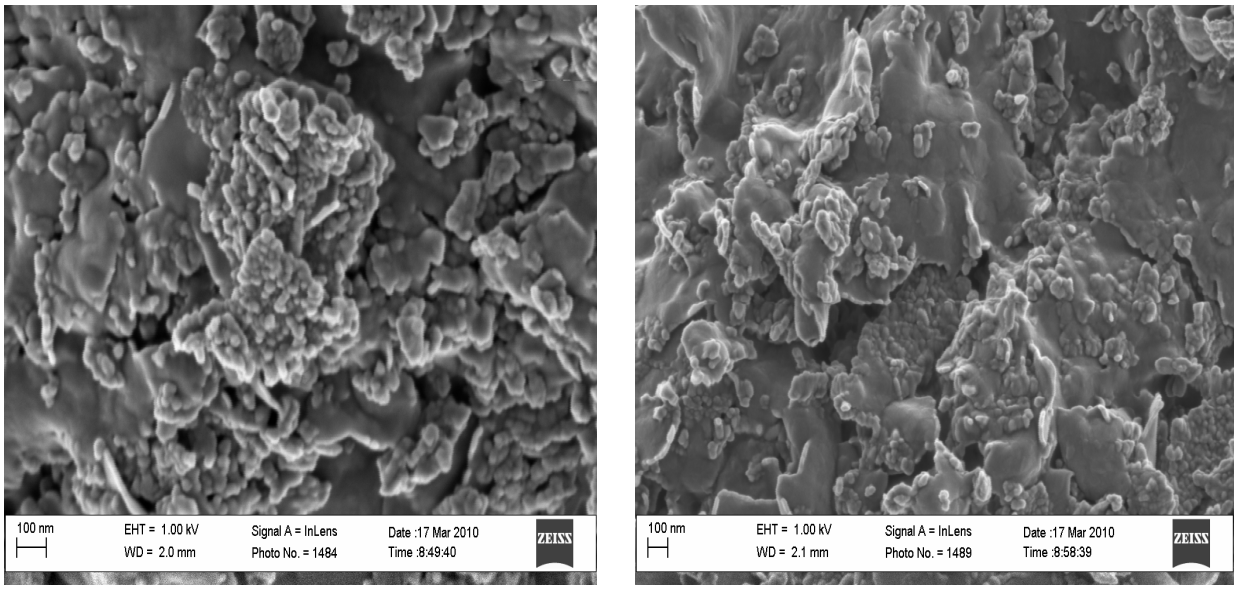

Figure 5. FESEM micrographs of untreated crude clay BP [A] and organically modified clay BSC14 [B]

Figure 5 shows the presence of rounded nano-sized particles on the surfaces of the clay mineral particles and also in aggregated form. Most of these particles were much smaller than 100 nm in size. The large aggregate shown in Figure 4 was attributed to the surface energy mismatch between the uncoated silica nanoparticles and the surfactant-coated bentonite flakes.

4.1.3 State of the intercalated alkylammonium ions

Organic cations introduced up to the CEC level by ion exchange (Lagaly, 1986) are electrostatically 'attached' to the clay mineral surfaces. The excess surfactant molecules are intercalated in their neutral salt form, i.e. together with their (hydrated) counter-ions (Klapyta et al., 2001; Lagaly, 1986). The incorporation of excess surfactant is driven by van der Waals interactions. Dense close-packing of the surfactants in the interlayer space improves the van der Waals interactions between long alkyl chains (Pan et al., 1997; Tahani et al., 1999; Yui et al., 2002; Janek and Lagaly, 2003; Kwolek et al., 2003; Calderon et al., 2008). Denser packing also requires better charge shielding of the same-charge surfactant head groups. Close-packing of long-chain surfactants can be facilitated by single-layer interdigitated intercalation, i.e. where the organic molecules are placed in such a way that the polar heads face opposite directions in order to minimise electrostatic repulsion between these head groups.

The state of the intercalated alkylammonium ions is derived by considering the basal spacing of the clay layers and the size and the shape of the guest molecule. The derived model compares the observed basal spacing and that calculated on the basis of the size and assumed shape of the guest alkylammonium. The model is accepted when good agreement between observed and calculated basal spacing is reached.

The physical arrangements of the alkyl chains of intercalated quaternary ammonium species (quats) have been the subject of intense debate (Lagaly, 1976; Lagaly, 1986; Vaia et al., 1994). At high surfactant loadings, two limiting cases are envisioned. One presumes that the chains are present as tilted, extended-chain paraffin-like arrangements. The alternative presumes disordered chain conformations containing numerous gauche conformers (Lagaly, 1976). These two different arrangements, although indistinguishable by XRD, nevertheless constitute very different molecular environments and interlayer structures (Vaia et al., 1994).

The d-spacing values observed for the present organobentonites are consistent with both options (Table 2).

Table 2. XRD basal spacings and FTIR CH_2 frequencies of bentonite samples

Sample	XRD *d*-spacing (Nm)	Chain tilt angle[1] °	FTIR $\nu_{as}(CH_2)$ (cm^{-1})	FTIR $\delta(CH_2)$ (cm^{-1})
BP	1.50	-	-	-
BSC12	1.82	25	-	-
BSC14	2.00	27	2920	1470
BSC16	3.81	32	2918	1470
BDC10	2.57	21	2924	1468
BDC16	3.89	33	2920	1469
BDC18	3.92	29	2918	1469
KP	1.52	-	-	-
KSC12	1.92	29	-	-
KSC14	1.84	22	2924	1476
KDC10	2.66	23	2925	1469
KDC16	3.82	32	2923	1468
KDC18	3.88	29	2918	1469

[1]Estimated from Equation (2) or Equation (3)

When the alkyl groups of intercalated surfactants adopt paraffin-like extended-chain conformations, they tilt at an angle α with respect to the plane of the clay mineral layers to yield a space-filled packing (Lagaly and Weiss, 1970a; Lagaly and Weiss, 1970b; Lagaly, 1986; He et al., 2006). The expected basal spacings for interdigitated monolayer intercalation and bilayer intercalation are given by the following approximate expressions (Lagaly and Weiss, 1970b; Kopka et al., 1998):

Monolayer: $$d_L = 1.18 + 0.127\, n_C \sin\alpha \quad (2)$$

Bilayer: $$d_L = 1.66 + 0.254\, n_C \sin\alpha \quad (3)$$

where:

d_L is the basal spacing

n_C is the number of carbon atoms in the alkyl chain

α is the tilt angle.

The values indicated for the constants in these equations are only approximate. They take into account the following contributions (Lagaly and Weiss, 1970a; Lagaly and Weiss, 1970b): the thickness of the bentonite layer (0.66 nm); the van der Waals radius of surface oxygen atoms (0.14 nm); the van der Waals radius of a methyl group (0.20 nm); the distance between a terminal methyl group and an oxygen atom (0.12 nm); the projected length of the C–N bond (0.12 nm); a correction accounting for the fact that methyl groups can actually penetrate the six-member oxygen rings of the silicate sheets (maximum depth 0.13 nm); and, finally, the gap between the terminal methyl groups for the case of bilayer intercalation (0.20 nm). These values yield separation distances of $xCH_3\cdots O \approx 0.12$ nm and $xN–CH_3\cdots O \approx 0.40$ nm.

The increased van der Waals energy between longer alkyl chains forces them into paraffin-type arrangements. Typically, alkylammonium chains are considered long at above eight carbon atoms. The strong interaction between long chains can shift the polar head groups out of their positions, for optimal hydrogen bond formation. Therefore, and in order that the volume accessible to the adsorptive surface will increase strongly, alkylammonium ions move from flat to perpendicular orientations (Utracki, 2004).

The powder XRD patterns for Boane crude and its organically modified derivatives are presented in Figure 6, while those for Koppies crude and its derivatives are shown in Figure 7. The measured basal spacings are presented in Table 2. The values obtained for single-chain surfactant-intercalated bentonites are consistent with a monolayer configuration. In turn, the basal spacings of the double-chain surfactant-intercalated bentonites are consistent with a bilayer configuration. The angle α at which the respective alkyl chains tilted with respect to the plane of the clay mineral layers is also presented in Table 2. The tilt angles were estimated from the measured basal spacing values using Equation (2) or Equation (3). The present angles are equivalent to about half the reported value of ca. 59 ° for typical paraffin-type conformations. This suggests that the chains adopted disordered conformations with numerous gauche conformers (Lagaly, 1986).

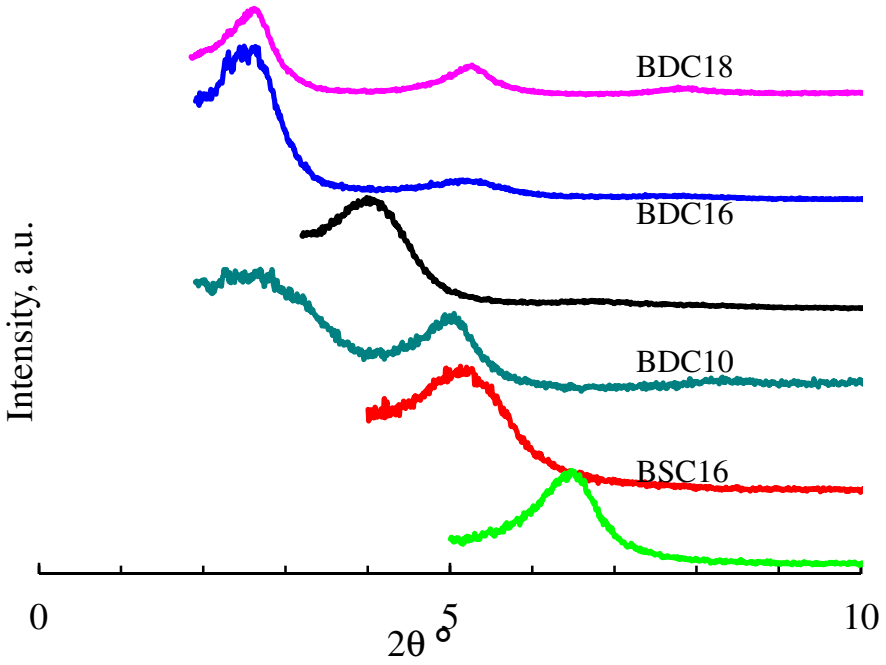

Figure 6. Powder XRD patterns for Boane crude and its organically modified derivatives

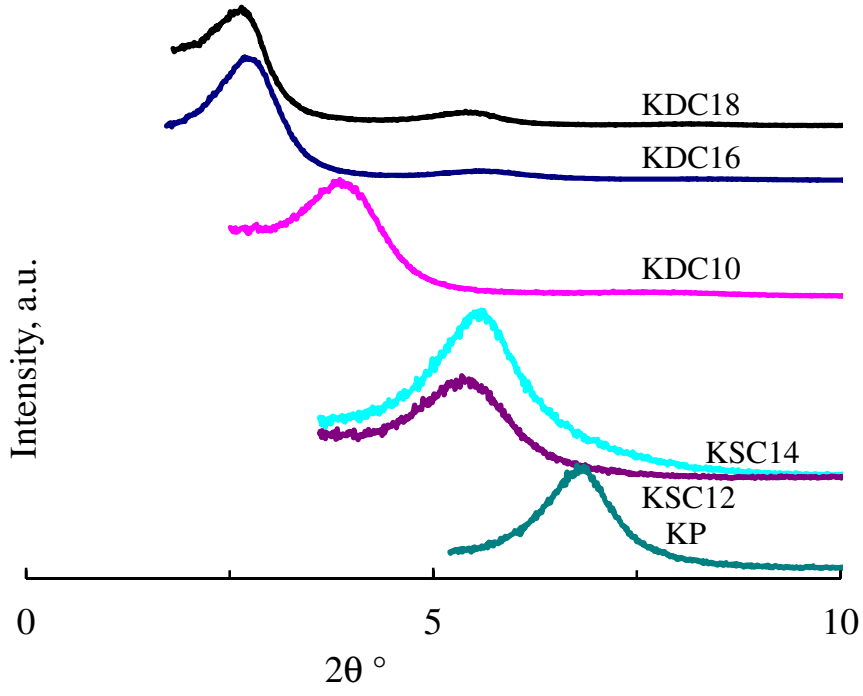

Figure 7. Powder XRD patterns for Koppies crude and its organically modified derivatives

The FTIR spectra for Koppies bentonite and its organoderivatives are shown in Figure 8 and those for the Boane counterparts are presented in Figure 9. Significant changes in the spectral profile of the organically modified samples can be observed. A more complex spectrum is observed for the organically treated samples than for the untreated samples. The spectra of the treated samples feature two strong bands in the wavenumber range 3000-2800 cm^{-1} (sharp bands at approximately 2920 and 2850 cm^{-1}), one additional band at 1470 cm^{-1} and another at 720 cm^{-1}. Altogether, these absorptions are indicative of the presence of a hydrocarbon with a long linear aliphatic chain. The strong band at about 2920 cm^{-1} may be assigned to $\nu_{as}(CH_2)$ stretching and that at 2850 cm^{-1} may be attributed to $\nu_s(CH_2)$ stretching. In turn, the band at 1470 cm^{-1} may be attributed to $\nu_{as}(CH_2)$ bending and that at 720 cm^{-1} may be assigned to $\nu_s(CH_2)$ bending. The presence of a weak band at approximately 1360 cm^{-1}, which is assigned to $\nu_s(CH_3)$ bending, corroborates the spectral data for the long linear aliphatic chain.

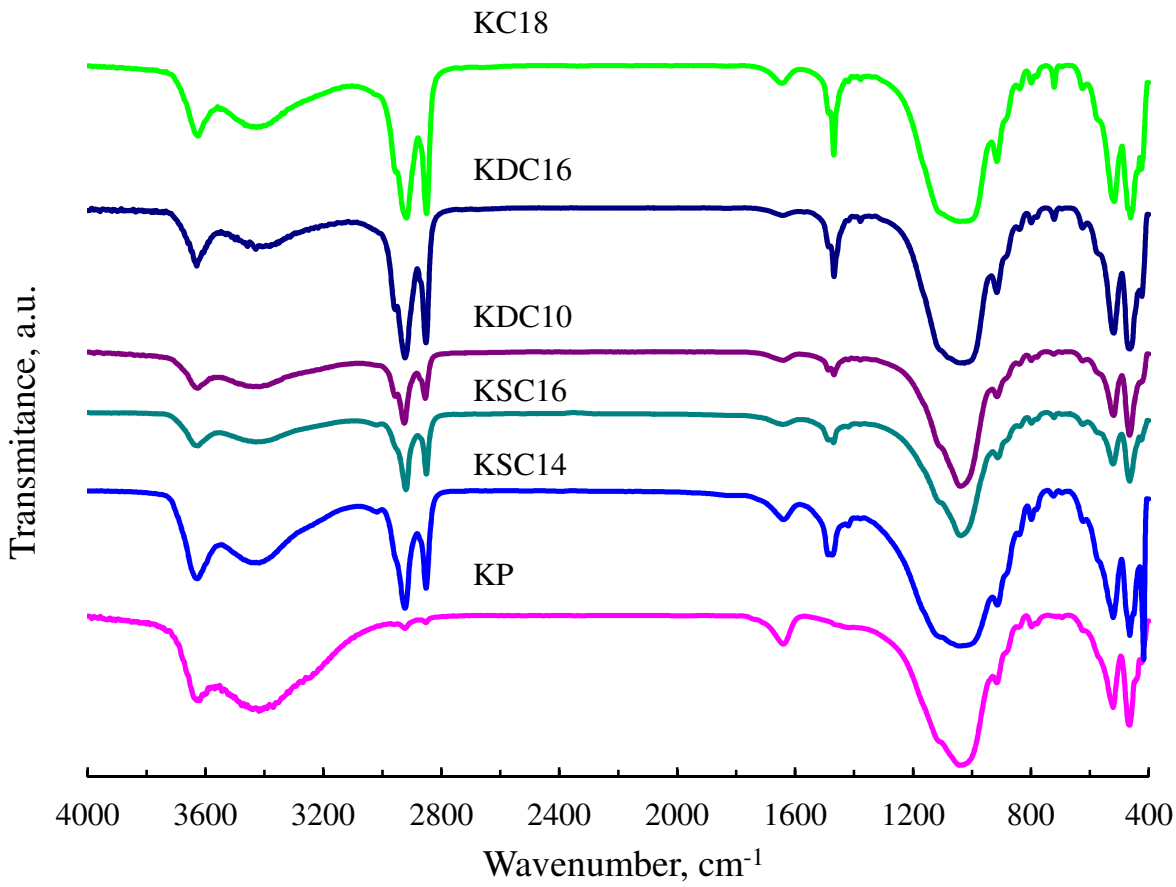

Figure 8. FTIR spectra for Koppies bentonite and its organoderivatives

The assignment of bands to CH_2 and CH_3 was based on a comparison of the relative intensities with increasing aliphatic chain length. The intensity of CH_2 absorption increases

with increasing chain length. Conversely, the intensity of the CH_3 band decreases with increasing chain length. The reverse is also true, i.e. the intensity of the CH_3 band increases with decreasing chain length, whereas the intensity of the CH_2 band decreases.

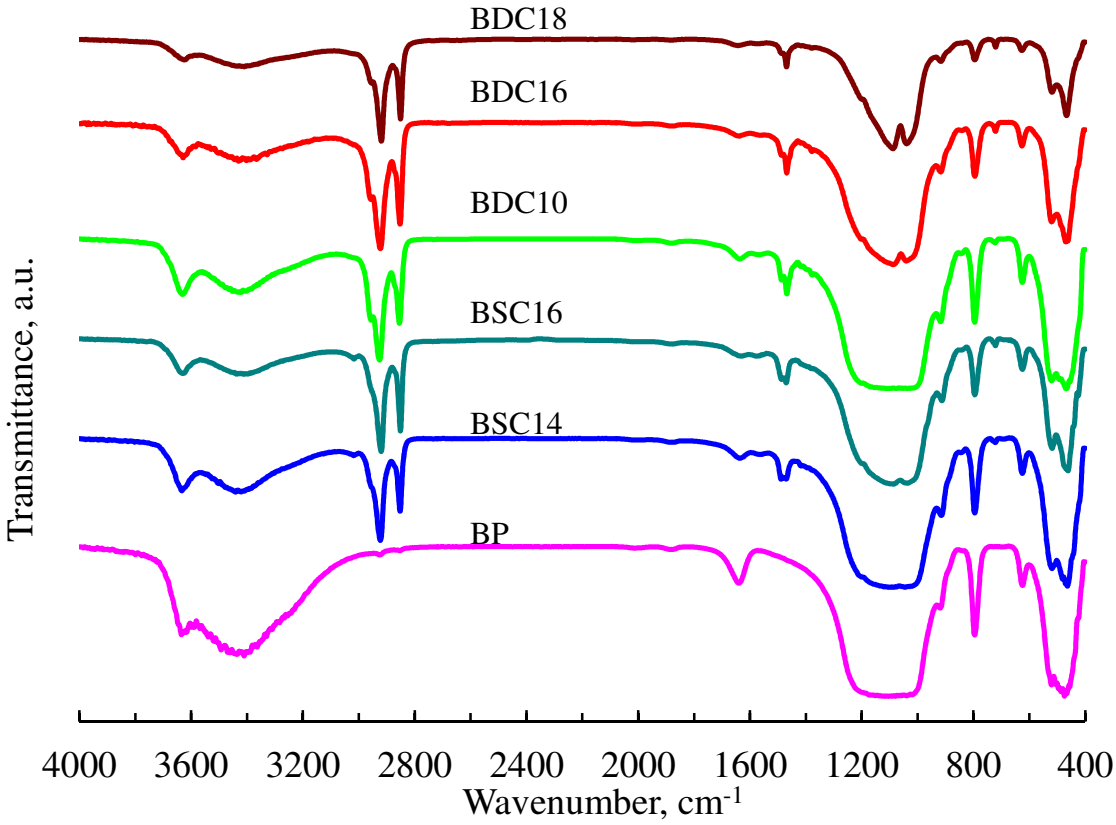

Figure 9. FTIR spectra for Boane bentonite and its organo-derivatives

Vaia et al. (1994) proposed the use of the $\nu_{as}(CH_2)$ band to probe the nature of the interlayer structure. Both the wavenumber and the width of this band are very sensitive to the gauche/trans conformer ratio and the packing density of the chain methylenes. The wavenumber varies from 2917.8 cm^{-1} for the methylene chains in the all-trans ordered state in a crystalline surfactant to 2928.9 cm^{-1} when the chains are in a liquid-like environment (Vaia et al., 1994; Hongping et al., 2004).

The frequencies of $\nu_{as}(CH_2)$ found for the present organobentonites are presented in Table 2. For all surfactants, regardless of the number of chains, the observed values shifted towards values more consistent with the all-trans ordered state with an increase in the alkyl chain lengths. It is speculated, however, that the intercalated alkyl chains did not adopt a rigid solid-like

configuration. Instead it is likely that they were mobile while simultaneously maintaining some degree of orientational order reminiscent of a liquid–crystalline state. Such trans-gauche disorder promotes dense packing of the chains and leads to improved surface mating between the terminal methyl groups and the silicate layers (Lagaly, 1976).

The FTIR CH_2 bending mode [$\delta(CH_2)$] reportedly provides useful additional information (He et al., 2004). A sharp and intense band located around 1472 cm^{-1} indicates strong interchain interactions. Conversely, band broadening coupled with decreased intensity at a position around 1466 cm^{-1} reflects reduced interactions between methylene groups on neighbouring chains (He et al., 2004). The $\delta(CH_2)$ wavenumbers found for the present organobentonites are presented in Table 2. Except for KSC12 and KSC14, the other $\delta(CH_2)$ wavenumbers were similar and were located in the middle of the range 1466-1472 cm^{-1}. As indicated above, the KSC12 and KSC14 organoclay samples feature interdigitated monolayer surfactant intercalation. The extent of interdigitation is such that interactions between different chain methylenes are intense. It is proposed, based on the XRD results, that BSC12 and BSC14 similarly feature interdigitated monolayer surfactant intercalation. However, the chains of the intercalated surfactants have weaker interactions. The other organobentonites comprise bilayer intercalated surfactants with weaker interactions between different chain methylenes.

Figure 8 and Figure 9 compare the FTIR spectra of organically treated clay with the spectra of untreated clay. A combination of narrow and broad absorption bands was observed for all samples between 3700-3200 cm^{-1}. The spectra are not affected, in terms of position (wavenumber), by the presence of organic cations and are characteristic for OH groups. Additional moderate and intense bands were observed from 1750-1360 cm^{-1}, as well as at about 1030 cm^{-1}; in the range 800-650 cm^{-1}they were used to investigate the nature of the OH group. The vibration at about 3618 cm^{-1} was assigned to the smectite structural OH-stretching band. This is a narrow band typical ofthe non-bonded hydroxy group. For clay minerals, OH absorption near 3620 cm^{-1} used to be assigned to inner hydroxyl groups – those located at the surface of octahedral sheets, opposite the tetrahedra. Madejová (2003) stated that smectites with high quantities of Al in the octahedra display absorption at 3620 cm^{-1} in the IR spectra. The broad OH band at approximately 3400 cm^{-1} was due to the presence of adsorbed water and resulted from the H–O–H vibrations of bound water. The intensity of this band decreases as water molecules are displaced by organic species with a larger size.

A typical broad Si–O stretching band is present in the spectra of all samples analysed at approximately 1030 cm^{-1} (Figure 8 and Figure 9). The bands at approximately 793 $cm^{-1}$are attributed to the presence of significant quantities of quartz in the samples. Bands at about 910 cm^{-1} may be assigned to Al_2OH (Madejová, 2003) or AlFeOH (Frost & Kloprogge, 2000). Two non-assigned bands were observed in the range 650-450 cm^{-1} for both untreated and treated clays.

The band structures between 3150 and 3000 cm^{-1} that were expected for KDC18 and BDC18, which would have been indicative of unsaturated aliphatic chains, were not observed. Neither were the C–H out-of-plane bending absorptions observed. Coates (2000) considers these bands to be the most informative regarding the location and spatial geometry of double bonds. The very low concentration of aliphatic C18 double-bonded chains in these samples may explain the absence of the C=C–H absorptions. The possibility that there might be an overlap obscuring the *cis* C–H out-of-plane bending was ruled out. This is because the $\nu_s(CH_2)$ bend at 720 cm^{-1} is not intense enough to obscure the *cis* C–H out-of-plane bending.

4.1.4 Thermal stability of organobentonites

Thermogravimetric analysis (TGA) provides information on the amount of intercalated surfactant (Xie et al., 2001; Xi et al., 2004; Xi et al., 2005; Li & Jiang, 2009). Figure 10 and Figure 11 report the TG mass losses recorded for samples based on Koppies and Boane bentonites respectively. As expected, mass loss increased with increasing number of alkyl chain substituents of surfactants. In addition, the mass loss increases mirrored the increase in the chain length, confirming its dependence on the amount of organic intercalated.

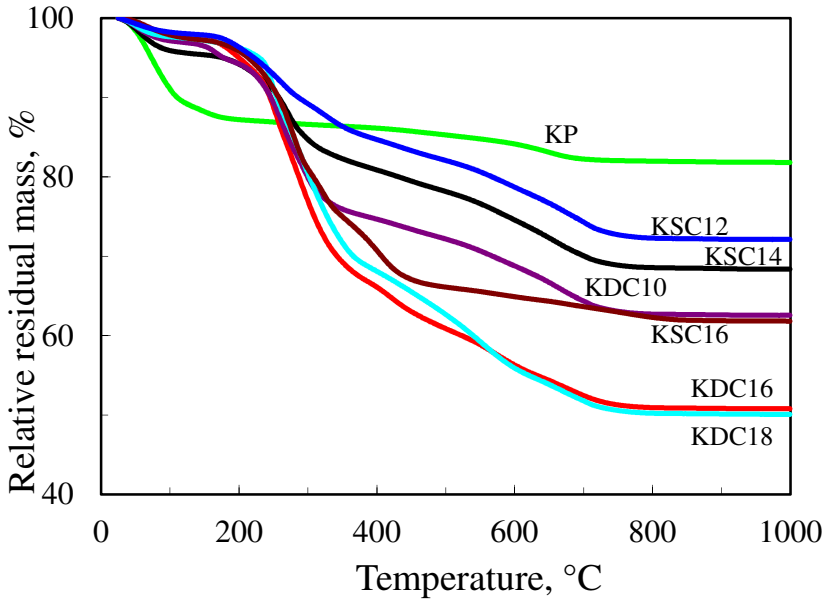

Figure 10. TG mass losses recorded for Koppies bentonite and its organoderivatives

The thermogravimetric decomposition onset temperature, T_{onset}, provides an indicator for the thermal stability of organoclays. T_{onset} is defined as the intercept of the tangent of the initial plateau and that of its main slope on the TG curves (Li & Jiang, 2009). The onset decomposition temperature of the present organobentonites is about 200 ºC (Figure 10 and Figure 11), irrespective of the alkyl chain length (Xie et al., 2001) and number of alkyl chains.

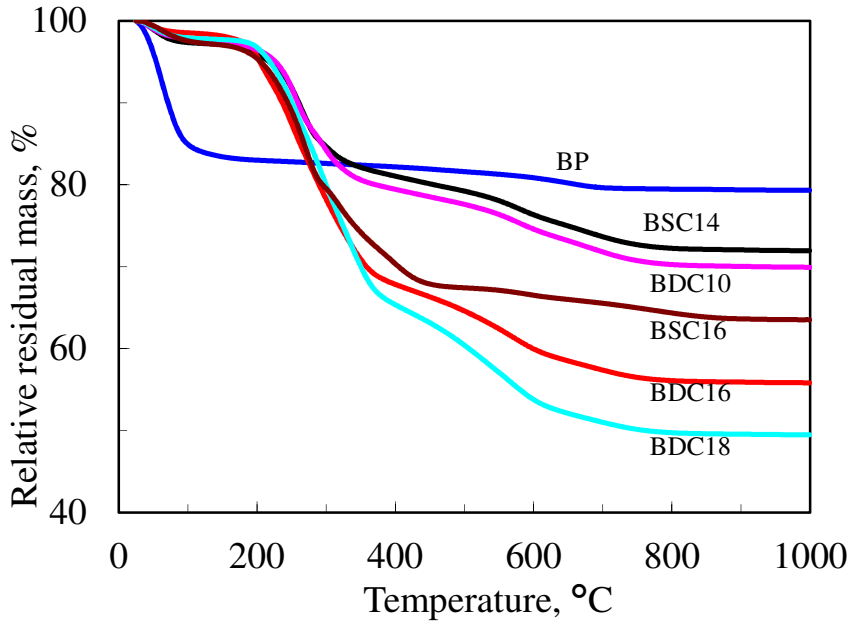

Figure 11. TG mass losses recorded for Boane bentonite and its organoderivatives

Figure 12 and Figure 13 present, respectively, the derivative TG curves for the Koppies and Boane bentonites and their respective organobentonites. These curves show several peaks, indicating that the degradation proceeds in several consecutive steps. These mass loss steps are related to the structure of the inserted molecule (Xi et al., 2004; Xi et al., 2005). For all the surfactants, most of the mass loss occurred in the same temperature range, i.e. 200-400 ºC, regardless of the length or number of alkyl chain substituents.

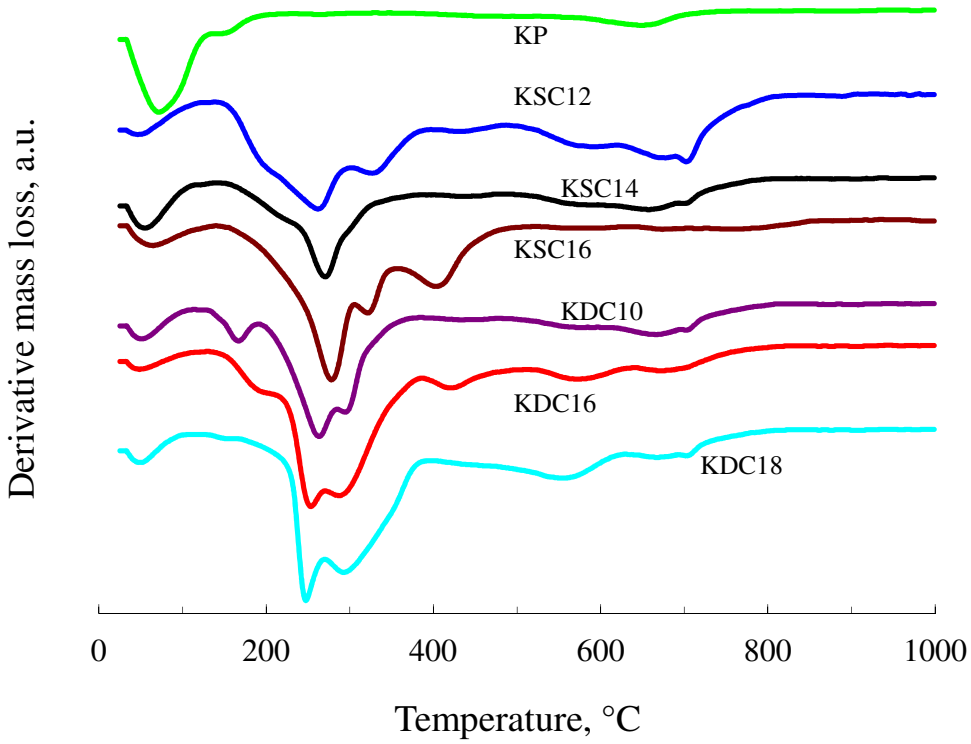

Figure 12. Derivative TG curves for Koppies bentonite and its organobentonites

The main decomposition step is tagged as T_{peak}, the peak temperature corresponding to the maximum mass loss rate. For single-chain intercalated surfactants, only hints of weak peaks were observed below T_{peak}. With the double-chain surfactants a more pronounced peak was observed below T_{peak}. The intensity of T_{peak} increased with chain length for single-chain surfactants. Conversely, T_{peak} decreased with increasing chain length for double-chain surfactants. Similar results for surfactants with two alkyl chains were previously reported (Li & Jiang, 2009). The decrease in T_{peak} was attributed to the development of ordered solid-like chain conformations (Li & Jiang, 2009). However, the T_{peak} trends observed for the present organobentonites are in contradiction to the trends indicated by the downward shift in FTIR

$\nu_{as}(CH_2)$. This suggests that the degradation mechanism of the surfactants might not be as sensitive to the molecular arrangements of the surfactants in the interlayer as has been surmised.

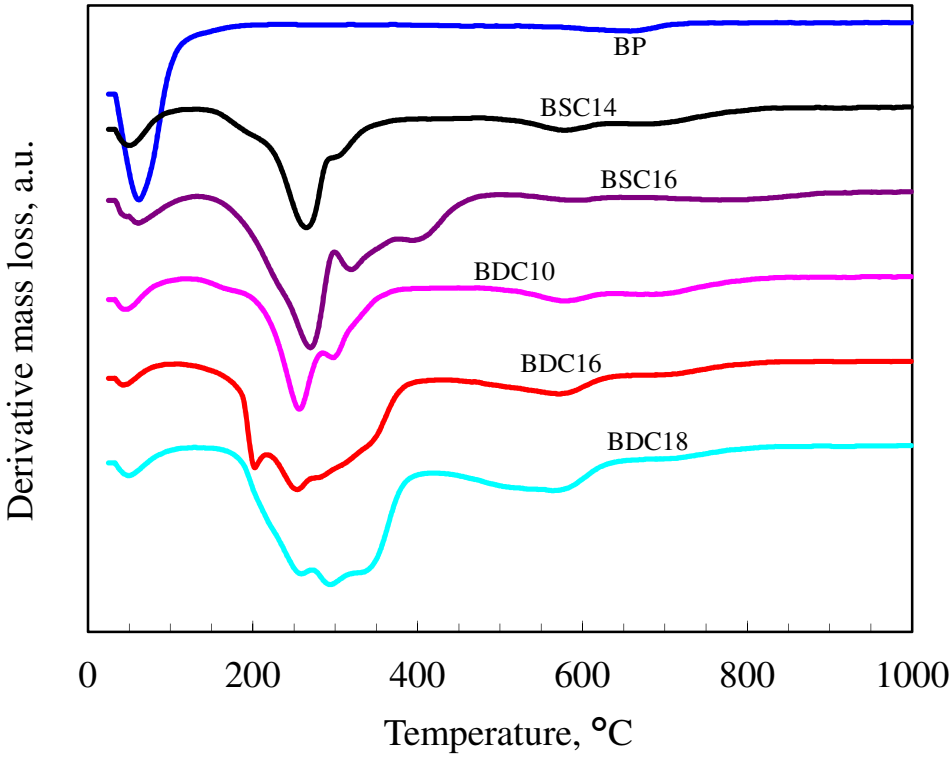

Figure 13. Derivative TG curves for Boane bentonite and its organobentonites

In the DTG curve of the crude bentonites (Figure 12 and Figure 13), only two major thermal events were observed. The DTG curves of the organobentonites showed additional thermal events. The endothermic peak displayed below 100 °C in the DTA curves (Figure 14 and Figure 15) was attributed to the loss of interlayer water. The mass loss associated with this dehydration event amounted to 16.6 mass % for crude bentonites and less than 4 mass % for organobentonites. The higher water content of the crude bentonites was expected as the Ca^{2+} and Na^{+} ions have a greater tendency for hydration than the oleophilic surfactant.

The DTA curves for the crude bentonites are almost featureless in the region between 150 and 600 ºC (Figure 14 and Figure 15). In contrast, the curves obtained for the organobentonites showed significant exothermic events in this temperature range. These were attributed to the oxidative decomposition of intercalated organic species in the air atmosphere (Hedley et al., 2007; Tiwari et

al., 2008). BSC14 and BDC10 featured broad exothermic peaks centred at ca. 330 and 350 ºC respectively.

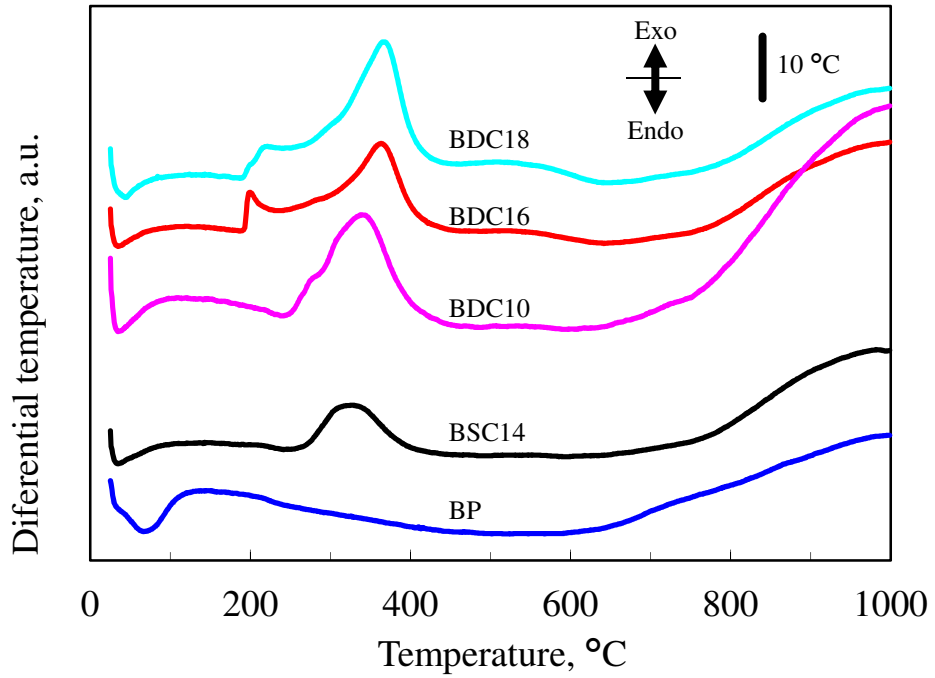

Figure 14. DTA curves for Boane bentonite and its organobentonites

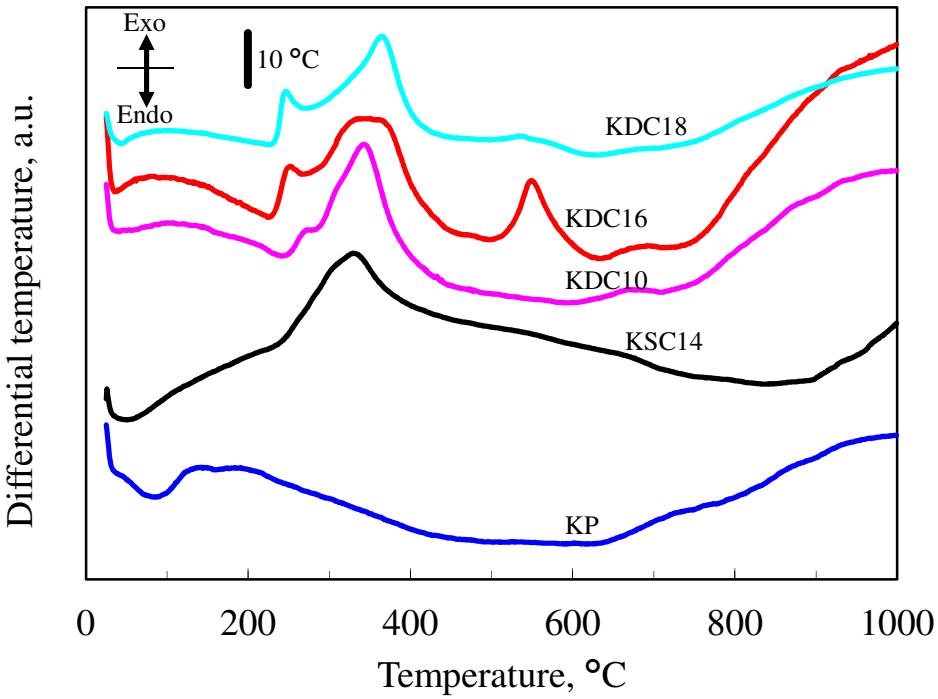

Figure 15. DTA curves for Koppies bentonite and its organobentonites

It is evident from Figure 14 that BDC16 and BDC18 organobentonites started to degrade earlier than all the other organobentonites. A well-defined exotherm onset was observed just below 200 ºC and was followed by a second broader peak centred at ca. 370 ºC (Figure 14). Nevertheless, current results seem to support the claim of Xie et al. (2001) that the decomposition onset temperatures of alkyl ammonium organoclays are independent of the alkyl chain length.

4.2 Characteristics of EVA–organobentonite composites

4.2.1 Morphological characteristics

The properties of clay-based nanocomposites are ultimately determined by their morphology. Homogeneous dispersion of large numbers of stiff high-aspect-ratio platelets in the polymer matrix is usually the desired outcome. This implies the need for extensive delamination and/or exfoliation of the clay particles during the preparation step. Factors that control the exfoliation of clay particles include the properties of the matrix and the organoclays, and the processing route used. Surfactant structural issues significantly affect the properties of organoclays and ultimately the nanocomposite morphology (Fornes et al., 2002). This study held the montmorillonite clay base, the polymer matrix and the melt processing technique constant and focused on the effect of the surfactant structure and its loading on the organoclay. Fornes et al. (2002) studied Nylon 6 composites and observed that decreasing the number of long alkyl chains from two to one, and using an equivalent amount of surfactant with the montmorillonite (as opposed to adding an excess) led to greater extents of silicate platelet exfoliation, increased moduli, higher yield strengths and lower values for the elongation at break. The current study found that the opposite holds for EVA-based micro-nanocomposites prepared by melt compounding. The present results are in better agreement with the findings of Shah et al. (2005) for nanocomposites from poly(ethylene-co-methacrylic acid) copolymers. In these systems four distinct surfactant structural effects lead to improved levels of delamination/exfoliation and higher stiffness for these nanocomposites. These effects are:(1) a higher number of alkyl chains on the amine rather than just one;(2) longer alkyl chains instead of shorter ones;(3) the use of 2-hydroxyethyl groups as opposed to methyl groups on the ammonium ion; and (4) an excess amount of the amine surfactant on the clay instead of an equivalent amount (Shah et al., 2005).

Figure 16 presents the XRD pattern of the soda ash-activated Koppies slurry (KS), neat Koppies powder (KP) bentonite and the organic derivatives. The diffractogram of KS is

featureless, indicating that the bentonite particles were present in an exfoliated form. The basal reflection observed at 2θ = 6.76º for KP bentonite corresponds to d_{001} = 1.52 nm (Table 2). This falls within the 1.2-1.6 nm range typical for smectite minerals under ambient temperature and humidity conditions (Utracki, 2004).

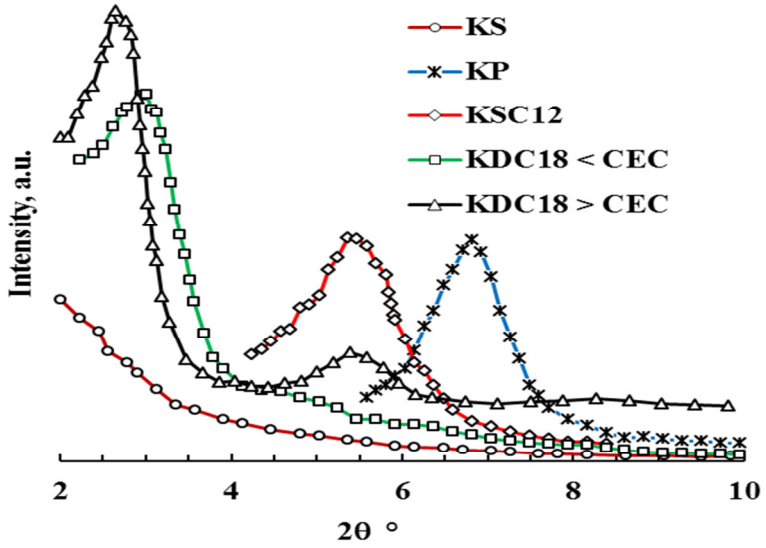

Figure 16. XRD pattern of the soda ash-activated Koppies slurry (KS), neat Koppies powder (KP) bentonite and the organic derivatives

The chain length, surfactant loading and configurations that the surfactant molecules assume in the interlayer determine the basal spacing of organoclays (Lagaly, 1986). The surfactant cations are electrostatically 'attached' to the clay surfaces with the alkyl chains preferring to pack tightly together in order to maximise van der Waals interactions. Excess surfactant intercalates in the neutral salt form, together with (hydrated) counter-ions (Lagaly, 1986; Klapyta et al., 2001).

The diffractograms for the organoclays showed reflections at lower 2θ values, confirming the intercalation of the surfactants. The observed XRD d-spacing for the single-chain surfactant organoclay sample KSC12 was 1.92 nm (Table 2). As previously reported by our laboratory (Massinga et al., 2010; Massinga &Focke, 2012), this value is consistent with interdigitated monolayer surfactant intercalation of the C12 single-chain surfactant. Organobentonites prepared in the presence of the C18 double-chain surfactant below and above the CEC of KP resulted in a nearly identical XRD diffractogram and content of intercalated surfactant

(Figure 16). The XRD-estimated d-spacings were 3.56 nm for the organoclay sample prepared with a stoichiometric amount (KDC18 < CEC) and 3.77 nm for the organoclay sample with an excess of the C18 double-chain surfactant (KDC18 > CEC). These values are consistent with bilayer surfactant intercalation. The additional reflection at 5.45°, in the diffractogram for the KDC18 > CEC sample, corresponds to a second-order basal reflection. This reflection was not observed for the KDC18 < CEC sample, suggesting that more ordered intercalation occurred in the former case.

The XRD diffractograms for EVA composites based on the C12 single-chain surfactant (Figure 17) did not show well-defined reflections, in contrast to those for the EVA-clay composites based on the C18 double-tail surfactant (Figure 18 and Figure 19).

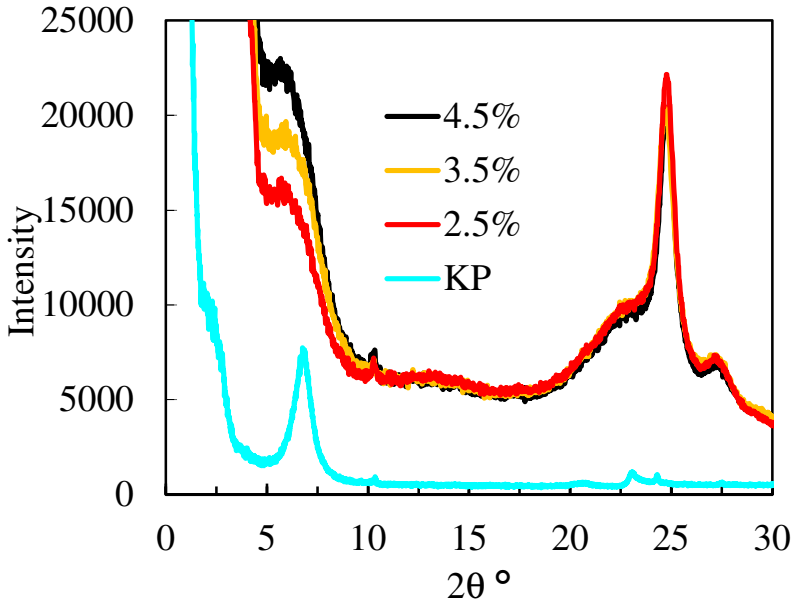

Figure 17. XRD diffractograms for EVA-organoclay composites based on Koppies bentonite with C12 single chain

The diffractogram for all the EVA composites with organoclays based on the C18 double-chain surfactant (Figure 18 and Figure 19) were virtually identical, irrespective of the clay loading. They all showed four clear reflections associated with an integral series of basal plane reflections. This indicates a homogeneous distribution of the alkylammonium cations in the MMT interlayers (Klapyta et al., 2001). Compared with the organoclays, the reflections

are sharper and their positions shifted to lower 2θ values. This implies an increase in perfection and an expansion of the clay gallery height to effect a d-spacing as high as 3.9 nm.

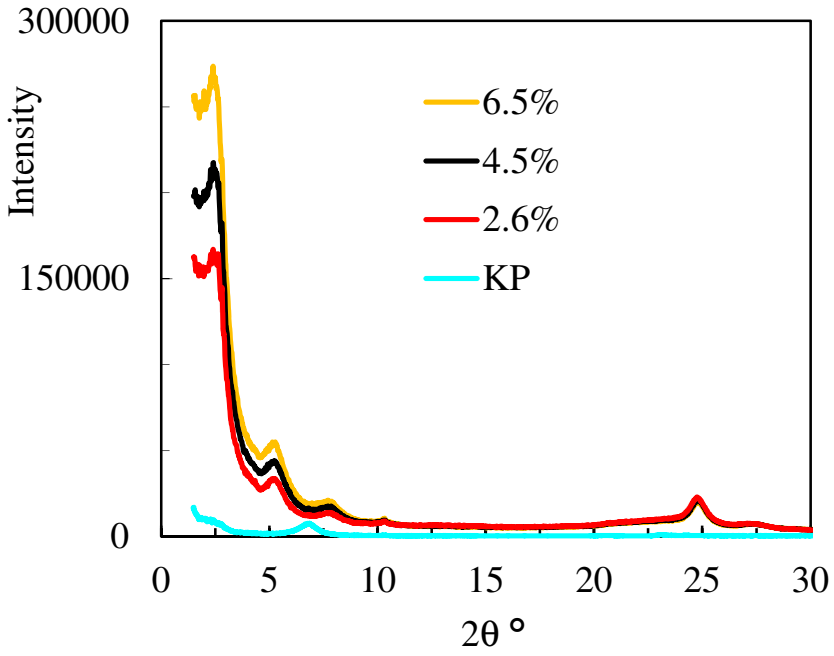

Figure 18. XRD diffractograms for EVA-organoclay composites based on Koppies bentonite with C18 double chain at CEC

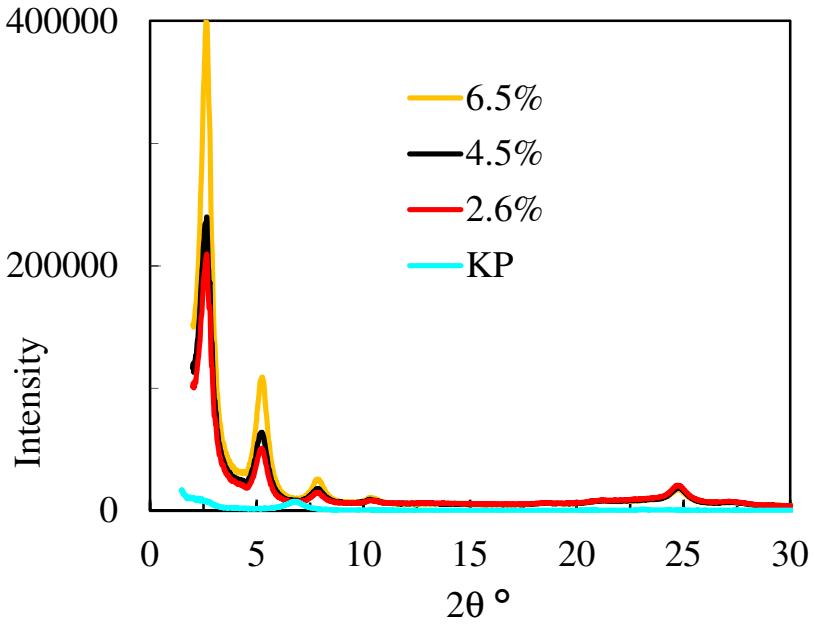

Figure 19. XRD diffractograms for EVA-organoclay composites based on Koppies bentonite with C18 double chain above CEC

The following tentative rationalisation for the results presented in this thesis is proposed. The XRD results indicated interdigitated monolayer intercalation of the single-tail surfactant in the clay, while the double-tail surfactant intercalated in a double-layer fashion (Massinga et al., 2010; Massinga & Focke, 2012). The basal spacing values of the neat organoclays were readily determined as the XRD diffractograms showed clear basal reflections. Incorporating the clays into the EVA by melt compounding changed these diffractograms dramatically. The XRD diffractograms of the KSC12-based nanocomposites became almost featureless, suggesting extensive disruption of the regular clay platelet stacking. Only hints of poorly resolved reflections remained. Such a drastic change is consistent with extensive clay delamination which reduces the remaining platelets to stacks comprising a few clay sheets. TEM provided some evidence for this possibility (Figure 20). An alternative possibility is a significant increase in the degree of disorder in the stacking of the platelets within the tactoids. Random co-intercalation of EVA polymer chains can result in such a severe disruption in the regularity of sheet stacking. The presence of a single hydroxyethyl substituent on the C12 surfactant appears sufficient to encourage co-intercalation of the EVA chains as it is capable of hydrogen bonding with the ester functional groups.

In contrast, the XRD diffractograms for the nanocomposites made using the double-tail surfactant showed sharpened reflections and, in some instances, the emergence of additional reflections attributable to multiple basal reflections. This is consistent with an increase in the structural order of the tactoids due to improved packing of the surfactants intercalated in the clay galleries. It is significant that the diffractograms, and thus the basal spacings, were virtually identical, irrespective of the amount of surfactant employed in the synthesis of the organoclays. Alexandre and Dubois (2000) previously noted an increase in the basal spacing of double-tail intercalated MMT when it was incorporated into EVA. They also found that the surfactant intercalated into the neat clay when both were individually dispersed in molten EVA (Alexandre et al., 2001). An increase in basal spacing has also been observed in other polymer matrices (Pavlidou & Papaspyrides, 2008) and it is generally taken as evidence that polymer intercalation into the clay galleries has occurred (Beyer, 2002). However, the sharpening of the reflection peaks observed in this study is not consistent with polymer intercalation into the clay galleries. Since the polymer chains vary in length and in composition, one would expect significant variations in the d-spacing values and thus a broadening of the XRD reflections if they were co-intercalated. This is in fact observed with

the clay intercalated with surfactant containing the hydroxyethyl substituent. The common shift to lower Bragg angles implies that, more likely, the EVA chains did not enter the clay galleries. Instead, it seems more probable that 'surplus' surfactant molecules released by the delamination and dispersion of the clay sheets during compounding were taken up in the remaining tactoids, resulting in improved ordering through tighter packing of the alkyl chains in the galleries. Nevertheless, it should be kept in mind that the XRD traces capture only the thicker tactoids and certainly not the well-dispersed single (exfoliated) clay sheets.

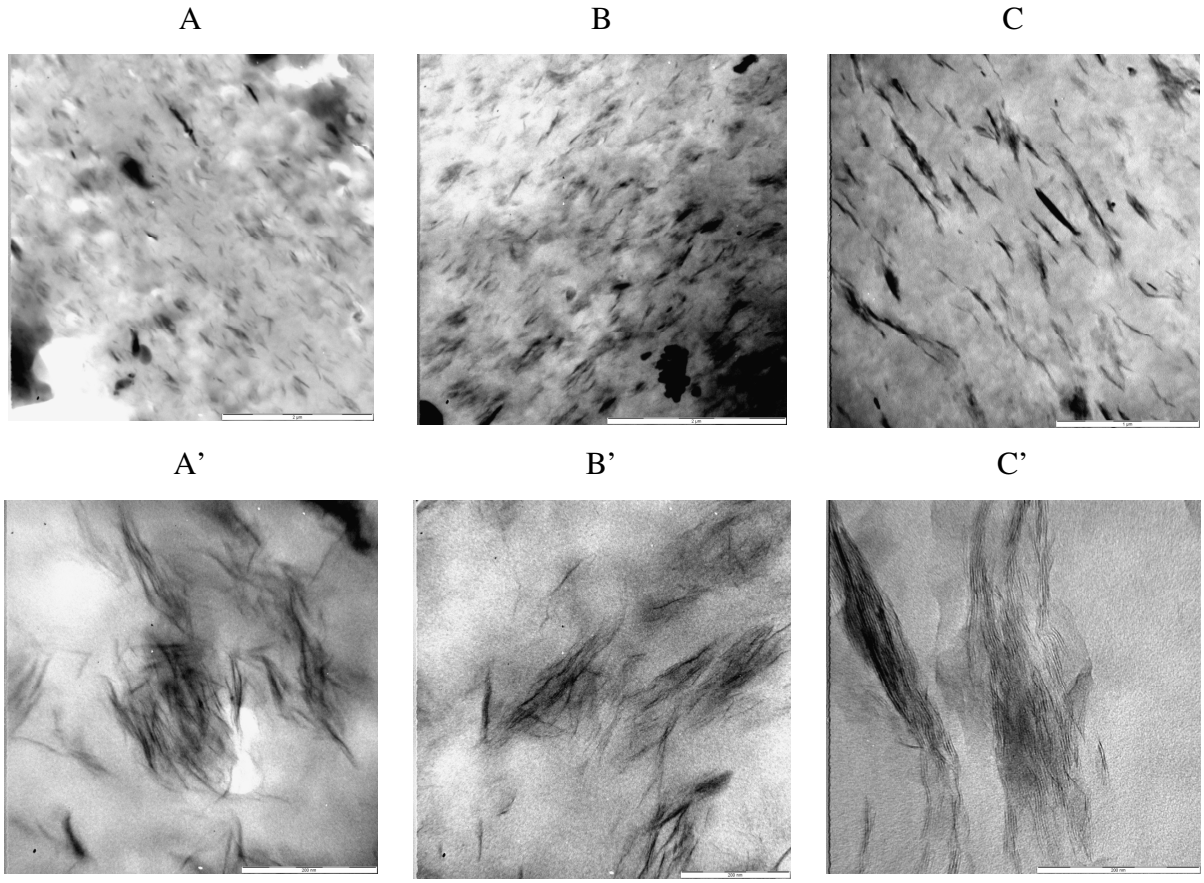

Figure 20. Representative TEM pictures for the EVA-organoclay composites at the micron scale (1 µm): [A] C12 single chain; [B] C18 double chain at CEC; [C] C18 double chain above CEC, and at the nanoscale (200 nm): [A'] C12 single chain; [B'] C18 double chain at CEC; [C'] C18 double chain above CEC

Figure 20 shows representative TEM micrographs of the EVA-organoclay composites at the micron scale (Figure 20A, B, C) and at the nanoscale (Figure 20A', B', C'). Small clay particles are visible at the micron scale but extensive delamination is evident in the

micrographs with nanoscale resolution. This implies that the EVA-organoclay compounds prepared in the present study were a combination of micro- and nanocomposites. The flake-like clay particles seen in the composites based on the single-tail organobentonite KSC12 were significantly smaller and thinner than those observed in the two composites comprising the double-tail surfactant. It seems reasonable to conclude that a surfactant with a single hydroxyethyl substituent facilitates clay sheet dispersions particularly well, similarly to those containing two hydroxyethyl substituents, when all other characteristics are similar.

4.2.2 Rheological and mechanical characteristics

The main consequence of delamination and exfoliation of clay particles is the enhancement of the viscosity of the liquid melt and the modulus in the solid state. Two main mechanisms operate to increase the modulus of composites comprising well-dispersed clay platelets (Pavlidou & Papaspyrides, 2008). The clay platelet particles are significantly stiffer than the polymer matrix. Thus, the first effect derives from their load-carrying ability. In addition, the apparent increase in matrix stiffness arises from the tendency of the clay surfaces to constrain the motion of adjacent polymer chains. Strong polymer chain-clay surface interactions strengthen this confinement effect. Both mechanisms benefit from an increase in the degree of clay exfoliation as the interfacial area also increases.

The rheological behaviour of molten polymer nanocomposites complements XRD and TEM information on the degree of exfoliation of clay platelets in a polymer matrix (Gupta et al., 2005). Figures 21-23 show the effect of clay content and shear rate on the melt viscosity of EVA-clay composites. The high viscosity at low shear rates points to strong interactions between the delaminated clay platelets and the polymer chains or, alternatively, the formation of network structures by clay particle interactions. Pronounced shear thinning indicates extensive clay exfoliation in certain systems (Wagener & Reisinger, 2003; Gupta et al., 2005; Szép et al., 2006). The nanocomposites' internal structure is retained at low shear rates but at high shear rates the clay network structures break down and the platelets tend to orient in the direction of flow. The resulting platelet alignment decreases the apparent viscosity so that it approaches that of the neat polymer melt (Wagener & Reisinger, 2003; Szép et al., 2006).

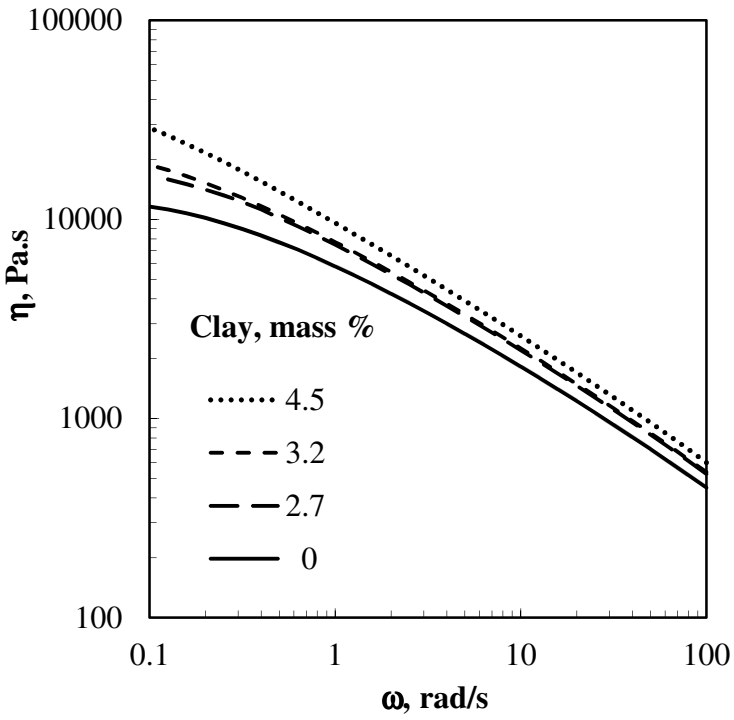

Figure 21. Rheology curves obtained at 170 °C for EVA-clay composites containing the clay prepared with C12 single chain

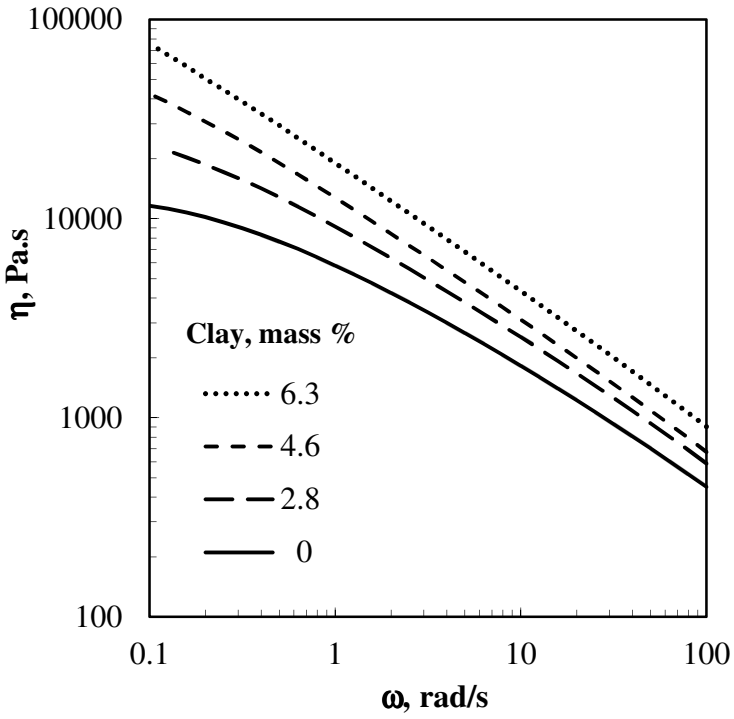

Figure 22. Rheology curves obtained at 170 °C for EVA-clay composites containing the clay prepared with C18 double chain at CEC

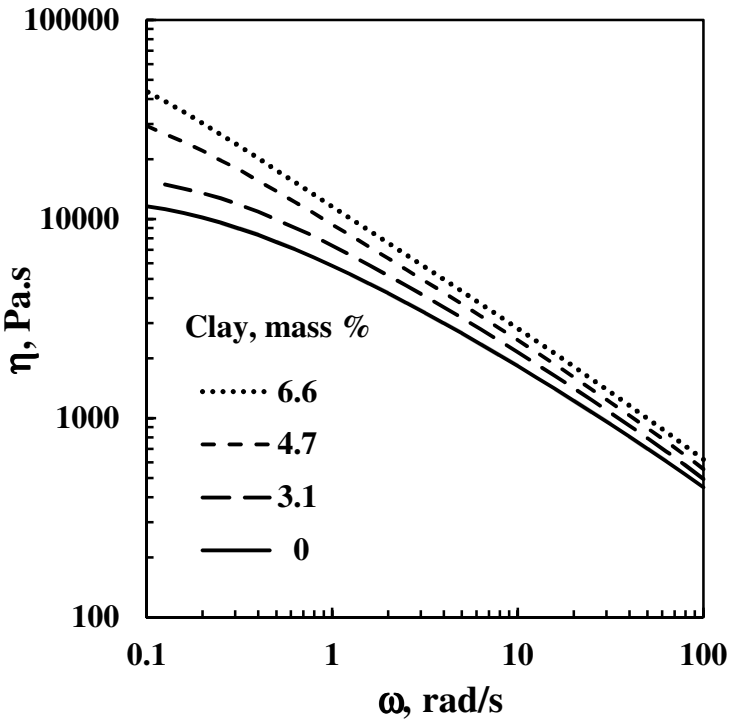

Figure 23. Rheology curves obtained at 170 °C for EVA-clay composites containing the clay prepared with C18 double chain above CEC

Figure 24 compares the relative viscosities scaled with respect to that of the neat EVA at a clay content of ca. 4.5 mass %. Interestingly, the highest melt viscosity is shown by the KDC18 < CEC sample. The melt viscosities of the other two clay composites were similar but significantly lower.

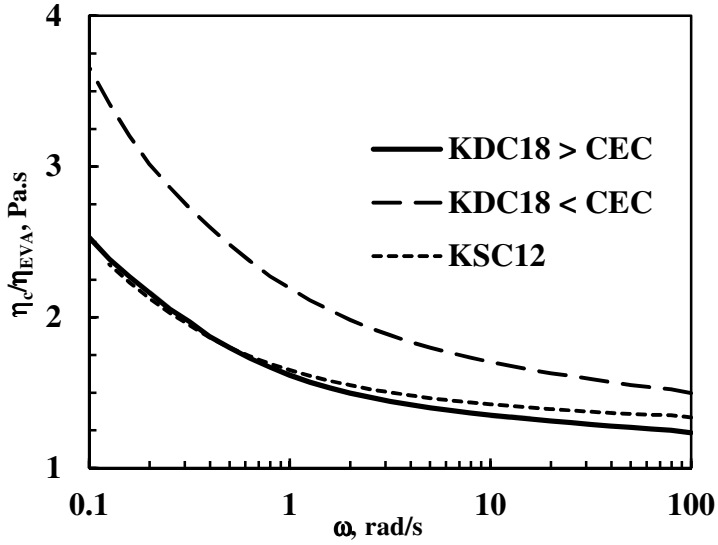

Figure 24. Relative viscosities of composites scaled with respect to that of the neat EVA at a clay content of ca. 4.5 mass %

Table 3 compare moduli for the composites at comparable clay contents. It is clear that the composites based on the double-tail modified clays performed better at modulus enhancement than the single-tail surfactant-modified clay, especially when intercalation beyond a CEC excess was achieved, despite the fact that the single-tail surfactant is more likely to interact with the EVA chains as discussed above. Thus it may be easier to exfoliate bilayer-intercalated clay than interdigitated monolayer intercalated clay. The increase in the melt viscosities mirrored the modulus enhancement for the composites based on the two clays prepared with an equivalent amount of surfactant. Surprisingly, this was not the case for the composite based on an excess of the DC18 surfactant. It provided the best performance in modulus improvement but featured a lower viscosity than the KDC18 < CEC sample. The lowering of the viscosity of the KDC18 > CEC composites was unexpected. However, this can be explained by assuming that some of the excess surfactant must have de-intercalated and that these surfactant molecules imparted an external lubrication effect.

Table 3. Clay content from TGA and mechanical properties of EVA-clay composites

EVA composite	Clay (mass %)	Tensile strength, (MPa)		Strain at break (%)		Young's modulus(MPa)		Tensile impact(MJ/m$^{2)}$	
Neat EVA	0.0	9.1	0.3	287	18	24.3	2.2	0.57	0.01
C12 single chain	2.7	9.0	0.2	250	14	34.1	2.4	0.41	0.06
(KSC12)	3.2	9.2	0.2	236	10	37.7	3.7	0.41	0.02
	4.5	9.3	0.2	245	12	33.1	2.6	0.39	0.02
C18 double chain	2.8	9.3	0.2	271	11	39.2	3.0	0.39	0.03
	3.9	9.4	0.3	274	19	37.3	2.9	0.40	0.02
(KDC18 < CEC)	4.6	9.3	0.2	274	7	42.3	2.5	0.45	0.03
	6.3	9.5	0.2	284	8	49.3	4.3	0.37	0.02
C18 double chain	3.1	12.4	0.3	445	19	38.1	1.5	0.40	0.03
(excess surfactant)	4.7	16.2	0.2	721	22	48.9	2.3	0.35	0.01
(KDC18 > CEC)	6.6	15.1	0.3	663	11	73.1	4.6	0.36	0.03

Note: The second number in each column indicates standard deviation in measured value.

Table 3 reports tensile and tensile impact properties for the EVA nanocomposites. The tensile impact strength decreased with clay loading for all samples. Adding clay reduced it by values between 21 and 38%, depending on the clay used. For the KSC12 and KDC18 < CEC composites, tensile strength increases marginally and elongation at break decreases slightly

with increase in clay content. In contrast, the KDC18 > CEC composites showed significant improvements in both tensile strength and ultimate elongation. Optimum results were obtained for the compound with intermediate clay content (4.7 mass % clay). In this case, the tensile strength and ultimate elongation were 78 and 151% higher than the corresponding values for the neat polymer. The tensile modulus data obtained from tensile strength tests, also summarised in Table 3, indicate that the composites differed markedly with respect to the increase in the Young's modulus. The composite based on the clay containing the double-tail surfactant intercalated in excess of the CEC showed the best performance. The modulus was three times higher than that of the neat EVA at a loading of 6.6 mass %. At a similar clay content, the composite prepared using the organoclay loaded with the same surfactant, but at a lower level, provided only a doubling of the modulus. Table 3 also shows that the increase in modulus with increasing clay content was less for the composites based on the single long alkyl chain surfactant. The nanocomposites displayed a large increase in the elongation at break. This could be due to the plasticising effect of the galleries, their contribution to the formation of dangling chains and conformational effects at the clay-matrix interface (Camargo et al., 2009).

4.2.3 Thermal and thermomechanical characteristics

Table 3 also reports the TGA-determined dry (inorganic) clay contents of the EVA-organoclay composites. Figures 25-27 show TGA results for EVA-organoclay composites based on Koppies bentonite intercalated with C12 single chain and C18 double chain below and above CEC.

Up to a temperature of about 400 °C, all samples showed a similar mass loss profile. Thereafter the observed mass loss was less for the samples with higher clay loadings. At high temperatures, the mass loss reached a plateau value corresponding to the calcined clay residue. This allowed the estimation of the actual clay content of the EVA composites from the residual mass observed at 1 000 °C.

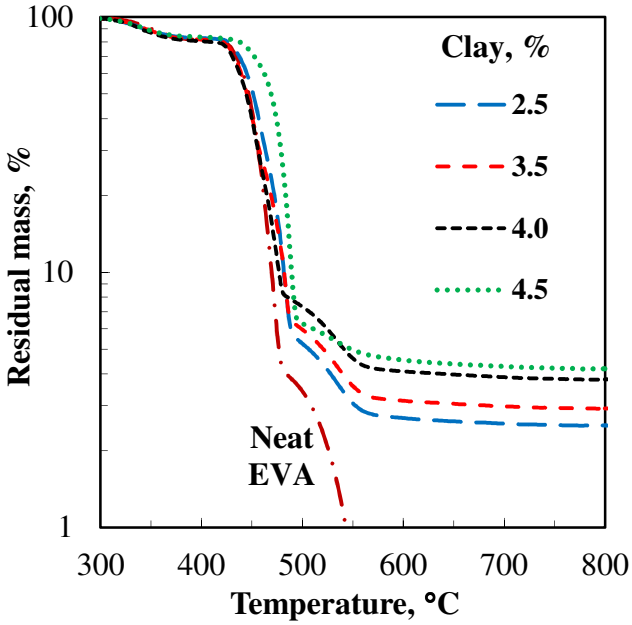

Figure 25. TGA curves for EVA-organoclay composites based on Koppies bentonite with C12 single chain

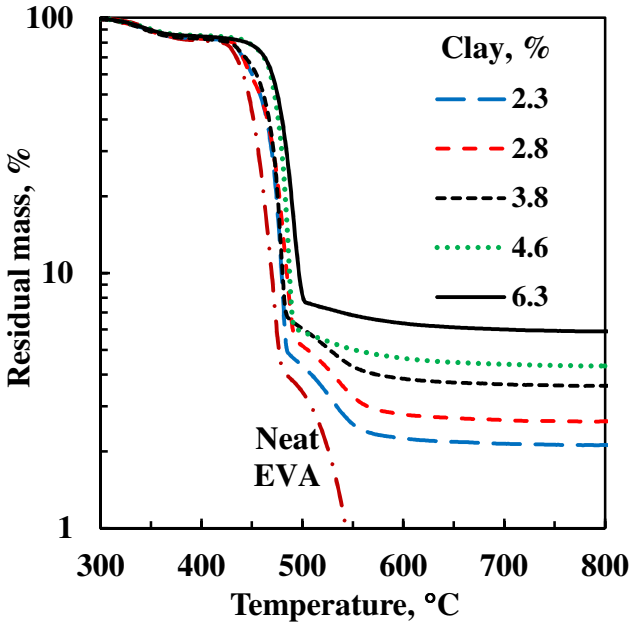

Figure 26. TGA curves for EVA-organoclay composites based on Koppies bentonite with C18 double chain at CEC

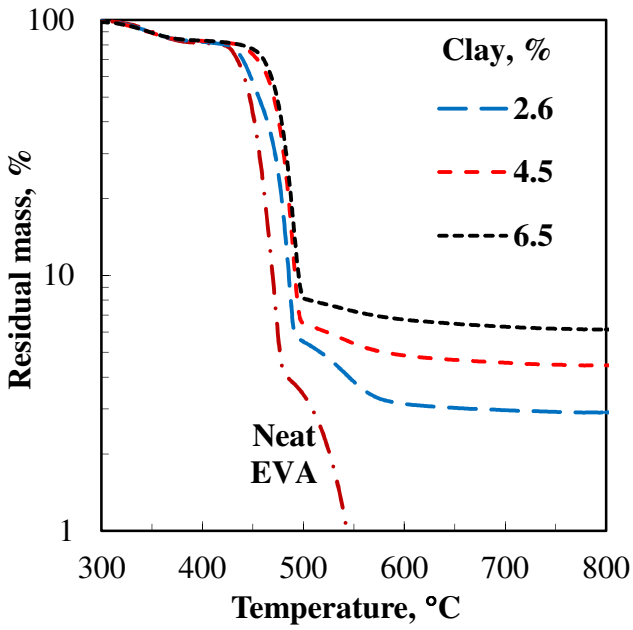

Figure 27. TGA curves for EVA-organoclay composites based on Koppies bentonite with C18 double chain above CEC

Figure 28 shows tan δ as a function of temperature and clay concentration for the composite based on the clay containing double-tail surfactant intercalated in excess of the clay CEC. The shape of the tan δ curve remains approximately the same, but the peak height decreases with increase in clay content. The tan δ curves for the composites made with the other two organoclays showed similar behaviour (Figure 29 and Figure 30). The peak in this curve can be associated with the glass transition temperature which was about -7 °C for the neat EVA as well as for all the composites. This suggests that the presence of the clay did not significantly affect the mobility of the polymer chains of the matrix.

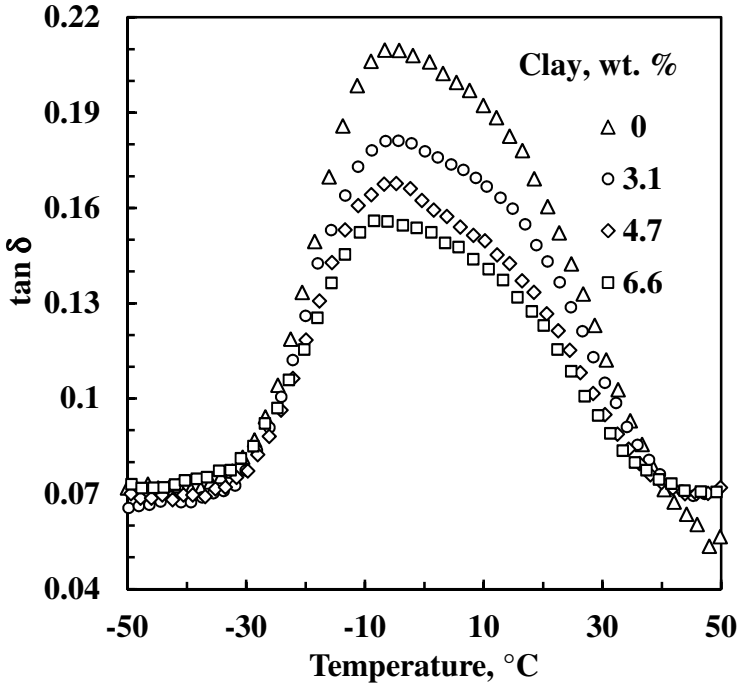

Figure 28. Effect of clay loading on tan δ for EVA-organoclay composites based on the clay containing C18 double chain above CEC

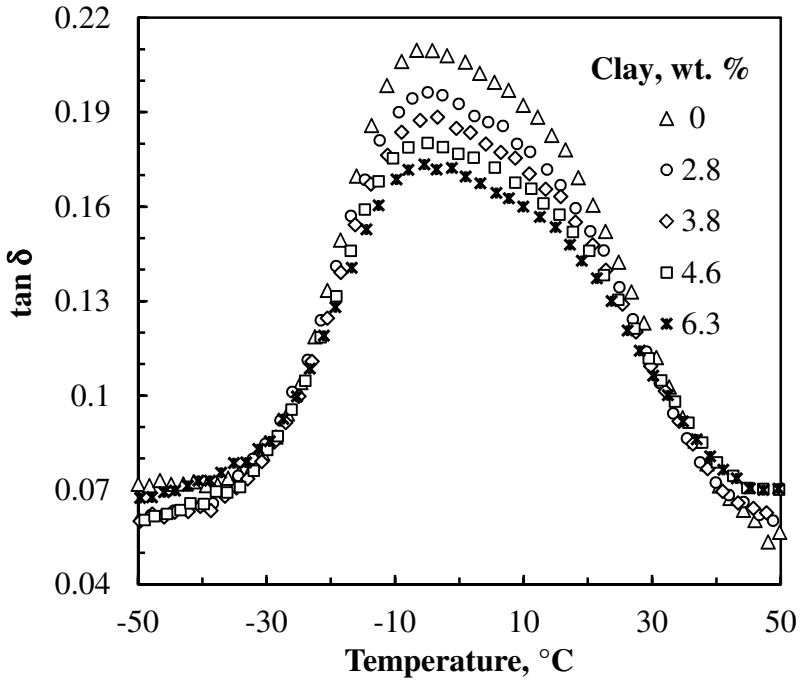

Figure 29. Effect of clay loading on tan δ for EVA-organoclay composites based on the clay containing C18 double chain at CEC

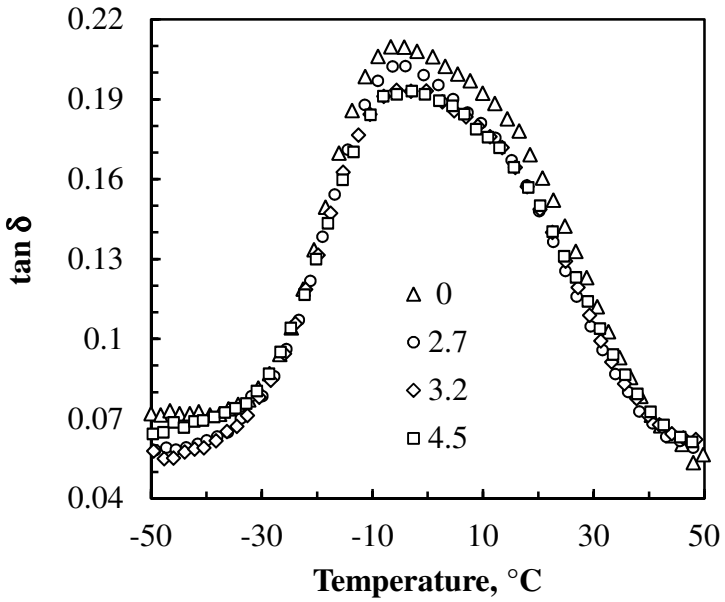

Figure 30. Effect of clay loading on tan δ for EVA-organoclay composites based on the clay containing C12 single chain

Figures 31-33 show the DMA-determined storage modulus as a function of temperature and clay concentration for the EVA-organoclay composites.The graphs show that the stiffness enhancement is limited at low temperatures where the polymer is in a glassy state and more pronounced in the temperature range corresponding to the rubbery plateau, i.e. above the glass transition temperature.

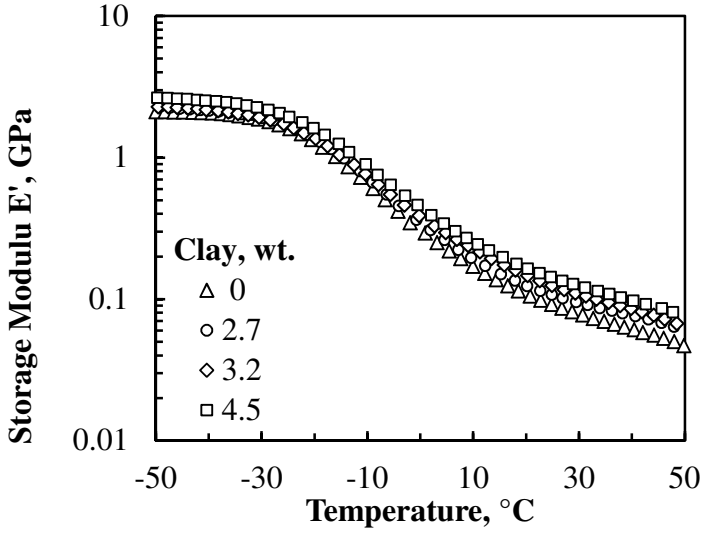

Figure 31. DMA-determined storage modulus for EVA-organoclay composites based on C12 single chain

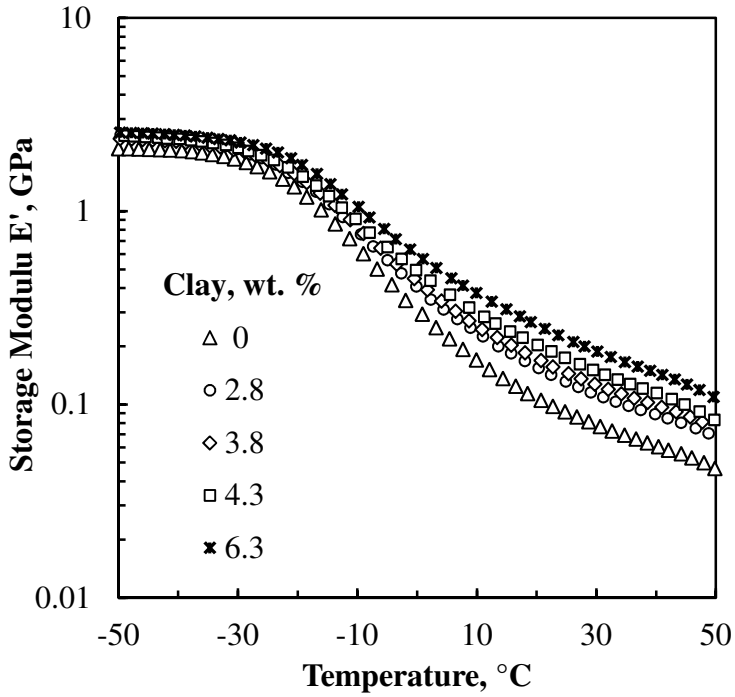

Figure 32. DMA-determined storage modulus for EVA-organoclay composites based on C18 double chain at CEC

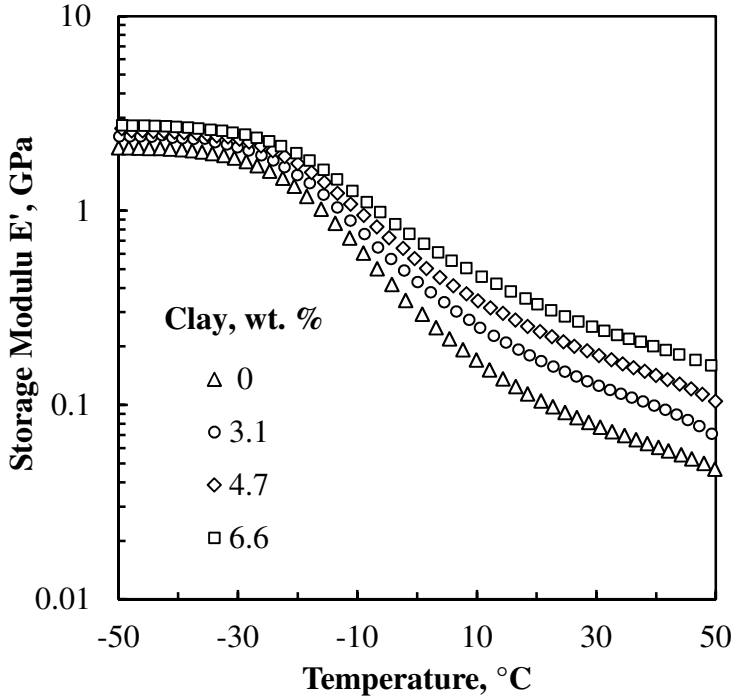

Figure 33. DMA-determined storage modulus for EVA-organoclay composites based on C18 double chain above CEC

Figure 34 compares the modulus enhancement E'_c/E'_p found for the composites containing approximately 4.5 mass % clay. Figures 31-34 confirm that the modulus enhancement trends observed with tensile testing (Table 3) hold over the full temperature range. They show that the enhancement achieved in the glassy region is small and similar for the different organoclay composites but that it becomes differentiated at elevated temperatures.

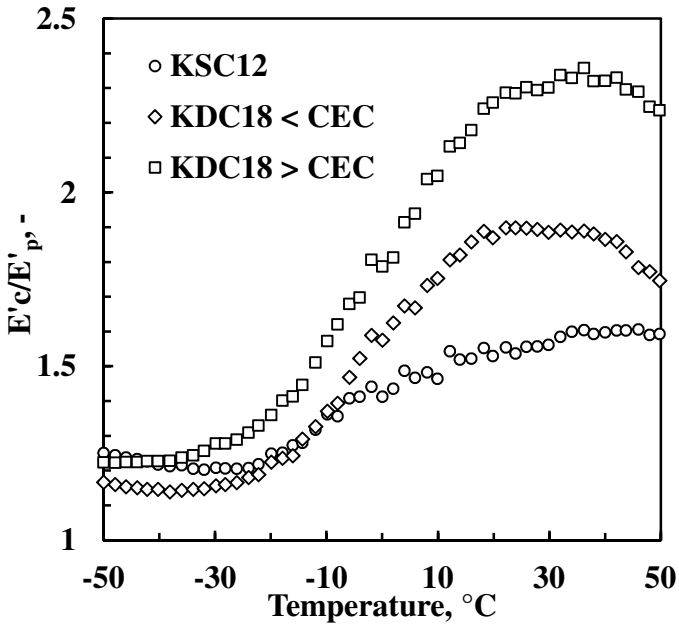

Figure 34. Modulus enhancement for the composites containing approximately 4.5 mass % clay

CHAPTER 5 CONCLUSIONS

Organobentonites were prepared using purified bentonites from the Boane deposit in Mozambique and from the Koppies mine in South Africa. Boane bentonite contained significant amounts of cristobalite that could not be removed cost-effectively. Quaternary ammonium surfactants (quats) were intercalated using soda ash-activated Koppies and Boane bentonite dispersions.

X-ray diffractometry (XRD), Fourier transform infrared (FTIR) spectroscopy and thermogravimetric analysis (TGA) were combined to describe the interlayer structures and their molecular environments. It was concluded that the organobentonite samples comprising single-chain C12 and C14 surfactant consist of monolayers of interdigitated surfactant configurations. The extent of interchain penetration caused strong hydrophobic interactions between the different chain methylenes. The single-chain C16 and double-chain C10, C16 and C18 alkyl surfactants intercalated as bilayers but XRD also hints at the presence of a minor phase comprising interdigitated surfactant configurations. However, FTIR analysis indicated disordered chain conformations. It is speculated that the intercalated alkyl chains did not adopt a rigid solid-like configuration. Instead it is likely that they were mobile while simultaneously maintaining some degree of orientational order reminiscent of a liquid–crystalline state. The interactions between the different chain methylenes of the organobentonites comprising bilayer intercalated surfactants were weaker.

The onset decomposition temperature of the present organobentonites, around 200 ºC, is within the typical range of polymer/organoclay processing temperatures. The thermal stability of the present organobentonites was independent of both the number of alkyl chain substituents and their length, as well as independent of the degree of clay intercalation.

TEM and XRD revealed that the EVA nanocomposites prepared by twin-screw melt compounding had mixed exfoliated/intercalated microstructures. The presence of a single hydroxyethyl substituent in the C12 surfactant appears to be sufficient to encourage co-intercalation of the EVA chains as it is capable of hydrogen bonding with the ester functional groups. It seems reasonable to conclude that a surfactant with a single hydroxyethyl substituent facilitates clay sheet dispersions particularly well, similarly to those containing two hydroxyethyl substituents, when all other characteristics are similar.

The XRD diffractograms for the nanocomposites made using the C18 double-tail surfactant showed sharpened reflections and, in some instances, the emergence of additional reflections attributable to multiple basal reflections. This is consistent with an increase in the structural order of the tactoids due to improved packing of the surfactants intercalated in the clay galleries. However, the sharpening of the reflection peaks observed does not seem consistent with polymer intercalation into the clay galleries. Since the polymer chains vary in length and in composition, one would expect significant variations in d-spacing values and thus a broadening of the XRD reflections if they were co-intercalated. This is in fact observed with the clay intercalated with the surfactant containing the hydroxyethyl substituent. The common shift to lower Bragg angles implies that, more likely, the EVA chains did not enter the clay galleries. Instead, it seems more probable that 'surplus' surfactant molecules released by the delamination and dispersion of the clay sheets during compounding were taken up in the remaining tactoids, resulting in improved ordering through tighter packing of the alkyl chains in the galleries.

Improved mechanical properties were realised, especially when using the bentonite containing the longer double-tail surfactant intercalated at levels in excess of the cation exchange capacity (CEC) of the clay. The nanocomposites showed improved tensile modulus and elongation at break values at the expense of a reduction in impact strength, while tensile strength was about the same as for the neat polymer. It is postulated that it was easier to delaminate these bilayer-intercalated clays and that excess surfactant acted as an external lubricant, thereby reducing the apparent melt viscosity.

CHAPTER 6 REFERENCES

Ahmadi, S., Huang, Y., Li, W., 2005. Fabrication and physical properties of EPDM-organoclay nanocomposites, *Compos. Sci. Technol*. 65, 1069-1076.

Alexandre, M., Dubois, P., 2000. Polymer-layered silicate nanocomposites: preparation, properties and uses of a new class of materials, *Mater. Sci. Eng*. 28, 1-63.

Alexandre, M., Beyer, G., Henrist, C., Cloots, R., Rulmont, A., Jéróme, R., Dubois, P., 2001. "One-pot" preparation of polymer/clay nanocomposites starting from Na^+ montmorillonite. 1. Melt intercalation of ethylene-vinyl acetate copolymer, *Chem. Mater*. 13, 3830-3832.

Bellucci, F., Camino, G., Frache, A., Ristori, V., Sorrentino, L., Iannace, S.,Bian, X., Guardasole, M., Vaccaro, S., 2006. Effect of organoclay impurities on mechanical properties of EVA-layered silicate nanocomposites, e-Polymers 014, 1-10.

Beyer, G., 2002. Nanocomposites: a new class of flame retardants for polymers, *Plastics Additives & Compounding* 4(10), 22-28.

Brown, G., Brindley, G., 1980. Crystal structure of clay minerals and their X-ray identification, Mineralogical Society, London, Monograph 5, 305-360.

Camargo, P., Satyanarayana, K., Wypych, F., 2009. Nanocomposites: synthesis, structure, properties and new application opportunities, *Mat. Res*. 12(1), 1-39.

Calderon, J., Lennox, B., Kamal, M., 2008. Thermal stable phosphonium-montmorillonite organoclays, *Appl. Clay Sci*. 40, 90-98.

Chacko, A., Sadiku, E., Vorster, O., 2009. The rheological and mechanical properties of ethylene-vinyl acetate (EVA) copolymer and organoclay nanocomposites, *J. Reinf. Plast. Comp.* 29, 558-570.

Chaudhary, D., Prasad, R., Gupta, R., Bhattacharya, S., 2005a. Morphological influence on mechanical characterisation of ethylene-vinyl acetate copolymer-clay nanocomposites, *Polym. Eng. Sci.* 45 (7), 889-897.

Chaudhary, D., Prasad, R., Gupta, R., Bhattacharya, S., 2005b. Clay intercalation and influence on crystallinity of EVA-based clay nanocomposites, *Thermochim. Acta* 433 (1-2), 187-195.

Coates, J., 2000. Interpretation of infrared spectra, A practical approach. In: Meyers, R. (Ed.), *Encyclopedia of Analytical Chemistry*, Chichester, Wiley, 10815-10837.

Costache, M., Jiang, D., Wilkie, C., 2005. Thermal degradation of ethylene-vinyl acetate copolymer nanocomposites, *Polymer* 46, 6947-6958.

Cser, F., Bhattacharya, S., 2003. Study of the orientation and the degree of exfoliation of nanoparticles in poly(ethylene-vinyl acetate) nanocomposites, *J. Appl. Polym. Sci*. 90, 3026-3031.

Cui, L., Ma, X., Paul, D., 2007. Morphology and properties of nanocomposites formed from ethylene-vinyl acetate copolymers and organoclays, *Polymer* 48, 6325-6339.

Dal Castel, C., Bianchi, O., Oviedo, M., Liberman, S., Mauler, R., Oliveira, R., 2009. The influence of interfacial agents on the morphology and viscoelasticity of PP/MMT nanocomposites, *Mat. Sci. Eng. C* 29 (2009) 602-606.

De Paiva, L., Morales, A., Diaz, F., 2008. Organoclays: Properties, preparation and applications, *Appl. Clay Sci*. 42, 8-24.

Duquesne, S., Jama, C., Le Brasa, M., Delobelb, R., Recourtc, P., Gloaguen, J., 2003. Elaboration of EVA-nanoclay systems-characterization, thermal behaviour and fire performance, Composites Science and Technology 63, 1141-1148.

Filippi, S., Paci, M., Polacco, G., Dintcheva, N., Magagnini, P., 2011. The interlayer spacing collapse of Cloisite® 30B organoclay, Polymer Degradation and Stability 96(5), 823-832.

Fischer, H., 2003. Polymer nanocomposites: From fundamental research to specific applications, *Mater. Sci. Eng. C* 23, 763-772.

Fornes, T., Yoon, P., Hunter, D., Keskkula, H., Paul, D., 2002. Effect of organoclay structure on nylon 6 nanocomposite morphology and properties, *Polymer* 43, 5915-5933.

Frost, R., Kloprogge, J., 2000. Vibrational spectroscopy of ferruginous smectite and nontronite, *Spectrochim. Acta A* 56, 2177-2189.

Garcia-Lopez, D., Picazo, O., Merino, J., Pastor, J., 2003. Polypropylene-clay nanocomposites: Effect of compatibilizing agents on clay dispersion, *Europ. Polym. J.* 39, 945-950.

Goldstein, A., Beer, M., 2004. Exfoliable organo-montmorillonite nano-fillers for polymer/ceramic composites, *J. Europ. Ceram. Soc.* 24, 3187-3194.

Greene-Kelly, R., 1955. Dehydration of the montmorillonite minerals. *Mineral Mag*. 228.

Gupta, R., Pasanovic-Zujo, V., Bhattacharya, S., 2005. Shear and extensional rheology of EVA/layered silicate-nanocomposites, *J. Non-Newtonian Fluid Mech*. 128, 116-125.

Guven, N., Grim, R., 1972. X-ray diffraction and electron optical studies on smectite and α-cristobalite associations, *Clays Clay Miner.* 20, 89-92.

Hang, P., Brindley, G., 1970. Methylene blue absorption by clay minerals. Determination of surface areas and cation exchange capacities (clay-organic studies xviii), *Clays Clay Miner*. 18, 203-212.

He, H.; Frost, R., Zhu, J., 2004. Infrared study of $HDTMA^+$ intercalated montmorillonite, *Spectrochim. Acta A* 60, 2853.

He, H., Frost, R., Bostrom, T., Yuan, P., Duong, L., Yang, D., Xi, Y., Kloprogge, T., 2006. Changes in the morphology of organoclays with $HDTMA^+$ surfactant loading, *Appl. Clay Sci*. 31, 262-271.

He, H., Ma, Y., Zhu, J., Yuan, P., Qing, Y., 2010. Organoclays prepared from montmorillonites with different cation exchange capacity and surfactant configuration, *Appl. Clay Sci*. 48, 67.

Hedley, C., Yuan, G., Theng, B., 2007. Thermal analysis of montmorillonites modified with quaternary phosphonium and ammonium surfactants, *Appl. Clay Sci*. 35, 180-188.

Hongping, H., Ray, F., Jianxi, Z., 2004. Infrared study of $HDTMA^+$ intercalated montmorillonite. *Spectrochim. Acta* 60, 2853-2859.

Janek, M., Lagaly, G., 2003. Interaction of a cationic surfactant with bentonite: A colloid chemistry study, *Colloid Polym. Sci*. 281, 293-301.

Jeon, C., Ryu, S., Chang, Y., 2003. Preparation and characterization of ethylene vinyl acetate copolymer/montmorillonite nanocomposite, *Polym. Int*. 52, 153-157.

Joseph, S., Focke, W.W., 2011. Poly (ethylene-vinyl co-vinyl acetate)/clay nanocomposites: Mechanical, morphology and thermal behavior.*Polym. Comp.*, 32(2), 252-258.

Klapyta, Z., Fujita, T., Iyi, N., 2001. Adsorption of dodecyl- and octadecyl trimethyl ammonium ions on a smectite and synthetic micas, *Appl. Clay Sci*. 19, 5-10.

Konta, J., 1980. Properties of ceramic raw materials. In: Bilke, W. E., Paetsch, D. (Eds), *Ceramic Monographs – Handbook of Ceramics,* Monograph 1.1.4, Freiburg, Germany, Verlag Schimdt GmbH.

Konta, J., 1995. Clay and man: Clay raw materials in the service of man, *Appl. Clay Sci*. 10, 275-335.

Kopka, H., Beneke, K., Lagaly, G., 1998. Anionic surfactants between double metal hydroxide layers, *J. Colloid Interf. Sci*. 123, 427-436.

Kornmann, X., Berglund, L., Sterte, J., 1998. Nanocomposites based on montmorillonite and unsaturated polyester, *Polym. Eng. Sci*., 38, 1351-1358.

Kwolek, T., Hodorowicz, M., Stadnicka, K., Czapkiewicz, J., 2003. Adsorption isotherms of homologous alkyl dimethyl benzyl ammonium bromides on sodium montmorillonite, *J. Colloid Interf. Sci*. 264, 14-19.

Lagaly, G., Weiss, A., 1970a. Anordnung und Orientierung kationischer Tenside auf Silicatoberflächen. II. Paraffinähnliche Strukturen bei den *n*-Alkylammonium-Schichtsilicaten mit hoher Schichtladung (Glimmer). *Kolloid-Z. u. Z. Polymere*237, 364-368.

Lagaly, G., Weiss, A., 1970b. Anordnung und Orientierung kationischer Tenside auf Silicatoberflächen. III. Paraffinartige Strukturen bei den *n*-Alkylammonium-Schichtsilicaten mit mittlerer Schichtladung (Vermiculite). *Kolloid-Z. u. Z. Polymere* 238, 485-493.

Lagaly, G., 1976. Kink-block and gauche-block structures of bimolecular films. *Angew. Chem. Int. Ed. Engl*. 15, 575-586.

Lagaly, G., 1986. Interaction of alkylamines with different types of layered compounds, *Solid State Ionics* 22, 43-51.

La Mantia, F., Tzankova Dintcheva, N., 2006. EVA copolymer-based nanocomposites: Rheological behavior under shear and isothermal and non-isothermal elongational flow, *Polym. Test*. 25, 701-708.

LeBaron, P., Wang, Z., Pinnavaia, T., 1999. Polymer-layered silicate nanocomposites: An overview, *Appl. Clay Sci.* 15, 11-29.

Lee, J., Lee, H., 2004. Characterization of organobentonite used for polymer nanocomposites, *Mater. Chem. Phys*. 85, 410-415.

Lee, H., Park, B., Choi, H., Gupta, R., Bhattachary, S., 2007. Preparation and rheological characteristics of ethylene-vinyl acetate copolymer/organoclay nanocomposites, J. Macromolecular Sci., Part B: Physics 46 B (2), 261-273.

Li, Z., Jiang, W., 2009. A thermogravimetric investigation of alkylammonium intercalation into rectorite, *Thermochim. Acta* 483, 58.

Madejová, J., 2003. FTIR techniques in clay mineral studies, *Vib. Spectrosc*. 31, 1-10.

Marini, J., Branciforti, M., Lotti, C., 2009. Effect of matrix viscosity on the extent of exfoliation in EVA/organoclay nanocomposites, *Polym. Adv. Technol.* 21 (6), 408-417.

Martins, C., Larocca, N., Paul, D., Pessan, L., 2009. Nanocomposites formed from polypropylene/EVA blends, Polymer 50, 1743-1754.

Massinga Jr., P.,Focke, W., De Vaal, P., Atanasova, M., 2010. Alkyl ammonium intercalation of Mozambican bentonite, *Appl. Clay Sci*., 49, 142-148.

Massinga Jr., P.,Focke, W., 2012. Intercalating cationic surfactants in Koppies bentonite, *Mol. Cryst. Liq. Cryst.*, 555(1), 85-93.

Mezger, T. (2006). *Rheology Handbook: For Users of Rotational and Oscillatory Rheometers*, 2nd ed.,Hanover, Germany, Vicentz Network GmbH.

Montanari, G., Cavallini, A., Guastavino, F., Coletti, G., Schifani, R., Di Lorenzo Del Casale, M., Camino, G., Deorsola, F., 2004. Microscopic and nanoscopic EVA composite investigation: Electrical properties and effect of purification treatment, Annual Report - Conference on Electrical Insulation and Dielectric Phenomena, CEIDP, 318-321.

Pan, J., Yang, G., Han, B., Yan, H., 1997. Studies on interaction of dodecyltrimethylammonium bromide with Na- and Al-montmorillonite, *J. Colloid Interf. Sci.*194, 276-280.

Pasanovic-Zujo, V., Gupta, R., Bhattacharya, S., 2004. Effect of vinyl acetate content and silicate loading on EVA nanocomposites under shear and extensional flow, *Rheolog. Acta*43(2), 99-108.

Patel, H., Somani, R., Bajaj, H., Jasra, R., 2007. Preparation and characterization of phosphonium montmorillonite with enhanced thermal stability, *Appl. Clay Sci*. 35, 194-200.

Paul, D., Zeng, Q., Yu, A., Lu, G., 2005. The interlayer swelling and molecular packing in organoclays, *J. Colloid Interf. Sci*. 292, 462-468.

Paul, D., Robeson, L., 2008. Polymer nanotechnology: Nanocomposites, M. *Polymer*, 49, 3187-3204.

Pavlidou, S., Papaspyrides, C., 2008. A review on polymer-layered silicate nanocomposites, *Prog. Polym. Sci*. 33, 1119-1198

Peeterbroeck, S., Alexandre, M., Jérôme, R., Dubois, P., 2005. Poly(ethylene-co-vinyl acetate)/clay nanocomposites: Effect of clay nature and organic modifiers on morphology, mechanical and thermal properties, *Polym. Degrad. Stab*. 90(2 Spec. Iss.), 288-294.

Pereira de Abreu, D., Losada, P., Angulo, I., Cruz, J., 2007. Development of new polyolefin films with nanoclays for application in food packaging, Europ. Polym. J. 43, 2229-2243.

Perez, E., 1974. Modificaciones de las Pastas Ceramicas por Medio de Electrolitos y Coloides Protectores, Madrid, Instituto Eduardo Torroja de la Construccion y del Cemento, 51.

Pistor, V., Lizot, A., Fiorio, R., Zattera, A., 2010. Influence of physical interaction between organoclay and poly(ethylene-co-vinyl acetate) matrix and effect of clay content on rheological melt state, *Polymer* 51, 5165-5171.

Powell, C., Beall, G., 2006. Physical properties of polymer/clay nanocomposites, *Curr. Opin. Solid State Mater. Sci.*10, 73-80.

Prasad, R., Gupta, R., Cser, F., Bhattachary, S., 2006. Experimental investigation of the linear viscoelastic response of EVA-based nanocomposites, *J. App. Polym. Sci*. 101, 2127-2135.

Preschilla, N., Sivalingam, G., Rasheed, A., Tyagi, S., Biswas, A., Bellare, J., 2008. Quantification of organoclay dispersion and lamellar morphology in poly(propylene)-clay nanocomposites with small angle X-ray scattering, *Polymer* 49, 4285-4297.

Rehab, A., Salahuddin, N., 2005. Nanocomposite materials based on polyurethane intercalated into montmorillonite clay, *Mater. Sci. Eng. A* 399, 368-376.

Riva, A., Zanetti, M., Braglia, M., Camino, G., Falqui, L., 2002. Thermal degradation and rheological behaviour of EVA/montmorillonite nanocomposites, *Polym. Degrad. Stab*. 77(2), 299-304.

Sinha Ray, S., Okamoto, M., 2003. Polymer/layered silicate nanocomposites: A review from preparation to processing, *Prog. Polym. Sci*. 28, 1539-1641.

Shah, R., Hunter, D., Paul, D., 2005. Nanocomposites from poly(ethylene-co-methacrylic acid) ionomers: effect of surfactant structure on morphology and properties, *Polymer* 46, 2646-2662.

Shenoy, A. (1999). *Rheology of Filled Polymer Systems*. London, UK, Kluwer Academic.

Suh, I., Ryu, S., Bae, J., Chang, Y., 2004. Effects of compatibilizer on the layered silicate/ethylene vinyl acetate nanocomposite, *J. Appl. Polym. Sci*., 94, 1057-1061.

Szép, A., Szabó, A., Tóth, N., Anna, P., Marosi, G., 2006. Role of montmorillonite in flame retardancy of ethylene vinyl acetate copolymer, *Polym. Degrad. Stab*. 91, 593-599.

Tahani, A., Karroua, M., Van Damme, H., Levitz, P., Bergaya, F., 1999. Adsorption of a cationic surfactant on Na-montmorillonite: Inspection of adsorption layer by X-ray and fluorescence spectroscopies, *J. Colloid Interf. Sci.*216, 242-249.

Tian, Y., Yu, H., Wu, S., Ji, G., 2004. Study on the structure and properties of EVA/MMT nanocomposites, J. Materials Sci. 39, 4301-4303.

Tiwari, R., Khilar, K., Natarajan, U., 2008. Synthesis and characterization of novel organo–montmorillonites, *Appl. Clay Sci*. 38, 203-208.

Utracki, L., 2004. *Clay-Containing Polymeric Nanocomposites*. Vol. 1, Shawbury, UK, Rapra Technology Limited.

Vaccari, A., 1998. Preparation and catalytic properties of cationic and anionic clays, *Catal. Today* 41, 53-71.

Vaia, R., Teukolsky, R., Giannelis, E., 1994. Interlayer structure and molecular environment of alkylammonium layered silicates, *Chem. Mater*. 6, 1017-1022.

van Olphen, H., 1964. Internal mutual flocculation in clay suspensions, J. colloid sci. 19, 313-322

Velde, B., 1985. *Clay Minerals – A Physico-Chemical Explanation of their Occurrence,* Amsterdam, Elsevier.

Voyutsky, S., 1978. *Colloid Chemistry*, Moscow, Mir Publishers, 560.

Wagener, R., Reisinger, T., 2003. A rheological method to compare the degree of exfoliation of nanocomposites. *Polymer* 44, 7513-7518.

Wang, S., Hu, Y., Zong, R., Tang, Y., 2004. Preparation and characterization of flame retardant ABS/montmorillonite nanocomposites, *Appl. Clay Sci*. 25, 49-55.

Xi, Y., Ding, Z., He, H., Frost, R., 2004. Structure of organoclays – An X-ray diffraction and thermogravimetric analysis study, *J. Colloid Interf. Sci*., 277, 116.

Xi, Y., Martens, W., He, H., Frost, R., 2005. Thermogravimetric analysis of organoclays intercalated with the surfactant octadecyl trimethyl ammonium bromide, *J. Therm. Anal. Calorim.*, 81, 91.

Xie, W., Gao, Z., Liu, K., Pan, W., Vaia, R., Hunter, D., Singh, A., 2001. Thermal characterization of organically modified montmorillonite, *Thermochim. Acta* 367-368, 339-350.

Xu, S., Boyd, S., 1995. Cationic surfactant adsorption by swelling and nonswelling layer silicates, *Langmuir*, 11, 2508-2514.

Yui, T., Yoshida, H., Tachibana, H., Tryk, D., Inoue, H., 2002. Intercalation of polyfluorinated surfactants into clay minerals and the characterization of the hybrid compounds, *Langmuir* 18, 891-896.

Zanetti, M., Camino, G., Thomann, R., Mülhaupt, R., 2001. Synthesis and thermal behaviour of layered silicate-EVA nanocomposites, *Polymer* 42(10), 4501-4507.

Zhang, W., Chen, D., Zhao, Q., Fang, Y., 2003. Effects of different kinds of clay and different vinyl acetate content on the morphology and properties of EVA/clay nanocomposites, *Polymer* 44 (26), 7953-7961.

Zhang, F., Sundararaj, U., 2004. Nanocomposites of ethylene-vinyl acetate copolymer (EVA) and organoclay prepared by twin-screw melt extrusion, *Polym. Comp.* 25(5), 535-542.

Zhu, R., Zhu, L., Zhu, J., Xu, L., 2008. Structure of cetyltrimethylammonium intercalated hydrobiotite, *Appl. Clay Sci*. 42, 224-231.

APPENDICES

Appendix A.1

The cation exchange capacity (CEC) of KP, from South Africa, is 0.85 meq/g of dry clay. The CEC of Mozambican BP clay is 0.70 meq/g of dry clay. These CECs were used to calculate the amount of each intercalating agent for intercalation experiments. The mass of organic cation (OC) equivalent to these clay CECs was calculated as follows:

$$\text{m OC (g)} = \text{Clay CEC (meq)} * \frac{1\,\text{eq}}{1000\,\text{eq}} * \frac{1\,\text{mol OC}}{1\,\text{eq OC}} * \frac{\text{M (g/mol) OC}}{1\,\text{mol OC}}$$

Where: m = mass; M = molar mass

Example

This example corresponds to the calculation for preparing KSC14 (Koppies slurry and quaternary ammonium salt SC14 (M = 336 g/mol). The CEC is 0.85 meq/g of dry clay.

$$m_{SC14} = 0.85\,\text{meq} * \frac{1\,\text{eq}}{1000\,\text{eq}} * \frac{1\,\text{mol C14TAB}}{1\,\text{eq C14TAB}} * \frac{336\,\text{g/mol C14TAB}}{1\,\text{mol C14TAB}} = 0.29\,\text{g}$$

The calculated mass of SC14 is equivalent to the CEC of 1 g of dry clay. However, for the synthesis of KSC14 an amount of clay slurry comprising 94.7 g of dry clay instead of 1 g was used. Therefore, the mass of SC14 required for 94.7 g of dry clay was:

$$m_{SC14} = 94.7 * 0.29 \text{ g SC14} = 27.45 \text{ g}$$

A mass of SC14 1.5 times the equivalent of the clay CEC was used instead of 27.45 g SC14.

$$M_{SC14\ (excess\ 50\%)} = 1.5 * 27.45 \text{ g C14TAB} = 41.2 \text{ g}$$

Since the intercalation experiments did not use dry clay, but clay slurry, it was necessary to calculate the amount of KS comprising 94.7 g of dry clay. In Figure 1, the solid content of

South African clay slurry KS was determined as 18.9 mass %. Therefore, the amount of clay slurry containing 94.7 g of dry clay was calculated as follows:

$$m_{KS} = \frac{94.7\text{g}}{0.189} = 501\,\text{g}$$

This mass of clay slurry was intercalated with 41 g of SC14, which is about 1.5 times the mass of organic cation equivalent to the clay's CEC.

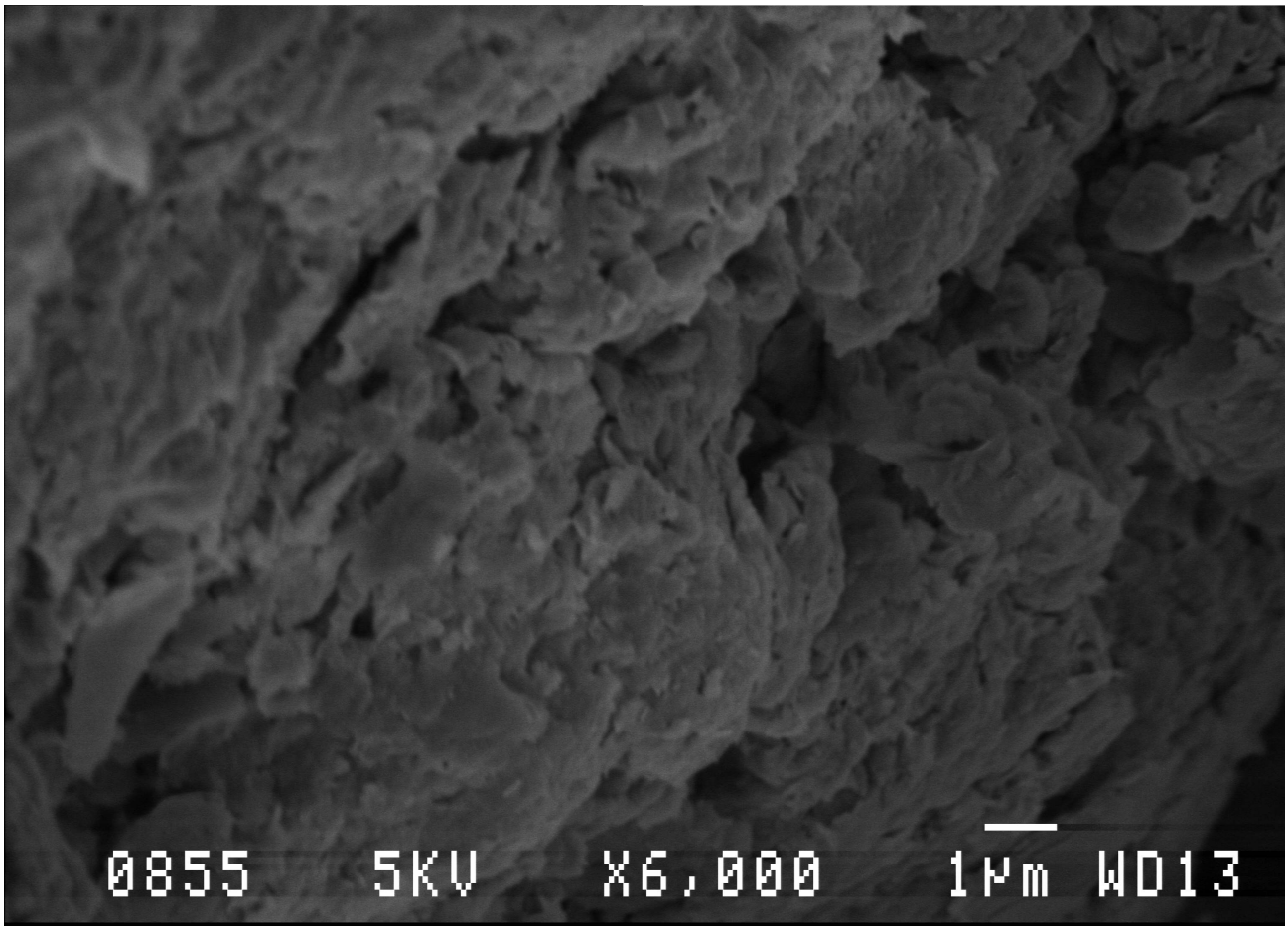

Figure A.1. Representative low-resolution SEM micrograph of organobentonite KSC14 revealed flake-shape particles

Table A.1. Summary of EVA melt intercalated with layered silicates in reviewed works

VA content (%)	MFI[a] (g/10 min)	Melting temperature (^oC)	Density g/cm^3	Reference
3	0.6	103[b]	(0.926[b])	Jeon et al., 2003
6	1.8	n.i.	n.i.	Zhang & Sundararaj, 2004
8	1	94[b]	0.930[b]	Jeon et al., 2003
9	n.i.	n.i.	n.i.	Cser & Bhattacharya, 2003; Pasanovic-Zujo et al., 2004; Chaudhary et al., 2005a; Chaudhary et al., 2005b; Costache et al., 2005
	1.1	n.i.	n.i.	Zang & Sundararaj, 2004
9.3	2	100	0.930	Cui et al., 2007
12	0.5	96	0.936	Alexandre et al., 2001a; Zanetti et al., 2001
	1.1	90[b]	0.932[b]	Jeon et al., 2003
12	0.8	n.i.	n.i.	Zang & Sundararaj, 2004
	0.3	95	0.929	Marini et al., 2009
14	0.3	93	0.935	La Mantia & Tzankova Dintcheva, 2006
14	0.3	93	0.935	Filippi et al., 2011
15	1.6	95[b]	0.938[b]	Jeon et al., 2003
18	n.i.	n.i.	n.i.	Pasanovic-Zujo et al., 2004; Chaudhary et al., 2005a; Chaudhary et al., 2005b
	1.6	n.i.	n.i.	Zhang & Sundararaj, 2004

VA content (%)	MFI[a] (g/10 min)	Melting temperature (^oC)	Density g/cm^3	Reference
18	2.5	88	0.941	Prasad et al., 2006; Cui et al., 2007
	2	86	0.940	Martins et al., 2009
	150	73	0.937	Marini et al., 2009
19	0.65	84	0.942	Alexandre et al., 2001a; Zanetti et al., 2001; Riva et al., 2002; Duquesne et al., 2003
	2	n.i.	n.i.	Costache et al., 2005
19	0.65	84	0.942	Bellucci et al., 2006
	2.1	86	0.940	Marini et al., 2009;
19	8	n.i.	n.i.	Marini et al., 2009
22	2	81[b]	0.945[b]	Jeon et al., 2003
22	3	87[b]	0.944[b]	Jeon et al., 2003
26	4	73[b]	0.950[b]	Jeon et al., 2003
27	3	71	0.951	Alexandre et al., 2001a; Alexandre et al., 2001b Peeterbroeck et al., 2005
28	n.i.	n.i.	n.i.	Beyer, 2001; Cser & Bhattacharya, 2003; Zhang et al., 2003; Pasanovic-Zujo et al., 2004; Tian et al., 2004; Chaudhary et al., 2005a; Chaudhary et al., 2005b; Costache et al., 2005; Szép et al., 2006

VA content (%)	MFI[a] (g/10 min)	Melting temperature (^oC)	Density g/cm^3	Reference
	3	71[b]	0.950[b]	Jeon et al., 2003
	3, 6, 25, 43, 150	n.i.	n.i.	Zhang & Sundararaj, 2004
	25	70	0.950	Gupta et al., 2005; Prasad et al., 2006
28	3	73	0.951	Cui et al., 2007
	150	68	0.950	Joseph & Focke, 2011
	2-3	100	0.920	Chacko et al., 2009
	24	73	0.947	Pistor et al., 2010
	25	70	0.921	Marini et al., 2009
	400	60	0.951	Joseph & Focke, 2011
40	n.i.	n.i.	n.i.	Zhang et al., 2003
	3	58	0.967	Cui et al., 2007; Lee et al., 2007
50	n.i.	n.i.	n.i.	Zhang et al., 2003
80	n.i.	n.i.	n.i.	Zhang et al., 2003

[a)] =measured at 190^o C under 2.16 kg load; [b)] = as indicated by the supplier; n.i. = not indicated

Table A.2. Summary of layered silicates and organic modifiers used in reviewed works

Code	Silicate mineral	CEC (meq/100 g)	Organic modifier	d_{001}, nm	Reference
OC_1	MMT	80–95	$(CH_3)_2N^+(HTallow)_2$	3.19 2.57	Alexandre et al., 2001a; Peeterbroeck et al., 2005;
OC_2	MMT	80–95	$(CH_3)_2[CH_3CH(CH_3CH_2)(CH_2)_4N^+(HTallow)$	2.07	Alexandre et al., 2001a; Peeterbroeck et al., 2005;
OC_3	MMT	80–95	$H_3N^+(CH_2)_{11}COOH$	1.63	Alexandre et al., 2001a
OC_4	MMT	80–95	$(CH_3)_3N^+(CH_2)_{21}COOH$	2.0	Alexandre et al., 2001a
OC_5	MMT	92	$(CH_3)_2N^+[(CH_2)_{17}CH_3]_2$	n.i.	Alexandre et al., 2001b
OC_6	MMT	n.i.	$(CH_3)_2N^+[(CH_2)_{17}CH_3]_2$	n.i.	Beyer, 2001
OC_7	FH	70–80	$H_2N(CH_2)_{11}COOH$	n.i.	Zanetti et al., 2001; Riva et al., 2002;
OC_8	FH	n.i.	$H_3N^+(CH_2)_{17}CH_3$	n.i.	Zanetti et al., 2001; Riva et al., 2002;
OC_9	MMT	n.i.	$H_3N^+(CH_2)_{17}CH_3$	n.i.	Zanetti et al., 2001
OC_{10}	MMT	n.i.	$(CH_2CH_2OH)_2N^+CH_3(Tallow)$	1.80	Riva et al., 2002; Costache et al., 2005; Cui et al., 2007

Code	Silicate mineral	CEC (meq/100 g)	Organic modifier	d_{001}, nm	Reference
OC_{11}	MMT	n.i.	$(CH_2CH_2OH)_2N^+CH_3(Tallow)$	1.88–1.84	Duquesne et al., 2003 Chaudhary et al., 2005a; Chaudhary et al., 2005b; Peeterbroeck et al., 2005; Prasad et al., 2006; Lee et al., 2007 Martins et al., 2009; Marini et al., 2009; Pistor et al., 2010;
OC_{11}	MMT	n.i.	$(CH_2CH_2OH)_2N^+CH_3(Tallow)$	1.88–1.84	Filippi et al., 2011
OC_{12}	MMT	n.i.	$(CH_3)_2N^+(HTallow)_2$	3.6	Riva et al., 2002
OC_{13}	MMT	85	$(CH_3)_3N^+(CH_2)_{15}CH_3$	1.96	Cser & Bhattacharya, 2003;
OC_{14}	MMT	n.i.	$(CH_2CH_2OH)_2N^+CH_3(CH_2)_{17}CH_3$	0.872	Jeon et al., 2003
OC_{15}	MMT	n.i.	$(CH_3)_2N^+[(CH_2)_{17}CH_3]_2$	2.239	Jeon et al., 2003
OC_{16}	MMT	n.i.	$(CH_3)_2(C_6H_5CH_2)N^+(CH_2)_{17}CH_3$	1.002	Jeon et al., 2003
OC_{17}	MMT	n.i.	$(CH_3)_2[CH_3CH(CH_3CH_2)(CH_2)_4N^+(CH_2)_{17}CH_3$	1.103	Jeon et al., 2003
OC_{18}	MMT	n.i.	$(CH_3)_3N^+(CH_2)_{17}CH_3$	1.983	Zhang et al., 2003
OC_{19}	MMT	n.i.	$(CH_3)_2N^+[(CH_2)_{17}CH_3]_2$	3.617	Zhang et al., 2003

Code	Silicate mineral	CEC (meq/100 g)	Organic modifier	d_{001}, nm	Reference
OC_{20}	MMT	n.i.	$CH_3N^+[CH_2)_{15}CH_3]_3$	3.723	Zhang et al., 2003
OC_{21}	MMT	n.i.	$(CH_3)_2N^+(HTallow)_2$	3.52	Chaudhary et al., 2005a;
OC_{21}	MMT	n.i.	$(CH_3)_2N^+(HTallow)_2$	3.52	Chaudhary et al., 2005b
OC_{22}	FH	70-80	$(CH_3)_2N^+(HTallow)_2$	4.55	Montanari et al., 2004; Bellucci et al., 2006
OC_{23}	MMT	85	$(CH_3)_2(CH_3CH_2)N^+(CH_2)_{15}CH_3$	2.00	Pasanovic-Zujo et al., 2004
OC_{24}	MMT	100	$H_3N^+(CH_2)_{17}CH_3$	2.01	Tian et al., 2004
OC_{25}	MMT	n.i.	$(CH_3)_2N^+(HTallow)_2$	2.4–2.7	Zhang and Sundararaj, 2004; Cui et al., 2007; Martins et al., 2009
OC_{26}	MMT	85	$(CH_3)_2(CH_3CH_2)N^+(CH_2)_{15}CH_3$	2.1	Gupta et al., 2005
OC_{27}	H	n.i.	$(CH_2CH_2OH)_2N^+CH_3(Tallow)$	2.1	Costache et al., 2005
OC_{28}	MG	n.i.	$(CH_2CH_2OH)_2N^+CH_3(Tallow)$	3.5	Costache et al., 2005
OC_{29}	FH	n.i.	$(CH_3)_2N^+(HTallow)_2$	3.11	Peeterbroeck et al., 2005
OC_{30}	MMT	n.i.	$(CH_3)_2N^+(Tallow)_2$	3.1–3.2	Montanari et al., 2004 Peeterbroeck et al., 2005; Bellucci et al., 2006; La Mantia & Tzankova Dintcheva, 2006

Code	Silicate mineral	CEC (meq/100 g)	Organic modifier	d_{001}, nm	Reference
OC_{31}	MMT	n.i.	$(CH_3)_2N^+(HTallow)_2$	2.24	Peeterbroeck et al., 2005
OC_{32}	MMT	n.i.	n.i.	1.82	Szép et al., 2006
OC_{33}	MMT	n.i.	$(CH_3)_3N^+(HTallow)$	1.8	Cui et al., 2007
OC_{34}	MMT	n.i.	$(CH_3)_2(C_6H_5CH_2)N^+(HTallow)$	1.865	Chacko et al., 2009

OC = organoclay; MMT = montmorillonite; FH = fluorohectorite; H = hectorite; MG = magadiite; n.i. = not indicated

Table A.3. Summary of equipment and parameters used to process the composites in reviewed works

Compounder/extruder	Temperature (°C)	Residence time (min)	Screw speed (rpm)	Reference
Two-roll mill (Agila)	160 EVA12) 130 (EVA19 & EVA27)	7	n.i	Alexandre et al., 2001a
Two-roll mill (Agila)	130	7	n.i.	Alexandre et al., 2001b
BUSS kneader	160	n.i.	n.i.	Beyer, 2001
Twin-screw minicompounder (DACA).	120	5 & 10	n.i.	Zanetti et al., 2001
Brabender	120	5	n.i.	Zanetti et al., 2001
Internal mixer (Brabender AEW330)	120±5	10	60	Riva et al., 2002
Twin-screw (Banbury)	80	40	70	Cser & Bhattacharya, 2003
Internal-mixer (Brabender Plasticorder PL2000)	160	n.i.	40/5/80	Duquesne et al., 2003
Mixer (Haake)	100	20	80	Jeon et al., 2003

Compounder/extruder	Temperature (°C)	Residence time (min)	Screw speed (rpm)	Reference
Rubber Mill	120	13	32 (3 min) & 64 (10 min)	Zhang et al., 2003
Leistriz ZSE27	140	n.i.	n.i.	Montanari et al., 2004
Twin-screw (Brabender)	80 (EVA28) & 90 (EVA18)	40	70	Pasanovic-Zujo et al., 2004
Twin-roll mill	120–125	10	n.i.	Tian et al., 2004
Twin-screw (Coperion, ZSK-25)	160	n.i.	200	Zhang & Sundararaj, 2004
Intermeshing counter-rotating twin-screw (Brabender)	110 (EVA9); 100 (EVA18 & EVA28)	25	70	Chaudhary et al., 2005a; Chaudhary et al., 2005b
Twin-screw (Brabender)	80	30	70	Gupta et al., 2005
Internal-mixer (Brabender Plasticorder)	120	20	60	Costache et al., 2005
Two-roll mill (AGILA)	140	12	15 m/s	Peeterbroeck et al., 2005
Internal mixer (Brabender)	125-130	3	60	Bellucci et al., 2006

Compounder/extruder	Temperature (°C)	Residence time (min)	Screw speed (rpm)	Reference
Single-screw (Brabender)	160	n.i.	60	La Mantia & Tzankova Dintcheva, 2006
Intermeshing counter-rotating twin-screw (Brabender)	160	n.i.	60	La Mantia & Tzankova Dintcheva, 2006
Twin-screw (Brabender)	100	n.i.	70	Prasad et al., 2006
Internal-mixer (Brabender Plasti Corder PL2000)	180	10	180	Szép et al., 2006
Intermeshing co-rotating twin-screw (Haake)	170	n.i.	280	Cui et al., 2007
Intermeshing counter-rotating twin-screw	110	25	70	Lee et al., 2007
Co-rotating twin-screw (Haake)	90–100	n.i.	280	Chacko et al., 2009
Twin-screw (B&P Process Equipment Systems)	195	n.i.	140	Martins et al., 2009

Compounder/extruder	**Temperature (°C)**	**Residence time (min)**	**Screw speed (rpm)**	**Reference**
Internal mixer (Haake Rheomix 600p)	150 150	5 (masterbatch) 5 nanocomposites)	120 120	Marini et al., 2009 Marini et al., 2009
Interpenetrating twin-screw co-rotating (MH-COR-20-32-LAB)	160	n.i.	400	Pistor et al., 2010
Static mixer (Brabender Plasticorder)	120	12.5	60	Fillippi et al., 2011
Two-roll mill	180	40	42	Joseph & Focke, 2011

Table A.4. Effect of processing equipment and conditions on dispersion of EVA composites

Nanocomposite	**Extruder/Compounder**	**Temperature (^oC)**	**Screw speed (rpm)**	**Reference**
EVA28 With OC_{11}	Counter-rotating intermeshing twin-screw	100	70	Chaudary et al., 2005a; Chaudary et al., 2005b
EVA28 with OC_{11}	Co-rotating interpenetrating twin-screw	160	400	Pistor et al., 2010
EVA14 with OC_{30}	Single screw	120–160	60	La Mantia & Tzankova Dintcheva, 2006
EVA14 with OC_{30}	Counter-rotating intermeshing twin-screw	120–160	60	La Mantia & Tzankova Dintcheva, 2006

Table A.5. Effect of organic modification of silicates on dispersion of EVA composites

Composite	Composite d_{001} (nm)	d_{002} (nm)	d_{003} (nm)	TEM results	O-clay load (mass %)	O-clay d_{001} (nm)	Reference
EVA9/OC_5	-	1.46	-	Int/exf & tactoids	5	1.820	Cui et al., 2007
EVA9/OC_{10}	4.41	Exists	-	Int & big tactoids	5	3.520	Chaudhary et al., 2005a
EVA9/OC_6	3.33	Exists	-	Int/exf & small tactoids	5	2.570	Cui et al., 2007
EVA9/OC_{25}	-	1.62	-	Tactoids	5	1.840	Cui et al., 2007
EVA18/OC_5	-	-	-	Int/exf & small tactoids	5	1.860	Chaudhary et al., 2005a
EVA18/OC_6	3.81	Exists	Exists	Int/exf & small tactoids	5	2.570	Cui et al., 2007
EVA19/OC_5	-	1.5	-	Exf & small tactoids	10	1.800	Riva et al., 2002
EVA19/OC_5	-	1.35	-	Exf & few tactoids	10	1.800	Duquesne et al., 2003
EVA19/OC_{4a}	-	1.4	-	Int/exf & small tactoids	10	2.000	Zanetti et al., 2001a
EVA19/OC_6	3.8	2	1.3	Int/exf & tactoids	10	3.600	Riva et al., 2002
EVA27/OC_5	-	Yes		Exf	5	1.800	Peeterbroeck et al., 2005
EVA27/OC_{23}	3.68	yes		Int/exf & tactoids	5	2.070	Peeterbroeck et al., 2005

Composite	Composite d_{001} (nm)	d_{002} (nm)	d_{003} (nm)	TEM results	O-clay load (mass %)	O-clay d_{001} (nm)	Reference
EVA27/OC_6	3.87	yes		Int/exf & tactoids	5	2.240	Peeterbroeck et al., 2005
EVA27/OC_{13}	4.02	yes		Int/exf & tactoids	5	2.900	Peeterbroeck et al., 2005
EVA28/OC_{19}	-	-	-	Exf & small tactoids	5	2.100	Gupta et al., 2002
EVA28/OC_1	4.4	yes	No	Int/exf & small tactoids	5	2.010	Tian et al., 2004
EVA28/OC_{27}	3.75	yes	Yes	Int & small tactoids*	5	2.620	Joseph and Focke, 2011
EVA28/OC_{13}	Yes	yes	Yes	Int/exf & small tactoids			Beyer, 2001
EVA28/OC_6	3.053	yes	Yes			2.293	Jeon et al., 2003

Int/exf = mixed morphology intercalated/exfoliated; * = Visualized in FESEM

Table A.6. Effect of VA content on dispersion of EVA composites

Composite	Composite d_{001} (nm)	d_{002} (nm)	d_{003} (nm)	TEM results	O-clay load (wt %)	O-clay d_{001} (nm)	Reference
EVA6/OC_6	3.2	Yes			2.5	2.500	Zhang and Sundararaj, 2004
EVA9/OC_6	3.5	Yes			2.5	2.500	Zhang and Sundararaj, 2004
EVA18/OC_6	3.81	Yes	Yes	Int/exf & small tactoids	5	2.570	Cui et al., 2007
EVA28/OC_6	3.85	Yes	Yes	Int/exf & small tactoids	5	2.570	Cui et al., 2007
EVA40/OC_6	4.18	Yes	Yes	Int/exf & small tactoids	5	2.570	Cui et al., 2007

Table A.7. Influence of composite structure on its mechanical properties

Material	Silicate content (%)	Internal structure	Modulus (MPa)	Strength (MPa)	Strain (%)	Reference
EVA27	0	-	12.1±1.2	28.4±0.7	1 406±28	Alexandre et al., 2001a
EVA27-OC_1	5	Int/exf	24.0±0.5	26.2±1.2	1 264±75	Alexandre et al., 2001a
EVA27-OC_2	5	Int/exf	23.1±1.0	27.0±0.8	1 341±16	Alexandre et al., 2001a
EVA27-OC_3	5	Int/exf	12.0±0.3	26.8±1.5	1 409±13	Alexandre et al., 2001a
*EVA15	0	-	58.8	15.7	800	Jeon et al., 2003
*EVA15-OC_{15}	2.5	Int***	80.4	14.7	760	Jeon et al., 2003
*EVA15-OC_{15}	5	Int***	94.1	14.2	756	Jeon et al., 2003
*EVA15-OC_{15}	7.5	Int***	101	12.7	711	Jeon et al., 2003
*EVA15-OC_{15}	10	Int***	109.8	11.3	678	Jeon et al., 2003
EVA6	0	-	84.5	-	1 146	Zhang & Sundararaj, 2004
EVA6-OC_{25}	2.5	Int***	97.7	-	946	Zhang & Sundararaj, 2004
EVA6-OC_{25}	5	Int***	113	-	600	Zhang & Sundararaj, 2004
EVA6-OC_{25}	10	Int***	127.2	-	36	Zhang & Sundararaj, 2004
EVA6-OC_{25}	20	Int***	152.4	-	18	Zhang & Sundararaj, 2004
*EVA9	0	-	8.6	15.6	-	Chaudhary et al., 2005a; Chaudhary et al., 2005b

Material	Silicate content (%)	Internal structure	Modulus (MPa)	Strength (MPa)	Strain (%)	Reference
*EVA9-OC_{11}	2.5	Int tactoid	54.3	7.8	-	Chaudhary et al., 2005a; Chaudhary et al., 2005b
*EVA9-OC_{11}	5	Int tactoid	64.3	8.9	-	Chaudhary et al., 2005a; Chaudhary et al., 2005b
*EVA9-OC_{11}	7.5	Int tactoid	74.3	9.4	-	Chaudhary et al., 2005a; Chaudhary et al., 2005b
*EVA18	0	-	5.7	13.3	-	Chaudhary et al., 2005a; Chaudhary et al., 2005b
*EVA18-OC_{11}	2.5	Int/exf	30	12.2	-	Chaudhary et al., 2005a; Chaudhary et al., 2005b
*EVA18-OC_{11}	5	Int/exf	34.3	15	-	Chaudhary et al., 2005a; Chaudhary et al., 2005b
*EVA18-OC_{11}	7.5	Int/exf	45.7	6.7	-	Chaudhary et al., 2005a; Chaudhary et al., 2005b
*EVA28	0	-	2.9	8.3	-	Chaudhary et al., 2005a; Chaudhary et al., 2005b
*EVA28-OC_{11}	2.5	Exf with small tactoids	8.6	5.3	-	Chaudhary et al., 2005a; Chaudhary et al., 2005b

Material	Silicate content (%)	Internal structure	Modulus (MPa)	Strength (MPa)	Strain (%)	Reference
*EVA28-OC_{11}	5	Exf with small tactoids	12.6	6.7	-	Chaudhary et al., 2005a; Chaudhary et al., 2005b
*EVA28-OC_{11}	7.5	Exf with small tactoids	17.1	5.6	-	Chaudhary et al., 2005a; Chaudhary et al., 2005b
EVA27	0	-	12.2±1.2	28.4±0.7	1406±28	Peeterbroeck et al., 2005
EVA27-OC_{31}	3	Int/exf & small tactoids	24.9±0.9	25.8±1.3	1231±46	Peeterbroeck et al., 2005
EVA27-OC_{2}	3	Int/exf & small tactoids	22.0±1.0	26.2±1.2	1259±25	Peeterbroeck et al., 2005
EVA27-OC_{11}	3	Int/exf & small tactoids	22.8±1.1	30.7±0.9	1266±24	Peeterbroeck et al., 2005
EVA27-OC_{1}	3	Int/exf & small tactoids	24.0±0.5	26.7±0.4	1291±45	Peeterbroeck et al., 2005
EVA27-OC_{29}	3	Int/exf & small tactoids	21.1±2.6	25.1±2.2	1270±51	Peeterbroeck et al., 2005
*EVA9.3	0	-	83.3	-	178.6	Cui et al., 2007
*EVA9.3-OC_{10}	1	Exf & small tactoids	91.7	-	174.2	Cui et al., 2007

Material	Silicate content (%)	Internal structure	Modulus (MPa)	Strength (MPa)	Strain (%)	Reference
*EVA9.3-OC_{10}	3	Exf & small tactoids	100	-	172.9	Cui et al., 2007
*EVA9.3-OC_{10}	5	Exf & small tactoids	125	-	160	Cui et al., 2007
*EVA9.3-OC_{10}	7	Exf & small tactoids	141.2	-	148.6	Cui et al., 2007
*EVA9.3-OC_{33}	1	Exf & small tactoids	79.2	-	174.2	Cui et al., 2007
*EVA9.3-OC_{33}	3	Exf & small tactoids	95.8	-	162.9	Cui et al., 2007
*EVA9.3-OC_{33}	5	Exf & small tactoids	104.2	-	157.1	Cui et al., 2007
*EVA9.3-OC_{33}	7	Exf & small tactoids	116.2	-	140	Cui et al., 2007
*EVA9.3-OC_{25}	1	Int/exf & small tactoids	112.5	-	170	Cui et al., 2007
*EVA9.3-OC_{25}	3	Int/exf & small tactoids	179.2	-	171.4	Cui et al., 2007

Material	Silicate content (%)	Internal structure	Modulus (MPa)	Strength (MPa)	Strain (%)	Reference
*EVA9.3-OC_{25}	5	Int/exf & small tactoids	250	-	151.4	Cui et al., 2007
*EVA9.3-OC_{25}	7	Int/exf & small tactoids	275	-	125.7	Cui et al., 2007
*EVA18	0	-	35.5	9.4	234.3	Cui et al., 2007
*EVA18-OC_{10}	1	Exf & small tactoids	45.2	-	242.9	Cui et al., 2007
*EVA18-OC_{10}	3	Exf & small tactoids	64.5	-	234.3	Cui et al., 2007
*EVA18-OC_{10}	5	Exf & small tactoids	90.3	-	234.3	Cui et al., 2007
*EVA18-OC_{10}	7	Exf & small tactoids	109.7	-	228.6	Cui et al., 2007
*EVA18-OC_{33}	1	Exf & small tactoids	38.7	-	251.4	Cui et al., 2007
*EVA18-OC_{33}	3	Exf & small tactoids	45.2	-	251.4	Cui et al., 2007

Material	Silicate content (%)	Internal structure	Modulus (MPa)	Strength (MPa)	Strain (%)	Reference
*EVA18-OC_{33}	5	Exf & small tactoids	58.1	-	257.1	Cui et al., 2007
*EVA18-OC_{33}	7	Exf & small tactoids	71.0	-	258.6	Cui et al., 2007
*EVA18-OC_{25}	1	Int/exf & small tactoids	51.6	10.1	257.1	Cui et al., 2007
*EVA18-OC_{25}	3	Int/exf & small tactoids	96.8	11.1	264.3	Cui et al., 2007
*EVA18-OC_{25}	5	Int/exf & small tactoids	161.3	11.9	248.6	Cui et al., 2007
*EVA18-OC_{25} *EVA18-OC_{25}	7 7	Int/exf & small tactoids	232.3 232.3	12.0 12.0	208.6 208.6	Cui et al., 2007 Cui et al., 2007
*EVA28	0	-	18	**	**	Cui et al., 2007
*EVA28-OC_{10}	1	Exf & small tactoids	21	**	**	Cui et al., 2007
*EVA28-OC_{10}	3	Exf & small tactoids	28.5	**	**	Cui et al., 2007

Material	Silicate content (%)	Internal structure	Modulus (MPa)	Strength (MPa)	Strain (%)	Reference
*EVA28-OC_{10}	5	Exf & small tactoids	36	**	**	Cui et al., 2007
*EVA28-OC_{10}	7	Exf & small tactoids	57	**	**	Cui et al., 2007
*EVA28-OC_{33}	1	Exf & small tactoids	19.5	**	**	Cui et al., 2007
*EVA28-OC_{33}	3	Exf & small tactoids	25.5	**	**	Cui et al., 2007
*EVA28-OC_{33}	5	Exf & small tactoids	36	**	**	Cui et al., 2007
*EVA28-OC_{33}	7	Exf & small tactoids	48	**	**	Cui et al., 2007
*EVA28-OC_{25} *EVA28-OC_{25}	1 1	Int/exf & small tactoids	24 24	** **	** **	Cui et al., 2007 Cui et al., 2007
*EVA28-OC_{25} *EVA28-OC_{25}	3 3	Int/exf & small tactoids	48 48	** **	** **	Cui et al., 2007 Cui et al., 2007
*EVA28-OC_{25}	5	Int/exf & small tactoids	72	**	**	Cui et al., 2007

Material	Silicate content (%)	Internal structure	Modulus (MPa)	Strength (MPa)	Strain (%)	Reference
*EVA28-OC_{25}	7	Int/exf & small tactoids	117	**	**	Cui et al., 2007
EVA28	0	-	7.1	4.05	454	Joseph & Focke, 2011
EVA28-OC_{25}	1	Int	7.8	4.10	483	Joseph & Focke, 2011
EVA28-OC_{25}	3	Int	10.9	4.13	473	Joseph & Focke, 2011
EVA28-OC_{25}	5	Int	15.8	4.46	475	Joseph & Focke, 2011
EVA28-OC_{25}	10	Int	20.1	3.80	391	Joseph & Focke, 2011
EVA28	0	-	3.96	1.62	374	Joseph & Focke, 2011
EVA28-OC_{25}	1	Int	4.2	1.68	427	Joseph & Focke, 2011
EVA28-OC_{25}	3	Int	5	1.7	508	Joseph & Focke, 2011
EVA28-OC_{25}	5	Int	5	1.7	509	Joseph & Focke, 2011
EVA19	0	-	43±1.1	25±0.5	820±22	Bellucci et al., 2006
EVA19-OC_{30}	5	Int	54±1.3	17±0.6	663±15	Bellucci et al., 2006
EVA19-OC_{22}	5	Exf	62±1.7	20±0.8	721±18	Bellucci et al., 2006

* = Estimated from graphs;** = Beyond instrument limit;***= Probed by XRD

Table A.8. Influence of composite structure on its steady shear rheological properties

Material	Silicate content (%)	Internal structure	η_0 (Pa.s)	T^a (^oC)	-n	G' (Pa)	Reference
EVA19	0	-		110		10^3	Riva et al., 2002
EVA19-OC_7	10	Tactoids		110		10^3	Riva et al., 2002
EVA19-OC_8	10	Int/exf		110		3.10^3	Riva et al., 2002
EVA19-OC_{10}	10	Int/exf		110		$1,5.10^4$	Riva et al., 2002
EVA19-OC_{12}	10	Int/exf		110		$1,9.10^3$	Riva et al., 2002
*EVA28	0	Int***					Pasanovic-Zujo et al., 2004
*EVA28-OC_{18}	3	Int***				10^9	Pasanovic-Zujo et al., 2004
*EVA28-OC_{18}	5	Int***					Pasanovic-Zujo et al., 2004
*EVA28-OC_{18}	10	Int***					Pasanovic-Zujo et al., 2004
*EVA28	0	-	4.10^3	130			Gupta et al., 2005
*EVA28-OC_{26}	2.5	Int***	$1,6.10^4$	130			Gupta et al., 2005
*EVA28-OC_{26}	5	Int***	4.10^4	130			Gupta et al., 2005
*EVA28-OC_{26}	7	Int***	9.10^4	130			Gupta et al., 2005
*EVA28-OC_{26}	10	Int***	$1,7.10^5$	130			Gupta et al., 2005
EVA14	0	-	$1,8.10^5$	160			La Mantia & Tzankova Dintcheva, 2006
EVA14-OC_{30}	5	Int tactoid	3.10^5	160	0.049		La Mantia & Tzankova Dintcheva, 2006
EVA14-OC_{30}	10	Int tactoid	$3,3.10^5$	160	0.058		La Mantia & Tzankova Dintcheva, 2006

Material	**Silicate content (%)**	**Internal structure**	**η_0 (Pa.s)**	**T^a (^oC)**	**-n**	**G' (Pa)**	**Reference**
EVA14	0	-	$1,6.10^5$	160			La Mantia & Tzankova Dintcheva, 2006
EVA14-OC_{30}	5	Int tactoid	$2,8.10^5$	160	0.042		La Mantia & Tzankova Dintcheva, 2006
EVA14-OC_{30}	10	-	$3,1.10^5$	160	0.054		La Mantia & Tzankova Dintcheva, 2006
*EVA28	0	-		130			Szép et al., 2006
*EVA28-OC_{32}	5	Int/exf	4.9	130	0.84		Szép et al., 2006
EVA40	0		$5,6.10^4$	130	0.62	3.10^3	Lee et al., 2007
EVA40-OC_{11}	2.5	-	$1,8.10^5$	130	0.49	$7,5.10^3$	Lee et al., 2007
EVA40-OC_{11}	5	Exf with small tactoids	4.10^5	130	0.34	$1,3.10^4$	Lee et al., 2007
EVA40-OC_{11}	7.5	Exf with small tactoids	$1,4.10^6$	130	0.25	$2,6.10^4$	Lee et al., 2007
EVA40-OC_{11}	10	Exf with small tactoids	$4,6.10^6$	130	0.22	$5,5.10^4$	Lee et al., 2007
EVA12	0	-	$5,5.10^5$	150	0.28		Marini et al., 2009
EVA12-OC_{31}	3	Int/exf & small tactoids	$6,6.10^5$	150	0.36		Marini et al., 2009
EVA19	3	Int/exf & small tactoids	4.10^4	150	0.02		Marini et al., 2009

Material	**Silicate content (%)**	**Internal structure**	**η_0 (Pa.s)**	**T^a (^oC)**	**-n**	**G' (Pa)**	**Reference**
EVA19-OC_{11}	3	Int/exf & small tactoids	10^5	150	0.08		Marini et al., 2009
EVA19	3	Int/exf & small tactoids	10^4	150	0.02		Marini et al., 2009
EVA19-OC_{29}	3	Int/exf & small tactoids	$4{,}2.10^4$	150	0.06		Marini et al., 2009
EVA28	0	-	$2{,}3.10^3$	150	0.02		Marini et al., 2009
EVA28-OC_{10}	1	Exf & small tactoids	$1{,}1.10^5$	150	0.46		Marini et al., 2009
EVA18	3	Exf & small tactoids	$2{,}4.10^2$	150	0.05		Marini et al., 2009
EVA18-OC_{10}	5	Exf & small tactoids	$3{,}8.10^4$	150	0.41		Marini et al., 2009
EVA19	0	-			0.22		Bellucci et al., 2006
EVA19-OC_{30}	5	Int			0.34		Bellucci et al., 2006
EVA19-OC_{22}	5	Exf			0.54		Bellucci et al., 2006
*EVA28	0	-	10^4	110		-	Prasad et al., 2006

Material	**Silicate content (%)**	**Internal structure**	**η_0 (Pa.s)**	**T^a (^oC)**	**-n**	**G' (Pa)**	**Reference**
*EVA28-OC_{11}	2.5	Exf & small tactoids	8.10^4	110	0.28	30	Prasad et al., 2006
*EVA28-OC_{11}	5	Int/exf & small tactoids	4.10^5	110	0.46	200	Prasad et al., 2006
*EVA28-OC_{11}	7.5	Int/exf & small tactoids	7.10^6	110	0.84	7.10^3	Prasad et al., 2006
*EVA18	0	-	$1,5.10^5$	110	0.25	-	Prasad et al., 2006
*EVA18-OC_{11}	2.5	Exf & small tactoids	$4,5.10^5$	110	0.33	100	Cui et al., 2007
*EVA18-OC_{11}	5	Exf & small tactoids	$1,2.10^6$	110	0.49	600	Prasad et al., 2006
*EVA18-OC_{11}	7.5	Exf & small tactoids	6.10^6	110	0.67	4.10^3	Prasad et al., 2006

η^o = Zero shear viscosity; T^a = Temperature; n = Shear thinning exponent; G'= storage modulus; *= Estimated from graphs

η^o and G' were taken at lower shear rates or frequencies

Table A.9. Influence of composite structure on its thermal properties

Material	Silicate content (%)	Internal structure	T_{max1} (°C)		T_{max2} (°C)		Reference
			Oxidative	Non-oxidative	Oxidative	Non-oxidative	
*EVA19	0	-	367	373	457	487	Beyer, 2001
*EVA28-OC_6	5		367	360	498	483	Beyer, 2001
EVA12	0				413		Zanetti et al., 2001
EVA12-OC_7	10				415		Zanetti et al., 2001
EVA12-OC_8	10				487		Zanetti et al., 2001
EVA12-OC_9	10				474		Zanetti et al., 2001
EVA19	0		335	348		468	Zanetti et al., 2001
EVA19-OC_7	10			348		468	Zanetti et al., 2001
EVA19-OC_8	10		288	283		479	Zanetti et al., 2001
EVA19-OC_9	10		335	296	475	468	Zanetti et al., 2001
*EVA19	0		332	350	423	464	Riva et al., 2002
*EVA19-OC_7	10		350	350	423	468	Riva et al., 2002
*EVA19-OC_8	10	Int/exf	293	284	477	470	Riva et al., 2002
*EVA19-OC_{10}	10	Int/exf	350	330	486	468	Riva et al., 2002
*EVA19-OC_{12}	10	Int/exf	350	350	486	457	Riva et al., 2002
EVA19	0		335		470		Duquesne et al., 2003
EVA19-OC_{11}	5		340		430		Duquesne et al., 2003

Material	Silicate	Internal	T_{max1} (°C)		T_{max2} (°C)		Reference
			Oxidative	Non-Oxidative	Oxidative	Non-Oxidative	
EVA19-OC_{11}	10		340		430, 470		Duquesne et al., 2003
*EVA27	0		352		448		Peeterbroeck et al., 2005
*EVA27-OC_1	3		352		490		Peeterbroeck et al., 2005
*EVA27-OC_{29}	3		352		504		Peeterbroeck et al., 2005
*EVA27-OC_{30}	3		352		476		Peeterbroeck et al., 2005
*EVA27	0		352		448		Peeterbroeck et al., 2005
*EVA27-OC_1	5		352		490		Peeterbroeck et al., 2005
*EVA27-OC_{29}	5		352		490		Peeterbroeck et al., 2005
*EVA27-OC_{30}	5		352		490		Peeterbroeck et al., 2005
*EVA28	0		341		458		Szép et al., 2006
*EVA28-OC_{32}	11		331		476		Szép et al., 2006

*Estimated from graphs

Table A.10. XRF analysis of major and trace elements in the bentonite samples

UNIVERSITEIT VAN PRETORIA
UNIVERSITY OF PRETORIA
YUNIBESITHI YA PRETORIA

XRF REPORT:

XRD & XRF Facility **Geology Department**

Direct Telephone: (012) 420-2137
Direct Telefax: (012) 420 2661 South Africa

CLIENT: Pedro

DATE: 12/03/08

ANALYSIS:

Should be considered semi-quantitative.

%	GSN Cert	GSN	KP	BP	KDC16	KDC10	KDC18>CEC	BSC14	BDC16	BDC10	BDC18>CEC	BDC18 >CEC
SiO_2	65.80	66.09	56.41	73.35	33.19	49.09	33.85	60.86	44.15	59.23	41.20	45.52
TiO_2	0.68	0.67	0.32	0.20	0.17	0.15	0.17	0.16	0.10	0.16	0.10	0.26
Al_2O_3	14.67	14.81	17.47	12.04	10.94	9.17	11.09	9.31	8.59	9.15	6.69	15.85
Fe_2O_3	3.75	3.73	5.00	2.47	3.13	1.11	3.10	1.83	1.40	1.81	1.42	5.25
MnO	0.06	0.05	0.13	0.03	0.03	0.00	0.03	0.01	0.00	0.00	0.01	0.05
MgO	2.30	2.19	3.74	2.43	2.21	1.39	2.20	1.29	1.54	1.26	0.96	3.14
CaO	2.50	2.46	2.53	0.13	0.42	0.00	0.45	0.00	0.32	0.00	0.06	0.70
Na_2O	3.77	3.76	0.32	0.78	0.07	0.57	0.04	0.02	0.80	0.14	0.49	0.05
K_2O	4.63	4.62	1.17	0.07	0.44	0.32	0.46	0.04	0.20	0.09	0.02	0.65
P_2O_5	0.28	0.28	0.15	0.00	0.47	0.01	0.43	0.01	0.01	0.01	0.00	0.62
Cr_2O_3	0.008	0.01	0.01	0.00	0.00	0.00	0.00	0.00	0.00	0.00	0.01	0.01
NiO	0.0043	0.01	0.00	0.01	0.00	0.00	0.00	0.00	0.00	0.00	0.02	0.01
V_2O_5	0.01	0.01	0.01	0.00	0.00	0.00	0.00	0.00	0.00	0.00	0.00	0.01
ZrO_2	0.03	0.02	0.02	0.05	0.01	0.04	0.01	0.05	0.04	0.05	0.12	0.04
LOI	1.32	1.29	10.72	7.65	47.75	37.58	48.51	25.89	43.05	27.04	49.47	28.69
TOTAL	99.82	100.0 0	97.99	99.22	98.85	99.44	100.36	99.47	100.21	98.96	100.56	100.85

ppm	GSNcert	GSN	KP	BP	KDC16	KDC10	KDC18>CEC	BSC14	BDC16	BDC10	BDC18>CEC	KSC14
As	1.6	3	3	3	3	4	3	228	6	7	3	5
Cu	20	27	10	9	11	13	8	121	37	95	66	11
Ga	22	20	20	23	11	14	11	22	11	16	10	17
Mo	1.2	1	1	1	1	1	1	1	1	1	1	1
Nb	21	20	25	92	5	10	5	64	66	61	37	15
Ni	34	38	13	9	8	11	8	23	15	15	10	9
Pb	53	52	34	21	5	11	8	3	11	18	13	15
Rb	185	182	52	3	18	23	17	58	2	2	2	31
Sr	570	578	150	36	30	34	27	3	3	3	3	66
Th	42	45	32	13	3	4	3	76	3	3	3	14
U	8	11	3	3	3	3	3	3	3	3	3	3
W*	450	543	6	10	6	6	6	8	8	8	6	6
Y	19	10	31	163	10	14	9	78	96	93	58	18
Zn	48	49	55	167	35	44	34	171	92	130	88	43
Zr	235	225	157	411	74	94	75	369	376	357	242	110
Cl*	450	692	697	5615	9560	4948	10916	114	13368	4329	19959	123
Co	65	69	6	2	7	167	8	2	2	3	2	14
Cr	55	57	7	7	7	7	7	7	7	7	7	24
F*	1050	2011	617	1328	611	837	668	1382	1451	1566	1431	100
S*	140	484	98	597	355	262	178	318	377	243	299	423
Sc	7	9	10	1	11	9	10	2	2	1	2	11
V	65	55	26	17	28	29	27	17	17	17	17	37
Cs	5	9	9	9	10	10	12	9	9	9	9	9
Ba	1400	1383	483	129	274	273	307	124	73	93	120	255

La	75	52	46	167	51	50	53	120	149	120	131	51
Ce	135	136	119	250	120	109	118	216	278	213	231	112

If you have any further queries, kindly contact the laboratory.

Analyst:

M.Loubser